

## Propagation properties of short density perturbations in Q-machine plasmas with double-humped ion velocity distribution functions

**Noauthor, Risø**

*Published in:*

Proceedings of the 3. International Conference on Quiescent Plasmas

*Publication date:*

1971

*Document Version*

Publisher's PDF, also known as Version of record

[Link back to DTU Orbit](#)

*Citation (APA):*

Twomey, D. (1971). Propagation properties of short density perturbations in Q-machine plasmas with double-humped ion velocity distribution functions. In Proceedings of the 3. International Conference on Quiescent Plasmas (pp. 95-102). (Denmark. Forskningscenter Risøe. Risøe-R; No. 250).

## DTU Library

Technical Information Center of Denmark

---

### General rights

Copyright and moral rights for the publications made accessible in the public portal are retained by the authors and/or other copyright owners and it is a condition of accessing publications that users recognise and abide by the legal requirements associated with these rights.

- Users may download and print one copy of any publication from the public portal for the purpose of private study or research.
- You may not further distribute the material or use it for any profit-making activity or commercial gain
- You may freely distribute the URL identifying the publication in the public portal

If you believe that this document breaches copyright please contact us providing details, and we will remove access to the work immediately and investigate your claim.

Danish Atomic Energy Commission  
Research Establishment Risø

---

Proceedings of the 3rd International  
Conference on Quiescent Plasmas,  
Elsinore September 20 - 24 1971

Sponsored by the European Physical Society and arranged by the  
Danish Atomic Energy Commission Research Establishment Risø

October 1971

*Sales distributor:* Jul. Ojellerup, 87, Sølvgade, DK-1307 Copenhagen K, Denmark

*Available on exchange from:* Library, Danish Atomic Energy Commission, Risø, DK-4000 Roskilde, Denmark



Proceedings of the 3rd International Conference on Quiescent Plasmas,  
Elsinore September 20 - 24 1971

Sponsored by the European Physical Society  
and arranged by the Danish Atomic Energy Commission,  
Research Establishment Ris5

Abstract

These proceedings contain fifty-one papers presented at the "3rd International Conference on Quiescent Plasmas". The papers are arranged according to the following subjects: Plasma Production, Ion Waves, Electron Waves, Drift Waves, Non-Linear Effects, and Special Topics.

To facilitate reproduction and speed up publication, the papers are reproduced directly from the best available copies, and no editorial alterations have been made.

ISBN 87 550 0107 6

## CONTENTS

|   | Page |
|---|------|
| <b><u>PLASMA PRODUCTION</u></b>   |      |
| The Helios Program. Harry S. Robertson .....  | 1    |
| The Structure of an Alkali-Plasma Column in a weak<br>Magnetic Field. P. H. Krumm, M. A. Hellberg and<br>G. R. Baker .....  | 9    |
| A Quiescent Plasma Sustained by High Frequency Fields.<br>Earl R. Ault and K. R. MacKenzie .....  | 17   |
| Magnetic Multipole Confinement of a Magnetic Field-Free<br>Plasma. Rudolf Limpaecher and K. R. MacKenzie .....  | 22   |
| Production and Application of a Uranium Plasma in the Q-Device.<br>M. Hashmi and A. J. van der Houven van Oordt .....   | 27   |
| <b><u>ION AND ELECTRON WAVES</u></b>  |      |
| Experimental Study of the First Order Ion Distribution Function<br>Related to Ionic Wave in a Q-Machine. P. Mills .....   | 33   |
| Exact Calculation of the Perturbed Distribution Functions<br>Associated with Electrostatic Waves. J. M. Buzzi .....   | 40   |
| Numerical Studies of Ion Acoustic Wave Propagation in the Non<br>Maxwellian Plasma of a Single Ended Q-Device. J. M. Buzzi ...  | 48   |
| Measurements of the Perturbed Ion Velocity Distribution at a<br>Wave-exciting Grid. G. B. Christoffersen .....  | 55   |
| Calculations and Measurements of the Perturbed Density and<br>Ion Velocity Distribution Function in Grid-Excited Waves in<br>a Q-Machine Plasma. G. B. Christoffersen, V. O. Jensen<br>and P. Michelsen ..... | 63   |
| Simulation of Pseudowaves and Ion Acoustic Waves.<br>K. Estabrook and I. Alexeff .....  | 71   |
| Excitation of Ion-Acoustic Waves by Parametric Heating and<br>Strong High-Frequency Fields. R. H. Abrams, Jr.,<br>T. Che and H. Lashinsky .....   | 79   |

|  | Page |
|--|------|
| Collective Interaction and Freely Streaming Ions in Density Perturbations and Waves in Q-Machines. V. O. Jensen .....  | 87   |
| Propagation Properties of Short Density Perturbations in Q-Machine Plasmas with Double-Humped Ion Velocity Distribution Functions. Dennis Twomey .....   | 95   |
| Propagation of Ions-Acoustic Waves in a Plasma with a Double-humped Ion Velocity Distribution Function. P. Michelsen and L. P. Prahm .....   | 103  |
| Two Ion Beam Instability in a Q-Machine with Inhomogeneous B-Field. D.R. Baker, C. Bartoli and M. Bitter .....   | 111  |
| Ion Heating Caused by Ion Acoustic Waves in an Ion-Streaming Plasma. T. Honzawa and Y. Kawai .....   | 119  |
| Ion Wave Excitation via a Modulated Electron Beam. J.M. Buzzi, H.J. Doucet and W.D. Jones .....  | 128  |
| Ion-Acoustic Collisionless Shocks in a Q-Machine. V. Vanek and T.C. Marshall .....   | 136  |
| Observation of the Propagation and Damping of Small Amplitude Electron and Ion Waves in Thermally Ionized Collisionless Alkali Metal Plasma. R.N. Franklin, S.M. Hamberger, G. Lampis and G.J. Smith ..... | 144  |
| Spatial and Temporal H. F. Plasma Response to an Externally Applied Pulse. P. Demuliere, M. Guillemot, J. Olivain, F. Perceval and A. Quemeneur .....  | 151  |
| Ion-Acoustic Resonances in Bounded Plasmas and Comparison with Refined Fluid Theory. R.R. Weynants, A.M. Messiaen and P.E. Vandeplass .....  | 161  |
| Ion-Acoustic Instability of a Two-Temperature, Collisional, Fully-Ionized Plasma. T.D. Rognlien and S.A. Self .....  | 169  |
| Wake Behind a Body in Motion in a Plasma, Parallel to the Magnetic Field. Theoretical Solution. J.P.M. Schmitt .....   | 177  |
| Wake behind an Obstacle in a single-ended Q-Machine and its Use as a Diagnostic of the Ion Distribution Function. J.P.M. Schmitt .....   | 185  |

DRIFT WAVES

|   |     |
|---|-----|
| <b>Current-Driven Collisional Drift Instability in a Q-Machine Plasma: Wave Induced Losses and Anomalous Resistivity.</b><br>R. F. Ellis and R. W. Motley .....   | 194 |
| <b>Effects of Parallel Wavelength on Collisional Drift Instability.</b><br>L. G. Schlitt and H. W. Hendel .....   | 201 |
| <b>Numerical Investigation of the Effect of Heat Transport on Collisional Drift Waves.</b> P. Brossier, P. Deschamps,<br>R. Gravier, R. Pellat and C. Renaud .....  | 209 |
| <b>Measurements of Temperature Waves in Connection with a Drift-Type Instability.</b> W. Friz, G. L. J. Müller and R. S. Palmer ....  | 217 |
| <b>Dynamic Stabilization of Transverse Kelvin-Helmholtz Instability.</b> Y. C. Lee and T. K. Chu .....  | 224 |
| <b>Passive Feedback Control of a Drift-Type Instability in a Q-Machine Plasma Column.</b> G. L. J. Müller and R. S. Palmer ..   | 230 |
| <b>Experimental Frequencies and Growth Rates of a Drift-Dissipative Instability in a Continuous r. f. Plasma.</b><br>B. E. Keen and M. W. Alcock .....  | 238 |
| <b>Resonant Characteristics of Collisionless Drift-Waves in Hydrogen Plasma - Comparison between Experimental Results and Linear Theory.</b> R. Boissier, P. Brossier, P. Deschamps,<br>R. Gravier, R. Pellat and C. Renaud ..... | 246 |
| <b>Experimental Measurement of Drift-Waves in a Strongly Sheared Magnetic Field.</b> P. E. Stott and J. Burt .....  | 254 |
| <b>High Frequency Fluctuations in the Density Gradient of an Alkali Plasma.</b> P. Brossier, P. Deschamps, R. Gravier and<br>C. Renaud .....  | 261 |
| <b>Interpretation of Dispersion Relations for Bounded Systems.</b><br>T. D. Roglien and S. A. Self .....  | 267 |

NON-LINEAR EFFECTS

|   |     |
|---|-----|
| <b>Amplitude of Electron Plasma Wave Echoes.</b> M. Guillemot,<br>J. Olivain, F. Perceval, A. Quemeneur and G. Matthieussent .. | 275 |
|---|-----|



|   | Page |
|---|------|
| Wave Growth in a Large Unmagnetized Electron-Beam-Plasma System. P. J. Barrett, D. Gresillon and A. Y. Wong .....                                   | 285  |
| Measurement of Velocity Diffusion in an Electron Beam-Plasma Interaction. P. J. Barrett, D. Gresillon and A. Y. Wong .....                          | 290  |
| Cross-field Current-driven Ion Acoustic Instability.<br>P. J. Barrett, B. D. Fried, C. F. Kennel, R. J. Taylor and<br>J. M. Sellen .....            | 297  |
| Large Amplitude Wave Interaction with a Plasma: Trapping Effects. M. Guillemot, J. Olivain, F. Perceval and<br>A. Quemeneur .....                   | 304  |
| Exchange of Energy between Large-amplitude Plasma Waves and the Electron Energy Distribution. E. P. Barbian and<br>B. Jurgens .....                 | 317  |
| Test Wave Amplification and Instability Caused by Electron Trapping. R. N. Franklin, S. M. Hamberger, H. Ikezi,<br>G. Lampis and G. J. Smith .....  | 327  |
| Trapped-Ion Instability in Ion-Acoustic Waves. H. Ikezi,<br>Y. Kiwamoto, K. Mima and K. Nishikawa .....   | 334  |
| Measurements on an Ion Sound Decay Instability Induced by a Large Amplitude Bernstein Mode in a Plasma. B. E. Keen and<br>W. H. W. Fletcher .....   | 341  |
| Observations of Nonlinear Scattering from a Plasma Column.<br>R. L. Bruce, F. W. Crawford and K. J. Harker .....                                    | 349  |
| <b><u>SPECIAL TOPICS</u></b>  |      |
| Acquisition and Processing of Plasma Fluctuation Data Using FFT Spectral Analysis Techniques. D. E. Smith, E. J. Powers,<br>and R. E. Rowberg ..... | 357  |
| Potential Surrounding a Moving Test-Particle in a Quiescent Plasma. K. C. Hines .....   | 365  |
| A Measurement of $T_{\perp}$ of Ba Plasma in a Q-Machine.<br>I. Katsumata .....   | 374  |
| A Small Electrostatic Energy Analyser. P. Michelsen .....   | 382  |

|   | <b>Page</b> |
|---|-------------|
| <b>Resonance Charge Exchange Cross Section for Cesium Measured<br/>around 2 eV. S. A. Andersen, V. O. Jensen and P. Michelsen ...</b> | <b>388</b>  |
| <b>AUTHOR LIST .....</b>  | <b>395</b>  |



The Helios Program\*

by

Harry S. Robertson

University of Miami, Coral Gables, Florida 33124, U.S.A.

Abstract

HELIOS (for Heated Lithium Ion System) is a nearly completed facility for quiescent, steady-state plasma studies. Lithium ions are injected through two rhenium ionizing nozzles into a 2- to -1 mirror field with four internal Ioffe bars. Electrons are heated by octave-band microwave noise over the electron gyrofrequency range, and ions are heated by wide-band noise around the ion gyrofrequencies. The boundaries of the plasma are formed by a cage of iron wires, each floating electrically and free to assume its own potential. The system is designed to minimize instabilities by eliminating, insofar as possible, all free-energy sources such as currents and temperature gradients. The stochastic heating is also helpful in suppressing certain instabilities, and the boundary cage not only prevents the naturally-present plasma potential differences from producing currents via the vacuum chamber walls, but also the local ripples in the magnetic field contribute to containment. Initial experiments in the partially completed system have produced plasmas with electron temperature of 35 eV, at densities of  $10^{17}/\text{cm}^3$  using 200 watts of microwave power.

Introduction

The Helios system was conceived as the solution to a design problem with a set of ten boundary conditions, listed below. These criteria were established before any device was considered, and the Helios system should be regarded as a vehicle for basic research studies, and not an end in itself. The design will doubtless be changed as the research progresses.

In the light of present knowledge of plasma instabilities and loss processes, university research needs, the present state of the art, and the kind of general plasma research device that seems to be needed as a second-generation replacement for the Q-machine, the following basic criteria were established:

- (1) Basically steady state (or long time constant).
- (2) Minimal sources of free energy to drive instabilities.

- (3) Ion and electron temperatures of the order of 100 eV.
- (4) High, controllable density (up to  $10^{13} - 10^{14}/\text{cm}^3$ ), at very high fractional ionization.
- (5) Dimensions of the plasma chamber  $>10$  ion gyroradii for interesting ion energy.
- (6) Favorable magnetic field geometry.
- (7) High degree of flexibility and versatility.
- (8) Modest size and cost.
- (9) Maximum utilization of present facilities.
- (10) High degree of current value, both as an educational vehicle and as a research tool.

The system to be described has produced interesting preliminary plasmas, but a number of the design features that should contribute to its good behavior have not yet been incorporated.

#### General Description

The Helios system may be described briefly as a stochastically heated lithium-ion plasma in a combined mirror and linear multipole field. As shown in Fig. 1, lithium is to be evaporated from its electrically heated niobium reservoir, through a tubular, incandescent, ohmically heated rhenium ionizer, into the one-meter-long plasma chamber. The cold ( $\sim 0.2\text{eV}$ ), partially ionized lithium spray is subjected to steady-state microwave heating by broad-band microwave noise power, introduced axially via radiators at the ends of the plasma chamber.

The stochastic heating field is intended to heat the electrons throughout the entire plasma volume to approximately the same temperature, thereby preventing instabilities that arise because of electron temperature gradients. A double-humped distribution with a population of run-away hot electrons is regarded as incompatible with criterion 2, and therefore to be avoided. Supplementary stochastic heating of the ions is also necessary.

The broad-band noise source, which operates over the spectrum of electron gyrofrequencies in the plasma, may be thought of as a microwave heat lamp, operating in a region of the spectrum for which the electron component of the plasma is highly absorbent. Even without detailed calculation, it is evident that this kind of heating is capable of producing a well-thermalized electron component of the plasma. Other advantages are that the phase incoherence of the heating source prevents the growth of electron-cyclotron waves and at the same time inhibits the growth of other micro-instabilities, since the electrons act as if they are being stirred so rapidly that collective effects are dispersed before they are sufficiently organized to become disruptive, yet so gently that the process of stirring causes no perturbation.

The approach to stability control through elimination of free-energy sources has been developed conceptually by Fowler<sup>2</sup>. The Helios design has attempted to eliminate every possible source of free energy that might drive instabilities, and the initial experiments will evaluate the relative success of alternate techniques. No velocity-space instability is expected, since both the electron and the ion distributions are intended to be close to Maxwellian. (There will be a modified mirror loss cone, but the combination of magnetic field geometry and plasma boundary design is expected to diminish it, and the heating method should minimize velocity space anisotropies.)

There are to be no essential imposed d.c. potentials. The plasma is in a cage, similar to that shown in Fig. 1, such that the electric fields at the boundaries minimize plasma losses (or maximize plasma density). The boundary fields are expected to be much more compatible with the natural boundary conditions of the plasma than are the usual metallic walls, and much less subject to build-up of electrostatic fields than is possible with insulating walls. Recent work by Geissler<sup>2</sup> shows that conducting walls impose an unnatural equipotential surface at the plasma boundary that enhances the plasma loss rate by orders of magnitude, whereas with insulating walls the non-classical part of the diffusion loss was much reduced. Similarly, Ferrari and Kuckes<sup>3</sup> have shown that the presence of a metal end in an ECR plasma is clearly destabilizing. On the other hand, an insulating wall, when clean, permits the accumulation of local charged spots and their resultant electric fields, whereas an accumulation of lithium can result after a time in essentially a metal-plated, conducting wall. A boundary of the type proposed here (and apparently not yet tried anywhere) seems to be the obvious and necessary means of minimizing the plasma-sheath free energy sources.

There are to be no direct or low-frequency currents in the Helios plasma, except perhaps a small differential particle current at the source (at low energy) to compensate for possible unequal ion and electron loss rates at the boundaries. No beams of energetic particles and no selective or highly localized heating of any component or element of the plasma should exist. Expansion free energy is minimized by favorable magnetic field geometry.

The one unavoidable source of free energy resides in the confinement of the plasma, with consequent pressure gradient, leading usually to some form of the universal instability. The stochastic heating field in Helios is expected to suppress instability growth of the drift-wave type, both by minimizing the internal pressure gradients that drive it and by continuously disorganizing the electrons. A suppression of this type has been reported by Puri<sup>4,5</sup>, and both Dandl's<sup>6</sup> group and Ferrari and Kuckes<sup>3</sup> have found an onset of a violent instability after removal of (coherent) heating power. Puri<sup>5</sup> was able to suppress instabilities in a small plasma with only 250 mW of noise power, and he demonstrated that a coherent field of the same power level had no such effect. (Presumably, in view of the observed suppression of instabilities at high coherent power levels<sup>3,5</sup>, it is possible to override and disrupt any instability that arises from collective and organized plasma motion, provided sufficient power is available. Recent work at Oak Ridge<sup>7,8</sup> shows the effectiveness of off-resonance heating in the suppression of instabilities, but the energy absorption by the plasma is so low that off-resonance heating turns out to be far less efficient than stochastic heating at frequencies around resonance.)

Plasmas of thermonuclear interest should at least be warm, dense enough to have Debye lengths small compared to the container dimensions, and as stable as possible. Single particle containment (or containment of very tenuous plasma) is often possible, but dense plasmas can be most elusive. Charge exchange and instabilities have been the principle loss mechanisms for most plasma systems. Helios quite effectively eliminates the former by the choice of lithium as the plasma source, since lithium neutrals are readily absorbed on the walls, where they effectively form an active gettering surface. At room temperature, the vapor pressure of the adsorbed background lithium is less than  $10^{-8}$  Torr, and the relatively low flux of

entering neutrals is expected to be singly ionized (and thus trapped) by the heated electron component of the plasma. Recombination neutrals are expected to be rare, since volume recombination cross sections are small, and the survival time of these (or any other) neutrals should be so short that any loss from this source is negligible.

Most, if not all, of the known instabilities should be suppressed by the magnetic field geometry and the stochastic heating field. Therefore the loss rate should be governed by almost classical diffusion up to a plasma density such that the stochastic field no longer penetrates enough to inhibit instabilities.

Three distinct features of the magnetic field geometry should be mentioned; e.g., the mirror field, the multipole field, and the boundary field. The mirror is formed by two sets of eight coils each set and run at 2100 Gauss at the center, with a 2/1 mirror ratio.

The use of a minimum-B configuration is well known to be effective in eliminating hydromagnetic and other low-frequency instabilities. The Helios quadrupole field is unusual in that it is inside the plasma system, as shown in Fig. 1. The reasons for so placing it are as follows: the multipole field drops off rather rapidly with distance from the currents that produce it, so it is most effective when close to the plasma. But if the so-called Ioffe-bars were outside the plasma chamber, ions and electrons drifting along field lines that intercept the wall would be lost. As Kerst<sup>10</sup> and other have shown, the multipole field itself may be regarded as a set of magnetic surfaces defining a region of stable confinement and another, unstable, region. The stable region surrounds the conductors producing it, so that the ions may be able to drift radially beyond the conductor, circle it, and return to the central region without being lost to the walls. The presence of the mirror field complicates the analysis of magnetic surfaces, but the same general effect should exist.

The presence of Ioffe bars within the plasma chamber is not expected to increase plasma loss on the walls (the Ioffe bars themselves) because the high currents in the Ioffe bars create a sufficiently great magnetic pressure barrier to repel incident plasma. Thus the stabilizing effect of the multipole field appears to be enhanced by the internal placement. The combined mirror and multipole field should improve the thermal mixing and help to eliminate temperature gradients arising from non-uniformities in the stochastic heating field. Puri<sup>1</sup> points this out and remarks that a non-uniform magnetic field tends to "Maxwellianize" the particle velocity distribution. He also shows that when the electric field bandwidth is large enough to span the mirror gyrofrequencies, all the particles have approximately the same heating rate. Helios is therefore expected to be a well-thermalized and well-stabilized plasma system, with almost all known instability sources eliminated by design.

The third feature of the magnetic field geometry, the boundary field, may be the most interesting. It should certainly be the subject of careful experimentation as an attempt to superpose localized small-scale perturbations on the main fields at the system boundary in order to inhibit plasma loss. The cage that bounds the plasma is made of nickel-plated iron wire, 0.63 cm in diameter, spaced 0.63 cm apart. In addition to the already discussed electrical advantages<sup>2</sup>, the radial cage boundary produces a locally

rippled magnetic field that presents, on the average, favorable curvature to the plasma, and the end boundary produces local modification of the mirror field that should reduce mirror losses by increasing the local magnetic gradient<sup>11</sup> (at least in one dimension), as shown in Fig. 2.

### Technical Details of Helios

General - A preliminary, semi-quantitative assessment of the design parameters of Helios is given as an indication of the kind of plasma that may be obtained when the system is fully operational and as a guide to points that need further experimental and theoretical attention. (It should be emphasized that the immediate attainment of the idealized plasma to be described here is neither expected nor essential to the value of Helios as a research tool. As is well known, plasmas almost never behave entirely as planned, and much of our knowledge of them arises in the attempt to understand their idiosyncrasies.)

For this development, the plasma is assumed to be operating in a steady state, free of instabilities, with the electron and ion temperatures,  $T_e$  and  $T_i$ , constant throughout the plasma. The ion and electron losses to the walls are compensated by a flux of new ions and electrons from the hot rhenium ionizers; the plasma density is assumed to be so high that the incoming ions and electrons are very quickly thermalized by collisions with their background species. At first, ions are assumed to be heated by electron-ion collisions, though modification of the calculations to include direct ion heating is easy. The total internal energy of the plasma is treated as if it were divided between the ions and the electrons, and denoted as  $U = U_i + U_e$ . (For present purposes, the assignment of energy is rather arbitrary; it is essential only that energy flows be properly evaluated.) In steady state, the time rate of change of each of the energies is zero.

Ions - The rate of change of the ion energy is given by

$$\dot{U}_i = (\dot{U}_i)_e + (\dot{U}_i)_c \quad (1)$$

where  $(\dot{U}_i)_e$  is the rate at which energy is given to the ions by the electrons and  $(\dot{U}_i)_c$  is the rate at which the ion energy changes because of ion losses from the system (containment losses). Since the total number of ions is taken to be constant, and the ion potential energy is not changed by heating, the term  $(\dot{U}_i)_e$  may be written as  $(3nk/2)\dot{T}_i$ , where  $\dot{T}_i$  is the rate at which the ion temperature would increase if the only effect were electron heating, and is given by

$$\dot{T}_i = (T_e - T_i)/\tau_{it} \quad (2)$$

where  $\tau_{it}$  is the ion thermalizing time for Coulomb collisions with electrons. A reasonably accurate expression for  $\tau_{it}$  is

$$\tau_{it} = [(2m_e m_i \epsilon_0^2 \pi^3)^{3/2} / q_e^2 q_i^2 n_i \lambda n A] [(kT_i/m_i) + (kT_e/m_e)]^{3/2}, \quad (3)$$

where  $n_i$  is the ion number density, the  $q$ 's are charges, and  $\lambda$  is the well known Debye cutoff factor. For calculations where it matters,  $\lambda n A$  will be taken as approximately 15, corresponding to a density of about  $10^{12} \text{ cm}^{-3}$  and a temperature of 10-100 eV.



The containment loss term may be written as

$$(U_i)_c = - \langle \epsilon_i \rangle N_i / \tau_{ic} \quad (4)$$

where  $\langle \epsilon_i \rangle$  is the average energy of the escaping ions and  $\tau_{ic}$  is the ion containment time.

The ions enter as  $Li^+$ , presumably, but they may be lost as  $Li^{2+}$  or  $Li^{3+}$ , thereby carrying away an energy equal to the difference in the ionization energies,  $\delta V_i$ . If ion potential energy is ignored, then, and if the escaping ions are assumed to have the same kinetic energy as the ions in the plasma, the factor  $\langle \epsilon_i \rangle$  may be written

$$\langle \epsilon_i \rangle = e\delta V_i + (3kT_i)/2. \quad (5)$$

When  $\dot{U}_i = 0$ , the ion energy balance yields the result

$$T_e = T_i (1 + \tau_{it}/\tau_{ic}) + (2e\delta V_i/3k)(\tau_{it}/\tau_{ic}). \quad (6)$$

It is thus evident that the electron temperature must exceed that of the ions, though the difference can be small if  $\tau_{it} \ll \tau_{ic}$ .

The dominant ion loss term is probably mirror leakage though the loss cone, and it is also the most difficult to calculate. Judd, MacDonald and Rosenbluth have produced a simplified calculation for the ion containment in a parabolic mirror (the lossiest of simple geometries) for a singly-charged particle. If the velocity distribution is Maxwellian, this confinement time reduces to

$$\tau_{im} = [6\sqrt{2} \pi^{3/2} e^2 m_i^{1/2} (kT_i)^{3/2} \log_{10} R] / [ne^4 \lambda nA], \quad (7)$$

where  $R$  is the mirror ratio. The ratio of the ion thermalization time, from Eq. (3), to  $\tau_{im}$  when the electron temperature is greater than that of the ions is

$$\tau_{it}/\tau_{im} = (m_i/m_e)^{1/2} (T_e/T_i)^{3/2} / 3\sqrt{2} \log_{10} R. \quad (8)$$

For singly ionized lithium in Helios, with the electron and ion temperatures equal and  $R = 2$ ,  $\tau_{it}/\tau_{im} = 89$ , a value that indicates the need for supplementary ion heating.

**Lithium Source** - The source of  $Li^+$  and of electrons is a pair of incandescent rhenium tubes, each about 0.63 cm in outside diameter and 2.5 cm long. The neutral lithium atoms enter the ionizer from the lithium reservoir at a pressure determined by the temperature of the reservoir (1000°C corresponds to about 50 Torr). The necessary flow rate is regulated by control of the reservoir temperature.

In order to supply ions at the simple mirror loss rate (calculated to be of the order of  $10^{20}$ /sec -- or about 1 mg/sec -- for density near  $10^{13}$ /cm<sup>3</sup>), the flux from the ion source must be  $n_i A v_i = 10^{20}$ /sec where  $n_i$  is the ion density in the source,  $A$  is the area of the aperture, presumably about  $4(10)^{-2}$  cm<sup>2</sup>, and  $v_i$  is the average ion velocity, approximately thermal at the

ionizer temperature, or  $\sim 2.5(10)^5$  cm/sec. Then  $n_5 = 10^{16}/\text{cm}^3$ , corresponding to an ion pressure (at the 0.2 eV ionizer temperature) of 2.6 Torr. Thus the niobium reservoir will be easily able to supply the requisite source pressure.

**Electrons** - Ions and electrons are supplied from volume ionization at the same rate. From the incandescent rhenium source, however, the ion input rate is determined by the reservoir pressure, whereas electrons are thermionically emitted from the hot rhenium at a rate governed by rhenium temperature and work function and by the space charge cloud near the rhenium surface. Q-machine experience has shown that the independent control of neutral atom influx and of ionizer temperature permits regulation of the ion and electron fluxes over a wide operating range. Electron containment and heating, rather than injection, are the main problems to be examined.

In keeping with Eq. (1), the time rate of change of the electron energy may be written,

$$\dot{U}_e = P_{me} + (\dot{U}_e)_i + (\dot{U}_e)_c + (\dot{U}_e)_r, \quad (9)$$

where  $P_{me}$  is the microwave heating power absorbed by the electrons,  $(\dot{U}_e)_i = -(\dot{U}_i)_e$  is the energy given to the electrons by the ions,  $(\dot{U}_e)_c$  is the time rate of change of electron energy attributable to imperfect containment, and  $(\dot{U}_e)_r$  is the loss rate as radiated power. For steady state,  $\dot{U}_e = 0$ , and appropriate substitutions into Eq. (9) yield

$$P_{me} = (3N_e k/2)(T_e - T_i)/\tau_{it} + \langle n_e \rangle N_e / \tau_{ec} + P_{re} + N_e \delta V_i / \tau_{ic}, \quad (10)$$

where the first term is the rate of heating of ions by electron, the second, containment loss term could be written with  $\langle n_e \rangle = (3/2)T_e$ .  $\tau_{ec}$  is the electron containment time,  $P_{re}$  is the power radiated by electrons or by electron-excited optical transitions, and the last term is the rate of energy loss via escape of  $\text{Li}^{2+}$  and  $\text{Li}^{3+}$ , where  $\delta V_i$  is here the average ionization potential energy gain of the entire ion population.

Although Helios will attempt to heat the ions as much as possible by electron collisions, the equalization of  $T_i$  and  $T_e$  usually seems to require supplementary ion heating. Either large  $\tau_{it}$  or direct heating of the ions, then, will normally reduce the first term to negligibility. The second term is difficult to evaluate and will be discussed later. The radiated power, except for optical radiation, may be shown to be quite small. The optical radiation is more complicated, but further analysis indicates that it, too, can be relatively small. The last term can be estimated crudely by the assumption that  $10^{20}$  ions/sec escape each carrying about 70 eV ionization energy -- a total of just over 1 kw, a figure expected to be a pessimistic upper limit for the initial stages of the Helios study.

The most difficult and least reliable estimate is the electron confinement time. If electron parameters are used in Eq. (7) to calculate the mirror-loss containment time, the result clearly indicates that electrons run out of the mirror throats in microseconds. But the electrically-floating ferromagnetic boundary cage should reduce mirror losses and become electrically charged so as to repel whichever particle would normally escape most rapidly. Therefore electron confinement time should be equal to ion confinement time.

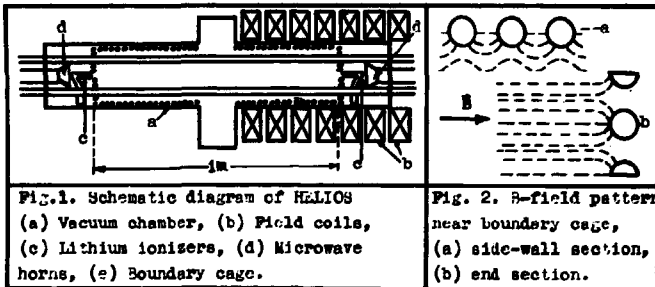
### Results

Operation to date has been with 200 watts of microwave heating of the electrons, no ion heating, no Ioffe bars, no boundary cage, and injection of lithium as neutral atoms from four points near the midplane of the system. The intent was to examine the plasma in its worst state and document the improvements as each omitted feature was added. The greatest problem arose from the lithium injection system, which was substituted because of a temporary unavailability of rhenium. A cold spot in the substitute system resulted in condensation of most of the lithium, and the high boiler temperature drove adsorbed hydrogen out of the lithium. We have observed electron-cyclotron-noise-heated hydrogen plasmas at densities of  $10^{11}/\text{cm}^3$  or greater and electron temperatures of 35-50 eV. The system is now being completed with proper rhenium injectors, and future results are expected to be much more interesting.

### References

- 1 T.K. Fowler, *Thermodynamics of Unstable Plasmas*, *Advances in Plasma Physics* (Interscience, 1968) p. 201.
- 2 K.H. Geissler, *Phys. Rev.* **171**, 179 (1968); *Plasma Physics* **10**, 127 (1968).
- 3 L.A. Ferrari and A.F. Kuckes, *Phys. Fluids* **8**, 2295 (1969).
- 4 S. Puri, *Phys. Fluids* **9**, 1043, 2043 (1966); *Phys. Letters* **26A**, 193 (1968); *Phys. Fluids* **11**, 1745 (1968); *Phys. Fluids* **12**, 472 (1969).
- 5 S. Puri, D.A. Dunn, and K.I. Thomassen, *Phys. Letters* **25A**, 694 (1967); *Phys. Fluids* **11**, 2728 (1968).
- 6 R.A. Dandl, A.C. England, W.B. Ard, H.O. Eason, M.C. Becker, and G.M. Haas, *Nucl. Fusion* **4**, 344 (1964).
- 7 R.A. Dandl, H.O. Eason, P.H. Edmonds, A.C. England, G.E. Guest, C.L. Hedrick, J.T. Hogan, J.C. Spratt, *Fourth Conference on Plasma Physics and Controlled Fusion*, Madison (1971) paper G-4.
- 8 W.B. Ard, R.A. Blanken, R.J. Colchin, J.L. Dunlap, G.E. Guest, G.R. Haste, C.L. Hedrick, W.H. Lazar, J.F. Lyon, and D.J. Sigmar, *ibid*, paper G-5.
- 9 H.S. Robertson, *Phys. Rev.* **188**, 288 (1969).
- 10 T. Okhawa and D.W. Kerst, *Phys. Rev. Letters* **7**, 41 (1961); *Nuovo Cimento* **22** 748 (1961).
- 11 L.G. Kuo, E.G. Murphy, M. Petrevic, and D.R. Sweetman, *J. Nucl. Energy* **C6**, 505 (1964).

\* This work supported by the U.S. Atomic Energy Commission.



THE STRUCTURE OF AN ALKALI-PLASMA COLUMN IN A WEAK  
MAGNETIC FIELD.

By  
P.H. Krumm, M.A. Hellberg<sup>+</sup> and G.R. Baker,  
University of Natal, Durban, South Africa.

ABSTRACT

In the single-ended Q-device of the University of Natal Plasma Group a Cs- or K- plasma is produced by surface ionization in the density range of  $10^8$  to  $10^9$  cm<sup>-3</sup>. A cylindrical plasma column is formed, by means of a collimator in front of the tungsten hot plate ( $T = 2.5 \times 10^3$  K) and diffuses along a weak axial magnetic field ( $B = 50 \dots 900$  G). The column structure is investigated by a floating potential method with electrostatic probes for various values of B. In all cases a radial electric field appears at the plasma edge together with a charge separation. Thus the plasma column consists of a quasineutral core surrounded by a charge double layer ("sheath") the position of which is independent of the magnetic field strength and is given by the collimator radius. The sheath width however increases with decreasing B.

The plasma column is surrounded by a metallic cylinder as boundary which can be earthed or biased, and is limited in the axial direction by a grounded endplate. Measurements of electron and ion fluxes to these boundaries for various values of B together with the comparison of potential, electric field and charge density profiles for both Cs and K plasmas support the view that for low magnetic field strength ( $B < 1$  kG) the structure of the plasma column is determined by the spatial distribution of the electrons to which the ions adjust themselves. This appears to be understandable in the light of the extremely different ion and electron Larmor radii, the ion Larmor radii being of the same order as the diameter of the plasma column. Models to explain the detailed structure are also discussed.

INTRODUCTION

In our group we are at present looking at the structure of an alkali plasma column in a weak axial magnetic field, i.e.  $B < 1$  kG. Such a structure could be interesting for the following reason. If one chooses the magnetic field such that the ion Larmor radius is large in comparison with the dimensions of the plasma column, e.g. the radius of the cylindrical column, and if on the other hand B is strong enough to keep the electron Larmor radius small w.r.t. the column radius, one could say that only the electrons "see" the magnetic field and are hindered in diffusing across the field lines whereas the ions are

<sup>+</sup> On leave at Princeton University.

unaffected by the magnetic field (at least within the plasma column) and diffuse unhindered across the lines. One would then expect the cross-sectional structure of the plasma column to be as in Fig. 1. One would expect to see a quasineutral circular region as defined by the hot plate (or the collimator if present). Beyond the edge of that region there should be little electron diffusion whereas the ions will escape until, under steady state conditions, a radial electric field has been established such that further ion diffusion is suppressed. This electric field crossed with the magnetic field will give rise to an azimuthal drift velocity  $V_D = E/B$ . The plasma column should thus consist of a quasineutral core surrounded by a charge double layer in which the particles drift azimuthally.

Experimental arrangement (Fig. 2).

The Cs or K plasma is produced in a single ended Q-machine by surface ionization at a tungsten plate heated by electron bombardment to a temperature of  $T = 2.5 \times 10^3$  K. To suppress the temperature gradient near the plate edge and to obtain a well defined cylindrical column, a copper collimator has been introduced, at a distance of 4 cm in front of the tilted hotplate. The structure of the column is investigated at two different positions by means of electrostatic probes using the floating potential method. Two different types of probes were used. For most of the time the probes were moved radially from the axis outwards, thus only giving half potential profiles. To check the symmetry of the plasma column, probe 1 was replaced by a U-shaped probe the tip of which pointed vertically into the plasma and which could be moved across the full width of the column. The magnetic field is produced by a solenoid to be homogeneous over a length of 32 cm. The column is terminated by an end grid which can be biased but usually is kept at ground potential. The plasma column is surrounded by a cylindrical wall as boundary which can be biased to give variable boundary conditions and to allow electron and ion currents to be measured.

The plasma parameters are:

|                        |                       |
|------------------------|-----------------------|
| collimator radius      | 5 mm                  |
| electron Larmor radius | 0.026 mm              |
| ion Larmor radius      | 12.8 mm               |
| mean electron velocity | $3 \times 10^5$ m/sec |
| mean ion velocity      | $6 \times 10^2$ m/sec |

mean free paths

mean free paths

|               |         |
|---------------|---------|
| e-i           | 11.8 cm |
| i-i           | 17.5 cm |
| e-e           | 17.5 cm |
| column length | 20 cm   |

Experimental results

1. Form of profiles

Fig. 3 shows the potential profile for the entire diameter, indicating reasonable asymmetry. The electric field distribution is shown in Fig. 4. It shows a field free region in the center, then a positive field near the edge followed by a strong negative field.

The space-charge distribution was found from the field assuming cylindrical geometry over the region of the probe, thus

$$\rho(r) = \epsilon_0 \left( \frac{dE}{dr} + \frac{1}{r} E(r) \right)$$

It is preferable to look at the charge distribution rather than the radial field profile because it is easier to define sheath position and width from the charge distribution. As a justification it can be stated that for those cases examined perfect correlation was found between sheath width and position as taken from the space charge profiles and peak position and half width of the radial electric field.

2. Sheath width and position

About 100 runs were analysed w.r.t. sheath position and width. Fig. 5 shows the result for two field strengths, i.e.  $B = 125 \text{ G}$  ( $\frac{1}{2}B = 80 \frac{1}{2}\tau$ ) and  $B = 775 \text{ G}$  ( $\frac{1}{2}B = 12.9 \frac{1}{2}\tau$ ). It can be seen that the position is almost unaffected by  $B$  whereas the width increases with  $\frac{1}{2}B$ .

A statistical analysis of all runs taken revealed that the position does not correlate with the magnetic field i.e. is roughly constant independent of the magnetic field (correlation coefficient = -0.02) whereas the sheath width does (c.c. = + 0.83)

Furthermore it was found that, when plotted against ion-Larmor-radius, the sheath widths for Cs and K profiles fell apart whereas when plotted against  $\frac{1}{2}B$  (i.e. proportional to the electron Larmor-radius) they coincide in their functional dependence upon  $\frac{1}{2}B$ . Fig. 6 shows plots of least square fits in the region below  $\frac{1}{2}B = 40 \frac{1}{2}\tau$  and of individual runs above  $\frac{1}{2}B = 40 \frac{1}{2}\tau$  for sheath position and width.

### Currents to wall and endplate

It is apparent from Fig. 5 that in the region surrounding the plasma the electric field and space charge density are not zero. Although care has to be taken in evaluating these results since the plasma equations might not hold in this region, it seems to be obvious that charged particles diffuse through the sheath into that region. Particle fluxes to the wall, the centred probe and the endplate for biases between - 10 V and + 10 V are therefore shown in Fig. 7.

Three different values for B were chosen i.e. B = 0, B = 210 G and B = 610 G, the result being that

- (i) the electron current gets suppressed with increasing B,
- (ii) the ion saturation current increases with increasing B,
- (iii) this agrees with the currents to the endplate where the dependence is reversed.

### Electron and ion profiles

The consistency of these results and the symmetry of the plasma column can be tested by taking ion-saturation current profiles ( $v_p = -25$  V) and electron-current profiles ( $v_p = 0$ ). (See Fig. 8 and 9).

There appears a sharp fall off in electron density beyond the plasma edge and an unsymmetry as far as the shape of the column is concerned. This unsymmetry might be due to the particular arrangement of hotplate and oven. The ion density decreases with decreasing B in the centre and outside the column which is in agreement with Fig. 7.

### DISCUSSION

There are several models one can construct in an attempt to explain the occurrence of the electric field near the plasma edge. The simplest model would be to treat the plasma as a conductor kept at a negative potential surrounded by an earthed wall. A surface charge would then be induced giving rise to a field falling off like  $1/r$ . This however is not in agreement with the observations. In a next attempt one could treat the electrons as fixed and give them an arbitrary but convenient distribution and let the ions adjust themselves to that distribution in the form  $n(x) = n_0 \exp(-e\phi(x)/kT)$ . A numerical solution of Poisson's equation was attempted but the results were not completely convincing. A third two-fluid model would allow for both electron and ion-diffusion, taking collisions especially in the sheath region

into account, since ions and electrons have large drift velocities. Working with a B-dependent electron diffusion coefficient and a B-independent ion diffusion coefficient it was possible to reproduce the form of the electric field. The diffusion coefficients turned out to be of the order of Bohm diffusion and are presently the subject of further tests. In addition the influence of the collimator on the sheath formation is being investigated.

#### CONCLUSION.

We observe, as expected, a strong negative electric field near the plasma edge of the right order of magnitude. The position of this field appears to be independent of B whereas its width increases with decreasing B, i.e. with increasing electron Larmor radius.

Attempts are continuing to find a suitable model reproducing the experimental observations.

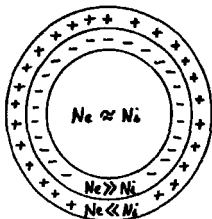
#### ACKNOWLEDGEMENTS.

The authors are indebted to Professor J.S. Martin, whose ideas started this project. They would like to thank Dr. D.T. Goodhead for valuable discussions and Mr. A.J. Hayzen for his help in the computer work and drawing of diagrams. This project was made possible by the skilful work of Mr. W.J. de Beer.

The work was supported in part by the South African Atomic Energy Board.



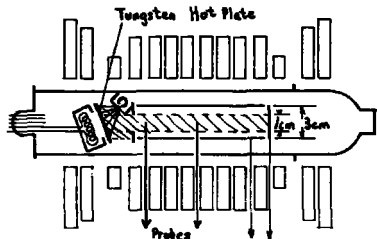
**FIG 1**



$N_e = N_i = 0$

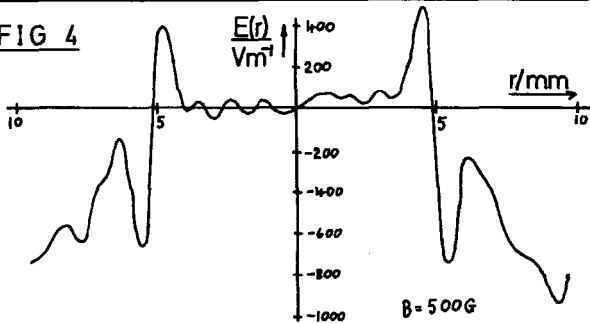
expected structure of the plasma column

**FIG 2**

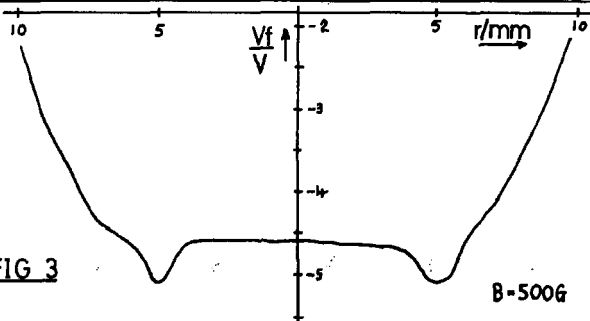


single ended q-machine

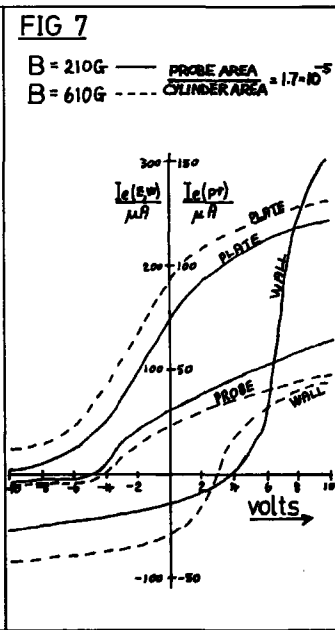
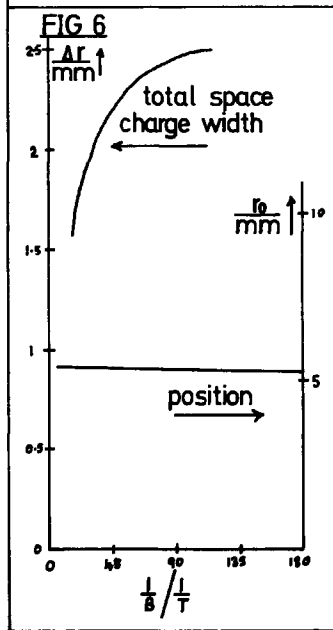
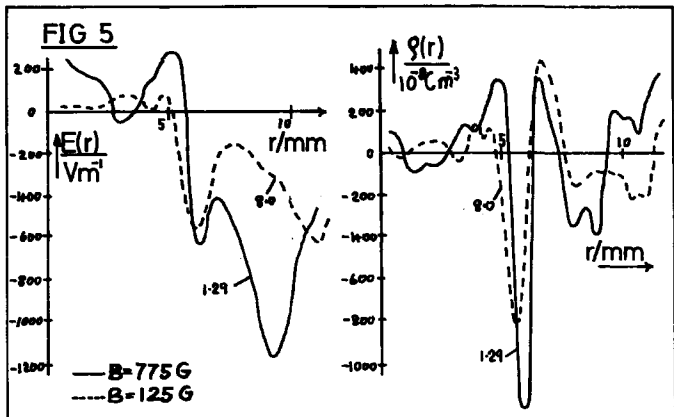
**FIG 4**

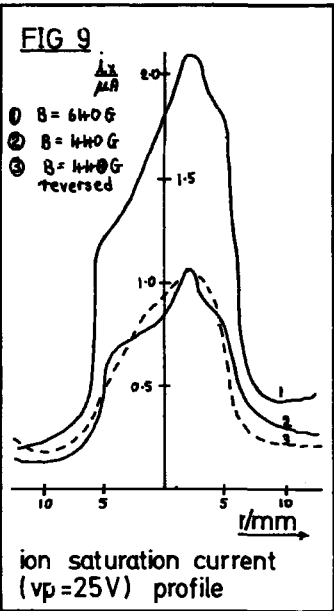
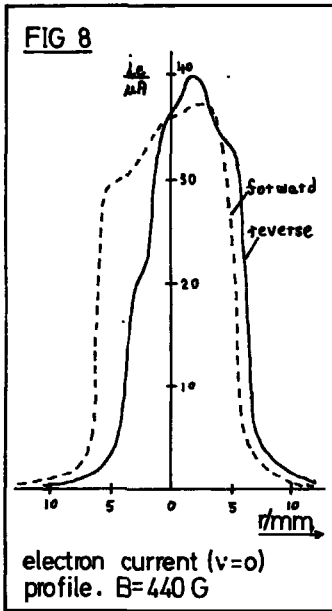


**FIG 3**



B = 500 G





## A Quiescent Plasma Sustained by High Frequency Fields\*

by

Earl R. Ault and K. R. MacKenzie

University of California, Los Angeles

### Abstract

A large volume quiescent laboratory plasma is sustained by an alternating voltage of 20 to 80 V rms (at 70 to 100 Mc) applied to an electrode consisting of 0.0025 cm tungsten wires stretched about 1 mm apart across a metal frame 30 cm in diameter. In the plasma a sheath forms around each wire with a thickness which decreases with density. In this sheath the ionizing electrons pick up energy by accelerating past the wire with the correct phase to utilize the transit time effect. (The fraction of electrons lost to the fine wire is small). Evidence for this mechanism is indicated by the fact that: 1) The electron plasma frequency is considerably higher than the applied frequency; hence the electric fields are confined to the sheath region; and 2), at normal operating voltages there is insufficient ionization to initiate the process. Some other means, such as a momentary discharge from a hot filament, a pulse of photoionization from a spark, or a large increase in pressure, is required to produce the initial plasma and set up the proper sheath conditions around each wire. This process has been used to sustain a plasma in argon at  $\approx 4 \times 10^{-4}$  Torr with a noise level,  $\langle \delta n/n \rangle \approx 2 \times 10^{-4}$ . Densities in the  $10^8$  to  $10^9$  range are produced in a volume of 30 liters. Linear ion waves and nonlinear shocks are easily produced in this device.  $T_e$  is of the order of 5 eV.

### Introduction

In this paper we describe a convenient low cost method of generating a very quiescent large volume collisionless plasma. By applying a high frequency voltage (70 to 100 Mc) to a special fine grid electrode, several liters of plasma can be generated, with a noise level  $\Delta n/n$  as low as  $2 \times 10^{-4}$ . Densities in the range from  $10^8$  to  $10^9$  are produced at background pressures around  $4 \times 10^{-4}$  Torr in argon or helium. Electron temperatures are as high as 5 eV.

### Apparatus

Small diameter tungsten wires (spaced 1 to 2 mm apart) are stretched across a stainless steel ring and spot welded at the ends to provide good contact for high frequency currents. The ring (fastened to vacuum feedthrough insulated rods approximately 1 cm in diameter) is mounted axially inside a 35 cm diameter stainless vacuum chamber 150 cm in length. The two feedthrough connectors are connected to ground through blocking capacitors (to permit dc biasing of the wires) and strap inductances which make the system resonant in the 70 to 100 Mc range. As shown in Fig. 1 the total inductance was split

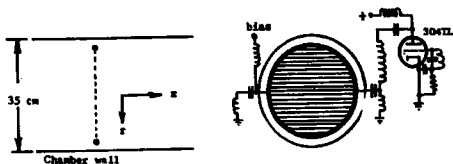


Fig. 1. Wires with diameter 0.0025 to 0.0075 cm have been successfully used.

into two parts (on opposite sides of the ring) to minimize voltage gradients on the wires (since the electrode is a sizable fraction of  $\lambda/4$  at these frequencies).

In the initial trials power was fed to the resonant system from a commercial generator with an output of 40 watts. A maximum of 60 V peak to peak could be obtained which was sufficient to produce only a weak plasma ( $\sim 10^8/\text{cc}$ ). The generator was then replaced by a tuned plate tuned grid oscillator (Fig. 1) with a high Q grid circuit to discriminate against the higher frequency anode circuit mode (which puts very little voltage on the resonator). With 1000 V dc on the anode and 250 mA anode current, over 200 V peak to peak could be applied to the wires with about 70% anode efficiency. We estimate that about 10% of this power is delivered to the plasma, the rest being lost in the rather low Q circuit, and the anode.

#### Qualitative Theory

The motivation for testing this variation of a high frequency discharge was straightforward. The ionizing energy given to an electron by a high frequency field should not be wasted by collision with an electrode! If an electrode is used, it should have a small collision cross-section such as an electrode consisting of fine wires.

Electrons which gain energy in passing such wires must utilize the transit time effect. In this process the transfer of energy is most effective if the field is confined in a small vacuum region around the wire (such as a sheath) where the plasma forms the outer conductor of the miniature "transmission line"). The high frequency energy will be largely confined in this manner if  $\omega_{pe}$  is well above the applied frequency. However, this feature implies that the energy transfer will only be efficient if the plasma is already in existence. Hence it was argued that the mechanism could sustain a plasma, but might have difficulty in the initiation stage.

But perhaps the most attractive feature in such a concept was the realization that the diameter of any sheath around the wire would decrease with density. Thus the discharge might be locally self-stabilizing, and therefore

possibly noise free.

### Results

In operation it was observed (as expected) that the discharge did not start by itself, but required initiation either by photoionizing the gas (by means of a high energy vacuum spark) or by ionization by electron bombardment from a filament. Once initiated, it was self-sustaining. Empirically, however, it was found that the discharge could be initiated by raising the pressure to around  $3 \times 10^{-3}$  Torr. After the pressure was returned to around  $4 \times 10^{-4}$  Torr, the uniformity was found to be quite reasonable. In the vicinity of the electrode the density changed by 8% over a distance of 30 cm along  $z$  and by 20% over a distance of 8 cm along  $r$  (see Fig. 1).

One of the features (obvious in retrospect, but not anticipated) is the fact that the fine wire grid collects electrons on the positive swing and assumes a negative bias with respect to the plasma. Preliminary data indicate that this bias is about half the applied high frequency to ground voltage. This negative bias ensures the existence of a sizable sheath, which is one of the required features in the postulated crude theory. It is also observed that the electron plasma frequency is above the applied frequency, implying that the high frequency energy is fairly well confined to the sheath region.

### Discussion

So far we have no direct evidence for the correctness of the proposed theory of operation, but all observations tend to support it-- especially the low noise level (which we attribute to the locally self-stabilizing feature).

Whether this plasma will be useful for studies near the electron plasma frequency remains to be seen. The applied high frequency can be expected to introduce interference effects. However, in the much lower frequency ion acoustic regime, with  $T_e$  in the range of 5 eV (where Landau damping is small) no such problems exist. Figure 2 shows a tone burst ion acoustic signal with  $\Delta n/n \sim 10^{-4}$ , which is clearly seen on a noise background only slightly higher.

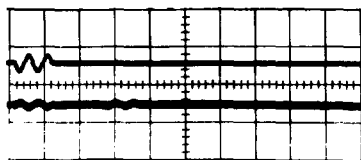


Fig. 2.

20  $\mu$ s/CM  
 ION WAVE AMPLITUDE  $\Delta n/n \sim 10^{-4}$   
 $X=10$  CM,  $T=5$  eV,  $N=10^8$

Figure 3 shows an ion acoustic shock where the initial overshoot is about 20% of the steady state level. (The trailing wave structure behind the shock is only partially understood).

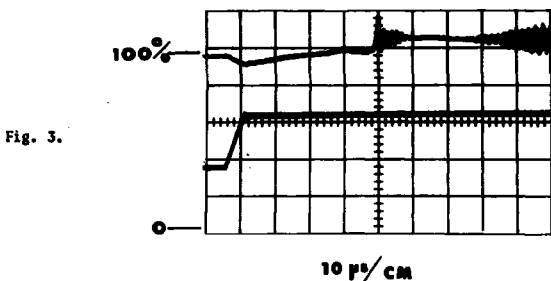


Fig. 3.

$$X = 15 \text{ CM}, T_e = 5 \text{ ev}, N_e = 10^8 \text{ CM}^{-3}$$

The signals in Figures 2 and 3 were both generated by the grid in cage method shown in Fig. 4.<sup>1</sup> This method is a variation (requiring no internal filaments) of the double plasma technique of generating an ion wave.<sup>2</sup>

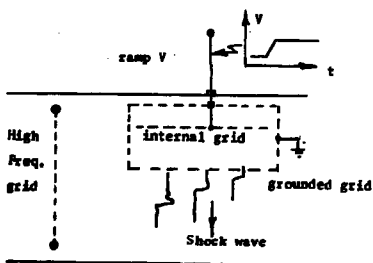


Fig. 4. High energy electrons produced by the High Freq. grid penetrate the grounded grid and produce plasma inside. Pulsing the inner grid positive by a ramp spills ions across the grid and excites a shock wave.

The frequency dependence of this discharge has not yet been investigated. We presume that even higher frequencies would be more desirable. However there is obviously a problem with electrode dimensions, since even in the configuration shown in Fig. 1 the size of the electrode is not a negligible fraction of a wavelength. Multiple electrodes would probably be the answer.

\*Supported in part by the United States Air Force Office of Scientific Research.

1. A technique developed by D. B. Cohn and R. J. Taylor, UCLA (private communication).
2. R. J. Taylor, D. R. Baker and H. Ikezi, Phys. Rev. Letters 24,206 (1970).



## Magnetic Multipole Confinement of a Magnetic Field-Free Plasma\*

by

Rudolf Limpaecher and K. R. MacKenzie

University of California, Los Angeles

### Abstract

The plasma vacuum chamber is lined with rows of permanent magnet bars 0.7 cm square, and 3.1 cm long, (spaced 0.7 cm apart), which are alternately oriented to provide a mirror cusp field with a maximum strength of about 1600 gauss at the pole faces, decreasing to the order of 5 gauss about 3 cm away from the multipole structure. The plasma is produced by electron emission of 1 to 100 mA from a short filament located in the internal field-free region. Densities up to  $10^{10}\text{cm}^{-3}$  and  $5 \times 10^{10}\text{cm}^{-3}$  are produced in helium and argon respectively at pressures less than  $10^{-4}$  Torr, with a uniformity in the field-free internal region of approximately 1%, and a noise level  $\langle \delta n/n \rangle = 3 \times 10^{-4}$ . An identical chamber, with nonmagnetized bars, showed density variations greater than 20% over the same region, and a noise level about 30 times higher. In the afterglow, the contained plasma decayed about 100 times slower than the identical control plasma.  $T_e$  could be varied from 2 to 5 eV, making this plasma a very convenient and economical device for wave studies.

### Introduction

The principle of plasma confinement by magnetic "walls" is used in all present fusion efforts. The large devices use multipole orders no higher than the octopole.<sup>1</sup> For confinement studies a multipole device (described by Sadowski<sup>2</sup>) uses a spherical arrangement of 32 electromagnets. The multipole principle, however, has apparently not been applied to the problem of containment of a large volume quiescent uniform plasma for basic studies in plasma physics. In this paper we report some characteristics of such a uniform plasma (in only the earth's magnetic field) surrounded by the multipole field of over 400 small permanent magnets. Electromagnets were considered briefly and then abandoned, since on a cost and convenience basis they cannot compete with most of the available permanent magnets at fields under 2 kg. Although too weak to effectively contain ions at fusion energies, such fields are found to effectively reflect most of the ions and electrons in ordinary laboratory plasmas, and thereby reduce the ionizing source requirements by one or two orders of magnitude. As an added benefit, the continual reflection at the boundaries yields a vast improvement in plasma uniformity in the field-free region.

Apparatus

The geometry tested is shown in Fig. 1. The magnets were 0.7 by 0.7 x 3.1 cm bars of alnico 5, spaced 0.7 cm apart and oriented alternatively north and south.

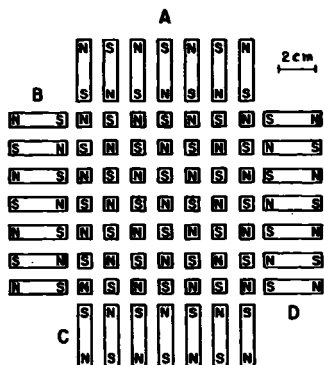


Fig. 1. Multimagnetic Mirror Plasma Device (hereafter referred to as M. P.I.). The side "walls" A,B,C,D, each consist of a 7 by 11 array of 0.7 by 3.1 cm alnico magnets. The spaces between the magnets are used for insertion of supports for filaments, grids, and probes.

The magnetic field due to such an array is shown in Fig. 2.

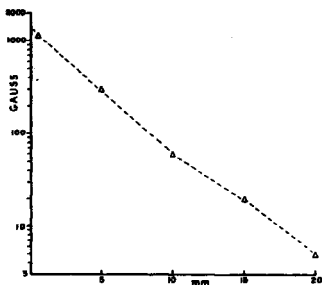


Fig. 2. The maximum magnetic field of 1100 gauss at the pole face center (normal to the pole face) drops to less than 5 gauss at a distance of 3 magnet spacings. Extension of the curve to larger distances was limited by the sensitivity of the magnetic field meter. (A maximum field of 1600 gauss, making an angle of 25 degrees to the normal, was obtained at the edge of each pole).

In such a box-like rectangular array (as shown in Fig. 1) the regular alternation of poles cannot be continuously extended to all six sides at once. Deviations occur at some of the side junctions. Since at this junction two like poles are side by side, only the effective pole geometry is changed and no extra particle loss is expected.

For comparison purposes an identical control "box" (designated as "CON.") was constructed with nonmagnetic bars. Both boxes were then enclosed in a common vacuum system. Plasma was generated by electron emission ranging from 1 to 100 mA from a single 0.025 cm diam Ta filament 9 cm long in each box,

(each filament biased at -60V). The magnetic and nonmagnetic pole faces served as anodes. Plasma density and electron temperature were measured in each box by a flat Ta probe with a total area of 25 mm<sup>2</sup>.

### Results

Figure 3 shows the central collected electron current (at 10mA emission) in argon and helium as a function of pressure. A set of curves was also obtained for nitrogen which is similar to the set shown for argon. (At 100 mA of emission and 10<sup>-3</sup> Torr of argon, a density of 2 x 10<sup>11</sup>/cc was measured).

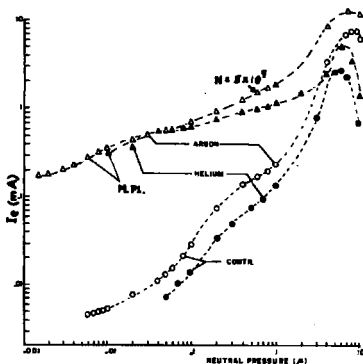


Fig. 3. Electron current collected by a 25 mm<sup>2</sup> flat tantalum probe (biased at the plasma potential) as a function of neutral density. Due to some uncertainties regarding the electron temperature, the raw data is presented. Electron current is converted to electron density at the point shown.

At high pressures, where collisions dominate the loss process, both boxes behave in similar fashion. At very low pressures however, the density and collected electron current in the magnetic box is about two orders of magnitude higher than in the control box. The fact that helium ions are as effectively contained as argon ions is of particular interest.

Figure 4 shows the uniformity in density for an argon plasma. The scale is normalized to the density at a distance of 5 magnet bar spacings. In the magnetic box the density is seen to be uniform over the magnetic field-free region to within the accuracy of the measurement ( $\sim 1\%$ ), whereas a large gradient exists in the nonmagnetic control box.

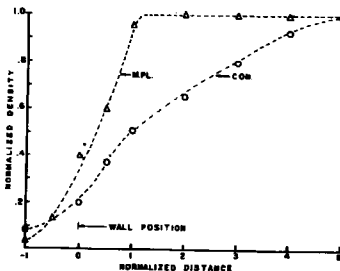
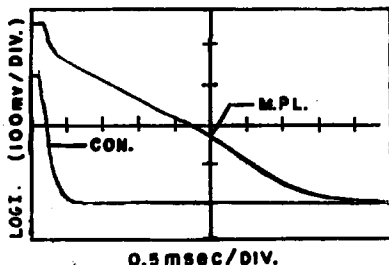


Fig. 4. Normalized plasma density in the multipole plasma device (CON.) as a function of the distance from the "wall" (or pole face position). The distance is measured in units of magnet spacing (1 unit = 0.7 cm).

Figure 5 shows the decay of the afterglow plasma when the  $-60$  V bias and the filament current are turned off simultaneously. The containment provided by the magnetic walls is very evident.



Logarithm of collected ion current as a function of time. A change of 58 mV corresponds to a change of  $\Delta N/N = (1 - e^{-1})$  in collected ion current.

Fig. 5

Figure 6 shows a linear ion acoustic wave generated by applying a 0.5V peak to peak signal at 60 kHz to a biased grid in the plasma in the magnetic box. The perturbed density  $\delta N/N$  is shown in percent where  $N = 2 \times 10^{19}/\text{cc}$  and  $T_e = 2.7$  eV. This picture shows that the noise level  $\langle \delta N/N \rangle$  is about 3 parts in  $10^4$ . A corresponding picture in the nonmagnetic box could not be obtained due to a much higher level of noise. Presumably one factor in the large reduction of noise in the magnetic box is the low ratio of primary electron to plasma electron current density near the filament.

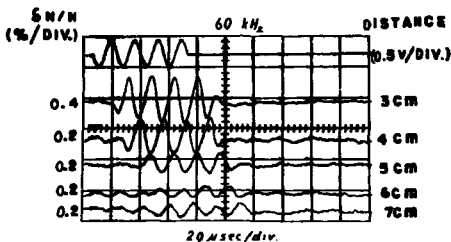


Fig. 6. Induced density perturbation in a gated linear ion acoustic wave train observed at several probe positions. The peak to peak noise ratio ahead of the wave train  $\langle \delta N/N \rangle$  is  $\sim 3 \times 10^{-4}$ .

We believe that these results herald a new era in producing quiescent laboratory plasmas. Small magnets which can produce local fields of 2 kg are inexpensive and can be arranged (we believe) in a more efficient configuration than the model tested. By investigating this geometry it can be seen that at the center of each local "square" there is a point of zero field, where any particle with exactly the right direction of entry can escape. A linear arrangement of magnets consisting of alternating rows of like magnets or long bar magnets will avoid this drawback. Losses in such a system occur only in the linear or point cusp regions. In this linear type of array the magnetic field does not fall off as rapidly, but this is deemed to be an advantage, since the reflection process sets in farther from the magnet poles. The particle orbits become more adiabatic and therefore reflection should be more effective. For the same reason it is also advantageous to use larger magnets with larger separations. Such a box, with much larger dimensions, is under construction.

We see no reason why this principle cannot be used to provide a quiescent uniform plasma with any desired dimensions. The power requirements are very small, and per unit volume they decrease with increasing volume. At the same time the percentage ionization (now  $< 1\%$ ) will rise. With small relative cost it appears that a large space simulation chamber could be filled with a quiescent uniform helium plasma with the electron temperature controllable over the range 1 to  $5 \text{ eV}^3$ , and perhaps higher.

\*Supported in part by the United States Office of Scientific Research, AFOSR Grant No. 1447D.

1. Tihoro Ohkawa and Masaji Yoshikawa, *Phys. Fluids* **11**, 2039 (1968).
2. M. Sadowski, *Rev. Sci. Instr.* **40**, 1545 (1969).
3. K. R. MacKenzie, R. J. Taylor, D. Cohn, E. Ault and H. Ikezi, *Appl. Phys. Letters* **18**, 529 (1971).

Production and Application of a Uranium Plasma in the Q-Device

by

M. Hashmi and A.J. van der Kouven van Oordt <sup>+</sup>)

Max-Planck-Institut für Plasmaphysik, Garching (Germany)

EURATOM-Association

Abstract

Uranium plasma has been produced in the single-ended operation of the Q-device BARBARA. The density and flux measurements are performed by different Langmuir probes. Our preliminary results are presented and discussed. The various application of such a uranium plasma are also mentioned.

Introduction

A Q-device plasma can be utilized as an ion source by using a grid. In this respect, the production of a high density uranium plasma in a Q-device is of special interest as it can be employed for the separation or enrichment of isotopes by means of a mass spectrometer.

To determine the probability of contact ionisation

$\gamma$  ( $= \frac{I_0}{I_0 + I_a}$ ) of uranium, the Langmuir function

$$I_a = \frac{g_+ + \sum_i g_i^e \exp\left(-\frac{E_i^e}{kT}\right)}{g_0 + \sum_i g_i^e \exp\left(-\frac{E_i^e}{kT}\right)} \exp\left\{-e \frac{(I - \phi_i)}{kT}\right\} \quad (1)$$

should be known.  $\phi_i^{(+)}$  and T are the work function and temperature of the plate respectively. I is the ionisation potential of the

<sup>+</sup>) EURATOM

<sup>++</sup>) The effective work function for contact ionisation  $\phi_i^+$  is different from the work function for electron emission  $\phi_e$ .

atoms.  $g_0$  and  $g_+$  are the statistical weight factors of the ionic and atomic ground levels respectively.  $g_+^{\ell}$  and  $g_0^{\ell}$  are the statistical weight factors of the ionic and atomic  $\ell$ -th excited level.  $E_+^{\ell}$  and  $E_0^{\ell}$  are the energies of excitation to the  $\ell$ -th quantum state of the ion and atom, respectively.  $e$  is the electronic charge and  $k$  the Boltzmann constant.

For alkaline and alkaline earth metals, the terms  $\sum g_+^{\ell} \exp(-\frac{E_+^{\ell}}{kT})$  and  $\sum g_0^{\ell} \exp(-\frac{E_0^{\ell}}{kT})$  in equation (1) can be neglected because  $kT < E_+^{\ell}$  and  $E_0^{\ell}$ . For uranium, on the other hand,  $kT \gg E_+^{\ell}$  and  $E_0^{\ell}$ . But it is still not possible to estimate  $\gamma$  theoretically from equation (1), as the configurations of uranium atom and ion are not known and therefore the ionisation potential of uranium <sup>+) cannot be determined.</sup>

The only reasonable way to determine  $\gamma$  is to perform an experiment.

The present paper describes such an experiment in the single ended operation of a Q-device. The results and application of such a plasma are discussed.

### Experiments

The uranium plasma was produced in the single ended operation of the Q-device BARBARA /2/. The Re endplate of 3.2 cm diameter was heated to 2500°K. The magnetic field was between 2 and 3 kG.

As the vapour pressure of metallic uranium is quite low, a high temperature oven (~2000°K) is necessary in order to obtain the required intensity of the atomic beam. The first oven

---

+) For the ionisation potential of uranium, the values varying between 4 V and 7 V are available in the literature /1/.

was made of tantalum and could be heated up to  $\sim 2000^{\circ}\text{K}$  by a direct passage of current (A.C. as well as D.C.). This kind of oven created the main difficulty. At high temperatures, a Ta-U alloy was formed first depressing the vapour pressure of uranium and finally the oven was broken. Another attempt was made with a BeO crucible.

The radial density distribution of plasma was measured by a single Langmuir probe. The total number of ions produced per sec,  $i_{+}$  was determined from the ion saturation part of the characteristic of a "spoon" probe which was larger than the plasma diameter. Under certain conditions, the total number of atoms per sec  $i_{0}$  "illuminating" the hot end plate can be evaluated from the knowledge of the oven temperature and vapour pressure of uranium.  $i_{+}$  and  $i_{0}$  turned out to be approximately equal indicating that almost all the uranium atoms were ionised at the hot end plate.

Fig. 1 shows a radial density profile of the plasma. Fig. 2 is the ion part of the characteristic of a single Langmuir probe.

Due to the fact that the atomic flux was limited by the oven temperature, the maximum ion current obtained by a "spoon" probe up to now was about 1 mA which will correspond to a plasma density of about  $10^{11}\text{ cm}^{-3}$ . In a cesium plasma, however, we have already been able to achieve quite easily the density up to  $10^{13}\text{ cm}^{-3}$ . Moreover, by using the value of volume recombination as given by D'ANGELO /3/ and HINNOV and HIRSCHBERG /4/, the equilibrium theory yields a maximum plasma density of about  $10^{14}\text{ cm}^{-3}$  /5/. This seems to be the limiting factor because the curves by LANGMUIR and TAYLOR /6/ show that the surface coating of the end plate at  $2500^{\circ}\text{K}$  is negligible up to the atomic densities of  $10^{15}\text{ cm}^{-3}$  which would correspond at an oven temperature of about  $2400^{\circ}\text{K}$ . Our aim is to achieve the maximum density of about  $10^{14}\text{ cm}^{-3}$  of a uranium plasma in the Q-device.



### Application

As mentioned above, uranium plasma may be used as an ion source for the separation of isotopes in commercial quantities if large amount of ions can be extracted from the plasma by means of a negatively biased grid. Assuming a density of  $10^{14} \text{ cm}^{-3}$  and a hot end plate of  $10 \text{ cm}^2$ , the total amount of about 250 kg uranium per year could be separated yielding 1.83 kg of  $\text{U}^{235}$  isotope per year. The radial mass spectrometer described by SMITH et al. /7/ seems to be able to separate this amount quite economically. Enriched uranium of any desired percentage could be produced by re-mixing the separated isotopes, without influencing the economy of this method. According to our estimate, the price of enriched uranium produced by this method seems to remain noticeably below the price fixed by the USAEC.

This work was performed under the terms of agreement between the Max-Planck-Institute for Plasma Physics, Munich-Garching, and EURATOM to conduct joint research in the field of plasma physics.

### References

- /1/ Smith, D.H., and Hertel, G.R., Jour. Chem. Phys., 51, 3105 (1969)
- /2/ Hashmi, M., van der Houven van Oordt, A.J., and Wegrowe, J.-G., Nucl. Fus. 10, 163 (1970)
- /3/ D'Angelo, N., Phys. Rev. 121, 505 (1961)
- /4/ Hinnov, E., and Hirschberg, J.G., Phys. Rev. 125, 795 (1962)
- /5/ von Goeler, S., Phys. Fluids 7, 463 (1964)
- /6/ Langmuir, I., and Taylor, J.B., Phys. Rev. 44, 423 (1933)
- /7/ Smith, L.P., Perkins, W.E., and Forrester, A.T., Phys. Rev. 72, 989 (1947)

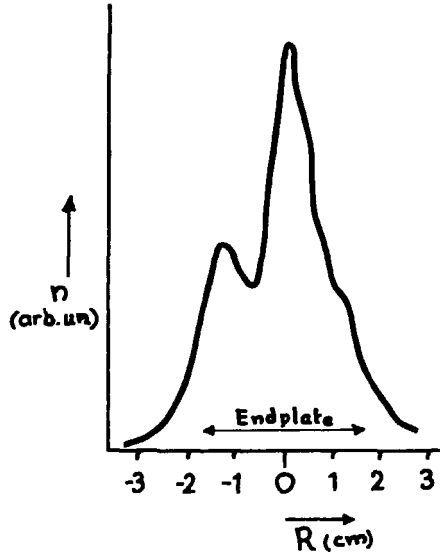


Figure 1 Radial density profile

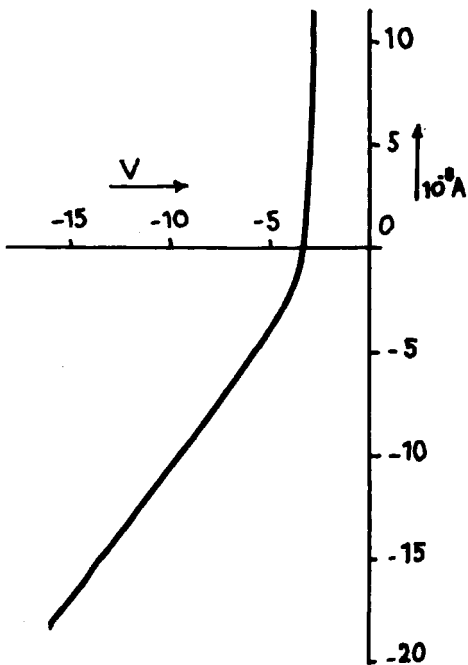


Figure 2 Ion part of the characteristic of a single Langmuir probe

EXPERIMENTAL STUDY OF THE FIRST ORDER ION DISTRIBUTION  
FUNCTION RELATED TO IONIC WAVE IN A Q MACHINE

P. MILLS

Laboratoire de Physique des Milieux Ionisés  
Ecole Polytechnique, Paris - France  
(Equipe de Recherche associée au C.N.R.S.)

ABSTRACT

In this paper we propose an experimental study of oscillations of the first order ion distribution function in an ionic wave and we have tried to point out if there are features related to collective effects or not.

I. INTRODUCTION

Numerous theoretical and experimental studies show that ion acoustic waves can be damped even in absence of collisions [1,2,...] but the perturbations in phase space oscillate indefinitely without damping. Observations of echoes is an indirect confirmation of this. [3]. In this paper we propose an experimental study of oscillations of the first order ion distribution function  $f_1(v,x,t)$  related to ionic wave and to compare the result with numerical calculations based on a theory elaborated by D. GRESILLON [4]. Our study which is similar to that of IKEZI and TAYLOR [5] differs by the fact that we study ballistic behaviour and Landau modes at the same time. In the experiments of IKEZI and TAYLOR the ratio of electrons temperature to ions temperature ( $\frac{T_e}{T_i} = 0,1$ ) prevents the propagation of Landau modes far from the grid. The observed phenomena are not plasma phenomena : the propagation of a perturbation in a collisionless neutral gaz would have the same characteristics.

II. EXPERIMENTAL SET-UP

The theory for which we will developped the principal features in party III is adapted to an experimental situation we will briefly described. A single ended Q machine has been used. Only one plate of tantalum is heated, the cold plate is the grid of an electrostatic analyzer and is maintained at a negative potential. A plasma which is confined by a static magnetic field flows from the hot plate to the cold plate. The density ( $10^7 < n < 10^9$  p/cm<sup>3</sup>) and the mean speed parallel to  $B_0$  are functions of neutral flux and hot plate temperature. A grid immersed in the plasma between hot and cold plate is biased to a constant potential plus a sinusoidal voltage of frequency  $m$ . Let  $f_{01}$ ,  $f_{02}$  be stationary ionic distri-

bution functions and  $V_{p1}$  and  $V_{p2}$  the plasma potentials upstream and downstream from the grid respectively [figure 1]. In figure 2 we have shown the distribution function  $f_{a2}$ . We see that the distribution of the ions accelerated by electronic sheath of the hot plate is that of an ion beam having a mean velocity which corresponds to the energy acquired in the sheath potential plus the ion thermal energy. We have determined the origine of these energies by two methods, first by analyzing the perpendicular energies of the ions of which the distribution is a maxwellian centred at origine ; secondly by injecting a beam of neutral caesium atoms in to the plasma perpendicularly downstream from the exciter. The analysis of ions created in this neutral beam by charge exchange permits the determination of the origine of these energies.[6]. We have experimentally determined the distribution functions  $f_{a1}$  and  $f_{a2}$  as function of the potential applied to the excitation grid, We have seen that the function  $f_{a2}$  is very close to  $f_{a1}$  when the potential  $V_{g1}$  applied to the grid is close to the plasma potential  $V_{p1}$ . In this case we take the perturbation to be linear. In an other case, for a potential  $V_{g1}$  which is very negative with respect to  $V_{p1}$  the ions with small energies are absorbed by the grid sheath. We can already expect for this range of polarisation the appearance of low energy bursts.

### III. THEORY

In everythings which follows we take the ions to have a speed parallel to  $B_0$  to be positive. After a Fourier transform in time the distribution functions  $f_0$  and  $f_1$  satisfy the one dimensionnal Vlasov equation. Let  $E_0$  and  $E_1$  be respectively the static field in the sheath of the exciter grid and the small alternative field. When polarisation is close to the plasma potential we can neglect the term  $\frac{eE_0}{m_i} \frac{\partial f_1}{\partial x}$  in the Vlasov equation. The general solution of the Vlasov equation is yet,

$$f_1(v, x, \omega) = - \frac{e}{m_i} \exp \left[ \frac{i\omega x}{v} \right] \int_0^x E_1(\xi, \omega) \frac{1}{v} \frac{\partial f_0}{\partial v} \exp \left( - \frac{i\omega \xi}{v} \right) d\xi \quad (1)$$

The field  $E_1$  can be separated into a field at the source ( $x = 0$ ) and a field which is zero in the range  $x = 0, -\infty$  and which is limited and damped in the range  $x = 0, +\infty$ ; this hypothesis does not take in account the capacitive field upstream and downstream of the grid. Solution (1) can be taken in the form :

$$f_1(v, x, \omega) = - \frac{e}{m_i} \exp \left( \frac{i\omega x}{v} \right) \left[ g(v) + \int_0^x E_1 \frac{1}{v} \frac{\partial f_0}{\partial v} \exp \left( \frac{-i\omega \xi}{v} \right) d\xi \right] \quad (2)$$

where the origine is the downstream abscissa where the sheath ends. If  $f_1(v, x, \omega)$  is zero for  $x < 0$  the first term in the bracket represents the free streaming of the perturbation at the source. The second term (2), we call  $M(v, x, \omega)$  represents at once the ballistic perturbation created by  $E_1$  and the Landau modes.

Now, let  $\phi_1(x) = \phi_1 \sum_{j=0}^{\infty} C_j \exp(ik_j x)$  be the potential from which  $E_1$  is derived, where the  $C_j$ 's are the excitation coefficients of the  $j^{\text{th}}$  pole and where the  $k_j$ 's satisfy the dispersion relation  $\epsilon(k_j) = 0$ .

In order to calculate  $f_1$ , we only look at the least damped pole  $k_0$ :

$$f_1(v, x, \omega) = \exp \frac{i\omega x}{v} g(v) - \underbrace{\frac{e\phi_1}{kT} \frac{1}{v} \frac{\lambda f_{02}}{\lambda v} k_0 C_0 \frac{\exp \left( \frac{i\omega x}{v} \right) - \exp(ik_0 x)}{k_0 - \frac{\omega}{v}}}_{M(v, x, \omega)}$$

The numerical calculation of  $M$ , where  $K_0$  is experimentally determined shows [4] that no strong singularity exists at the phase velocity [7]. As a matter of fact, a singularity can exist only if the imaginary part of  $K_0$  is very small. But  $\frac{1}{k_0}$  is proportionnel to  $\frac{1}{\left( \frac{\lambda f_{02}}{\lambda v} \right)^2}$  [8], yet a singularity exist only for particle velocities in the tail of the distribution and does not affect a great number of particles. The effect at the phase speed  $v_0$  is clearer if we look at the modulus of  $f_1$ ; for small  $\beta$  ( $\beta = \frac{\omega x}{v}$ ) there is no resonance at  $v_0$ . The resonance becomes very sharp and occurs at  $v_0$  only for very large  $\beta$ .

#### IV. EXPERIMENTAL RESULTS

We have remarked in part III we need to know  $E_1$  in order to calculate  $M(v, x, \omega)$ . The experimental determination of  $E_1$  and especially its variations along the  $x$  axis is done from the interferometer output of the wave response versus distance from the exciter grid. [figure]

In the experiments  $\frac{k_i}{\omega} = 0,04$  and the mean velocity of ions is  $V_0 \approx 2 a_i$ ,  $a_i = \sqrt{\frac{2kT}{m_i}} = 512 \text{ mkr s}^{-1}$ ,  $\beta = \frac{\omega x}{v} = 20 \pi$ .

The measurements of  $f_1(v, x, t)$  is performed with an electrostatic analyzer which have a good energy resolution and which is at the opposite of the hot plate. The energy analysis is performed by the collector, the grid of the analyzer being negatively biased. The collector current is :

$$I_c = \frac{e^2 s}{m_i} \int_{v_c}^{\infty} (V_c - V_p) F(E) dE \quad E = \frac{1}{2} m v^2$$

After linearisation the collected current is  $I = I_0 + I_1$ . A synchronous detection [9, 5, 4] gives the mean value of the product  $c(\theta)$  of which is variable. A synoptic view of the experimental arrangement is seen in Figure 7. In figure 7 we have presented the experimental results for  $f_1$  and its modulus. We see that the curves are very close to the calculated values of  $M(v, x, t)$  which represents the Landau modes and the ballistic modes created by the self consistent electric field  $E_1$  in the ionic wave. We see also that there is a resonance like behaviour of the modulus of  $(f_1)$ , unfortunately this pseudo-resonance can be created by the term  $\frac{\lambda f_D}{\lambda v}$ .

In another experiment we have measured the contribution of the fast ions in an ion wave. In figure 8 and 9 we have reproduced the interferometer output signal versus the distance from the exciter grid when the input signal is the current collected by the analyzer for a variable cut-off voltage  $V_c$ . Let

$$N_1(x) = \int_0^{\infty} f_1(v, x) dv \quad \text{and} \quad N^2(x) = \int_{V_c}^{\infty} f_1(v, x) dv$$

The measure of  $N_1(x)$  gives the wave number  $k_0$  and the Landau damping rate, in this case all the particles are collected. If we only collect the particles having an energy greater than  $eV_c$  the wave is drastically less damped [Fig 8]. For a cut off voltage  $V_c$  corresponding to a high energy of ions a theoretical study predicts that the wave can grow in space. We can see this result on figure 9 although the signal is yet very small with regard to the noise.

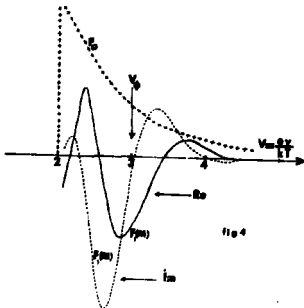
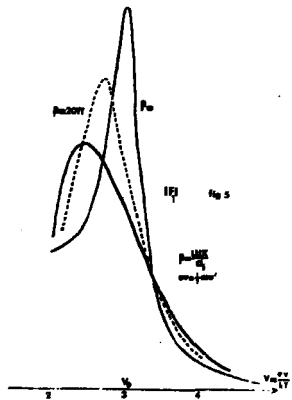
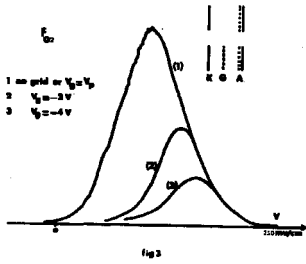
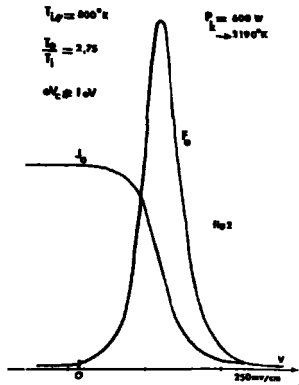
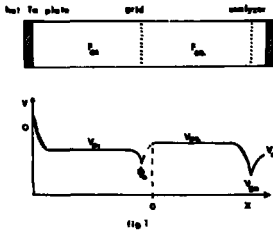
#### V. CONCLUSION

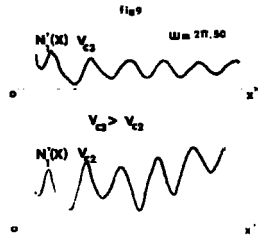
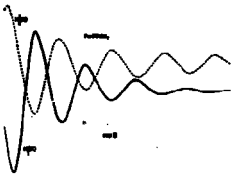
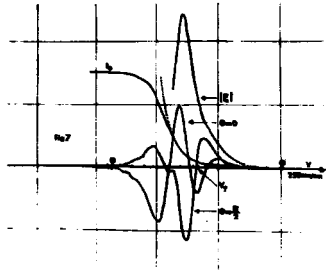
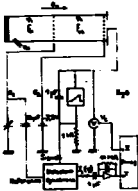
In conclusion experimental measurements are in quite good agreement with the theoretical predictions. Nevertheless the agreement between the measurements and the calculated term  $M(v, x, t)$  is not a sufficient proof of the existence of collective effects. Indeed we have not calculated the term  $g(v)$  for the sheath structure around the exciter grid is very complicated in a Q machine, and we cannot claim that it is very different from  $M(v, x, t)$ .

- REFERENCES -

- [1] A.Y WONG and al. Phys. Rev., 133, A 436, (1964)
- [2] L.LANDBAU. J. Phys. (USSR), 10, 45, (1946)
- [3] H. IKEZI and al., Phys. Lett., 20, 140, (1968)
- [4] D. GRESILLON, thèse d'Etat, Paris, June 1970.
- [5] H. IKEZI and al. Phys. Lett., 22, 923, (1969)
- [6] S.A. ANDERSEN and al. Phys. Lett. 31, 395 (1970)
- [7] D. GRESILLON and al. B. Ame. Phys. Soc, 1456, (1970)
- [8] D. GRESILLON and al. Rep. P.M.I. 449, Paris, (1970)
- [9] D. GRESILLON and al. Rep. P.M.I. 455, Paris, (1970)







EXACT CALCULATION OF THE PERTURBED DISTRIBUTION  
FUNCTIONS ASSOCIATED WITH ELECTROSTATIC WAVES

J.M. BUZZI

Laboratoire de Physique des Milieux Ionisés  
Ecole Polytechnique, Paris - France

ABSTRACT

We consider, for forced oscillations, the complete calculation of the perturbed distribution function  $F_1(x, v, t)$  associated with electrostatic waves, using the classical linear kinetic theory. Analytical expressions give the general properties of  $F_1(x, v, t)$ . Numerical results for maxwellian plasmas are presented for ion and electron plasma waves excited by a dipole.

I - INTRODUCTION.

Measurements of perturbed distribution functions associated with electrostatic waves have been reported recently in the literature <sup>1,2</sup>. However, as far as we know<sup>3</sup>, no exact calculation of the linear perturbed distribution function corresponding to any experimental conditions (forced oscillations) has been published. We present here analytical and numerical results obtained for  $F_1(x, v, t)$  in maxwellian plasmas for excitations by plane transparent grids.

II - THEORY.

In order to clarify the presentation we describe in detail the theory only in the case of electron waves. Ion waves show no particular difficulty.

Let us consider the linearized unidimensionnal Vlasov's equation without magnetic field for a homogeneous and stable plasma of electrons :

$$(1) \quad \frac{\partial F_1}{\partial t} + v \frac{\partial F_1}{\partial x} = - \frac{q_e}{m_e} E(x, t) \frac{dF_0}{dv}$$

$F_1(x, v, t)$  is the perturbed distribution,  $F_0(v)$  is the equilibrium distribution ;  $q_e$  and  $m_e$  are respectively the charge and mass of the electron.  $E(x, t)$  is the electric field which satisfies Poisson's equation:

$$(2) \quad \frac{\partial E}{\partial x} = \frac{q_e}{\epsilon_0} \int_{-\infty}^{+\infty} F_1(x, v, t) dv + \rho_{ex} / \epsilon_0$$

where  $\rho_{ex}(x, t)$  is a system of external charges which represents the excitation. Moreover we assume that that  $\rho_{ex}(x, t) = \rho(x) e^{-i\omega_0 t}$  where  $\omega_0$  is real.

We define the Fourier-Laplace transform by :

$$g(k, \omega) = \int_0^{\infty} e^{i\omega t} \left\{ \int_{-\infty}^{+\infty} g(x, t) e^{-ikx} dx \right\} dt$$

with  $\text{Im}(\omega) > 0$ .

For the forced oscillations regime, the transform of  $F_1$  is:

$$(3) \quad F_1(k, v, \omega) = \frac{q_e}{m_e} \frac{dF_0}{dv} \frac{\bar{E}(k, \omega)}{(\omega - \omega_0)(\omega - kv)}$$

where :  $\bar{E}(k, \omega) = \rho(L) / ik \epsilon_0 \epsilon(\omega, k)$

$\epsilon(\omega, k)$  being the usual longitudinal dielectric constant. Inversion of the Laplace transform (3) for  $t \rightarrow +\infty$  gives :

$$F_1(k, v, t) = \frac{q_e}{m_e} \frac{1}{v} \frac{dF_0}{dv} \bar{E}(k, \omega_0) \beta(k, \omega_0, v) e^{-i\omega_0 t}$$

where  $\beta(k, \omega_0, v)$  is the Schwartz distribution :

$$\beta(k, \omega_0, v) = P \frac{i}{k - \omega_0/v} - \pi \text{sign}(v) \delta(k - \omega_0/v)$$

Therefore,  $F_1(x, v, t) = F_1(x, v) e^{-i\omega_0 t}$

$$(4) \quad F_1(x, v) = \frac{q_e}{m_e} \frac{1}{v} \frac{dF_0}{dv} \frac{1}{2\pi} \int_{-\infty}^{+\infty} \bar{E}(k, \omega_0) \beta(k, \omega_0, v) e^{ikx} dk$$

#### A. The different contributions to the perturbed distribution function.

We assume that  $\rho(k)$  is an entire function of  $k$ . This restrictive assumption allows us, however, to consider excitation by dipole, monopole and multigrids. After elementary transformations Eq. 4 becomes :

$$(5) \quad F_1(v, x) = -i \frac{q_e}{\omega_0 \epsilon_0 m_e} \frac{dF_0/dv}{\omega_0 \epsilon_0 m_e} \{ A(x, \omega_0) + B(x, v, \omega_0) + C(x, v, \omega_0) + D(x, v, \omega_0) \}$$

The first contribution corresponds to the capacitive electric field:

$$(6) \quad A(x, \omega_0) = \text{sign}(x) \rho(k=0) / 2(1 - \omega^2 / \omega_{pe}^2)$$

The contribution  $B(x, v, \omega_0)$  represents the free-streaming of the perturbation induced by the local excitation:

$$(7) \quad E(v, x, \omega_0) = -\rho(k = \omega_0/v) e^{i\omega_0 x/v} Y(vx)$$

where  $Y$  is the Heavieside step function.

The contribution  $C(x, v, \omega_0)$  corresponds to the collective effects :

$$(8) \quad C(x, v, \omega_0) = -Y(vx) \rho(k = \omega_0/v) e^{i\omega_0 x/v} Q(\omega_0, k = \omega_0/v) / \epsilon(\omega_0, k = \omega_0/v)$$

with  $Q(\omega, k) = 1 - \epsilon(\omega, k)$

Unlike the previous contributions,  $D(x, v, \omega_0)$  is damped in space as macroscopic quantities such as the electric field :

$$(9) \quad D(x, v, \omega_0) = \frac{i}{2\pi} \int_{-\infty}^{+\infty} \psi(v, k, \omega_0) e^{ikx} dk$$

where  $\psi(v, k, \omega_0)$  is an analytical function of  $k$  for  $k < 0$  and  $k > 0$  (but not for  $-\infty < k < +\infty$ )

$$\psi(v, k, \omega_0) = \frac{\rho(k)/\epsilon(\omega_0, k) - \rho(0)/(1 - \omega^2/\omega_0^2)}{k} - \frac{\rho(k)/\epsilon(\omega_0, k) - \rho(\omega_0/v)/\epsilon(\omega_0, \omega_0/v)}{k - \omega_0/v}$$

It is important to note that at large distances, the undamped contribution  $C(x, v, \omega_0)$  can represent the most spectacular collective effect, i.e. the appearance of resonant particles at the phase velocity  $v_\varphi$ . As a matter of fact,  $1/\epsilon$  can have a peak near  $v_\varphi$  when the damping is weak. Moreover, we shall show in the next section that resonant particles appear only when the electric field is damped. Therefore,  $F_1(v, x)$  for large distances cannot be reduced in the general case to a purely free-streaming effect.

#### B. Expansion of $F_1(x, v)$ in plasma wave functions.

The explicit calculation of  $F_1(x, v)$  (Eq.5) can be carried out according to two methods. The first one is similar to that used by Gould<sup>4</sup> for the calculation of the potential. It consists in the numerical integration of Eq.9. This method gives satisfactory results provided the damping is not too weak, because, in the opposite case, the integrand of (9) is a very strongly peaked function of  $k$  which makes any numerical integration difficult.

The second method is similar to that used by H. Derfler and T.C. Simonen<sup>5</sup> in the calculation of the electric field. Then  $F_1(x, v)$  is represented by the sum of plasma wave functions, each of them corresponding to a root of the dispersion relation. This method leads to analytical results which allow us to discuss the general features of  $F_1(x, v)$  particularly in the balance between damped and undamped contributions.

The disadvantage of the second method is that for some distances and excitation frequencies a considerable number of plasma wave functions must be taken into account. However, in our numerical calculation (sec.III and IV), we avoid the difficulties of both methods by calculating the plasma wave function of the

first Landau pole only and by evaluating the contribution of the higher order poles by a Fourier transform according to Gould's method.

We consider here a dipole excitation which is the most interesting from the theoretical point of view. Calculations for monopole and multi-grids excitation system have been made which yield the same general results.

For dipole excitation we obtain :

$$(10) \quad F_1(v>0, x>0) = -\frac{q_e V_0}{m_e} \frac{1}{v} \frac{dF_0}{dv} \left[ e^{i\omega_0 x/v} + \sum_n \varphi_n(v, x) \right], \quad \omega_0 > 0$$

$V_0$  is the applied voltage between the two grids. The indices  $n$  correspond to the roots  $k_n$  of the dispersion relation :

$$(11) \quad \epsilon^+(\omega_0, k) = 0$$

In Eq.10 the term proportionnal to  $e^{i\omega_0 x/v}$  corresponds to the free streaming of the perturbation induced by the grids (term  $B(x, v, \omega_0)$ , Eq.5).  $\varphi_n(v, x)$  represent the collective effects since for  $\epsilon(\omega_0, k) = 1$  we have no dispersion relation.  $\varphi_n$  can be written :

$$\varphi_n(x, v) = D_n(v) [ e^{ik_n x} - e^{i\omega_0 x/v} ] + R_n(v, x)$$

where  $R_n(v, x)$ , given in appendix A, is damped in space and :

$$D_n(v) = \frac{v}{v - \omega_0/k_n} \left[ k \frac{\partial \epsilon^+(\omega_0, k)}{\partial k} \right]_{k=k_n}^{-1}$$

Equation (12) shows that collective effect gives a damped (corresponding to  $D(x, v, \omega_0)$ , Eq.9) and an undamped contribution (corresponding to  $C(x, v, \omega_0)$ , Eq. 8) which is proportionnal to  $D_n(v) \exp(i\omega_0 x/v)$ . At large distances, free-streaming and undamped collective contribution gives :

$$(13) \quad F_1(x \rightarrow +\infty, v) = -\frac{q_e V_0}{m_e} \frac{1}{v} \frac{dF_0}{dv} e^{i\omega_0 x/v} \left[ 1 - \sum_n D_n(v) \right]$$

$$\text{or} \quad F_1(x \rightarrow +\infty, v) = -\frac{q_e V_0}{m_e} \frac{1}{v} \frac{dF_0}{dv} e^{i\omega_0 x/v} / \epsilon^+(\omega_0, k = \omega_0/v)$$

Now it is interesting to point out how resonant particles appear. They have a velocity corresponding to the phase velocity  $v\varphi = \omega_0 / \text{Re}(k_1)$  of the first Landau pole  $k_1$  and can be observed only if  $\text{Im}(k_1) / \text{Re}(k_1) \ll 1$ .

In this case, for distances where the electric field is not strongly damped and not too near of the grids (few Debye

lengths), the contribution  $\psi_1(x, v, \psi)$  dominates the others contributions and  $R_1(v, \psi)$ . Therefore :

$$(13) \quad F_1(x > 0, v, \psi) \sim - \frac{q_e V_0}{n_e} \frac{1}{v_\psi} \left( \frac{dF_0}{dv} \right)_{v_\psi} \frac{v_\psi e^{i\omega_0 x/v_\psi}}{(v_\psi - \omega_0/k_1)} [e^{-\text{Im}(k_1)x} - 1]$$

Formula (13) shows that the modulus of  $F_1(x > 0, v, \psi)$  increases with distance, i.e. resonant particles at phase velocity appear only when the wave is damped. The physical meaning of this result is very simple. As a matter of fact, the resonant particles are produced by the energy exchange between electric field and particles. Hence it is only when this phenomena is ended, i.e. after the wave damping, that the perturbed distribution can have a resonant feature.

### III. NUMERICAL CALCULATION FOR ELECTRON WAVES.

In this section we consider the case of electron waves excited by a dipole at frequencies  $\omega_0 > \omega_{pe}$  in a Maxwellian plasma. The calculations give the reduced distribution  $f_1(x, v, t)$  :

$$F_1(x, v, t) = \left( \frac{q_e V_0}{k T_e} \right) \frac{n_0}{a_e} f_1(x, v, t) ; a_e^2 = 2kT_e/m_e$$

In Fig. 1 we have represented  $|f_1|$  for distances where the electric field is negligible. Three regimes can be distinguished :

**Regime A** : for  $\omega_{pe} < \omega_0 \lesssim 1.2\omega_{pe}$  ( $0 < \text{Im}(k_1)/\text{Re}(k_1) \lesssim 0.05$ ), we have a regime of strongly collective behaviour, characterized by the appearance of resonant particles.

**Regime B** : for  $1.2\omega_{pe} \lesssim \omega_0 \lesssim 2\omega_{pe}$  ( $0.05 \lesssim \text{Im}(k_1)/\text{Re}(k_1) \lesssim 0.4$ ), there

are no longer resonant particles. Nevertheless, the energy exchange between electric field and particles reduces the number of particles having low speeds (with respect to the free streaming solution) and increases the number having high speeds. The phase velocity  $v\psi$  of the first Landau pole still has a meaning for  $|f_1|$ : when  $v > v_\psi$  a sudden decrease in  $|f_1|$  occurs.

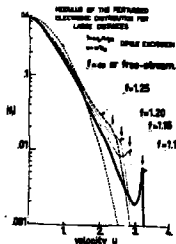


FIG. 1

Regime C : for  $\omega_0 \gtrsim 2\omega_{pe}$  ( $\text{Im}(k_1)/\text{Re}(k_1) \gtrsim 0.4$ ),  $|f_1|$  is very near the free-streaming solution and  $v_\varphi$  loses any particular meaning for  $|f_1|$ .

It is important to note that if other excitations are studied, the general shape of  $|f_1|$  can be drastically changed. Particularly with multi-grids systems,  $|f_1|$  is modulated and the corresponding maxima must not be mistaken as being due to collective effects.

In fig.2 we have represented  $|f_1|$  for a frequency  $\omega_0 = 1.15\omega_{pe}$ , corresponding to regime A. The modulation of  $|f_1|$  is to be observed in phase space

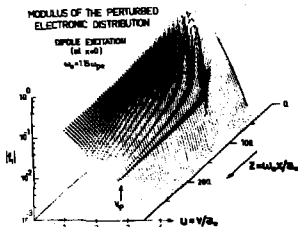


FIG.2

We note that all oscillations of  $|f_1|$  disappear at large distances except one which produces the peak of resonant particles.

#### IV. NUMERICAL CALCULATION FOR ION WAVES.

In fig.3 and 4 we represent results similar to those of fig.1 and 2, but for the perturbed ion distribution function, with  $T_e/T_i = 20$  (we assume that the electrons follow Boltzmann's law). Fig.3 allow us to distinguish three frequency regimes, similar to the case of electrons. Since the limits of the regimes depend on  $T_e/T_i$ , it is better to define them in terms of the pa-

to be observed in phase space and is relative to the phase mixing between the damped and undamped collective contributions, which can be explained by Eq.(12) applied to the first pole :

- for  $v$  fixed,  $|f_1|$  oscillates like :

$$\exp\{i\omega_0 x \left( \frac{1}{v} - \frac{1}{v} + i \frac{\text{Im}(k_1)}{\omega_0} \right)\}$$

- for  $z$  fixed,  $f_1$  oscillates like  $\exp[i\omega_0 x/v]$



FIG.3



parameter  $\text{Im}(k_1)/\text{Re}(k_1)$ . The transition between these regimes corresponds to values of this ratio which are nearly the same as for the electrons.

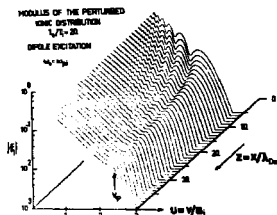


FIG. 4

In fig. 4 we have represented  $|f_1|$  for a frequency  $\omega_0 = \omega_{p1}$ , corresponding to regime B. The modulation in phase space has the same meaning as for the electrons except that, since the collective effects are not so strong, the ripples are not so pronounced and no resonant particles appear at large distances.

#### V - CONCLUSIONS.

The theoretical results presented here give a more obvious idea of the manner by which collective effects can be shown in measurements of the perturbed distribution.

As a matter of fact it seems that collective effects can be observed following two ways :

- The first one is to observe a collective phenomenon almost independent of the excitation, i.e., resonant particles at the phase velocity. This phenomena can be observed only with very weakly damped waves ( $\text{Im}(k_1)/\text{Re}(k_1) \lesssim 0.05$ ) and at distances where the electric field is almost completely damped. This condition is realized at distances where diffusion in phase space caused by collisions will probably destroy the strong oscillations of  $F_1$  near  $v_p$ . Moreover, the detection of a linear phenomena requires a very high resolution in energy.
- The second possibility is to measure  $F_1$  not too far from the excitation, but the interpretation of the measurements must be done with a precise knowledge of the unperturbed distribution function and of the excitation. However, measurements of  $F_1(x, v, t)$  can certainly give interesting qualitative information on the excitation process of electrostatic waves.



ACKNOWLEDGMENTS

It is a pleasure to acknowledge useful conversations on  $F_1$  calculation with G. MATTHIEUSANT, stimulating discussions with Dr. M.R. FEIX, Dr. H.J. DOUCET and J.P.M. SCHMITT, and the help of M. COULON, Head of the Computer Center of the Ecole Polytechnique.

This work was supported by Ecole Polytechnique, by Centre National de la Recherche Scientifique, and by Direction des Recherches et Moyens d'Essais.

APPENDIX A

For  $x$  and  $v$  positive  $R_n(v, x)$  is given by :

$$R_n(v, x) = -\frac{i}{2\pi} \left( D_n(v) \left[ \psi^+(ik_n x) - \psi(i\omega_0 x/v) \right] \dots \right. \\ \left. \dots - D_n^*(v) \left[ \psi^-(ik_n^* x) - \psi(i\omega_0^* x/v) \right] + D_n^*(v) \sigma(-k_n^*) e^{ik_n^* x} \right)$$

where :  $\psi^\pm(v) = e^{v E_1(v \pm i0)}$ ,  $E_1$  being the exponential integral defined in Ref. 6. Moreover :

$$\sigma(a) = 1 \text{ if } 0 < \arg(a) \leq \pi/2$$

$$\sigma(a) = 0 \text{ if } \pi/2 < \arg(a) < 2\pi$$

REFERENCES

- (1) H. IKEZI, R.J. TAYLOR, Phys. Fluids, 13, 2348, (1970).
- (2) D. GRESILLON, J. de Phys., 32, 269 (1971).
- (3) G. MATTHIEUSANT, from the Laboratoire de Physique des Plasmas de la Faculté des Sciences d'ORSAY (FRANCE), works now on this problem and solves it by other methods.
- (4) R.W. GOULD, Phys. Rev. 136, A991, (1964).
- (5) H. DERFLER, in Proceedings of the Seventh International Conference on Phenomena in Ionized Gases, B. Perovich and D. Toshich, Eds. (Grade-vinska Knjiga, Beograd, Yugoslavia, 1966), Vol. II, p. 282.
- T.C. SIMONEN, SUIPR Rep. n°100, Stanford University, Stanford, California, (1968).
- (6) M. ABRAMOWITZ, I. STEGUN, Handbook of Mathematical Functions, Dover Pub., p.228, (1965).

NUMERICAL STUDIES OF ION ACOUSTIC WAVE PROPAGATION  
IN THE NON MAXWELLIAN PLASMA OF A SINGLE ENDED Q DEVICE

J.M. BUZZI

Laboratoire de Physique des Milieux Ionisés  
Ecole Polytechnique, Paris - France

---

ABSTRACT

We represent first the experimental ion distribution function found in Q machines by an entire function and compare the dispersion curves of this analytical model to the one obtained by a drifted Maxwellian. Then we calculate the plasma response using two other models which may be applied to the case of experimentally measured distribution functions. The first model uses Hermite polynomials, the second is derived from the "Water-Bag". We compare the results of these two models to the analytical solution and give the respective advantages and inconveniences of the two models.

---

I. INTRODUCTION.

In single ended Q devices, the ion distribution functions are not Maxwellian, but according to the collisionless<sup>1</sup> theory are of the type :

$$(1) \quad F_i(v) = N \exp(-m_i v^2 / 2kT) \cdot Y(v - v_0)$$

$$v_0 = \{-2q_i V_p / m_i\}^{1/2}$$

where Y is the Heaviside step function,  $V_p$  the plasma potential and T the emitter temperature. The measurements of  $F_i(v)$ <sup>1</sup> agree with (1) except that the truncation is smoother.

The problem of the introduction of this non Maxwellian function in the linear kinetic theory can be approached by different ways. For example, one can calculate the incomplete plasma dispersion function<sup>2</sup> corresponding to (1) or represent the ions by a drifted Maxwellian<sup>3</sup>.

In this paper we represent first  $F_i(v)$  by an analytical function nearer to (1) than the drifted Maxwellian. In section II we compare the dispersion predicted by the two analytical models.

However, the distribution functions measured experimentally cannot be represented accurately by analytical functions. These experimental functions can be introduced in the linear kinetic theory by two general methods.

The first one consists in the analytical continuation in the complex  $v$  plane of a function known on the real axis only. Among the possible models solving this problem "à la Landau", we have chosen Hermite polynomials. (Section III).

In the second method we "stick" to the real axis. To solve this problem "à la Van Kampen", we have utilized a model derived from the "Water-Bag"<sup>6</sup> (Section IV).

## II. ANALYTICAL MODEL.

In this model we represent  $F_1(v)$  by the entire function

$$(2) F_1(v) \approx \varphi_i(u) = (A/\sqrt{\pi}) \cdot \exp(-u^2) \{1 + \operatorname{erf}[(u-u_0)/a]\}$$

$u = v/a_i$ ;  $a_i^2 = 2kT/m_i$ ;  $T$  is the emitter temperature.

$\varphi_i(u) \rightarrow \exp(-u^2)$  for  $u \rightarrow \infty$  in agreement with Eq.1 and the truncation is smoothed according to the experiments. Then the dispersion relation is :

$$D(\omega, k) = 1 - k_{D_i}^2 / k^2 \{Q'(\xi) + Z'(m\xi)\}; \quad \xi = \omega/k a_i$$

with  $m = (m_e/m_i)^{1/2}$ ;  $Z'$  is the derivative of the usual plasma dispersion function (the electrons are supposed to be Maxwellian at the emitter temperature) and  $Q'(\xi)$  is the Hilbert transform of

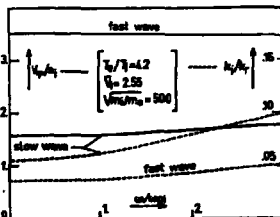


FIG. 1

Phase velocity  $V_\phi$  and reduced damping  $k_i/k_r$  of the two dominating Landau nodes. The thermal ion velocity  $a_i$  and mean velocity  $\bar{U}_i$  are defined by Eq. 3. The ion distribution function is given by Eq.2. The electrons are Maxwellian,  $T_e = T$ , emitter temperature.

$d\varphi_i/du$ .  $Q'(\xi)$  is calculated numerically and the roots of  $D(\omega, k)$  are searched for real  $\omega$  in the  $k$  plane. An example of dispersion

curves is given in fig.1. As in the Maxwellian case, we find two dominating modes travelling in opposite direction in the plasma frame, but here the waves are streaming in the same direction because of the plasma mean velocity,  $\bar{u}_i$  :

$$(3) \quad \bar{u}_i = \int \varphi_i(u) u \, du ; \quad T_i/T_e = (2m_i/k) \int \varphi_i(u) (u - \bar{u}_i)^2 \, du$$

If we compare, for example, the dispersion curves obtained using drifted Maxwellian for the ions with the same values of  $\bar{u}_i$  and  $T_i/T_e$  as in fig.1, we note a very good agreement for the phase velocity of the two modes. But there is a discrepancy of about a factor of 1.3 between the  $k_i/k_r$  ratios, although for the chosen values of  $\bar{u}_i$  and  $T_i/T_e$  the two distribution functions are very near.

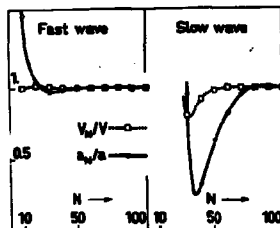
### III. HERMITE POLYNOMIALS.

In this model the zero order distribution function is represented by Hermite polynomials, i.e., its moments, truncated at order  $N$  :

$$(4) \quad f_0(v) \approx f_{0N}(v) = \exp(-u^2) \sum_0^N a_n H_n(u) / \sqrt{\pi}$$

FIG.2

Comparison between the roots of the dispersion relation given by the analytical model (Section II) and those given by the Hermite model v.s. the truncation order of the Hermite model.  $v$  is  $v_0/a_i$  and  $a = k_i/k_r$  given by the analytical model,  $v_N$  and  $a_N$  are the same quantities obtained by Hermite model truncated at order  $N$ . The conditions are the same as in fig.1, but the frequency is fixed,  $\omega = 0.5 \omega_{pi}$



From the point of view of the Hilbert transform, this expansion is very interesting since :

$$(5) \quad Q'(\xi) \approx Q'_N = \int \frac{df_{0N}/du}{u-\xi} = \sum_0^N (-1)^n a_n Z^{(n+1)}(\xi)$$

where the  $a_n$  coefficients are the same as in Eq.3 and  $Z^{(n+1)}(\xi)$  is the  $(n+1)^{th}$  derivative of the plasma dispersion function. The-

refore, the knowledge of the moments of an experimental distribution function allows us to make the analytical continuation of this function in the complex  $v$  plane by means of formulae (4) and (5).

It is interesting to point out that this treatment differs from the usual utilization of Hermite polynomials in the linear kinetic theory<sup>5</sup>. Here it is not the perturbed part of the distribution which is expanded but the zero order distribution. Therefore, the problem of the representation of the strong oscillating structure of the perturbed distribution function by Hermite polynomials<sup>5</sup> does not appear here. Moreover, the obtained dispersion relation has its roots in the complex  $k$  plane instead of the real axis<sup>5</sup>. These roots can be compared directly with those obtained by analytical models.

The most important question is now the convergence of  $Q'_N(\xi)$ . The answer depends of course on the zero order distribution function considered.

We have studied numerically this problem by applying the Hermite model to the ion distribution given by Eq.2. We have calculated the roots of the approximate dispersion relation  $D_N(u, k)$  corresponding to an Hermite expansion of  $\psi_i(u)$  truncated at order  $N$ . Typical results are shown in fig.2. It must be noted that the convergence is better for the phase velocity than for the damping. The convergence decreases when damping increases (this phenomenon is true also for higher order poles). The slowness of the convergence in our case is probably caused by the fact that  $\psi_i(u)$  differs strongly from  $\exp(-u^2)$ .

#### IV. MULTIPLE-WATER-BAG MODEL.

The Multiple-Water-Bag (M.W.B.) model<sup>4</sup> is very similar to Dawson's multi-beam model<sup>6</sup>. The distribution function is represented by  $N$  step functions :

$$f_0(v) = \sum_{n=1}^N h_n \mathcal{Y}(v-v_n)$$

Therefore, the Hilbert transform of  $df_0/dv$  becomes :

$$Q'_N(\xi) = \sum_{n=1}^N \frac{h_n}{v_n - \xi}$$

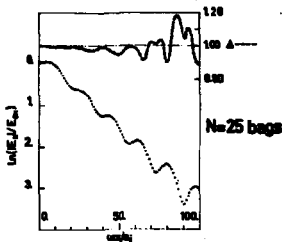


FIG.3

Amplitude of the electric field  $E_N$  v.s. distance.  $E_N$  is calculated using the M.W.B. model with  $N$  "bags".  $E_{0N} = E_N(x=0)$  and  $\Delta = E/E_N$  where  $E$  is given by the analytical model (Eq.6). The conditions are the same as in Fig.1 but  $\omega/\omega_{pi} \approx 0$ .

The most interesting property of the corresponding dispersion relation in contrast to the multibeam model, is that only real roots appear for stable distribution functions in the  $\omega$  plane, even if the number of "bags" is finite. The sum of the oscillating and undamped contributions of each root gives, by phase mixing, for not too long time or distances, the Landau damping : this correspond to a discrete form of the Van Kampen treatment, like the multi-beam model but more practical because of the above mentioned property.

We have applied the M.W.B. to the distribution function given by Eq.2 and we have calculated the corresponding spatial dependence of the electric field  $E_N$  for dipole excitation. We compare with the analytical model,  $E$  being calculated following the Gould method<sup>7</sup> :

$$(6) \quad E(x) / \ell^3 = i/\pi \int_0^{\infty} \text{Im}(1/D) e^{i\eta x} d\eta$$

$f = \omega/\omega_{pi}$  ;  $\eta = k a_i/\omega$  ;  $D$  being the dispersion relation for ion distribution function given by Eq.2. Fig.3 shows that M.W.B. gives satisfactory results with a reasonable number of "bags" in the considered case (for Maxwellian ions with  $T_e = T_i$ , the M.W.B. requires a higher number of "bags" than for a drifted distribution, 100 to 200 in order to obtain good results).



## V. DISCUSSION AND CONCLUSIONS.

An accurate comparison between theory and experiments in the study of electrostatic waves cannot be made without taking into account the real distribution functions if they differ strongly from a Maxwellian as in single-ended Q devices.

Our numerical results, particularly those concerning the "multi-water-bag" model, show conclusively that it is possible to introduce without any serious difficulty, an experimental distribution function in the linear kinetic theory.

As regards single-ended Q machine plasmas, it is interesting to point out that the mean ion velocity allows us to observe theoretically, for dipole excitation, the interferences of two waves (Fig. 3). Other excitation models like monopole or multigrids can reduce or suppress theoretically the interferences and we intend to check this point experimentally in order to have more information on the excitation process of ion acoustic waves in Q machines.

## ACKNOWLEDGEMENTS.

We are very indebted to Dr. M.R. FEIX for his many helpful suggestions about the Hermite and M.V.B. models and the fruitful general discussions we have had about this work.

REFERENCES.

- (1) S.A. ANDERSEN, V.O. JENSEN, P. MICHELSEN, P. NIELSEN,  
Phys. Fluids, 14, 728 (1971).  
J.M. BUZZI, H.J. DOUCET, D. GRESILLON,  
Phys. Fluids, 13, 3041 (1970).
- (2) H. DERFLER,  
Phys. Fluids, 7, 1625 (1964).
- (3) E.D. FRIED, A.Y. WONG,  
Phys. Fluids, 9, 1084, (1966).
- (4) P. BERTRAND, M. HAVET,  
Phys. Letters, 34A, 117 (1971).
- (5) F.C. GRANT, M.R. FEIX,  
Phys. Fluids, 10, 703, (1967) ;  
Phys. Fluids, 10, 1356, (1967).
- (6) J.M. DAWSON,  
Phys. Rev., 118, 381, (1960).
- (7) R.W. GOULD,  
Phys. Rev., 136, A991, (1964).

Measurements of the Perturbed Ion Velocity  
Distribution at a Wave-exciting Grid

by

G. B. Christoffersen

Danish Atomic Energy Commission Research Establishment Risø,  
Roskilde, Denmark

Abstract

Theoretical treatment of propagation of ion-acoustic perturbation based on the Vlasov equation necessitates knowledge of  $g(v)$ , the perturbed ion velocity distribution function at the grid. This knowledge is also important in connection with experimental investigations.

In a single-ended Q-machine  $g(v)$  is measured with an electrostatic energy analyser. The measurements show that both the shape and the size of  $g(v)$  are drastically changed with the various parameters, particularly the dc grid potential.

Introduction

In the following, experimental investigations of the interaction between a grid and the plasma in a single-ended Q-machine are described. Further knowledge of the mechanism in this interaction is of great interest because introduction of perturbations in the plasma column by means of a grid has been the most used method in several important experiments. In this connection may be mentioned Wong's, D'Angelo's and Motley's experiments<sup>(1)</sup> where the "Landau damping" of ion-acoustic waves is observed.

Perturbations by means of grids have also been used in the following more recent measurements: Propagation of ion-acoustic waves in a partly ionized plasma<sup>(2, 3)</sup>, investigations of non-linear effects<sup>(4, 5)</sup>, and finally

experiments concerning echo-phenomena in ion-acoustic waves (6, 7).

In all these experiments waves have been generated by means of grids placed perpendicularly on the magnetic field lines in the plasma column. Waves have been launched by impressing an oscillating negative potential on the grid, but the mechanism by which the waves are generated has not been investigated before.

The purpose of most of the experiments has been to verify Landau's (8) theory on waves in a collision-less plasma or other theoretical predictions based on the same model (9, 10). When the experimental results and the theories have been compared, it has normally been assumed that details in the excitation mechanism are without importance in the propagation of the waves. This is equivalent to ignoring the effect that results from an impressed perturbation of the velocity distribution of the ions, as thus only the so-called "natural modes" are considered. However, there is no reason not to take this perturbation of the velocity distribution into account as discussed by V. O. Jensen (11).

#### Experimental Set-up

This paper describes how the perturbation  $g(v)$  in the ion velocity distribution can be measured. Fig. 1 shows a schematic drawing of the experimental set-up. The circuit on the right-hand side of the figure determines the unperturbed velocity distribution  $f_0(v)$ . As described by S. A. Andersen et al. (12) we get  $f_0(v) = f_0 [v = \frac{2e}{m}(\varphi_a - \varphi_{pl})^{1/2}]$ , (where  $\varphi_a$  is the collector voltage,  $\varphi_{pl}$  the plasma potential,  $e$  and  $m$  the charge and mass of the ion) by differentiation of the collector current voltage characteristic with respect to  $\varphi_a$ . This differentiation can be obtained electrically. Through the transformer a 3 kc/s 0.03 V peak-to-peak voltage from the generator in the lock-in amplifier is added to the collector dc voltage,  $\varphi_a$ . The part of the ac current to the collector that is in-phase with the transformer voltage is proportional to  $di(\varphi_a)/d\varphi_a$  or  $f_0(v) = f_0 [v = \frac{2e}{m}(\varphi_a - \varphi_{pl})^{1/2}]$ . After determination of  $\varphi_{pl}$ , e.g. by means of charge exchange processes (12), we get  $f_0(v)$ .

The experimental procedure is as follows: First the unperturbed ion velocity distribution,  $f_0(v)$ , in which the experiment is to be performed is obtained by adjustment of the temperature of the hot plate and the Cs oven. The dc grid potential  $V_G$  is superimposed on an ac voltage  $V_g$  of the order of 200-400 mV peak-to-peak and with a frequency,  $f_2$ , of  $\sim 30$  c/s from

the generator in the other lock-in amplifier. This ac voltage perturbs the plasma and with it  $f_0(v)$ . The part of  $f_0(v)$  that is in-phase with  $V_g$  gives  $g(v)$ .

Fig. 2 shows quite clearly how  $f_0(v)$  is perturbed. The regular oscillation in  $f_0(v)$ , curves (A) - (C), is due to the impressed grid voltage,  $V_g$ . One can see, e. g. in (B), how the ions situated in the low and the middle areas of the energy interval are perturbed very much while ions with energy of  $\sim 1$  eV not at all are perturbed. The curves (a) - (c) show  $g(v)$  corresponding to (A) - (C). The sign of  $g(v)$  is chosen so that  $g(v)$  is positive if a positive change,  $dV_G$ , of  $V_G$  corresponds to more particles per velocity interval. (a) and (b) in fig. 2 show a very interesting thing: A double-humped  $g(v)$  where the humps have opposite signs. This means that a positive change of  $V_G$  (in (a) from  $-3.65$  V to  $-3.35$  V and in (b) from  $-9.15$  V to  $-8.85$  V) implies fewer particles in the low end of the energy interval, while it implies more particles in the middle and high ends.

### Results

Figs. 3 to 5 show three bands of curves of  $f_0(v)$  and the corresponding  $g(v)$  with  $V_G$  as parameter. The curves are deduced from photos of oscillograms as the ones in fig. 2. In all three cases the ac grid potential,  $V_g$ , is  $\sim 300$  mV peak-to-peak. A reduction of this voltage does not change the form of  $g(v)$ , only the amplitude is decreased. These three examples are characteristic for the change in  $f_0(v)$  and  $g(v)$  as functions of the dc grid potential,  $V_G$ .

When  $V_G$  is going through more and more negative values, the first thing that happens is generally that  $f_0(v)$  gets more particles in the low end of the velocity interval and fewer in the higher end, which implies the double-humped nature of  $g(v)$ . The flux decreases, while the density has not changed much because of the decreasing mean velocity. As  $V_G$  becomes more negative, more particles disappear in the whole velocity interval. This means that  $g(v)$  is now single-humped. In the beginning more of the slow particles vanish, whereas the quicker ones to some extent pass through. This appears as an increasing mean velocity of  $g(v)$ . Generally an increasing density or an increased spacing between the grid wires means that a more negative voltage is required to obtain a single-humped  $g(v)$ .

None of the investigated cases showed a change in the plasma potential. This indicates that the grid for small negative values of  $V_G$  spreads the

particles in the potential around the wires (this explains the displacement of particles towards lower velocities), and when  $V_G$  becomes more negative, an absorption of particles dominates. This absorption is most effective for the slow ions.

#### Conclusion

In investigations of propagation of ion-acoustic waves, particularly in a Q-machine, it is important to know  $g(v)$  because, as discussed by V. O. Jensen<sup>(11)</sup>, the motion of the ions where a wave is present is more or less freely streaming. In previous works it has been assumed that  $g(v)$  and  $f_0(v)$  have had the same form and could be approximated to Maxwellian distributions. But one has to be very careful,  $g(v)$  and  $f_0(v)$  generally do not have the same form, and often it is necessary to approximate  $g(v)$  with two opposite Maxwellian distributions.

#### References

1. A. Y. Wong, N. D'Angelo, and R. W. Motley, *Phys. Rev. Letters* 9, 415 (1962), *Phys. Rev.* 133, A436 (1964).
2. H. K. Andersen, N. D'Angelo, V. O. Jensen, P. Michelsen, and P. Nielsen, *Phys. Fluids* 11, 1177 (1968).
3. H. J. Doucet, and D. Gresillon, in *Plasma Physics and Controlled Nuclear Fusion Research* (International Atomic Energy Agency, Vienna, 1968, 1, 659).
4. J. M. Buzzi, D. Gresillon, and H. J. Doucet, *Bull. Am. Phys. Soc.* 13, 1569 (1968).
5. N. Sato, H. Ikezi, N. Takahashi, Y. Yamashita, and T. Obiki, *Institute of Plasma Physics, Nagoya University, Japan, Report IPPJ-62* (1967).
6. D. R. Baker, N. R. Ahern, and A. Y. Wong, *Phys. Rev. Letters* 20, 318 (1968).
7. H. Ikezi, N. Takahashi, and K. Nishikawa, *Phys. Fluids* 12, 853 (1969).
8. L. Landau, *J. Phys. (USSR)* 10, 25 (1946).

9. R. W. Gould, Phys. Rev. 136, A991 (1964).
10. R. W. Gould, T. M. O'Neil, and J. H. Malmberg, Phys. Rev. Letters 19, 219 (1967).
11. V. O. Jensen, These Proceedings.
12. S. A. Andersen, V. O. Jensen, P. Michelsen, and P. Nielsen, Phys. Fluids 14, 728 (1971).

Figure Captions

Fig. 1. Experimental set-up.

Fig. 2. (A) - (C): Measured  $f_0(v)$  curves. (a) - (c): Measured  $g(v)$  curves. 0.5 V/large division.

Fig. 3. (a)  $f_0(v)$ . (b)  $g(v)$ ;  $n \approx 10^8 \text{ cm}^{-3}$ ; grid spacing  $\approx 0.5 \text{ mm}$ . The numbers 1-4 correspond to  $V_G$  values: -2 V, -3 V, -6 V and -6.5 V.

Fig. 4. (a)  $f_0(v)$ . (b)  $g(v)$ ;  $n \approx 2 \times 10^9 \text{ cm}^{-3}$ ; grid spacing  $\approx 0.5 \text{ mm}$ . The numbers 1-4 correspond to  $V_G$  values: -4 V, -6.5 V, -9.5 V and -14 V.

Fig. 5. (a)  $f_0(v)$ . (b)  $g(v)$ ;  $n \approx 7 \times 10^8 \text{ cm}^{-3}$ ; grid spacing  $\approx 1.2 \text{ mm}$ . The numbers 1-5 correspond to  $V_G$  values: -3.5 V, -4.2 V, -9.0 V, -11.0 V and -24 V.

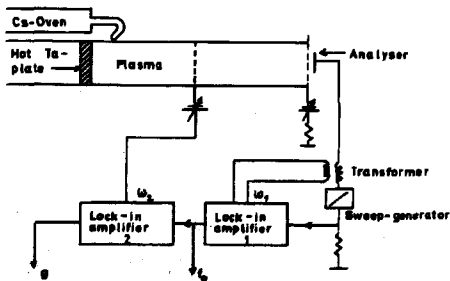


FIG1

FIG 2

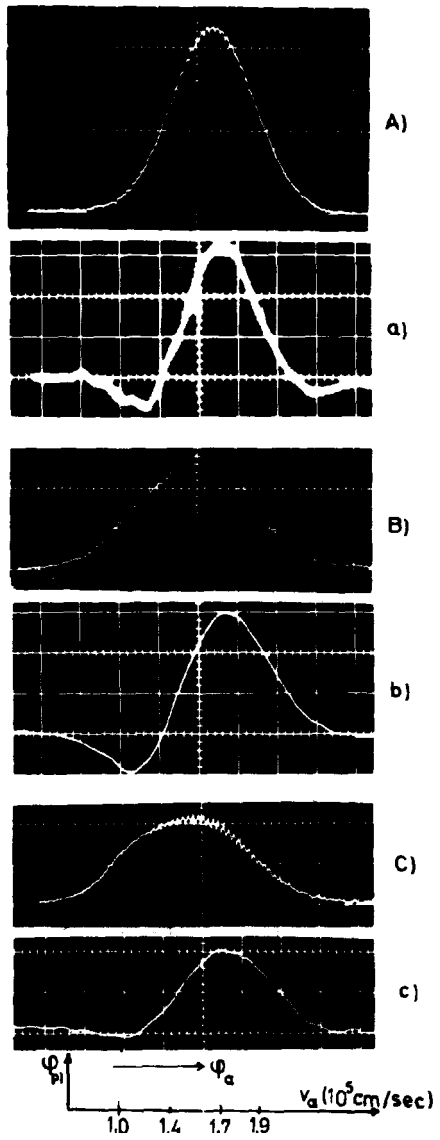




FIG 3

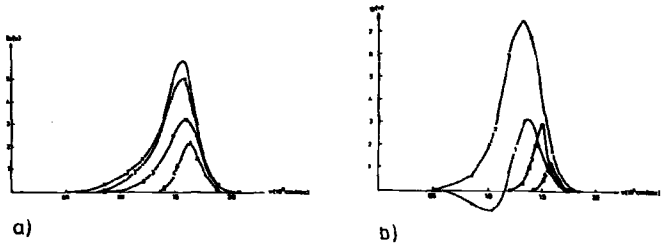


FIG 4

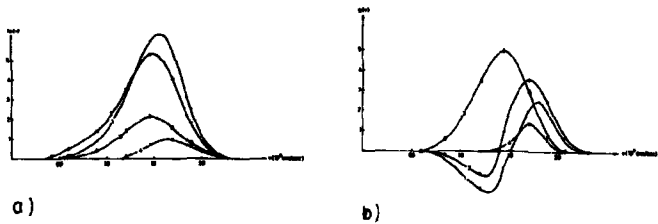
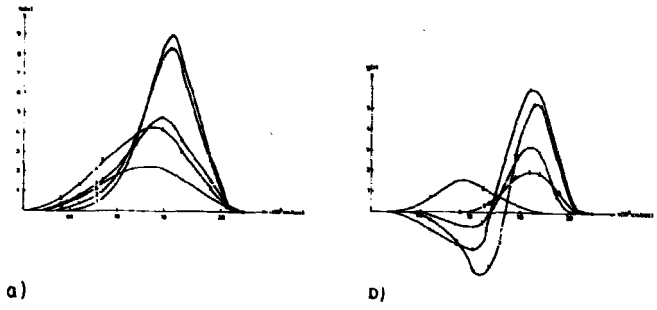


FIG 5



\_\_\_\_\_

Calculations and Measurements of the Perturbed  
Density and Ion Velocity Distribution Function  
in Grid-Excited Waves in a Q-Machine Plasma

by

G.B. Christoffersen, V.O. Jensen, and P. Michelsen  
Danish Atomic Energy Commission, Research Establishment Risø  
Roskilde, Denmark

Abstract

On the basis of the linearized quasi-neutral Vlasov equation we calculated the density perturbation  $n(x,t)$  and the perturbed ion velocity distribution function  $f(x,v,t)$  for ion-acoustic waves. We report on this theory, the results obtained and on experimental measurements that support our theoretical results.

Introduction

This paper treats the propagation of ion-acoustic waves excited by a grid in a collision-less plasma. We attempted to solve the linear Vlasov equation, using only the assumptions relevant for the experimental possibilities in a single-ended Q-machine. Preliminary measurements on the propagation of the ion flux and the perturbed ion velocity distribution function are presented and compared with theory.

Although much work has been done on linear ion-acoustic waves, our opinion is that there are still important details involved in the propagation of ion waves that are not well understood. We may here refer to the work by Gould<sup>(1)</sup>, in which it is concluded that "in general, ion waves cannot be interpreted by simply examining a single root of the dispersion relation". Hirschfield et al.<sup>(2)</sup> conclude that strong wave damping may in some cases be interpreted as phase mixing of freely streaming particles. In another paper of Hirschfield et al.<sup>(3)</sup> other "effects which can enter measurements of signal decay under conditions typical of some laboratory studies" are pointed out. In a paper by Andersen et al.<sup>(4)</sup> the necessity of knowing the undisturbed ion distribution function as well as the disturbed one at the grid position was stated.

In order to extend theory and experiments to the non-linear regime, it seems to be of importance to clarify these problems, and to compare linear theories and experiments carefully.

The main purpose with our work is to examine whether it is possible experimentally to distinguish wave particle interaction from the freely streaming contribution. From theoretical considerations this should be difficult as long as the electron to ion temperature ratio  $\theta \approx 1$ , and the steady-state ion distribution function,  $f_0(v)$ , and the perturbed ion distribution function are not known very accurately. Our measurements support this conclusion. Direct proof of wave - particle interaction seems to be obtained more easily with other kinds of wave propagation as shocks<sup>(5)</sup> or pulses<sup>(4)</sup>. Measurements of the perturbed ion velocity distribution have earlier been made by Ikeda et al.<sup>(6)</sup>. The temperature ratio was in their experiment  $\approx 0.5$ , and as expected the ions were moving as freely streaming particles. This has been shown from measurements of the phase relation  $e^{-i\omega t}$ . We verified this relation in our plasma where  $\theta \approx 1$ . The theory only shows significant deviation from the straight phase lines if  $\theta \gtrsim 5$ . The amplitude of the wave changes more with  $\theta$ , but cannot be measured as accurately as the phase and is more affected by irrelevant phenomena.

#### Theory

We shall here present a calculation of the propagation of grid-excited ion-acoustic waves. The method used resembles that of Gould<sup>(1)</sup>. The differences between the present work and that of Gould are mainly due to the fact that we attempted to use only those assumptions that are relevant for our experimental situation. The results could, however, also be obtained as integrals over the Green functions as in ref. 4. Furthermore, besides the calculation of the density propagation, we calculated the perturbation in the ion velocity distribution.

The experimental situation is: We can measure the zero-order ion distribution function,  $f_0(v)$ , the perturbed distribution function at the grid position,  $g(v)$ , and the latter away from the grid,  $f(x, v, t)$ .

Our starting point is the linearized Vlasov equation. We assume quasi-neutrality, except close to the grid. Further we assume the electrons to behave as an isothermal fluid. With the time variation  $e^{-i\omega t}$  for all perturbed quantities we then get:

$$-i\omega f(x, v) + v \frac{\partial f(x, v)}{\partial x} = c_s^2 \frac{d f_0(v)}{d v} \left\{ \frac{\partial \phi(x)}{\partial x} + \lambda \delta(x) \right\} \quad (1)$$

where  $c_s^2 = kT_e/n_e$ . The last term on the right-hand side is introduced because the quasi-neutrality relation between density and potential is not valid across the grid. A density jump at  $x = 0$  (grid position) is not necessarily

accompanied by a potential drop. The constant  $\lambda$  times the  $\delta$ -function accounts for this mathematically, while the physical situation is that we might have a charge distribution in the region consisting of the grid and the grid sheath. We now separate  $f(x, v)$  and  $n(x)$  into two terms,

$$f = f_1 + f_2 \quad \text{and} \quad n = n_1 + n_2$$

where index 1 refers to the contribution due to freely streaming particles (i.e. the solution to the left-hand side of eq. (1)), and index 2 refers to the contribution from the collective interaction. This involves

$$f_1(x, v) = g(v)e^{i\omega x/v}; \quad n_1(x) = \int_0^{\infty} g(v)e^{i\omega x/v} dv, \text{ for } x > 0,$$

and to simplify the calculations, we assume  $g(v) = 0$  for  $x \leq 0$ .

We now apply Fourier transformation to eq. (1)

$$(-i\omega + \lambda kv)f_2(k, v) = \kappa_e^2 f_0(v) \{ ik[n_1(k) + n_2(k)] + \lambda \} \quad (2)$$

where

$$n_1(k) = \frac{1}{ik} \int_0^{\infty} \frac{v g(v)}{v - \omega/k} dv \quad (3)$$

Solving this we get the result:

$$\begin{aligned} n(k) &= n_1(k) + n_2(k) \\ &= \frac{1}{ik} \frac{\int_0^{\infty} \frac{v g(v)}{v - \omega/k} dv + \kappa_e^2 \lambda \int_0^{\infty} \frac{f_0(v)}{v - \omega/k} dv}{1 - \kappa_e^2 \int_{-\infty}^{\infty} \frac{f_0(v)}{v - \omega/k} dv} \equiv \frac{1}{ik} H\left(\frac{\omega}{k}\right). \end{aligned} \quad (4)$$

To evaluate the velocity integrals we assume  $\omega$  has a small positive imaginary part. This implies that the integration path runs above the pole at  $v = \omega/k$  if  $k < 0$ , and below if  $k > 0$ . For this reason we split up the  $k$ -integration into two parts

$$n(x) = \frac{1}{2\pi} \int_{-\infty}^0 n_-(k) e^{ikx} dk + \frac{1}{2\pi} \int_0^{\infty} n_+(k) e^{ikx} dk, \quad (5)$$

where  $n_-(k)$  and  $n_+(k)$  represent the  $n(k)$  function above and below the branch cut  $k = \omega/v$  ( $v$  real) respectively. The relation between these two functions is

$$n_-(k^*) = -n_+(k) \quad (6)$$

Because the  $n(k)$  function has no poles in the upper half plane, we may deform the contour of the first integral so that it runs in along the positive  $k$ -axis just above the branch cut as shown in fig. 1. Doing this we get

$$n(x) = \frac{1}{2\pi i} \int_0^{\infty} \left[ \frac{1}{v} [H_+(v) - H_-(v)] \right] e^{i \frac{\omega x}{v}} dv \quad (7)$$

From relation (6) we get

$$n(x) = \frac{1}{\pi} \int_0^{\infty} \frac{1}{v} \text{Im} H_+(v) e^{i \frac{\omega x}{v}} dv \equiv \int_0^{\infty} h(v) e^{i \frac{\omega x}{v}} dv. \quad (8)$$

To obtain a finite integral for  $x = 0$  we must choose

$$\lambda = - \int_0^{\infty} g(v) dv$$

i.e. minus the density perturbation at  $x = 0$ . In cases where the zero order and the perturbed distribution function are Maxwellians, the  $h$ -function can be expressed in terms of the plasma dispersion function, and numerical calculations of (8) are rather simple.

The calculation of  $f(x, v)$  is similar to that of  $n(x)$ . From eqs. 2 and 3 and with the definition of  $H$  in (4) we find:

$$f(k, v) = \frac{1}{i k (v - \omega/k)} \left[ v g(v) + c_e^2 f_0'(v) \left\{ H\left(\frac{\omega}{k}\right) + \lambda \right\} \right] \quad (9)$$

Performing the inverse  $k$ -integration we get a residue contribution from the pole at  $k = \omega/v$ , and a branch cut contribution from the term containing  $H\left(\frac{\omega}{k}\right)$ :

$$f(x, v) = \left\{ g(v) + c_e^2 f_0'(v) \frac{1}{v} [\text{Re} H_+(v) + \lambda] \right\} e^{i \frac{\omega x}{v}} + c_e^2 f_0'(v) P \int_0^{\infty} \frac{1}{v} \frac{H(v)}{v - v'} e^{i \frac{\omega x}{v}} dv \quad (10)$$

Numerical calculations were performed of both  $f(x, v)$  and  $n(x)$ . From this kind of calculation it is possible to examine the relative importance of the interaction term, the validity range of the "first pole assumption", and to compare with measurements.

#### Experimental Set-up

The experiment was performed in the Rief Q-machine of which a schematic is shown in fig. 2.

With the electrostatic analyser, which is movable along the column, the

steady-state ion distribution function,  $f_0(v)$ , and the perturbed ion distribution function  $f_1(x, v, t)$ , can be measured. The electronic circuit shown in fig. 2 is used to obtain amplitude and phase of  $f_1(v)$ . A small (100 mV) 30 Hz voltage is applied to the analyzer collector to differentiate the signal. The ion current is measured across the resistor and detected in the lock-in amplifier 1 (phase sensitive amplifier PAR) which is adjusted to the frequency applied to the wave-exciting grid. The output is fed into lock-in amplifier 2 whose reference signal is used for differentiation (30 Hz). The phase measured at 1 is adjusted to give maximum signal on 2. The phase at 1 is now the phase of the wave, while the signal on 2 is the amplitude of the wave.

### Discussion

Although many interesting features can be found by numerical calculations of expressions (8-10) in the theoretical part of this contribution, we shall here only discuss the results relevant for comparison with the experiment.

The phase relation mentioned in the introduction states that

$$\text{phase of } f(v) \propto e^{i \frac{v x}{v}}$$

This is correct if we have no wave - particle interaction. We verified this relation (see fig. 3) in our plasm. If the relation is valid down to  $x = 0$ , the phase measurement can be used for determination of the plasm. potential. This method agrees with plasm. potential determination with charge exchange ions.

An example of amplitude and phase measurements is shown in fig. 4. The measurements were performed in the following way: First the steady-state ion velocity distribution function,  $f_0(v)$ , was measured<sup>(7)</sup>. In this example  $f_0(v)$  was very close to a drifting Maxwellian with the data:

$$T_i = 0.25 \text{ eV}, \quad T_e = 0.2 \text{ eV}, \quad \frac{T_e}{T_i} = 0.8,$$

$$v_{\text{drift}} = 1.9 c_i, \quad c_i = \left( \frac{2 m_e T_i}{m_i} \right)^{1/2},$$

$$n = 3.5 \cdot 10^9 \text{ cm}^{-3}$$

The perturbation at the grid position,  $g(v)$ , was then measured as described in ref. 8.  $g(v)$  has the data:

$$T_1 = 0.25 \text{ eV}$$

$$V_{\text{drift}} = 2.4 \cdot c_1.$$

The oscillating amplitude on the grid was made small enough ( $\Delta V = 0.1 \text{ V}$ ) to ensure linear excitation.

Then the perturbed distribution function  $f(x,v)$  was measured versus  $x$  by moving the analyser.

In Fig. 4a are shown the calculated curves and measured points for amplitude and phase of the ion flux. In figs. 4b-d corresponding curves and points are shown for  $f(x,v)$  at three velocities:

$$v = 3.1, \quad 2.8, \quad \text{and} \quad 2.1 \cdot c_1.$$

According to theory,  $f(x,v,t)$  is undamped in a collision-less plasma. In practice a damping will take place because of the finite resolution of the energy analyser. As seen, the damping is much less than for the flux curves. Because of the measuring technique the resolution varies inversely proportionally to  $v$ . This might be the reason for the relatively strong damping of  $f(x,v)$  in 4d with the lowest velocity. But apart from this, the experimental points of the amplitude seem to indicate collective effects for small  $x$ -values. In case of freely streaming particles, the amplitude should be independent of  $x$ .

In conclusion we may still say that the propagation properties of ion acoustic waves in the case where  $\theta \lesssim 1$  are mainly caused by freely streaming particles, and only slightly affected by collective effects.

#### Acknowledgements

The authors want to thank L. Prahm for help with the measurements, and L. Prahm and H. Pecseli for discussions on the theoretical part.

#### References

1. R.W. Gould, Phys.Rev. 135, 991 (1964)
2. J.L. Hirshfield and J.H. Jacob, Phys.Fluids 11, 411 (1968)
3. J.L. Hirshfield, J.H. Jacob, and D.E. Baldwin, Phys.Fluids 14, 615 (1971)
4. S.A. Andersen, G.B. Christoffersen, V.O. Jensen, P. Michelsen, and P. Nielsen, Phys.Fluids 14, 990 (1971)



5. R.J. Taylor, D.R. Baker, and H. Ikezi, *Phys.Rev.Letters* 24, 206 (1970)
6. H. Ikezi and R.J. Taylor, *Phys.Fluids* 12, 2348 (1970)
7. S.A. Andersen, V.O. Jensen, P. Michelsen, and P. Nielsen, *Phys.Fluids* 14, 728 (1971).
8. G.B. Christoffersen, in *Risø Report No. 250* (1971) 55-62.

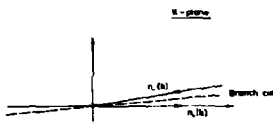


Fig. 1. Integration contour

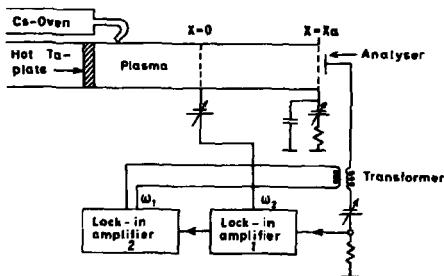


Fig. 2. Experimental set-up

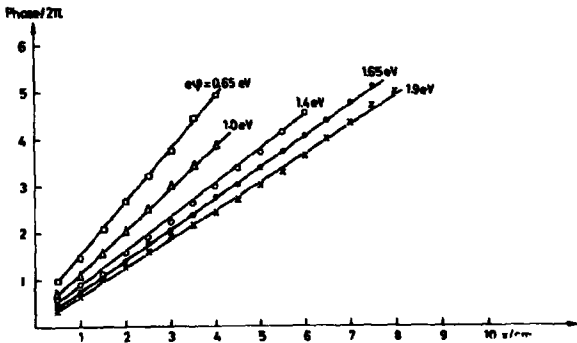


Fig. 3. Phase of  $f(x, v)$  versus  $x$ . Frequency 100 kHz,  $v = (2e\phi/m_e)^{1/2}$

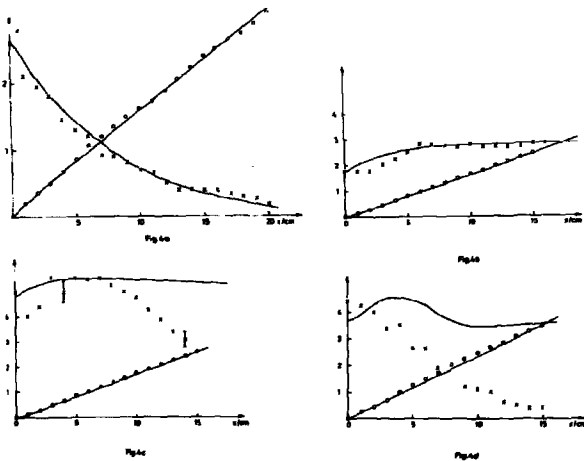


Fig. 4. Amplitude,  $x$ , and phase,  $\phi$ , of: a, ion flux; b-d, perturbed ion distribution function  $f(x, v)$ ; b,  $v = 3.1 \cdot c_1$ ; c,  $v = 2.8 \cdot c_1$ ; d,  $v = 2.1 \cdot c_1$ . Frequency 30 kHz. The amplitude is in arbitrary units, the phase is in units of  $2\pi$

SIMULATION OF PSEUDOWAVES AND ION ACOUSTIC WAVES

K. ESTABROOK, I. ALEXEFF

Oak Ridge National Laboratory  
Oak Ridge, Tennessee 37830, U.S.A.

---

ABSTRACT

The time evolution of the ion distribution is numerically calculated from the ion Vlasov and Poisson equations for oscillating negative potentials applied to a grid. The electron density model is  $\exp(e\phi/kT_e)$ . It is found that pseudowaves dominate the ion acoustic waves for frequencies greater than  $f_{pi}$  and grid potential less than  $-T_i$ . For frequency  $.25 f_{pi}$ , temperature ratio  $T_e/T_i > 1$ , and maximum potential  $-kT_e/e$ , the ion acoustic waves marginally dominate the pseudowaves.

---

A great deal of experimental research has been reported on ion waves excited by a negative time varying potential applied to a grid immersed in a plasma<sup>1-6</sup>. At frequencies greater than the ion plasma frequency, waves were observed with a speed greater than the ion acoustic speed and with very little damping in contrast to theory<sup>1</sup>. Such waves had a velocity which were independent of exciting amplitude but which did depend on  $(\omega x/a_i)^{1/3}$  where  $\omega$  is the frequency,  $x$  is the distance from the grid and  $a_i$  is the ion thermal velocity<sup>2</sup>. When excited by negative pulses of width greater than  $1/\omega_{pi}$ , the waves had a velocity maximum of  $\sqrt{2e\phi(\text{grid})/m_i}$  and a minimum of near zero<sup>3</sup>. Thus the wavelength was a function of distance. It was suggested that these fast waves were free streaming bursts of ions<sup>4,5</sup>.

The theoretical problem of describing a plasma surrounding a negative grid is inherently non-linear even for low excitation potentials since the electric field and velocity gradient of the distribution function changes very quickly in the sheath.

The purpose of this paper is to present the result of a series of numerical solutions to the one dimensional, non-linear, ion Vlasov-Poisson equations to determine the ion distribution function about a grid with time varying negative potential applied.

The equations to be solved are :

$$\text{ion Vlasov equation : } \frac{\partial f}{\partial t} + v \frac{\partial f}{\partial x} - \frac{e}{M} \frac{\partial \phi}{\partial x} \frac{\partial f}{\partial v} = 0$$

$$\text{electron thermal equilibrium : } n_e = n_0 \exp [e\phi/kT_e]$$

$$\text{Poisson's equation : } \frac{\partial^2 \phi}{\partial x^2} = \frac{e}{\epsilon_0} [n_e - \int_{-\infty}^{\infty} f dv]$$

where  $f$  is the ion distribution function,  $n_e$  is the electron density,  $T_e$  is the electron temperature, and  $\phi$  is the potential.  $f(x,v)$  is represented as numbers at discrete points at intervals  $\delta x$  and  $\delta v$  on the one dimensional phase space plane, typically three, two dimensional matrices of 71 to 251 points in  $x$  space and 65 to 301 points in  $v$ , space are stored in the computer, for the past, present and future  $f(x,v,t)$ . The future  $f(x,v,t+\delta t)$  is found from the past  $f(x,v,t-\delta t)$  from the present derivatives by the following recursion formula<sup>6</sup>:

$$f(x,v,t+\delta t) = f(x,v,t-\delta t) - \frac{\delta t}{\delta x} v [f(x+\delta x,v,t) - f(x-\delta x,v,t)] + \frac{\delta t}{2\delta x \delta v} \frac{e}{M} [\phi(x+\delta x,t) - \phi(x-\delta x,t)] [f(x,v+\delta v,t) - f(x,v-\delta v,t)]$$

After the future is found for all the points, the future array  $f(x,v,t+\delta t)$  is loaded into the present, the new ion density is found, Poisson's equation is solved and the process repeats itself with the new potential. There are 250 to 628 timesteps per ion plasma period. Since  $f$  is not represented as the continuous function that in nature it very nearly is, unphysical numerical instabilities arise that are smoothed by means of an upstream downstream algorithm to advance the distribution function every third timestep<sup>6-7</sup>.

The simulation results will be presented in four parts. First, pseudowave excitation by a negative oscillating potential  $kT_e/e \gg kT_i/e$ , frequency  $2 f_{pi}$ ; second, pseudowave and ion acoustic wave generation by oscillating potential  $kT_e/e \gg kT_i/e$ , frequency  $f_{pi}$ ; third, excitation by oscillating potential  $kT_i/e \ll kT_e/e$ , frequency  $f_{pi}$ ; and finally, pseudowave and ion acoustic wave generation by oscillating potential  $kT_e/e \gg kT_i/e$ , frequency  $.25 f_{pi}$ .

The plasma for all the simulations is chosen to be a Maxwellian at time zero. When a negative potential is placed on the grid, the electrons are blown out to the sheath distance  $[\epsilon_0 \phi(\text{GRID})/ne^2]^{1/2}$ . This "transient sheath"<sup>8</sup> forms in a few electron plasma periods which is short compared to the ion time scale. The electrons are considered to flow freely into and out from the

sheath region to a reservoir of isothermal electrons surrounding the grid which adds to the validity of the isothermal electron model.

Ions in the negative potential well are accelerated by the negative potential and then are released as the potential is made more positive<sup>3-6</sup>. After escaping the sheath, the fast ions propagate by their own inertia. Such ballistic bursts of ions are little affected by the self consistent electric field and are consequently called pseudowaves.

Figure 1 is the ion distribution function after the potential on the grid has oscillated from zero to  $-15kT_e/e$  twice and then to  $-15kT_e/e$ . The potential on the grid is :

$$\phi(\text{grid}) = [-Z_5 + Z_5 \cos(4\pi f_{pi} t)] kT_e/e.$$

The graph plots  $f(x,v,t)$  as a function of position  $x$  and velocity  $v$  at the single point in time  $t$ . The distance scale is the ordinate and is marked in Debye lengths from the grid. The velocity scale is the abscissa and is marked in units of  $\sqrt{kT_e/m_i} = v_a$  from zero velocity at the center. The ions on the left move up and the ions on the right move down. Each line within the graph is the velocity distribution  $f(\text{fixed } x, v, \text{ fixed } t)$  at the single plane in space indicated by the intercept of the line with the  $x$  axis. The height of the line above its  $x$  intercept is the phase space density  $f(x,v)$ .

The pseudowave farthest from the grid was generated during the first oscillation, the next pseudowave was generated by the second oscillation and the sheath about the grid at the time of fig.1 is produced by the  $-15kT_e/e$  potential on the grid. If the potential were allowed to oscillate to zero after this time, the fast ions in the sheath would free stream to form the third pseudowave. At this time and distance from the grid, no ion acoustic-wave is observed. The maximum velocity of the pseudowaves is less than  $\sqrt{2e\phi_{\text{max}}(\text{grid})/m_i}$  since the ions are retarded as they leave the grid region by the slowly rising potential.

If the excitation amplitude is dropped to  $-kT_e/e = -30kT_i/e$ , then both ion acoustic waves and pseudowaves may be observed on the distribution function. The density perturbation, however, is dominated by the pseudowaves. Fig.2 shows the

ion distribution function after the following potential was applied to the grid :

$$\phi(\text{grid}) = -0.5 kT_e/e, \quad 0 < t < 2/f_{pi}$$

$$\phi(\text{grid}) = [-.5 + .5 \sin(2\pi f_{pi} t)] kT_e/e \quad 0 < t < 5/f_{pi}$$

Three pseudowaves may be clearly seen outside the near Maxwellian and an ion acoustic wave may be seen in the near Maxwellian between 10 and 25 Debye lengths. The density perturbation is still dominated by the pseudowaves.

If the amplitude of the oscillating potential is reduced to the ion temperature, then the ion acoustic waves emerge first and may be clearly separated from the pseudowaves which follow.

The exciting potential used to generate the exciting potential used in fig.3 is the following :

$$\phi(\text{grid}) = -.5 kT_i/e, \quad 0 < t < 1/f_{pi}$$

$$\phi(\text{grid}) = [-.5 + .5 \sin(2\pi t f_{pi})] kT_i/e, \quad (1 < t < 4)/f_{pi}$$

$$\phi(\text{grid}) = -.5 kT_i/e, \quad (4 < t < 10)/f_{pi}$$

The ion acoustic waves in figure 3 can only be seen with difficulty. Figure 4 shows the perturbation [ $f(x,v) - f(\text{Maxwellian})$ ] of figure 3. The ion acoustic waves are seen to be in the form  $f_1(v) \approx \overbrace{v^2}^{v=0}$ , that is in the form of a shifted Maxwellian.

There are density maxima at 3.4, 8.6, and 13.8  $\lambda_D$  and density minima at 5.6 and 11.6 Debye lengths. The electric field is at a maximum between the density maxima and minima and drives the ion acoustic wave to advance 1/4 wavelength, 1/4 ion plasma period later. The pseudowaves emerging later in time (since they are slower than the ion acoustic speed) are not considered ion acoustic waves since they are not coherently driven by an electric field even though the pseudowaves do have electric fields with them. Note that the pseudowaves are faster than  $\sqrt{2e\phi_{\text{max}}(\text{grid})/m_i}$  due to thermal spread.

A computer plot (fig.5) of the ion density vs. time at 9 Debye lengths shows the ion acoustic waves followed by the pseudowaves. Laboratory verification of this effect has been observed as shown in fig. 6. The oscillogram shows the ion acoustic waves followed by the pseudowaves in the same form as the simulation.

If the exciting frequency is much less than the ion plasma frequency, the ion acoustic waves will dominate the pseudowaves for excitation potential  $kT_e/e$ . Fig.7 shows the ion distribution function after 3 voltage oscillations on the grid from zero to  $-kT_e/e$  at frequency  $.25/f_{pi}$ . Two pseudowaves may be seen parallel to the Maxwellian. The slower pseudowave is the tail of the first pseudowave generated. A faster pseudowave is the second to be generated. A third pseudowave may be seen moving away from the grid where it has been generated. The front of the second pseudowave is about to detach from its "tail" and will beat with the ion acoustic wave since its velocity is slightly faster than  $v_A$ .

In conclusion, time varying potentials applied to a grid inherently produce free streaming bursts. For frequency  $\approx f_{pi}$ , ion acoustic waves may be separated from the pseudowaves on a tone burst basis if a low excitation potential is used. For frequencies  $< f_{pi}$ , ion acoustic waves marginally dominate the pseudowaves for low excitation potentials. However pseudowaves are also generated and may beat with the ion acoustic waves to produce what may appear to be non-linear Landau damping.

#### ACKNOWLEDGEMENT.

This research was sponsored by the U.S. Atomic Energy Commission under contract with Union Carbide Corporation.

It is a pleasure to acknowledge many valuable conversations with L.A. BERRY, J.M. BUZZI, H.J. DOUCET, O.C. ELDRIDGE, M. FEIX, E.G. HARRIS, K. LONNGREN, M. WIDNER and W.R. WING.

REFERENCES

1. G.M. SESSLER, G.A. PEARSON,  
Phys. Rev. 162, 108 (1967).
2. H.J. DOUCET, D. GRESILLON,  
Phys. Fluids, 13, 773, (1970).
3. I. IKEZI, R.J. TAYLOR,  
J. Appl. Phys., 41, 738, (1970).
4. I. ALEXEFF, W.D. JONES, M. WIDNER,  
Phys. Fluids, 13, 1519 (1970).
5. K. LONNGREN, D. MONTGOMERY, I ALEXEFF, W.D. JONES,  
Phys. Letters, 25A, 79 (1968) ;  
H.J. DOUCET, D. GRESILLON,  
Phys. Letters, 28A, 257, (1968) ;  
Y. YAMASHITA, H. IKEZI, N. SATO, N. TAKAHASHI,  
Phys. Letters, 27A, 79 (1968) ;  
I. ALEXEFF, W.D. JONES, K. LONNGREN,  
Phys. Rev. Letters, 21, 878, (1968).
6. K. ESTABROOK,  
PH.D. Thesis, University of Tennessee, Knoxville,  
TENNESSEE, U.S.A., (1971).
7. R.D. RICHTMYER, K.W. MORTON,  
"Difference methods for initial value problems",  
Interscience, Wiley, New-York, 1969).
8. I. ALEXEFF, W.D. JONES, K. LONNGREN, D. MONTGOMERY,  
Phys. Fluids, 14, 1792, (1971).



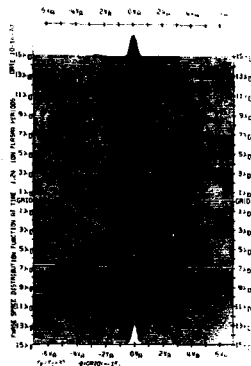


FIG. 1 - Two pseudowaves plus a sheath generated by a negative potential of amplitude  $15kT_e/e$  and frequency  $2f_{pi}$ .



FIG. 2 - Three pseudowaves produced by a negative oscillating potential of amplitude  $kT_e/e$  and frequency  $f_{pi}$ . Part of an ion acoustic wave may be observed between 10 and  $25\lambda_D$ .

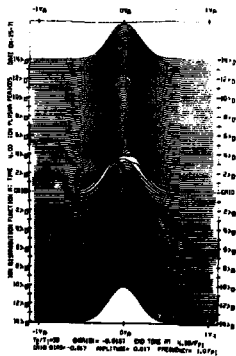


FIG. 3 - Ion distribution function of three pseudowaves and ion acoustic waves.



FIG. 4 - Amplified perturbation to distribution function of fig. 3. Waves on both sides of velocity space are the ion acoustic waves and the ridges moving away from the grid are the pseudowaves.

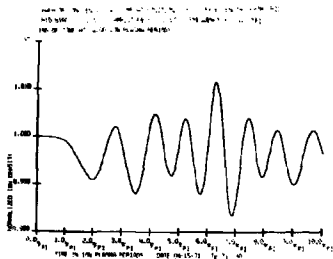


FIG.5 - Computer oscillogram of ion acoustic waves followed by pseudowaves.

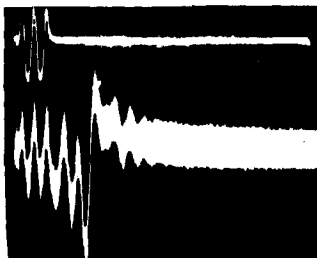


FIG.6 - Laboratory oscillogram of ion acoustic waves. At  $15\lambda_D$  from grid. The exciting potential applied to the grid was a negative oscillating voltage of amplitude  $4kT_1/e$  and frequency  $f_1$ .



FIG.7 - Ion acoustic waves and pseudowaves produced by three cycles of negative potential applied to the grid.

Excitation of Ion-Acoustic Waves by Parametric Heating and Strong High-Frequency Fields

by

R. H. Abrams, Jr., T. Ohe and H. Lashinsky

University of Maryland, College Park, Maryland USA

Abstract

Parametric excitation of ion-acoustic waves has been demonstrated in the bounded plasma column in a single-ended Q-machine. The electron temperature is controlled by radio-frequency heating and is varied periodically by amplitude modulation of the radio-frequency power at a modulation frequency equal to twice the frequency of the ion-acoustic wave, causing the ion-acoustic velocity to be modulated at this same frequency. The experimental results are in agreement with an analysis based on the Mathieu equation and the linear ion-acoustic damping can be directly related to the threshold value of the modulation index. Similar results are obtained with microwave heating of the electrons. Parametric excitation provides a convenient method for the excitation of ion-acoustic waves for experimental purposes and can also be used in diagnostic applications.

The parametric excitation of a resonance in a physical system can be described by the Mathieu equation<sup>1</sup>, in which a suitable time-periodic coefficient is used to represent the periodic variation of the system parameter that corresponds to the "restoring force." When this parameter is modulated at a frequency  $\omega_1$  a resonance at the frequency  $\omega_0$  can be excited when  $\omega_1 = 2\omega_0/n$ , where  $n$  is an integer. The classic experiment in parametric excitation is the Melde' experiment<sup>2</sup>, in which transverse oscillations of a string (one end fixed and the other tied to a longitudinally vibrating support) are observed when the propagation velocity i.e., the string tension  $S$ , is modulated periodically at a frequency  $\omega_1 = 2\omega_0$ , where  $\omega_0$  is the resonance frequency;  $S = S_0(1 - M \cos \omega_1 t)$  where  $M$  is the modulation index, which must exceed some threshold value in order for excitation to occur.<sup>1</sup> Parametric amplifiers are, of course, also well-known in electronics and quantum optics.<sup>3</sup>

In this paper we report the experimental observation of parametric excitation of ion-acoustic waves in a plasma in which the ion-acoustic velocity

i.e., the electron temperature, is modulated periodically; it is found that the behavior of the excited waves follows closely the predictions of the Mathieu analysis.<sup>4</sup> The work reported here will thus be recognized as a plasma analog of the classic Melde' experiment.

Parametric effects have been observed in plasma experiments on drift waves in which the plasma is perturbed by a monochromatic external signal which excites an intermediate pump mode.<sup>5</sup> The intermediate pump mode couples energy from the external pump field into the resonant plasma modes through the time variation of an unspecified plasma parameter. However, it is necessary to know the nonlinear mode-mode coupling coefficient and the identity of the time-varying parameter in order to relate the losses in the system to the threshold power required for excitation. Parametric excitation of the ion-acoustic waves in a plasma has also been reported in an experiment in which the boundary conditions are varied periodically in time.<sup>6</sup> A feature of the work reported here, on the other hand, is the fact that the losses in the system can be directly related to the threshold value of the modulation index of the time-varying parameter, which is known to be the electron temperature.

We consider the propagation of ion-acoustic waves in a finite plasma column that is bounded at both ends by material boundaries. The waves are described by a wave equation in which the phase velocity is given by  $c_s = (\kappa T_e / m_i)^{1/2}$  ( $\kappa$  is the Boltzmann constant,  $T_e$  is the electron temperature, and  $m_i$  is the ion mass). It is assumed that the electron temperature varies as  $T_e = T_e^0 (1 - M_T \cos \omega_1 t)$ , where  $T_e^0$  is the steady-state electron temperature,  $M_T$  is the temperature modulation index ( $M_T < 1$ ), and  $\omega_1$  is the modulation frequency. If the wave equation in the finite plasma column is Fourier-analyzed in space, subject to the appropriate boundary conditions at the ends of the column, the system can be described in terms of discrete normal modes with frequencies  $\omega_0^2 = k_z^2 \kappa T_e / m_i$ , where  $k_z$  is the longitudinal wave number.<sup>7,8</sup> The resonant ion-acoustic modes are standing waves with fundamental wavelength equal to  $2L$ , where  $L$  is the length of the column, so that  $k = n\pi/L$  for the fundamental mode. The equation that describes the time behavior of a given Fourier mode is

$$\frac{d^2 x}{dt^2} + 2\alpha \frac{dx}{dt} + \omega_0^2 (1 - M_T \cos \omega_1 t) x = 0, \quad (1)$$

where the quantity  $x$  represents a characteristic variable of the ion-acoustic wave, say the density, and the phenomenological term  $2\alpha$  is introduced to take account of losses in the system due to Landau damping, end effects, etc.

Equation (1) can be reduced to the standard form for the Mathieu equation

if the first-order term is eliminated by the transformation  $x = ye^{-\alpha t}$ . With the new parameters  $a \equiv (4/\omega_1^2) (\omega_0^2 - \alpha^2)$  and  $q \equiv 2M_T \omega_0^2 / \omega_1^2$ , and the new independent variable  $s = \omega_1 t / 2$ , Eq. (1) becomes

$$\frac{d^2 y}{ds^2} + (a - 2q \cos 2s)y = 0, \quad (2)$$

which exhibits a resonance at the fundamental frequency  $\omega_0$  when  $\omega_1 = 2\omega_0$ .

For a parametric system with dissipation, such as described by Eq. (1), it can be shown that growing oscillations can be excited only if<sup>1</sup>

$$M_T > 4\alpha/\omega_0. \quad (3)$$

This threshold criterion corresponds to the requirement that the time-averaged energy pumped into the resonant mode must exceed the time-averaged losses if the mode is to grow.

The experiments described here were carried out in a single-ended Q-machine operated under collisionless conditions with the following typical plasma parameters: electron density  $10^9 \text{ cm}^{-3}$ , ionizer temperature  $2200^\circ \text{K}$ , column length 20-60 cm, magnetic field 2000 G, and mean-free paths for ions and electrons, about 100 cm.

An rf heating technique, first reported by Demirkhanov *et al.*<sup>9</sup>, is used to control the electron temperature. In this method an rf voltage (7 MHz) is applied directly to the cold endplate that terminates the plasma column. Although the rf heating mechanism is not completely understood, it is found that the application of the rf voltage increases the effective temperature of the plasma, as reported by Demirkhanov. Evidence for an increased electron temperature is provided by two independent methods. First, for a constant rf frequency it is observed that  $\omega_0$ , the frequency of the ion-acoustic mode, increases with increasing rf voltage, reaching a saturation point at high rf voltages. (The present experiments are performed for parameter values such that the experimental mode frequency is proportional to the rf voltage,  $V_{\text{rf}}$ , so that  $T_e^0$  is proportional to  $V_{\text{rf}}^2 = [V_{\text{rf}}^0 \cos \omega_{\text{rf}} t]^2$ .) Second, the electron temperature, as determined from Langmuir probe characteristics, is found to increase monotonically with  $V_{\text{rf}}$ .

Modulation of the electron temperature for the parametric excitation experiments is accomplished in a straightforward way by amplitude modulation of the rf voltage applied to the endplate. Because of the quadratic dependence of the temperature on the rf voltage noted above  $M_T = 2M_V / (1 + M_V^2/2)$ , where  $M_V$  is the voltage modulation index. In the present experiments the rf source is a low-power commercial transmitter provided with a built-in modulator, typical rf voltages actually applied to the plate being approximately 5 V.

The rf power is applied to the endplate through a transmission line which is terminated in its characteristic impedance. As in Ref. 9 it is found that the drift wave is quenched at rf voltage levels one to two orders of magnitude below those used for rf heating.

The experiments are carried out as follows. The resonant frequency of the ion-acoustic mode without rf heating,  $\omega_0$ , is known approximately from earlier work in which the modes were excited by passing current through the plasma.<sup>8,10</sup> It is also found, as reported by Demirkhanov, that oscillations that satisfy the dispersion relations for ion-acoustic waves are observed at rf power levels much higher than those used in the parametric pumping experiments. The phase velocity of these waves is the ion-acoustic velocity and the frequencies are inversely proportional to the column length and are independent of the magnetic field; these waves exhibit all of the properties of the ion-acoustic waves reported earlier.<sup>8</sup> Parametric excitation is then accomplished at low rf power levels by modulating the rf voltage at a frequency approximately equal to twice the estimated mode frequency.

As the modulation frequency is swept through the parametric resonance frequency for various values of the modulation index  $M_T$ , a signal from a negatively biased Langmuir probe shows the instability growing from the thermal noise level. Figure 1 is a raster display<sup>11</sup> for a large value of  $M_T$ . The parametric resonance at  $\omega_0$  when  $\omega_1 \approx 2\omega_0$  is shown in Fig. 1a. On the other hand, an ac voltage at the modulation frequency applied directly to the endplate does not excite the mode, indicating that the resonance is not produced by a sheath effect. This result is shown in Fig 1b.

In order to provide a comparison between the experimental results and the well-known stability diagram associated with the Mathieu equation a tone-burst technique is used to map out the zones of stability and instability in the  $a$ - $q$  plane associated with Eq. (2). In this case the modulation signal is applied to the rf generator through a tone-burst generator so that the rf voltage at the endplate is modulated in bursts. When the modulation is gated on the oscillation either grows or is damped, depending on the location of the coordinates  $a$  and  $q$  in the stability diagram. Figures 2a and 2b show this behavior for two sets of values of  $a$  and  $q$  that correspond to growth and damping, respectively. This is believed to be the first experimental observation of parametric damping in the literature. The locus of experimental points at which the modulation burst has no visual effect on the background is then

taken to be the stability boundary between regions of stability and instability. The tone-burst technique also offers a convenient method for the measurement of growth and damping rates, as can be seen from the expanded trace in Fig. 2c.

A comparison of theory and a preliminary experiment is shown in Fig. 3. This figure shows the stability diagram for the Mathieu equation with four theoretical stability-boundary curves, plotted for various values of the loss parameter  $\alpha/\omega_0$  as noted in the figure. The experimental points in the figure indicate sets of values of  $a$  and  $q$  that correspond to the stability boundary as obtained by the tone-burst technique described above. It is evident that a reasonable fit for this particular case can be obtained for  $\alpha/\omega_0 = 0.05$ . We note that most of the experimental points used in fitting the curve lie in the wings of the curve. The loss parameter  $\alpha/\omega_0$  can also be determined from  $q_{\min}$  i.e., the minimum value of  $q$  for which excitation occurs in Fig. 3. Inspection of Fig. 3 gives  $q_{\min} \approx 0.08$ . Now, using the definition of  $q$  given in connection with Eq. (2) together with the criterion in Eq. (3) and the parametric resonance condition  $\omega_1 = 2\omega_0$ , we find  $\alpha/\omega_0 = 0.04$ . The qualitative agreement between these two determinations of the loss parameter  $\alpha/\omega_0$  is regarded as satisfactory in view of the preliminary nature of these experiments and indicates consistency between the shape of the experimental parametric resonance curve and the experimental excitation threshold.

These results indicate that ion-acoustic waves in a bounded plasma can be described phenomenologically by an extension of concepts used in the analysis of lumped-parameter systems.<sup>7</sup> Parametric excitation also provides a technique for the determination of growth rates under various plasma conditions and appears to be a useful method for the excitation of ion-acoustic waves when other methods are not desirable.

We are indebted to Dr. R. M. Goldman for discussion and R. M. Monblatt and W. E. Crowe for help in the experiments. This work was supported by the U. S. Atomic Energy Commission [AT-(40-1)-3405] and the U. S. Air Force Office of Scientific Research [AF-1016-69].

References

- \* Present address: Aeronomy Laboratory, ERL, ESSA, Boulder, Colorado.
1. N.W. McLachlan, Theory and Application of Mathieu Functions, Dover Publications, New York, 1964.
  2. J.W. Strutt, Lord Rayleigh, Phil. Mag. 24, 147, (1887).
  3. W.H. Louisell, Coupled Mode and Parametric Electronics, John Wiley, New York, 1960.
  4. E.J. Yadlowsky, Ph.D. Thesis, Institute for Fluid Dynamics and Applied Mathematics, University of Maryland, 1970.
  5. A.Y. Wong, M.V. Goldman, F. Hai and R. Rowberg, Phys. Rev. Letters 21, 518 (1968).
  6. H. Tanaka and S. Watanabe, J. Phys. Soc. Japan 24, 969 (1968).
  7. H. Lashinsky, in Nonlinear Effects in Plasmas, G. Kalman and M. Feix ed., Gordon and Breach, New York, 1969.
  8. E.J. Yadlowsky, R.H. Abrams, Jr., and H. Lashinsky, Proc. 2-nd International Conference on the Physics of Quiescent Plasmas, Ecole Polytechnique, Paris, 1969.
  9. R.A. Demirkhanov, G.L. Khorasanov and I.K. Sidorova, ZhETF Pis'ma Red. 6, 861 (1967) [JETP Letters 6, 300 (1967)]; R.A. Demirkhanov, G.L. Khorasanov and I.K. Sidorova, in Proceedings of 3-rd International Conference on Plasma Physics and Controlled Nuclear Research, Novosibirsk, U.S.S.R., 1968 (International Atomic Energy Agency, Vienna, Austria, 1969).
  10. N.A. Buchel'nikova, R.A. Salimov and Yu. I. Eidel'man, Nuclear Fusion 6, 255 (1966).
  11. H. Lashinsky, in Proceedings of 2-nd International Conference on Plasma Physics and Controlled Nuclear Fusion Research, Culham, England, 1965 (International Atomic Energy Agency, Vienna, Austria 1966).



Figure Captions

Fig. 1a. Raster display showing the excitation of the ion-acoustic wave at 4 kHz when the frequency at which the electron temperature is modulated is varied between 6 and 12 kHz. The raster is formed by using the output signal from a spectrum analyzer to intensity-modulate an oscilloscope whose horizontal sweep is synchronized with the sweep of the spectrum analyzer. The spectrum analyzer displays simultaneously the ion-acoustic mode and the modulation signal. The oscilloscope trace is moved vertically at a slow constant rate as the modulation frequency is varied.<sup>11</sup> Fig. 1b. Raster display showing the absence of ion-acoustic waves when the modulation voltage is applied directly to the cold endplate.

Fig. 2. Photographs showing the parametric excitation and parametric damping of an ion-acoustic wave at 8.0 kHz when the modulation of the electron temperature ( $\sim 50\%$ ) is gated on and off through the use of the tone-burst technique described in the text. In Fig. 2a the amplitude and frequency of the modulation correspond to parameter values that lie in the parametric excitation region of the stability diagram associated with the appropriate Mathieu equation, with the temperature modulated at 15.6 kHz. In Fig. 2b the parameters lie in the parametric damping region, with modulation at 9.8 kHz, and the background noise level is reduced by the parametric effect. Figure 2c, with an expanded sweep, shows the details of the growth of the unstable mode. Time scales: Fig. 2a, 1 msec/cm; Fig. 2b, 2 msec/cm; Fig. 2c, 0.5 msec/cm. Time increases from left to right.

Fig. 3. Stability diagram and experimental points for parametric excitation of ion-acoustic waves in a bounded plasma. Stable regions are shown by cross-hatching and the two straight lines denote the stability boundaries for a lossless plasma while the curved lines denote the stability boundaries for various values of the loss parameter  $\alpha/\omega_0$  as indicated in the diagram. The experimental points indicate combinations of the amplitude and frequency of modulation of the electron temperature that correspond to neutral stability. The parameters in the Mathieu equation [Eq. (2)] are defined by  $a \equiv (4/\omega_1^2)(\omega_0^2 - \alpha^2)$  and  $q \equiv 2M_T \omega_0^2/\omega_1^2$ , where  $\omega_0$  is the mode frequency,  $\omega_1$  is the pump frequency,  $\alpha$  is the loss term, and  $M_T$  is the temperature modulation index.



Fig. 1

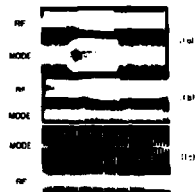


Fig. 2

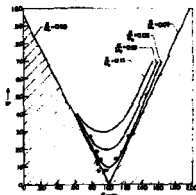


Fig. 3

Collective Interaction and Freely Streaming Ions  
in Density Perturbations and Waves in Q-Machines

by

V. O. Jensen

Danish Atomic Energy Commission  
Research Establishment Risø, Roskilde, Denmark

Abstract

The propagation properties of grid-excited density perturbations and ion waves in single-ended Q-machines are calculated from the linearized Vlasov equation. The calculations are exact as they take into account the dielectric properties of the plasma as well as the ion velocity distribution in the density perturbation at the grid. The results are compared with the approximate ones obtained in a normal Landau treatment in which only dielectric properties are considered. The effect of collective interaction compared with that of freely streaming ions is discussed.

Text

This paper discusses the propagation properties of grid-excited longitudinal density disturbances in Q-machine plasmas. Emphasis is on the extent to which the properties can be explained by freely streaming ions, by linear collective interaction and by non-linear effects.

It is assumed that the electrons behave isothermally and that quasi-neutrality prevails i.e. that the electric field is

$$E = - \frac{kT_e}{q} \frac{1}{n_0} \frac{\partial n}{\partial x} \quad (1)$$

where  $n_0$  is the undisturbed density. The assumption on which (1) is based is valid for slow ( $t \ll 1/\omega_{pi}$ ), long wave length ( $l \gg \lambda_D$ ) perturbations of the type which is most commonly studied in Q-machines. Use of the electron Vlasov equation instead of (1) would require more lengthy calculations, but the conclusions of this paper would not be changed.

With (1) the non-linearized ion Vlasov equation can be written

$$\frac{\partial F(x,v,t)}{\partial t} + v \frac{\partial F(x,v,t)}{\partial x} = c_e^2 \frac{1}{n_0} \frac{\partial F(x,v,t)}{\partial v} \frac{\partial n(x,t)}{\partial x} \quad (2)$$

where  $c_e^2 = kT_e/n_1$ . All other symbols have their usual meaning.

The Vlasov equation (2) is normally linearized by setting  $F(x,v,t) = f_0(v) + f(x,v,t)$  [ $f_0(v) \gg f(x,v,t)$ ], in which case it can be written

$$\frac{\partial f}{\partial t} + v \frac{\partial f}{\partial x} = c_e^2 \frac{1}{n_0} \frac{df_0(v)}{dv} \frac{\partial n}{\partial x} \quad (3)$$

The rhs term in (2) and (3) is the most interesting one as it takes into account collective interactions between the electric field and the ions.

Without this term (3) takes the form

$$\frac{\partial f}{\partial t} + v \frac{\partial f}{\partial x} = 0 \quad (4)$$

and simply describes freely streaming ions. Eq. (4) is obtained directly from (3) in the limit  $T_e \rightarrow 0$ .

The density associated with a perturbed velocity distribution is

$$n(x,t) = \int_{-\infty}^{\infty} f(x,v,t) dv \quad (5)$$

Recently much work has been done to demonstrate experimentally phenomena that can only be predicted from either the linearized Vlasov equation (3) or from full equation (2). The well-known works of Wong et al.<sup>1)</sup> on Landau damping of ion acoustic waves and some of the recent works on ion wave echoes are examples of experiments claimed to demonstrate collective effects as described by (3). Very recently some authors<sup>2,3)</sup> have claimed to have seen phenomena caused by non-linear effects as described by (2).

The work of Wong et al.<sup>1)</sup> has been discussed by various authors. Hirshfield and Jacob<sup>4)</sup> assumed a simple interaction mechanism between the wave-exciting grid and the plasma and could thus calculate the perturbed velocity distribution function at the grid. Assuming ions just outside the grid region to be freely streaming, they showed that the wave amplitude would decrease owing to simple phase mixing at a rate similar to that predicted by Landau damping (i.e. by collective effects). Similarly the phase velocity calculated on the basis of (4) is very close to that predicted by the linearized Vlasov equation (3). Therefore the experiments on grid-excited ion acoustic waves cannot be taken as clear-cut experimental proof of collective interaction.

We consider a single-ended Q-machine in which the ion velocity distribution function can be approximated by a drifting Maxwellian<sup>5)</sup>. Density perturbations propagating in the downstream direction are generated by varying the potential of a grid at  $x=0$ . Calculation of the ion velocity distribution  $g(v)$  in the density perturbation close to the grid is very complicated.  $g(v)$  is determined by the interaction between grid and plasma, which is a combination of absorption of ions hitting the wires, deflection or even reflection (see ref. 6) of ions passing close by the wires, and acceleration or deceleration of ions passing the sheath at the grid during the time the grid potential changes. In calculations of  $g(v)$  only the latter is normally considered<sup>4,7)</sup>. Rather than to try to calculate the shape of  $g(v)$  we use  $g(v)$

functions of the type measured by Christoffersen<sup>8)</sup>.

The following discussion is divided into two parts. First we consider a short pulse applied to the grid which thereby releases a short density pulse. The propagation of this pulse is given by a Green's function which can be calculated from (3) and (4). We give examples of the Green's function for various  $T_1/\tau_1$ -values and for various  $g(v)$ -functions. Next we consider grid-excited ion acoustic waves, whose properties are calculated as convolution integrals of the Green's functions.

Pulses. We consider a single-ended Q-machine in which the plasma flows through a grid at  $x = 0$  biased to  $\phi_0$ . The ion velocity distribution function,  $f_0(v)$ , in the downstream plasma is measured with an electrostatic analyser<sup>5)</sup>. During a short time interval,  $\Delta t$ , the grid potential is changed to  $\phi_0 + \Delta\phi$ , and the flux of ions with velocity  $v$  passing the grid is changed from  $v f_0(v)$  to  $v(f_0(v) + g(v))$ , [ $g(v) \ll f_0(v)$ ]. The propagation properties of the released density perturbation can be calculated as an initial value problem with  $f(x, v, t=0) = \Delta t v g(v) \delta(x)$ . By applying Laplace transformation in time and Fourier transformation in space to (3) we get

$$n(k, \omega) = - \frac{\Delta t \int_{-\infty}^{\infty} \frac{v g(v)}{\omega/k - v} dv}{1 + \frac{c_s^2}{v_0} \int_{-\infty}^{\infty} \frac{f_0(v)}{\omega/k - v} dv} = - \frac{\Delta t}{ik} H\left(\frac{\omega}{k}\right) \quad (6)$$

The inverse transformation of (6) can be performed with the technique described in ref. 9. We find that

$$n(x, t) = \frac{1}{t} h\left(\frac{x}{t}\right) \quad \text{and} \quad f(x, v, t) = \frac{1}{t} k\left(\frac{x}{t}, v\right) \quad (7)$$

i.e. pulses propagate in a self-similar manner. Functions  $h$  and  $k$  depend on  $f_0$  and  $g(v)$ . We shall show and discuss some examples of calculated  $n(x, t)$  and  $f(x, v, t)$ .

Fig. 1a shows the results obtained when  $f_0(v)$  and  $g(v)$  have the form  $\exp(-v/1.7 c_1)^2 / c_1^2$  (drifting Maxwellian with drift velocity  $1.7 c_1$ ) and when  $T_2=0$  (freely streaming ions). Shown are  $tn\left(\frac{x}{t}\right)$  and  $tf\left(\frac{x}{t}, v\right)$  for four  $v$ -values. In the calculations it was assumed that the  $f$ -curves were measured with an analyser with resolution  $c_1/4$ . Fig. 1b shows the same functions calculated for  $T_2=0.74 T_1$ . Comparison between a) and b) shows the effect of the interaction term in (3): a narrowing of the  $n$ -curves and "undershoot" on the  $f$ -curves. The narrowing of the  $n$ -curve is not very pronounced, and its shape is found to depend strongly on  $g(v)$ , which is difficult to measure experimentally.  $n$ -measurements therefore do not clearly indicate collective inter-

action. As shown in ref. 10, the undershoot is caused by collective deceleration of ions behind the pulse. This undershoot was demonstrated experimentally in ref. 9, and so was the self-similarity.

The curves in fig. 2 show the effect of changing the drift velocity of the ions in the perturbation. These curves were calculated for  $f_0(v)$  with the same form as in fig. 1, but with  $g(v)$  as a fast drifting Maxwellian of the form  $\exp(-(v-4c_1)^2/c_1^2)$ . By comparing the curve for  $T_0=0$  with fig. 1a one sees that the only effect of increasing the drift velocity of  $g(v)$  is that the pulse moves faster and thus appears earlier. This is expected because with  $T_0=0$  the ions are freely streaming. By comparing the two curves in fig. 2 we again see the effect of collective interaction: a narrowing of the density curve. In fig. 2, however, the effect of the collective interaction is much weaker than in fig. 1. The reason is clear: The propagation velocity of the pulse is essentially equal to the drift velocity of  $g(v)$  ( $=4c_1$ ). The collective interaction term in (3) is proportional to  $f_0^2(v)$  for  $v \lesssim 4c_1$ . At such high velocities  $f_0^2$  is very small, and the interaction term therefore becomes unimportant. We can therefore conclude that if  $g(v)$  has a drift velocity very different from that of  $f_0(v)$ , the ions in the perturbation will move through the plasma as nearly freely streaming particles.

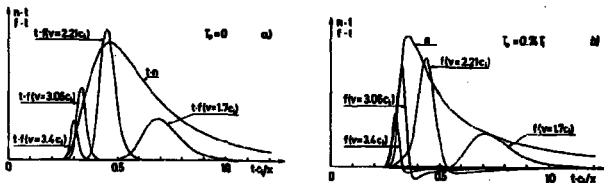


Fig. 1. Density and ion velocity distribution function in pulses.

$$v_{\text{drift}, f_0} = v_{\text{drift}, g} = 1.7 c_1$$

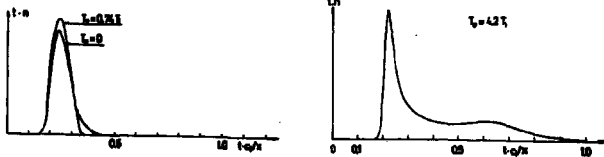


Fig. 2. Density in pulses.

$$v_{\text{drift}, f_0} = 1.7c_1 \quad v_{\text{drift}, g} = 4c_1$$

Fig. 3. Density in pulses.

$$v_{\text{drift}, f_0} = v_{\text{drift}, g} = 3c_1$$

The  $n$ -curve in fig. 3 is calculated for  $f_0(v)$  and  $g(v)$  as Maxwellians with drift velocity  $3c_1$  and  $T_e/T_i = 4.2$ . In this case we find a second maximum on the curve at  $tc_1/x \sim 0.6$ . To understand physically what causes this we calculated the curves in fig. 4. They show the quantities  $n$  as functions of  $x/t \cdot c_1$  for various  $T_e/T_i$ -values.  $f_0(v)$  and  $g(v)$  are drifting Maxwellians with drift velocity  $4c_1$ . For  $T_e/T_i \ll 1$  the collective interaction term in (3) is small, and the density perturbation propagates as a single pulse whose shape is almost only determined by the freely streaming particles in  $g(v)$ . As  $T_e/T_i$  is increased, the density perturbation splits up into two pulses. This splitting up is caused by the collective interaction term getting stronger and stronger. Seen from a system of reference moving with the drift velocity we get two pulses, one moving in each direction with the same speed. This is what one would expect when a density perturbation is excited in a medium with high restoring force. Note that we see both pulses on the downstream side only if the drift velocity of the plasma is higher than the propagation velocity of the pulse. Because of the  $t^{-1}$ -dependence the second pulse will occur at a probe in the plasma with a much smaller amplitude than that of the first pulse. This is in agreement with fig. 3. Some evidence, but not clear-cut proof, of this splitting-up has been seen in experiments at the Rice Q-machine.

Waves. When a sinusoidal potential with frequency  $\omega$  is applied to a biased grid in a plasma, an ion acoustic wave is generated. In calculating the propagation properties of waves we used the Green's function (?) and performed convolution integrals of the form

$$n_p(x,t) = \int_{-\infty}^t \exp(-\omega t') \frac{1}{t-t'} h\left(\frac{x}{t-t'}\right) dt'$$

The amplitude,  $amp_n$ , and the phase,  $\phi_n$ , of the density are calculated as functions of the dimensionless distance,  $x/c_1$ , from the grid. In fig. 5 we present the results obtained at three  $T_e/T_i$ -values for  $f_0(v)$  and  $g(v)$  as drifting Maxwellians with drift velocity  $3c_1$ .

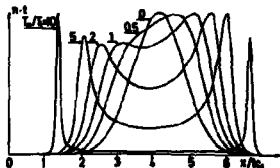


Fig. 4. Density in pulses calculated at various  $T_e/T_i$ -values  
 $v_{\text{drift}, f_0} = v_{\text{drift}, g} = 4c_1$ .

From the figure we note that close to the grid, characteristically within one wave length, the damping increases with increasing electron temperature. This feature is not found in a Landau treatment of the problem. Far away from the grid our results for  $T_e = T_i$  and  $T_e = 5T_i$  agree with those obtained by a Landau treatment. For  $T_e = 0$ , where the damping is wholly caused by phase mixing, a Landau treatment does not apply because the denominator in (6) has no zeros.

For the same values of the parameter  $T_e/T_i$  we also calculated the amplitude,  $\text{amp}_f$  and the phase,  $\phi_f$ , of the perturbed velocity distribution function,  $f(x, v, t)$ .  $\text{amp}_f$  and  $\phi_f$  are calculated for the three velocities  $v = 2.5c_i$ ,  $3c_i$  and  $3.5c_i$ , and the results are shown in fig. 6a-c. For freely streaming ions ( $T_e = 0$ ) in fig. 6a,  $\text{amp}_f$  is independent of  $x$ , and the phase increases linearly with  $x$  (slope  $v^{-1}$ ). Fig. 6b shows the results for  $T_e = T_i$ . We note that except for a weak oscillation in  $\text{amp}_f$  for  $v = 2.5c_i$  and  $3.5c_i$ , the results are very similar to those obtained for  $T_e = 0$ . Finally the results obtained in the case of strong interaction ( $T_e = 5T_i$ ) are shown in fig. 6c. Here we note a rather irregular oscillation in the  $\text{amp}_f$ -curves for  $v = 2.5c_i$  and  $3.5c_i$ .

The physical explanation of the feature seen in the figs. 6a-c is simple: For  $v = 3c_i$  we expect  $\text{amp}_f$  to be constant as for this special  $v$ -value the collective term in (3) disappears ( $f'_0(v) = 0$  for  $v = 3c_i$ ). For  $v = 2.5c_i$  and  $3.5c_i$  we expect oscillations in  $\text{amp}_f$  because  $f'_0(v) \neq 0$  for those  $v$ -values. For  $T_e = 0$  as in fig. 6a,  $\text{amp}_f$  is constant for all  $v$ -values because the collective interaction term in (3) is zero.

Conclusions. From the linearized Vlasov equation (3) the propagation properties of grid-excited pulses and waves were calculated for different  $g(v)$ -

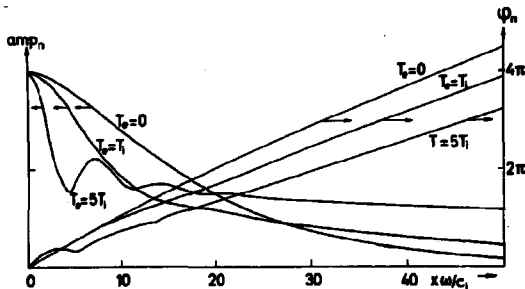


Fig. 5. Amplitude and phase of wave density.  $v_{\text{drift},e} = v_{\text{drift},g} = 3c_i$ .



functions and  $T_e/T_i$ -values. The main conclusions are:

For  $T_e \approx T_i$  as in most Q-machine experiments, the results are so close to those obtained in the freely streaming case ( $T_e=0$ ) that it is very difficult to perform experiments that clearly demonstrate collective interaction. The undershoot on the  $f$ -curves in fig. 1b is an exception seen experimentally<sup>9</sup>.

For  $T_e > T_i$  the collective interaction causes pulses to split up into

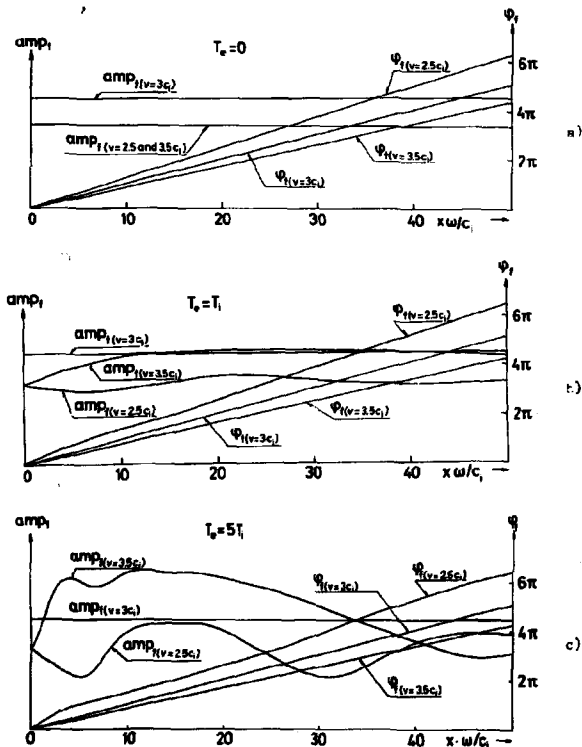


Fig. 6. Amplitude and phase of ion velocity distribution function in a wave.  $v_{\text{drift}, f_0} = v_{\text{drift}, g} = 3 c_1$ .

a fast one and a slow one. In the case of waves this splitting-up causes oscillations in the amplitude near the grid. Physically the oscillation is caused by a beating between the fast and the slow wave associated with the two pulses. It should be noted that amplitude oscillations were seen experimentally and explained as being caused by non-linear effects<sup>2</sup>. It should further be noted that amplitude oscillations also appears without collective interaction for  $g(v)$  as double-humped distribution function.

Close to the grid a normal Landau treatment does not give a satisfactory result. For  $g(v) \propto f_0(v)$  as considered here, a Landau treatment applies approximately one wave length away from the grid. For more complicated  $g(v)$ -functions as discussed in ref. 8 one has to go further away to find good agreement.

A more comprehensive collection of calculated propagation properties of pulses and waves will be published elsewhere<sup>11</sup>.

#### Acknowledgements

The author wants to thank P. Michelsen for many discussions and for doing most of the computer programming.

#### References

- 1) A.Y. Wong, R.W. Motley, and N. D'Angelo, *Phys.Rev.* 133, A436 (1964)
- 2) K. Kawai and H. Ikegami, *Plasma Physics*, 13, 463 (1971)
- 3) N. Sato, H. Ikezi, N. Takahashi and Y. Yamashita, *Phys.Rev.* 183, 278 (1969)
- 4) J.L. Hirshfield and J.H. Jacob, *Phys.Fluids* 11, 411 (1968)
- 5) S.A. Andersen, V.O. Jensen, P. Michelsen, and P. Nielsen, *Phys.Fluids* 14, 728 (1971)
- 6) S.A. Andersen, V.O. Jensen, and P. Nielsen, *Phys.Fluids* 12, 2694 (1964)
- 7) K. Estabrook, M. Widner, I. Alexeff, and W.D. Jones, *Phys.Fluids* 14, 1792 (1971)
- 8) G.B. Christoffersen, in *Risø Report No. 250* (1971) 55-62
- 9) S.A. Andersen, G.B. Christoffersen, V.O. Jensen, P. Michelsen, and P. Nielsen, *Phys.Fluids*, 14, 990 (1971)
- 10) S.A. Andersen, V.O. Jensen, P. Michelsen, and P. Nielsen, *Phys.Lett.* 32A, 413 (1970)
- 11) V.O. Jensen and P. Michelsen, *Risø Report to be published* 1972.

Propagation Properties of Short Density Perturbations in  
Q-Machine Plasmas with Double-Humped Ion  
Velocity Distribution Functions

by

Dennis Twomey

Danish Atomic Energy Commission  
Research Establishment Risø, Roskilde Denmark

Abstract

In a single-ended Q-machine the propagation of ion density perturbations through a plasma with a "double-humped" ion velocity distribution may be treated by a Green's Function technique, provided the distribution does not lead to growing solutions. A series of curves are calculated, and some effects due to Landau damping and free-streaming are shown.

Introduction

Andersen et al<sup>1)</sup> have investigated the propagation of density perturbations in a Q-Machine. They calculated the perturbed ion velocity distribution Function by means of a Green's Function technique. The results reported here follow from a similar analysis, except that we no longer assume the plasma to be quasi-neutral.

Andersen et al <sup>1)</sup> assumed the unperturbed ion velocity distribution function to be a "single-humped" Maxwellian, and showed (as have many others, e. g. Jackson <sup>2)</sup>) by a simple Nyquist analysis that this was "well behaved", i. e. that in a normal Landau treatment of wave propagation <sup>3)</sup> such distributions lead only to stable or damped solutions.

It will be assumed here that the unperturbed distribution function is made up of two Maxwellians which add to form a "double-humped" velocity distribution. Such distributions can be produced in Q-machines <sup>4)</sup>. The discussion will be limited to those distributions which a Nyquist analysis shows to be well-behaved, since the subsequent treatment is invalid for other distributions.

Following the analysis of Andersen et al leads to an expression for the perturbed distribution function,  $f(x, v, t)$ :

$$f(x, v, t) = \Delta t \lambda(v) \delta(x-vt) + \frac{\Delta t}{\epsilon} \frac{n_i}{n_e} \frac{C_s^2}{2m} h\left(\frac{x}{\epsilon}\right) P\left(\frac{dP_0(v)}{dv} \frac{1}{v - \frac{x}{\epsilon}}\right)$$

where

$$\lambda\left(\frac{x}{\epsilon}\right) = h\left(\frac{x}{\epsilon}\right) \left[ 1 - \frac{n_i}{n_e} \frac{C_s^2}{2m} P \int_{-\infty}^{\infty} \frac{dP_0(v)}{v - \frac{x}{\epsilon}} dv \right]$$

$$h\left(\frac{x}{\epsilon}\right) = \frac{1}{\pi} \text{Im} \left\{ H_1\left(\frac{x}{\epsilon}\right) \right\}$$

and

$$H_1\left(\frac{\omega}{k}\right) = \frac{\int_{-\infty}^{\infty} \frac{v g(v)}{\frac{\omega}{k} - v} dv}{1 + \frac{n_i}{n_e} \frac{C_s^2}{2m} \int_{-\infty}^{\infty} \frac{dP_0(v)/dv}{\frac{\omega}{k} - v} dv}$$

$g(v)$  is a truncated displaced Maxwellian of the form:

$$g(v) \propto \exp - \left( \frac{v - v_d1}{c} \right)^2 + \exp - \left( \frac{v - v_d1}{c} \right)^2 \quad v \geq 0$$

$$\propto 0 \quad v < 0$$

These are essentially the results of Andersen et al except that  $C_e$  is now the electron thermal velocity ( $\sqrt{2kT_e/m_e}$ ) and in addition we define  $n_e$  and  $n_i$  as the electron and ion number densities, and  $m$  as the ion to electron mass ratio.

Experimentally results may be obtained in the form of two types of curve:

- (i) a curve showing ion flux or ion saturation current to the analyser

$$\text{flux} = \int_0^{\infty} v f(x, v, t) dv$$

which is obtained when the analyser is set to collect all velocities.

- (ii) various  $S_{va}$  curves

$$S_{va}(x, t) = \int_0^{\infty} v f(x, v, t) \exp - \left( \frac{v - va}{vr} \right)^2 dv$$

where the resolution function of the analyser is assumed to be Gaussian in  $v$ , with a resolution  $vr$ .

These curves are obtained when the analyser is set to collect only ions of velocity  $va$ .

To calculate these curves in the "single-humped" case it is convenient to normalise equations 4 and 5 with respect to the ion thermal velocity ( $\sqrt{2kT_i/m_i}$ ). However in the "double-humped" case the ions in the two humps may have different temperatures and masses and therefore the normalisation is carried out with respect to the electron thermal velocity.

The expressions for flux and  $S_{va}$  are now given by:

$$P_{\text{flux}} = \frac{h(x) C_e}{t} \left[ X(1 - \phi_1 - \phi_2) + \theta_1 + \theta_2 \right]$$

where

$$\phi_j = \left( \frac{n_i}{n_e} \right)_j \left( \frac{C_e}{C_i} \right)^2 \frac{1}{4m_j} Z' \left\{ \left[ X - m_0 \right] \left( \frac{C_e}{C_i} \right)_j \right\}$$

$$\theta_j = \left( \frac{n_i}{n_e} \right)_j \left( \frac{C_e}{C_i} \right)^3 \frac{1}{2m_j} \int_{x-u}^{\infty} \frac{u}{x-u} (u - m_0) \exp \left\{ - \left( u - m_0 \right)^2 \left( \frac{C_e}{C_i} \right)_j^2 \right\} du$$

where  $j$  is a subscript referring to the first or second hump.

$$S_{\text{va}} = \frac{h(x) C_e}{t} \left[ X \exp - \left( \frac{X - m_0}{m\tau} \right)^2 (1 - \phi_1 - \phi_2) + \psi_1 + \psi_2 \right]$$

$$\psi_j = \left( \frac{n_i}{n_e} \right)_j \left( \frac{C_e}{C_i} \right)^3 \frac{1}{2m_j} \int_{x-u}^{\infty} \frac{u}{x-u} (u - m_0) \exp \left\{ - \left( u - m_0 \right)^2 \left( \frac{C_e}{C_i} \right)_j^2 + \left( \frac{u - m_0}{m\tau} \right)^2 \right\} du$$

$u$  = independent variable normalised to  $C_e$ ,  $X = \frac{x}{C_e}$ ,  $m_0 = \frac{vd}{C_e}$ ,  $ma = \frac{va}{C_e}$ .

$m\tau = \frac{v\tau}{C_e}$ , and  $Z'$  is the derivative of the plasma dispersion function.

Calculations have been carried out for a variety of values of the parameters,  $(C_e/C_i)_j$ ,  $n_j$ ,  $(n_i/n_e)_j$ ,  $m_0$  and usually for four values of  $va$  (each side of the two humps, see figure 1). The ratio  $C_e/C_i$  may be reduced to  $C_e/C_i = m\tau_e/T_i$ .

For the case where: both humps contain the same number of ions of the same type, the normalised hump velocities are 0.01 and 0.004 and the temperature ratio  $T_e/T_i = 4$ , we obtain the curves in figure 2. These are the curves that might be expected from the simple addition of the curves for two "single-humped" distributions.

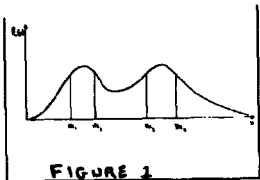


FIGURE 1

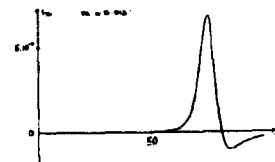
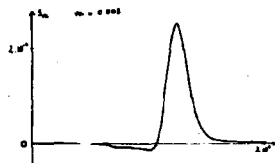
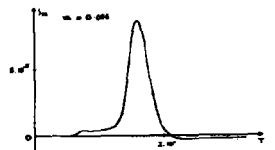
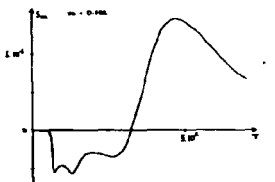
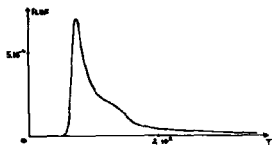


FIGURE 2

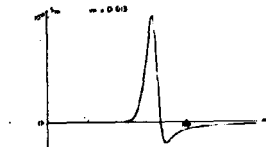
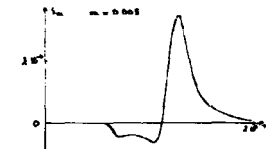
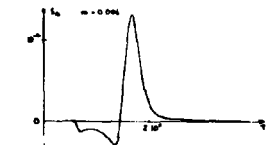
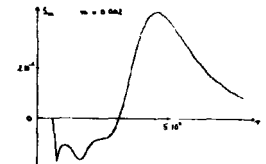
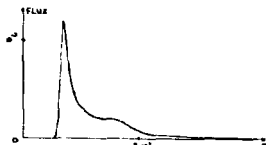


FIGURE 3

If we make the ratio of ions in the fast hump to ions in the slow hump equal to four we get the curves in figure 3. These are very similar to results which might be expected for a single-humped distribution with a drift velocity equal to that of the faster hump. The faster of the two humps appears

to have "absorbed" the slower one. This effect may also be obtained by setting  $T_e/T_i = 7$  for the faster hump.

An equivalent effect occurs if we modify the parameters of the slower hump rather than those of the faster hump.

In an experiment it may be more convenient to make a "double-humped" distribution by using ions of different mass. Figure 4 shows calculated curves for a plasma produced from potassium and rubidium.

The undershoot observed in the Sva curves arises from the interaction term in the Vlasov equation <sup>1)</sup>. To demonstrate this consider the case where the temperature ratio is very small (this is equivalent to making the interaction term very small <sup>5)</sup>). For  $T_e/T_i = 0.01$  we get the results in figure 5. No undershoot is observed.

The damping may be investigated by examining the flux curves. In all cases the amplitude of the second, slower peak is less than that of the faster peak, because its longer stay in the plasma causes it to suffer more damping. If there were no damping of any sort both peaks would have the same amplitude. Thus the amplitude of the slower peak relative to that of the faster peak gives some measure of the damping.

Stringer <sup>6)</sup> has calculated the conditions under which "double-humped" ion distributions lead to instability (see figure 6). If the velocity separation between the humps is fixed and all other parameters except the temperature ratio, are kept constant, then we can calculate flux curves for a set of temperature ratios ( $T_i/T_e$  in this case to be compatible with Stringer) which gradually approaches the instability limit

However, we would not expect the second peak in the flux curves to reach the same amplitude as the first. Even if there were no Landau damping the



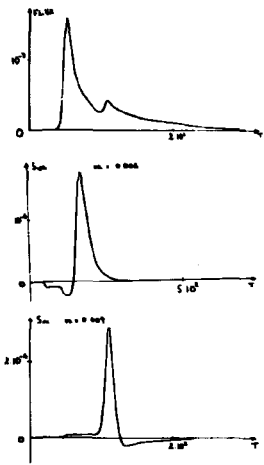
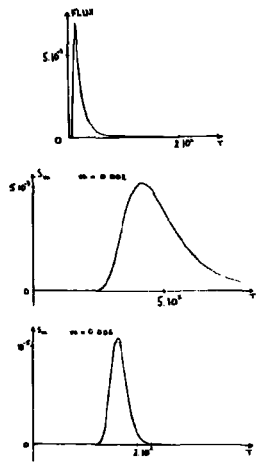


FIGURE 4



FIGURES

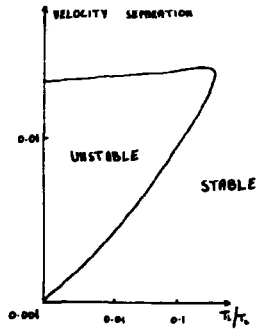


FIGURE 6

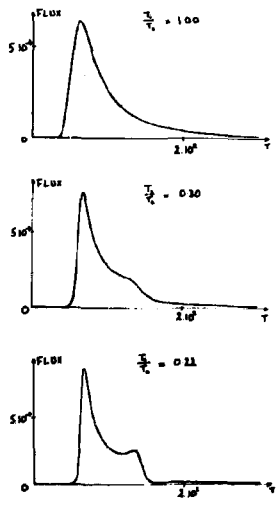


FIGURE 7

slower peak would still be more heavily damped as a result of free-streaming<sup>7)</sup>.

The effect of gradually approaching the instability limit is shown in figure 7. The second peak is initially unobservable, but grows in amplitude relative to the faster peak as  $T_1/T_e$  decreases.

- 1) Andersen, S. A., Christoffersen, G. B., Jensen, V. O., Michelsen, P., and Nielsen, P., *Phys. Fluids*, 14, 990 (1971)
- 2) Jackson, J. D., *J. Nuc. Ener. Part C*, 1, 171 (1960)
- 3) Landau, L. D., *J. Phys. (USSR)*, 10, 25 (1946)
- 4) Andersen, S. A., Jensen, V. O., Michelsen P., *Phys. Lett.* 31A, 395 (1970)
- 5) Jensen, V. O., *in Risø Report No. 250* (1971) 87-94
- 6) Stringer, T. E., *J. Nuc. Ener. Part C*, 4, 267 (1964)
- 7) Hirshfeld, J. L., and Jacob, J. H., *Phys. Fluids*, II, 411 (1968)



Propagation of Ion-Acoustic Waves in a Plasma  
with a Double-humped Ion Velocity Distribution Function

by

P. Michelsen and L. P. Prahm

Danish Atomic Energy Commission  
Research Establishment Risø  
Roskilde, Denmark

Abstract

It is possible to form a double-humped ion velocity distribution function in a Q-machine. Under certain circumstances such a plasma is "Landau unstable". Propagation of grid-excited, stable and unstable ion-acoustic waves is calculated by solving the one-dimensional linearized Vlasov equation as a boundary value problem.

Introduction

Great interest is taken in plasma instabilities. We shall here present calculations of micro instabilities caused by grid-excited ion-acoustic waves in a plasma with a double-humped ion velocity distribution function. Several works on this double-humped instability, also called the two-stream instability, have been published during the past ten years. Those calculations have, however, been worked out as initial value problems<sup>(1, 2)</sup>. Also numerical computer simulation has been used to investigate the instability in counter-streaming ion beams<sup>(3)</sup>. Attempts to investigate micro-instabilities in experimental equipment for quiescent plasmas, e. g. Q-machines, make calculations worked out as boundary value problems desirable. In this way Weitzner<sup>(4)</sup> looked at propagating pulses. Grid-excited ion-acoustic

waves will be treated in the following.

Theory

The problem is attacked by assuming a half-infinite, one-dimensional, collision-less plasma string. In this situation the Vlasov-equation for electrons and ions will give the correct description of the system

$$\frac{\partial f_{i,e}(x,v,t)}{\partial t} + \frac{\partial f_{i,e}(x,v,t)}{\partial x} - \frac{e_{i,e}}{m_{i,e}} \frac{\partial \Phi(x,t)}{\partial x} \frac{\partial f_{i,e}(x,v,t)}{\partial v} = 0$$

where the potential is given by the Poisson equation.

$$\frac{\partial^2 \Phi(x,t)}{\partial x^2} = - \sum_{i,e} \frac{e_{i,e}}{m_{i,e}} \int_{-\infty}^{+\infty} f_{i,e}(x,v,t) dv$$

All symbols have their usual meaning. We now use the same procedure as described by G. Christoffersen et al. <sup>(6)</sup> to determine the Fourier transform of the density perturbation  $n(k)$ .

The Vlasov equation is linearized. Assuming quasi-neutrality (except close to the grid), and that the electrons behave like an isothermal fluid, we get with the time variation  $e^{-i\omega t}$  for all quantities:

$$-i\omega f(x,v) + v \frac{\partial f(x,v)}{\partial x} = C_e^2 \frac{df_e(v)}{dv} \left[ \frac{\partial n}{\partial x} + \lambda \delta(x) \right]$$

$$C_e^2 = \frac{\partial T_e}{m_i}$$

Applying Fourier transformation we obtain after some calculations <sup>(6)</sup>

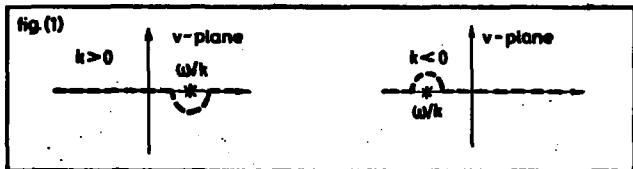
$$n(k) = \frac{1}{ik} \frac{\int_0^{\infty} \frac{v g(v)}{v - \omega/k} dv + \lambda C_e^2 \int_{-\infty}^{+\infty} \frac{df_e(v)}{v - \omega/k} dv}{1 - C_e^2 \int_{-\infty}^{+\infty} \frac{df_e(v)}{v - \omega/k} dv} = \frac{1}{ik} H\left(\frac{\omega}{k}\right)$$

where  $f_0(v)$  is the zero-order ion velocity distribution function, and  $g(v)$  is the perturbed distribution function at the grid. From this expression we find the phase and amplitude of the density perturbation:

$$n(x) = \frac{1}{2\pi} \int_{-\infty}^{\infty} n(k) e^{ikx} dk$$

### Pole Analysis

Before the inverse Fourier transformation is discussed, we shall look at the velocity integrals in the expression for  $n(k)$ . Assuming a complex  $\omega = \omega_r + i\omega_i$ ,  $\omega_i > 0$ , and real  $k > 0$ , the  $v$ -integration contour should in accordance with the theory of Landau<sup>(7)</sup> pass below the pole  $v_p = \frac{\omega}{k}$ . For real  $k < 0$ , the contour should then pass above the pole. Setting  $\omega_i = 0$ , we then get the integration contours as shown in fig. 1.



For this reason we split the inverse Fourier integration up into two contributions:

$$n(x) = \frac{1}{2\pi} \int_{-\infty}^0 \frac{1}{ik} H_-(k) e^{ikx} dk + \frac{1}{2\pi} \int_0^{\infty} \frac{1}{ik} H_+(k) e^{ikx} dk$$

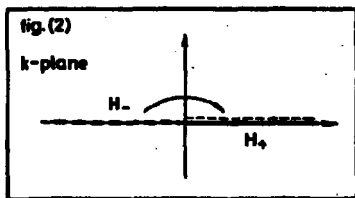
where the velocity integrals in  $H_+$  are taken below and in  $H_-$  above the pole  $\omega/k$ . This gives the relation

$$H_+(k) = H_-^*(k^*)$$

The inverse Fourier integration should be taken along the real  $k$ -axis. For  $k < 0$  the contour is, however, moved through the positive imaginary half plane and placed just over the positive real  $k$ -axis (see fig. 2). The  $v$  integrations in  $H_+(k)$  and  $H_-(k)$  are now alike, apart from the different direction around the singular point  $\omega/k$  (fig. 1). Substituting  $v = \omega/k$ , we get

$$n(x) = \frac{1}{2\pi i} \int_0^{\infty} \frac{1}{v} [H_+(v) - H_-(v)] \exp(i \frac{\omega x}{v}) dv$$

$$n(x) = \frac{1}{\pi} \int_0^{\infty} \frac{1}{v} \text{Im} \{ H_+(v) \} dv$$



The change of the  $K$ -integration contour can be done without any problems if  $H_-(k)$  is analytic in the upper imaginary half plane. Poles can only arise from zeros in the denominator of  $H_-(k)$ , and this is the same as looking for zero of the classical dielectric function  $\epsilon(\omega, k)$ .

For a stable ion distribution function the solutions to  $\epsilon = 0$  are the well-known branches in the  $\omega/k$  plane. Assuming quasi-neutrality the solutions reduce to points with  $k = 0$ . A weak unstable plasma with a non-symmetric velocity distribution function will have a single zero just above the real  $\omega/k$  axis:  $\frac{\omega}{k} = v_r + i v_i$  where  $v_i > 0$ . In the complex  $k$  plane we get

$$K = K_r + i K_i = \frac{\omega}{v_r + i v_i} \Rightarrow K_i < 0$$

$H_+(k)$  will then have a pole in the lower half plane, and  $H_-(k)$  a pole in the upper half plane.

Calculations for the stable plasma are described by G. Christoffersen et al. (6). For the unstable situation we have to add the residue contribution when changing the  $K$ -integration.

$$n(x) = \frac{1}{\pi} \int_0^{\infty} \frac{1}{v} \operatorname{Im} \{ H_+(v) \} \exp(i \frac{\omega x}{v}) dv + \frac{1}{v_0} \operatorname{Res} \{ H_-(v_0) \} \exp(i \frac{\omega x}{v_0})$$

$$\operatorname{Res} \{ H(v_0) \} = \left[ \frac{\int_0^{\infty} \frac{v g(v)}{v-v_0} dv + \lambda C_e^2 \int_{-\infty}^{\infty} \frac{\frac{\partial f(v)}{\partial v}}{v-v_0} dv}{\frac{\partial}{\partial v} \left[ 1 - C_e^2 \int_{-\infty}^{\infty} \frac{\frac{\partial f(v)}{\partial v}}{v-v_0} dv \right]} \right]_{v=v_0}$$

The constant  $\lambda$  is determined from the requirement that  $n(0) = \int_0^{\infty} g(v) dv$

$$\lambda = \lambda_1 + \lambda_2$$

$$\lambda_2 = - \int_0^{\infty} g(v) dv$$

$$\lambda_2 = \frac{\int_0^{\infty} v \frac{g(v)}{v-v_0} dv + \lambda_1 \int_{-\infty}^{\infty} \frac{\frac{\partial f(v)}{\partial v}}{v-v_0} dv}{\left[ \frac{\partial \mathcal{E}(v)}{\partial v} \right]_{v=v_0} \left[ 1 - 1/C_e^2 \int_{-\infty}^{\infty} \frac{\frac{\partial f(v)}{\partial v}}{v-v_0} dv \right] - \int_{-\infty}^{\infty} \frac{\frac{\partial f(v)}{\partial v}}{v-v_0} dv}$$

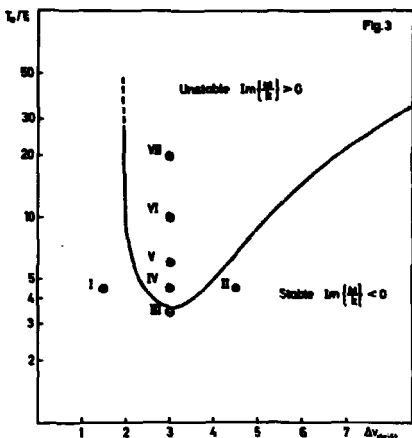
where for a stable plasma we use  $\lambda_2 = 0$ .

### Numerical Calculations

Assuming that the ion velocity distribution is a sum of Maxwellian distributions, we calculated the phase and amplitude for the density propagation of an ion-acoustic wave. The numerical work is done in Algol on a Borroughs 6700 computer.

Each calculation starts with an iteration to the zero for  $\epsilon$  with the largest imaginary part of  $\omega/k$  in the complex  $\omega/k$  plane, and thus it is determined whether the plasma is stable or not. If we have two drifting ion Maxwellian distributions with the same temperature,  $T_i$ , and the electron temperature is  $T_e$ , we find the well-known instability area as shown in fig. 3. The difference in the drift velocity is called  $\Delta V_D$ , and all velocities are normalized with respect to the ion thermal velocity. For  $T_e/T_i = 3.5$  the plasma is not unstable caused by the double-humped distribution, but drift instability between electrons and one ion group can appear at large drift velocity. This instability is not covered by our system of equations.

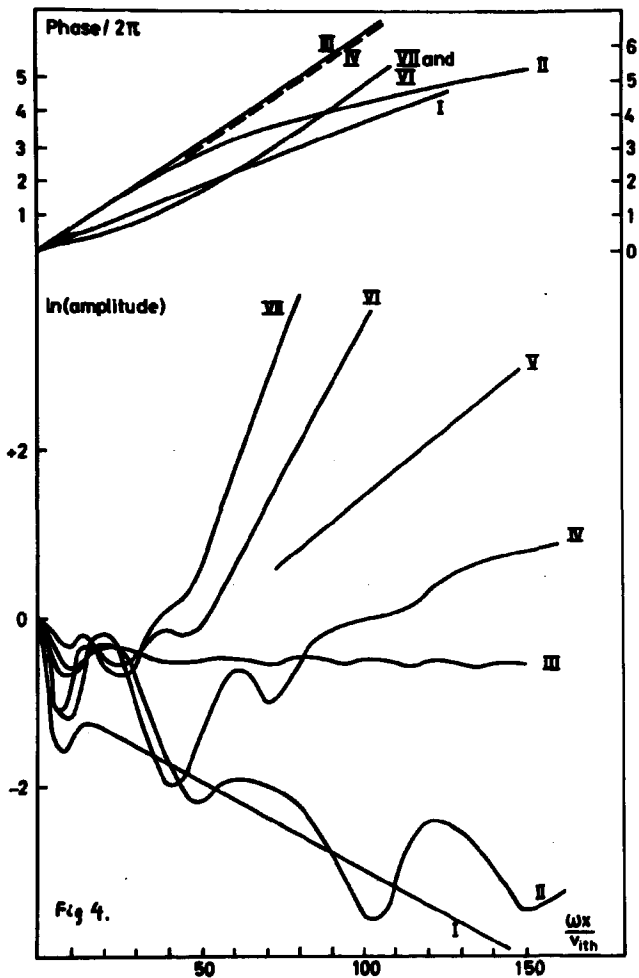




In fig. 4 is shown the phase and amplitude for two situations with  $T_e/T_i = 4.5$  corresponding to points I and II in fig. 3. The amplitude oscillates heavily for the large  $\Delta V_d$ , but is smooth when  $\Delta V_d$  is so small that the ion velocity distribution tends to be single-humped. For  $\Delta V_d = 3$ , examples are shown with different  $T_e/T_i$  values.

After a few wavelengths the amplitude grows or decays exponentially. The phase velocity is situated approximately between the two ion groups, for unstable zero-order distributions and distributions close to the stability limit (see fig. 5). For heavily damped oscillations the phase velocity is situated in front of the fastest ion group. From the table is also seen that phase velocity and damping or growth rate are well determined from the highest zero of the dielectric function  $\epsilon$ . The phase mixing is unimportant after a couple of wave-length.

Experimental investigation of the double-humped instability may be performed on a Q-machine. A slow ion group can be produced by means of charge-exchange processes<sup>(8)</sup> or by means of ions with different masses. Sufficiently high electron temperature can be obtained with RF heating<sup>(9)</sup>.



( At fig. 4 is  $g(v)$  proportional to the velocity distribution of the slow ion group)

In order to determine when the unstable waves stop growing, one has to extend the theory and consider non-linear calculation.

| Numerical Exampels |              |               |                          |                   |  |  | Fig 5.                               |
|--------------------|--------------|---------------|--------------------------|-------------------|--|--|--------------------------------------|
| Input Data         |              |               |                          | Calculated Data   |  |  |                                      |
| Grid No:           | $\Delta k_z$ | $\frac{v}{k}$ | $\frac{v_0 - v_{00}}{2}$ | Higest zero for E | $\Rightarrow \frac{1}{2R} \frac{R_r}{R_i}$ | $\frac{\omega}{\lambda}$ for $\frac{m\omega}{v_0} > 100$ | Phasevel. $\frac{\omega}{v_0} > 100$ |
| I                  | 1.5          | 4.5           | 175                      | 4.27 + i 0.319    | +2.1                                       | +2.1   | 4.30                                 |
| II                 | 4.5          | 4.5           | 3.25                     | 7.24 + i 0.359    | +3.2                                       |  | inf                                  |
| III                | 3.0          | 3.5           | 2.50                     | 2.50 + i 0.001    | +4.00                                      |  | 2.50                                 |
| IV                 | "            | 4.5           | "                        | " + i 0.105       | 3.8  | 3.8  | 2.53                                 |
| V                  | "            | 5.0           | "                        | " + i 0.281       | 1.8  | 1.9  | 2.54                                 |
| VI                 | "            | 10.0          | "                        | " + i 0.399       | 1.0  | 1.0  | 2.56                                 |
| VII                | "            | 20.0          | "                        | " + i 0.598       | 0.6  | 0.6  | 2.64                                 |

### References

- 1) J.D. Jackson, J. Nucl. Energy Part C: Plasma Physics 1, 171 (1960).
- 2) T.E. Stringer, Plasma Physics (J. Nucl. Energy Part C) 6, 267.
- 3) D.W. Forslund and C.R. Shonk, Phys. Rev. Lett. 25, No. 5, 281 (1970).
- 4) H. Weitzner, Phys. Fluids 5, No. 8, 933 (1962).
- 5) S.A. Andersen et al., Phys. Fluids, 14, No. 5, 990 (1971).
- 6) G.B. Christoffersen et al., in Risø Report No. 250 (1971) 63-70
- 7) L. Landau, Journ. of Phys. (USSR) 10, No. 1, 25 (1946).
- 8) S.A. Andersen, V.O. Jensen, and P. Michelsen, Phys. Lett. 31 A, 395 (1970).
- 9) E. Baarblian, T. Matti and B. Jürgens, IV European Conference on Controlled Fusion and Plasma Physics, 188 (1970). Rome 31 Aug. - 4 Sep.

Two Ion Beam Instability in a Q-Machine  
with Inhomogeneous B-Field

by

D.R. Baker, C. Bartoli and M. Bitter

European Space Research Institute (ESRIN)  
C.P. 64, 00044 Frascati (Rome), Italy

Abstract

The enhancement of thermal noise and the growth of excited ion acoustic waves is studied in the presence of a two beam plasma with a high temperature ratio. The two ion beams are created in a single-ended Q-machine with a localized neutral Cs cloud similar to the method described by Andersen et al.<sup>1)</sup>. The electrons are heated by 50 to 100 milliwatts of a  $\mu$ -wave power at the upper-hybrid resonance. An inhomogeneous field (inverse magnetic mirror or nozzle) is used to transfer the perpendicular energy of the electrons into parallel energy. In this configuration it is possible to obtain a temperature ratio ( $T_e/T_i$ ) between 3 and 10, and a ratio of beam velocity to ion thermal velocity of between 1.5 and 3.0 with various ratios of density between the two beams.

Introduction

We report the observation of a two ion beam instability in a Cs plasma with  $T_e/T_i > 1$ . The unstable waves are the ion acoustic waves travelling parallel to the beam velocity. This is commonly called the ion-ion or i-i instability. This instability has been investigated by numerous authors<sup>2-5)</sup>. This instability is of current interest because of its possible role in the formation of collisionless electrostatic shocks<sup>4-7)</sup>. We have measured the region in parameter space (beam velocity,  $T_e$ ,  $T_i$ ,  $T_D$ , etc.) in which the instability occurs by observing the enhancement of

thermal noise and by measuring the growth or damping of excited ion acoustic waves. The ion distribution function was measured on a retarding potential energy analyzer<sup>1,8,9</sup>).

#### Experimental Arrangement

The experiment was performed in a modified single-ended Q-machine. A schematic of the experiment is shown in Fig. 1. The two ion beams are created in a manner similar to that used by Andersen et al.<sup>1</sup>). The fast ions are created by surface ionization on the 3 cm diameter tantalum hot plate and accelerated into the plasma by the hot plate sheath<sup>1,9</sup>). The slow ions are created by a neutral Cs cloud localized in a copper tube which is located 20 cm downstream from the hot plate. These neutrals are ionized in part by a microwave discharge at the upper-hybrid resonance and in part by charge exchange with the fast ions. The microwave is fed into the copper tube which acts as a quasi-cavity. This creates two ion beams with temperatures of about 0.1 eV with a difference in drift velocity of about  $1.5 a_i$  to  $3.0 a_i$  ( $a_i = \sqrt{2 kT/m_i}$ ). The electrons created by the hot plate at a temperature of about 0.2 eV are too cold for the plasma to be unstable. The microwaves are used to heat the electrons sufficiently to obtain an unstable condition.

The microwave gives the electrons energy in the perpendicular direction. At the ion densities used in this experiment ( $n_i \approx 10^9$  and  $n_e \approx 10^{11}$ ) the electron mean free path is extremely long and the perpendicular energy is not transferred into a parallel temperature by collisions. An inhomogeneous B-field which acts like a reverse magnetic mirror is used to transfer the perpendicular energy into parallel energy. The maximum field gradient is at the microwave position and serves to stabilize the resonance position.

Using this technique it is possible to obtain parallel electron "temperatures" of between 0.3 eV and 1.0 eV near the discharge position. The inhomogeneous B-field means that the parallel electron temperature increases down the column until the region of homogeneous field is reached. This leads to some difficulty in the comparison of the data with theory. This is alleviated to some extent by measuring the plasma parameters close

to the discharge region in the area where the instability should be initiated.

The copper tube which contains the discharge region has coarse grids (spacing  $\gg \lambda_{de}$  and  $< r_{ci}$ ) on either end to help contain the microwave. The downstream grid is also used to excite ion waves by biasing it negatively and applying a voltage pulse or sine wave<sup>10)</sup>.

#### Summary of Theory

Since the theory related to this two ion instability has been treated in detail elsewhere only a brief summary will be given here. If we assume that the electrons are at rest with respect to the slow ions the dispersion relation can be written, using the notation of Fried and Wong<sup>3)</sup>, as

$$2k^2/k_i^2 = Z'(u) + na^2 Z'[a(u-v)] + (n+1)T Z'(u a_i/a_e)$$

where  $u = \frac{\omega}{ka_i}$ ;  $a_j = \sqrt{2T_j/m_j}$ ;  $a = a_i/a_b$ ;  $n = n_b/n_i$ ;

$v = v_d/a_i$ ;  $T = T_i/T_e$  and we have assumed  $n_e = n_i + n_b$ .

The subscript i refers to the slow ions or plasma ions and the subscript b refers to the fast ions or beam ions.  $Z'(u)$  is the plasma dispersion function<sup>11)</sup>. This dispersion relation was analyzed to find the limit of marginal stability using both the method of Fried and Wong<sup>3)</sup> and the method of Penrose<sup>12)</sup>. Both methods gave the same results. The marginal stability curves are shown in Fig. 2 for various values of T and n, for comparison with the experimental data.

It is also of interest to determine the growth rates as a function of frequency and the plasma parameters. This was done by Stringer<sup>2)</sup> for the case of colliding plasmas in the limit of small growth rates and can simply be modified for the case we are considering of an ion beam passing through a plasma. Typical results are shown in Fig. 3. It is difficult to make a direct comparison of the theoretical growth rates and the experimental data because of the dependence of plasma parameters on position. However, it is useful for a qualitative explanation of some of the experimental results.

### Experimental Results

The determination of whether the plasma is stable or not can be made either by observing the growth of the thermal noise or the growth of an excited wave as a function of position. It was most convenient to observe the behaviour of an excited pulse with a width  $\approx \frac{2}{\omega_{pi}}$ . (Excited pulse is shown in Fig. 5.) When the pulse amplitude grew larger as a function of position the plasma was classified as unstable. When the pulse amplitude became smaller or stayed the same the plasma was classified as stable. The results are shown in Fig. 2 and compared with theory. The plasma parameters ( $T_e$ ,  $T_i$ ,  $T_D$ ,  $n_h$ ,  $n_i$ , etc.) were measured at a point 4 cm from the discharge region and excitation grid. This point was chosen because it is far enough away from the discharge region so that the energy analyzer does not affect the discharge but close enough so that the growing waves are detectable but not large enough to effect the zero order distribution.

The ion distribution shown in figure 4 was measured with a typical retarding potential energy analyzer with diameter of 2 cm and a grid mesh of 200/cm. The resolution of the analyzer was measured using the method of Andersen et al.<sup>1)</sup> and found to be approximately 0.1 eV. This width of resolution is about the same as the width in measured voltage of the slow or plasma ions (the beam ions have a much larger width because of their high drift velocity). This means we must make a correction to the measured temperature of the slow or plasma ions by using a resolution function of finite width in the expression for the distribution function measured by the analyzer<sup>1,9</sup>).

$$f_m(v_R) = \int_0^\infty v f(v) R[(v-v_R)/v_s] dv$$

where  $f_m$  is the measured distribution function,  $v_R$  is the velocity corresponding to the retarding voltage,  $v_s$  is the spread in velocity corresponding to the resolution. The resolution function  $R$  would have a shape similar to a gaussian.

Since it is difficult to measure  $R[(v-v_R)/v_s]$  directly we have assumed it to be a gaussian of the form  $R[(v-v_R)/v_s] = 1/v_s \exp - (v-v_R)^2/v_s^2$ . If  $f(v)$  is of the form  $\exp - (v-v_D)^2/a_i^2$  and we set  $v_s = \delta a_i$ , we can find an approximate expression for the actual temperature

$T_i$  in terms of the measured temperature  $T_m$ ,  $T_i \approx T_m/(1+\delta^2)$ . Our determination of the analyzer resolution gives  $\delta \approx 1$ , and thus  $T_i \approx T_m/2$ . This is the value of  $T_i$  used in the determination of the plasma parameters.

The ion and beam temperatures are determined from the measured distribution function by the following relation<sup>9</sup>).

$$T = m_1/2 |(v_1 - v_2)/2|^2$$

where  $v_1 > v_2$  and  $f(v_1) = f(v_2) = f_{\max}/e$ .

This effective temperature is equal to the actual temperature if the beams are drifting maxwellians. It is seen that within the range of possible variation of experimental parameters there is relatively good agreement between observation and theory.

An example of a growing excited pulse is shown in Fig. 5. The oscillogram shows the time response of the plasma to the excited pulse and various positions downstream. The velocity of the growing pulse is less than the drift velocity of the beam and lies on the plasma ion side of the minimum in the distribution. The velocity of the damped pulse is greater than the drift velocity of the beam. An interesting feature of the growing pulse is that near exciting grid the pulse has about the same width as the exciting pulse, but as the pulse grows it tends to become broader then finally damps. This behaviour is confirmed in observation of excited CW sine waves and the background noise. The higher frequencies grow up faster saturate, and damp sooner than the lower frequencies. This behaviour can be explained qualitatively by the theoretical results for the growth rates shown in Fig. 3.  $|k_I|$  increases with  $k_R$  until maximum is reached then  $|k_I|$  falls rapidly to zero. The value of  $k_R$  corresponding to  $|k_I|_{\max}$  depends on the plasma parameters. As the two ion species move along the column they heat up and the maximum value of  $k_R$  for which growth occurs would decrease as one proceeds down the column bearing out the experimental results.

Of current interest is the quasi-linear interaction of the unstable waves on the zero-order distribution. This should cause the minimum of the ion distribution to fill in. We do indeed observe a filling-in, which is faster than should be accounted for by collisions and also is a bit faster in the presence of the



instability than without but we are not able to attribute this to a quasi-linear effect. This is in part due to the fact that the instability depends on the presence of the  $\mu$ -wave discharge and the discharge in turn depends slightly on the position of the energy analyser which is one boundary of the plasma. This combined with the fact that there are longitudinal inhomogeneities in the magnetic field and radial inhomogeneities in the plasma potential makes it difficult to verify these second order effects.

We would like to acknowledge interesting discussions with Dr. N. D'Angelo and Dr. K. Lackner, the help of Dr. M. Ianuzzi with the  $\mu$ -wave, help of J.J. Belliaro and G. Farina in the construction of the energy analyzers and operation of the Q-machine.

#### References

1. S.A. Andersen, V.O. Jensen, P. Michelsen, and P. Nielsen, Phys. Fluids 14, 728 (1971).
2. T.E. Stringer, J. Nucl. Energy, Part C 6, 267 (1964).
3. B.D. Fried and A.Y. Wong, Phys. Fluids 9, 1084 (1966).
4. C.F. McKee, Phys. Rev. Letters 24, 990 (1970).
5. D.W. Forslund and C.R. Shonk, Phys. Rev. Letters 25, 281 (1970).
6. D.W. Forslund and C.R. Shonk, Phys. Rev. Letters 25, 1699(1970).
7. C.F. Kennel and R.Z. Sagdeev, J. Geoph. Res. 72, 3303 (1967).
8. H. Ikezi and R.J. Taylor, Phys. Rev. Letters 22, 923 (1969).
9. J.M. Buzzi, H.J. Doucet, and D. Gresillon, Phys. Fluids 13, 3041 (1970).
10. A.Y. Wong, N. D'Angelo, and R.W. Motley, Phys. Rev. Letters 9, 415 (1962); Phys. Rev. 133, A436 (1964).
11. B.D. Fried and S.D. Conte, Plasma Dispersion Function, Academic Press (1961).
12. O. Penrose, Phys. Fluids 3, 258 (1960).

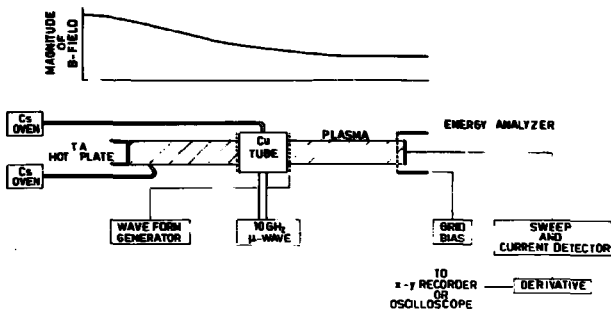


FIG 1 SCHEMATIC OF EXPERIMENT

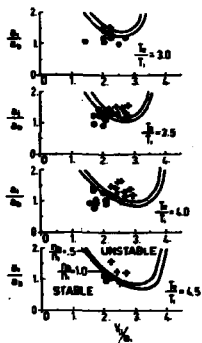


FIG 2  
STABILITY LIMITS  
THEORETICAL CURVES  
AND DATA POINTS  
FOR VARIOUS PLASMA  
PARAMETERS  
+ UNSTABLE o STABLE

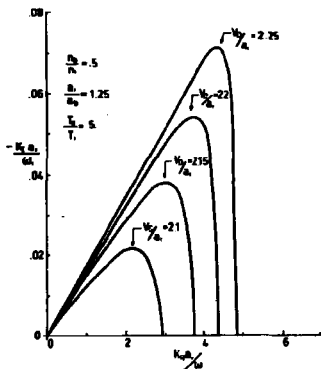
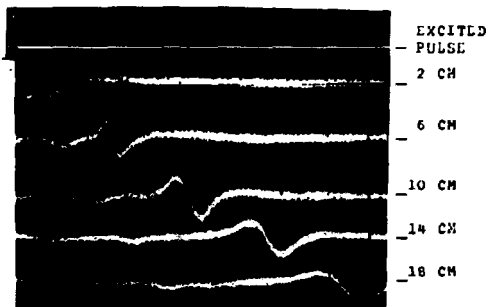


FIG 3  
GROWTH RATES FOR ION-ION INSTABILITY  
 $k = k_0 - k_1$   $k_1 = 0$  MEANS INSTABILITY



VOLTAGE →

FIGURE 4: SIGNAL OF ENERGY ANALYZER. TOP TRACE IS CURRENT VS VOLTAGE. BOTTOM TRACE IS THE DERIVATIVE OF THE CURRENT VS VOLTAGE OR THE DISTRIBUTION FUNCTION. HORIZONTAL SCALE 1 V/CM.



TIME →

FIGURE 5: DETECTED PULSES AT DIFFERENT DISTANCES FROM THE DISCHARGE REGION. TWO WAVES ARE VISIBLE. A SLOW ONE WHICH GROWS AND A FAST ONE WHICH IS HIGHLY DAMPED. HORIZONTAL SCALE IS 20  $\mu$ SEC/CM.

Ion Heating Caused by Ion Acoustic Waves  
in an Ion-Streaming Plasma

T. Honzawa and Y. Kawai

Institute of Plasma Physics, Nagoya University  
Nagoya, Japan

Abstract

It is experimentally shown that ion heating occurs because of ion acoustic waves driven by streaming electrons in an ion-streaming plasma characterized by  $T_e/T_i \leq 1$ . The excitation of the waves and the mechanism of ion heating in such a plasma are also discussed.

Introduction

Many theoretical and experimental studies<sup>1)</sup> have been carried out on excitation and damping of ion acoustic waves in plasmas so far. These results have shown that the ion-component plays an important role in the damping of the waves, in particular, in plasmas characterized by  $T_i > T_e$ <sup>2)</sup>. However, there have been only a few works to measure directly the energy absorption by ions from ion acoustic waves in a laboratory plasma<sup>3)</sup>.

Here we will report the results of our experiment showing that ion acoustic waves are driven by streaming electrons

and damped by streaming ions in an ion-streaming plasma characterized by  $T_i \gg T_e$ , which results in ion heating because of some non-linearities.

Apparatus

A view of the experimental apparatus is shown in Fig.1. A plasma source is of back-diffusion type<sup>4-5)</sup>, which consists of an array of pipelike oxide-coated cathodes (K), two sheets of grids ( $G_1$  and  $G_2$ ) and a metallic plate (A). In operation K and A are grounded and  $G_1$  and  $G_2$  are kept at a positive potential  $V_A$ , so that electrons emitted from K are accelerated between K and  $G_1$  and ionise residual gaseous atoms or molecules in the region between  $G_1$  and  $G_2$  to produce a plasma. A part of ions in the plasma are accelerated between K and  $G_1$  and gain a kinetic energy of  $eV_A$  to form an ion-beam, which is neutralized by thermal electrons from K. Thus we obtain an ion-streaming plasma, which includes an ion-beam with a controllable energy  $W_i = eV_A$ .

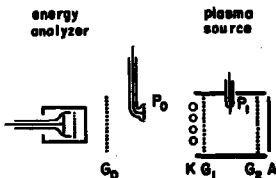


Fig.1. Experimental setup.

In most cases argon gas was used at a pressure from 2 to  $8 \times 10^{-4}$  torr. Under these conditions the densities of plasmas thus obtained were of the order of a few times  $10^7 \text{ cm}^{-3}$ ,

and the electron- and ion-temperatures were about 0.2 and 0.5 eV respectively. Therefore these plasmas are characterized by  $T_i \geq T_e$ <sup>5)</sup>.

The drift of electrons in such a plasma was excited by an electric field externally given between K and  $G_0$  (a positively-biased grid). So we could externally control the electron drift velocity in plasma rather easily.

Measurements of plasma parameters were made using a cylindrical probe ( $P_1$ ), a plane probe ( $P_0$ ) and a Faraday cup.  $P_0$  being rotative about its axis has only a sensitive surface. The estimations of  $T_e$  and  $N_e$  were made from the characteristic curve of  $P_0$  facing downstream. The increment ( $\Delta I = -N_e e v_d$ ) of electron-saturation-current due to the drift motion of electrons was measured with  $P_0$  facing upstream. The energy distribution of ions was measured with the Faraday cup. From the distribution we could estimate  $T_i$  assuming that the distribution was drift-Maxwellian.

For observation of ion acoustic waves  $P_0$  or  $P_1$  was used as a receiver, the signals from which were led to a Panoramic frequency analyzer or an oscilloscope.

#### Experimental Results

*Drift of Electrons:* As mentioned earlier, the drift of electrons arised from an electric field externally given by applying a positive potential  $V_G$  to  $G_0$ . Consequently it was easy to control the electron drift velocity  $v_d$ . The result obtained indicates that  $v_d$  is roughly proportional to  $V_G$ .

*Ion Acoustic Waves:* When  $v_d$  is settled at a proper value,

ion acoustic waves with many harmonics as shown in Fig.2 can be excited. The waves are of standing wave mode. From the dependence of the frequencies of the waves on the kinetic energy of an ion-beam included in plasma, the phase velocity of the waves in the laboratory frame was found to be nearly equal to the ion-beam velocity  $v_1$ . This fact enables us to estimate the wavelengths of ion-waves.

The relation between the amplitudes of ion-waves and  $v_d$  was carefully studied. The result obtained is illustrated in Fig.3, which indicates that there exists an optimum range in  $v_d$  for the excitation of the waves. Observations of ion-waves on an oscilloscope and analyses of their frequency spectrum make it possible to estimate the fluctuating ion-density  $\tilde{N}_n$  for the n-th harmonic.  $\tilde{N}_1$  for the fundamental wave is of the order of

$9 \times 10^5 \text{ cm}^{-3}$ , so that

$\tilde{N}_1/N_e = 4\%$ , whereas

$\tilde{N}_2/N_e = 0.6\%$ , etc.

Ion-waves as described above were observed only in the region between K and  $G_0$ . No signals were received in the region between  $G_1$  and  $G_2$  and on the downstream side beyond  $G_0$

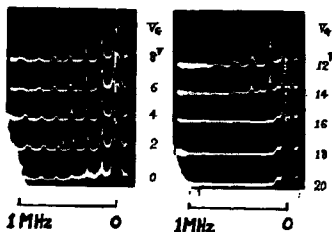


Fig.2. Photograph of the frequency spectrum of ion-waves.

(except in the vicinity of  $G_0$ ). When the potential of  $G_0$  was pulsively modulated, it was found that ion-waves were observable only in the phase, when the drift of electrons was excited.

**Ion Temperature:** In an ion-streaming plasma, where  $T_e/T_i \leq 1$ , it is theoretically expected that ion-waves are strongly Landau-damped due to ions<sup>2)</sup>. In order to study the energy absorption by ions from the ion-waves, we made energy analyses of ions by means of a Faraday cup. From the decaying slope with increasing energy of the energy distribution of ions we could estimate  $T_i$  assuming that the distribution was Maxwellian. The value of  $T_i$  was obtained as a function of  $V_G$  or  $v_d$ . The comparison of  $T_i$  and the amplitudes of the waves corresponding to various values of  $v_d$  tells us that there is a good correlation between these quantities as seen in Fig.4.

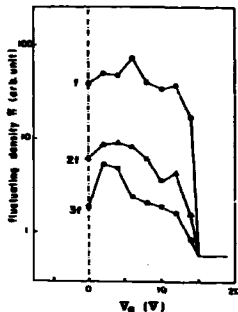


Fig.3. Relation between the amplitudes of the waves and  $V_G$ .

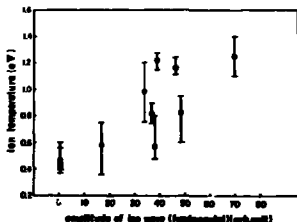


Fig.4. Correlation between  $T_i$  and the amplitude of the fundamental ion-wave.



Discussions

*Excitation of Ion Acoustic Waves:* Here we will show that the system of interest becomes possibly unstable against ion acoustic instability regardless of  $T_i \geq T_e$ , if  $v_d$  has a proper value, and estimate an optimum range in  $v_d$  for the excitation of ion acoustic waves.

The growth rate  $\eta$  of the instability is deduced from the linear theory as long as the amplitudes of the waves are infinitesimally small. For this calculation we use the one-dimensional Boltzman and Poisson equations, where a finite value of  $T_i$  ( $\geq T_e$ ), the drifts of electrons and ions and ion-neutral collisions are taken into consideration. These equations are solved under such an assumption as the absolute value of the imaginary part of  $\omega_j^*$  ( $-\omega - kv_j = \xi_j + i\eta$ ), which means the Doppler-shifted frequency of the wave with respect to j-species ( $= e, i$ ), is much smaller than that of the real part, that is  $|\xi_j| \gg |\eta|$ . The solution for  $\eta$  is represented as the following form<sup>6)</sup>,

$$\eta = T_i K(v) \left\{ \frac{1}{m} \left[ \frac{d}{du} f_0(u) \right]_{u=\frac{\omega}{k} - v_d} + \frac{Z_i^2}{K} \left[ \frac{d}{du} F_0(u) \right]_{u=\frac{\omega}{k} - v_d} \right\} - \frac{\nu}{T}, \quad (1)$$

where  $f_0(u)$  and  $F_0(u)$  are the zeroth order velocity distribution functions of electrons and ions respectively,  $m$  and  $M$  electronic and ionic masses,  $Z_i$  the charge number of ions,  $\nu$  the ion-neutral collision frequency and  $K(v)$  a positive factor of about  $10^6$  common to the first two terms in eq.(1). Supposing that both  $f_0(u)$  and  $F_0(u)$  are Maxwellian, the condition, under which the system is unstable, can be obtained

by putting  $\eta > 0$  in eq.(1). Here we put  $k > 0$ . From this inequality we can estimate the optimum range in  $v_d$  for the excitation of ion-waves in a graphical method. In the case that  $v_i = 2.2 \times 10^6$  cm/s ( $W_i = 100$  eV (Ar)),  $T_e = 0.2$  eV,  $T_i = 0.5$  eV,  $Z_i = 1$  and  $\nu = 2\pi \times 80$  kHz ( $p = 7 \times 10^{-4}$  torr),

$$v_i + 0.3 a < v_d < v_i + 1.2 a, \quad (2)$$

where  $a$  is the thermal velocity of electrons. The range of  $v_d$  given in (2) roughly agrees with the experimental result. Consequently it is concluded that streaming electrons can excite the ion acoustic waves regardless of  $T_e/T_i \leq 1$ , if their effect to make the ion acoustic instability grow overcomes the Landau damping by ions and other types of dampings, for example, the damping due to ion-neutral collisions.

*Mechanism of Ion Heating:* It is explained that the increase of  $T_i$  observed in this experiment comes from two types of randomization (the so-called Landau damping by ions and ion-neutral collisions) of the energies of ion-waves.

The coherently varying energy of an ion in the  $n$ -th harmonic wave  $\tilde{W}_n$  is estimated as

$$\tilde{W}_n = Mv_i (\tilde{v}_i)_n \approx (2(T_e + T_i)W_i)^{1/2} (\tilde{N}_n/N_e), \quad (3)$$

where  $W_i$  and  $v_i$  are the zeroth order energy and velocity of the ion in the laboratory frame respectively and  $(\tilde{v}_i)_n$  and  $\tilde{N}_n$  mean the fluctuating quantities for the  $n$ -th harmonic. In the present case, where  $W_i = 100$  eV,  $T_e = 0.2$  eV,  $T_i = 0.5$  eV and  $\tilde{N}_1/N_e = 0.045$ ,  $\tilde{W}_1$  is of the order of 0.6 eV. This value is comparable to the increments of  $T_i$  measured in our experiment.

The rates of energy absorption by ions from the waves for the two processes mentioned above can be quantitatively estimated. For the Landau damping the damping rate of the waves divided by the frequency, that is,  $|2\pi\omega_i^*/\omega_r^*|_{LD}$  is calculated to be about 0.36 under our experimental condition<sup>7)</sup>. On the other hand, the damping rate of the waves due to ion-neutral collisions,  $|2\pi\omega_i^*/\omega_r^*|_{coll}$ , is estimated to be about 0.49<sup>8)</sup>. The comparison of these quantities shows that the ion-neutral collisions are a little more effective to the damping of the waves than the Landau damping by ions. However, it is considered that the Landau damping has a little larger effect on the heating of ions, because ions can gain on the average only a half of the coherent energies through collisions with neutrals.

#### Conclusion

Here we could observe the increases of  $T_i$  caused by ion acoustic waves in an ion-streaming plasma. The waves were excited by streaming electrons, whose drift velocity  $v_d$  was externally controlled. It was found that there existed an optimum range in  $v_d$  for the excitation of the waves. The onset of the ion acoustic instability is well interpreted by means of the linear theory. Further it was found that there was a good correlation between  $T_i$  and the amplitudes of the waves. The increments of  $T_i$  were of the same order as the wave energies. These facts lead us to conclude that the heating of ions observed here occurs through some randomizations of the wave energies. Two types of randomizing processes seem to be

possible; one of them is the Landau damping and the other is ion-neutral collisions.

References

- 1) E.A.Jackson, Phys. Fluids 3, 113 (1960), I.Alexeff and R.V.Neidigh, Phys. Rev. 129, 516 (1963), A.Y.Wong, R.W. Motley and N.D'Angelo, Phys. Rev. 133, A436 (1964), H. Tanaca, A.Hirose and M.Koganei, Phys. Rev. 161, 94 (1967), etc.
- 2) B.D.Fried and R.W.Gould, Phys. Fluids 4, 139 (1961)
- 3) Y.Kawai, J. Phys. Soc. Japan 29, 1354 (1970), Y.Kawai and H.Ikegami, Plasma Phys. 13, 463 (1971)
- 4) K.Takayama, H.Ikegami and S.Aihara, Proc. 8th Intern. Conf. Phenomena in Ionized Gases p552 (1967), T.Honzawa, Japan. J. Appl. Phys. 1, 139 (1971)
- 5) T.Honzawa, Report of Institute of Plasma Phys., Nagoya Univ., IPPJ-109 (1971)
- 6) E.P.Gross, Phys. Rev. 82, 232 (1951), L.Landau, J. Phys. (USSR) 10, 25 (1946), S.Ichimaru, Ann. Phys. 20, 78 (1962)
- 7) B.D.Fried and S.D.Conte, *The Plasma Dispersion Function* (Academic Press Inc. New York and London, 1961)
- 8) Y.Hatta and N.Sato, Proc. 5th Intern. Conf. Phenomena in Ionized Gases Vol.1. p478 (1961)

ION WAVE EXCITATION VIA A MODULATED ELECTRON BEAM

J.M. BUZZI - H.J. DOUCET

Laboratoire de Physique des Milieux Ionisés  
Ecole Polytechnique, Paris - France

and

W.D. JONES

Physics Department, University of South Florida  
TAMPA, FLORIDA 33620, U.S.A.

---

ABSTRACT

We report the results of a preliminary study of a new technique for generating ion acoustic waves in a simple, predictable, and controlled manner with very small voltage perturbation to the plasma in the excitation region. Experimentally, this technique uses a tenuous modulated beam of energetic electrons to produce in the plasma a small volume in which the ion density is periodically increased above the equilibrium plasma density at the modulation frequency of the beam. Theoretically, using a model which assumes negligible perturbation to the particle velocities but which introduces a production (or loss - by grid collection, for example) term in the Vlasov equation, we have compared the excitation properties of the modulated beam with those of a grid. In good agreement with experimental observations, the amplitude of the perturbed electron current to a small probe, for example is predicted to be almost independent of frequency (for  $f \ll \omega_{pe}$ ) for the beam excitation but to decrease linearly with frequency for grid excitation. Also in good agreement with theory, the beam excitation is found to produce negligible direct coupling in comparison with that produced by grid excitation.

I. INTRODUCTION

Grid excitation of ion acoustic wave has received a great deal of interest, both theoretically and experimentally, in many laboratories (1). But as far as we know, all theoretical models use purely transparent grids whereas experiments use real grids which collect particles. This collection effect can be important in some experiments, particularly in single-ended Q machines where the density of the plasma flowing through the grid is known to be strongly dependent on the grid voltage. Therefore a complete treatment needs to include not only velocity perturbations around the grid, but also collection of particles.

In order to understand the properties resulting from this collec-

tion (or production) of particles, we study here an excitation in which the velocity perturbation is negligible with respect to the change in the number of particles. We have produced such an excitation using a modulated electron beam in a weakly ionized plasma. The beam produces periodically an additional ionization of the neutral gas in a thin slab defined by the beam shape, with no important perturbation to the velocity distributions.

## II. THEORY

Model of excitation via a modulated electron beam.

If we introduce a very tenuous modulated electron beam in a fully ionized plasma, we will produce a weak excitation of ion acoustic waves which can be described by the theory used for wave excitation by a purely transparent grid. But if we introduce the electron beam in a weakly ionized plasma, the electron beam can produce an additional ionization of the neutral gas. In this case, the perturbation of particle velocities due to the electron beam can be neglected with respect to the production of new particles in the plasma.

In previous theoretical modes (1), the Vlasov and Poisson equations are used. In these models it is assumed that the number of particles is constant and an external charge is introduced through Poisson's equation.

We present here a model using the Vlasov equations, but with source terms added, and the Poisson equation without external charge. It can be shown that this model reduces to the above models if we make a proper choice of the source term. In addition, however, this model can also describe the effects of collection or creation of particles.

In our model, we obtain for each particle species, after linearization :

$$\frac{\partial f_{is}}{\partial t} + v \frac{\partial f_{is}}{\partial x} + \frac{q_s}{n_s} E \frac{\partial f_{os}}{\partial v} = | \sqrt{g_s(v)} \delta(x) e^{-im_0 t} , \quad (1)$$

where the term on the right hand side has the dimensions of  $\partial f$  where  $v = v \delta(x)$  ;  $g_s(v)$  is the production (or collection) term which will be assumed later to be proportional to  $f_o(v)$ . Our use of the absolute value of  $v$  allows us to assume two boundary conditions :  $f_1 = 0$  for  $(v > 0, x \rightarrow -\infty)$  and for  $(v < 0, x \rightarrow +\infty)$ .

The Fourier-Laplace transform of (1) gives

$$f_{1B}(v, k, \omega) = - \frac{iq_B}{m_B} \frac{df_{0B}}{dv} \frac{E(k, m)}{m - kv} - \frac{|v| g_B(v)}{(m - \omega_0)(m - kv)} \quad (2)$$

and Poisson's equation becomes :

$$E(k, m) = i E(k, m) n_1 / (m - \omega_0) \quad (3)$$

where  $n_1 = \int g(v) dv$  is the neutralized density perturbation in the excitation for both electrons and ions, and

$$E(k, m) = \frac{q_e S_e(\omega, k) + q_i S_i(\omega_1, k)}{\epsilon_0 k^2 \epsilon(k, m)} \quad (4)$$

$S_e(\omega, k)$  being the Hilbert transform of the source term

$$S(\omega, k) = \frac{1}{n_1} \int_{-\infty}^{+\infty} \frac{g(v) |v|}{v - \frac{\omega}{k}} dv \quad ,$$

and  $\epsilon(k, m)$  the dielectric constant.

Solving the grid excitation problem by the classical model we find :

$$\bar{E}(k, \omega) = \frac{\rho(k)}{ik \epsilon_0 \epsilon(k, m)} \quad (5)$$

In Eq. 4, the Fourier transform  $\rho(k)$  of Eq. 5 becomes  $k^{-1} \sum_B q_B S_B(\omega, k)$ . In this expression, for most source terms, the factor  $1/k$  is the main difference between the two models. It will be responsible for the particular variations of all the macroscopic quantities (electric field, density, current, etc...) as functions of the frequency. We will show that electron beam excitation will produce at low frequencies an amplitude variations of the ion acoustic wave roughly independent of the frequency, whereas grid excitation produces a wave amplitude proportionnal to the frequency.

Using the expression for  $\bar{E}(k, m)$  given in Eq. 4, we can now calculate  $f_1(v, k, \omega)$  in Eq. 2 :

$$f_{1B}(v, k, \omega) = n_1 \left\{ \frac{q_B}{m_B} \frac{df_{0B}}{dv} \frac{\bar{E}(k, m)}{(m - \omega_0)(m - kv)} - \frac{|v| g_B(v)}{n_1 (m - \omega_0)(m - kv)} \right\} \quad (6)$$

It is necessary to use care in the inversion of Eq. 6 because  $|v|$  can introduce for  $S(\omega, k)$  a branch cut in the  $\omega$  plane. It turns out, however, that such a branch cut will produce a contribution only in the transient signal. To be able to compare with experimental results, we calculate the perturbation of the electron current  $j_e$ , collected on a small probe, for both elec-

tron-beam and grid excitation :

$$j_g(v, k, \omega) = q_0 \int f_{1e}(v, k, \omega) v dv. \quad (7)$$

After Laplace and Fourier inversions, we obtain for electron-beam excitation, using Eq. 6 and for  $x > a$ , for instance (in the Gould notations (1)) :

$$j_{e1}(x, v, t) = A \frac{1}{2\pi} \int_{-\infty}^{+\infty} \frac{e^{i\pi z} (S_i - S_0)}{f^2 \mathcal{E} \pi^2} d\pi + \int_{-\infty}^{+\infty} q_0(v) v \exp \frac{i\omega x}{v} dv, \quad (8)$$

where A

is independant of the frequency, and the integral is varying only slowly with frequency, when  $f \ll f_{pi}$ . To show the weak dependence of the integral on frequency, we can write the denominator  $f^2 \mathcal{E}$  as :

$\pi^2 \mathcal{E} = f^2 \pi^2 - [Z'(\frac{1}{2}) - 2 \frac{T_i}{T_e}]$ , where  $f^2 \pi^2$  is negligible with respect to the bracket in the low-frequency range. Therefore the denominator in the integral is independant of frequency.

In the monopolar grid excitation, the corresponding electron current perturbation is found to be :

$$j_{ie}(x, v, t) = [-2 \frac{T_i}{T_e} \frac{q_0^2}{m_0} \frac{E_0}{k_{d1}^2}] \frac{1}{2\pi} \int_{-\infty}^{+\infty} \frac{e^{i\pi z} d\pi}{f^2 \mathcal{E} \pi^2}. \quad (10)$$

The amplitude is now seen to be proportionnal to the applied frequency  $\omega_0$ , the integral still varying only slowly with  $f$  when  $f \ll f_{pi}$ .

Some other properties of the electron beam excitation can be pointed out : - 1 - The excitation can be easily linear, which is not true for grid excitation due to the large negative d.c. voltage generally applied on the grid ; - 2 - There is no direct coupled signal due to the fact that charge neutrality is conserved in the excitation region ; - 3 - Both wave and free streaming contributions present a non vanishing behavior at low frequencies. An additional, but weak, free-streaming term appears due to diffusion of the additional particles produced in the excitation.

### III. EXPERIMENT.

We have made some preliminary experiments of excitation of ion acoustic wave using a modulated electron beam in a classical xenon diffusion plasma (2). The plasma density is  $10^{19} - 5 \times 10^{19} \text{ cm}^{-3}$  and the electron temperature a few eV. The neutral gas is  $10^{-4} - 10^{-3}$  Torr.



The Electron beam generator is shown in Fig. 1. Electrons emitted from the hot negatively biased filament are modulated by a time varying potential on the grid and collimated into a thin slab. This results in a nearly monoenergetic density modulated beam passing through a small volume of the plasma, terminated by the collector.

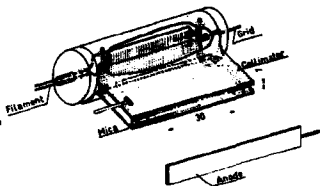


Fig . 1 . Electron beam device

The exact shape of the beam in the plasma is sensitive to such parameters as gas pressure, beam voltage, grid voltage, collimator voltage and filament temperature.

That the method of excitation is via ionization is verified by observing that : - 1 - no wave is detected when the beam energy is less than the ionization energy of the gas ; and - 2 - for beam energies higher than the ionization energy, the amplitude of the detected signal is observed to have approximately the same energy dependence as the ionization cross-section. Classical time-of-flight measurements suggest that, indeed, only ion acoustic waves are being generated. From a knowledge of the characteristics of the beam and the ionization cross section, we can calculate in reasonable agreement with observation, the amplitude of the generated wave. In high density plasmas, excitation at frequencies greater than 100 kHz have been possible with no detectable direct-coupled signal.

To check the theoretical predictions, we have made a preliminary experimental comparison of the excitation properties of electron beam and grid excitation as a function of frequency in the same plasma. A grid having 85% geometrical transparency and a grid spacing comparable to the electron Debye length was used. Figures 2 and 3 show the results of this study for continuous wave excitation.

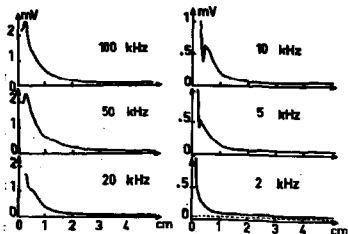


Fig. 2  
Grid excitation

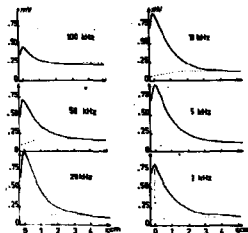


Fig. 3  
Electron beam excitation

Variations of the perturbations of electron current to a probe as functions of distance for several frequencies.

Qualitatively it is observed that the grid excitation exhibits a much stronger dependence on frequency than does the beam, especially at the lower frequencies. Also near the excitation region, there is observed to be a strong direct coupled signal in the case of the grid, whereas no such signal is seen for the beam excitation.

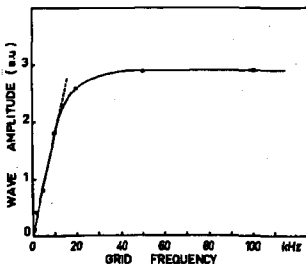


Fig. 5

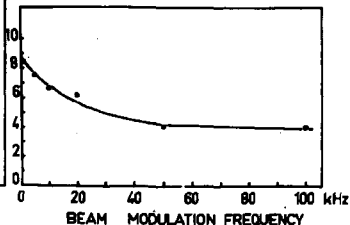


Fig. 4

Extrapolated amplitude to zero distance versus the frequency

In figures 4 and 5 we show the dependence of the extrapolated (to zero distance) wave amplitude as a function of frequency. In the case of the

beam excitation, Fig. 4, correction has been made to include an observed dependence of the beam intensity on frequency. For the case of the grid excitation, due to the strong direct coupled signal near the grid, the extrapolation had to be based on the smooth amplitude variation observed somewhat away from the grid region. In good agreement with the prediction of the above theory, the amplitude of the excited wave generated by the grid is seen to decrease strongly with frequency at low frequencies. Also qualitatively in agreement with theory, the amplitude dependence on frequency for waves generated by the modulated electron beam is seen to be much weaker at the lower frequencies. Thus qualitatively, the two generation mechanisms are quite different, both experimentally and theoretically. It is found experimentally that in beam excitation the signal is less distorted than in case of grid excitation. This effect can be considered as an additional evidence of the dependence of wave amplitude on frequency in the case of grid excitation.

#### IV. SUMMARY AND DISCUSSION

We have made a preliminary study, both theoretical and experimental, of a new method of ion acoustic wave excitation and have compared the results with the excitation properties of a grid. Two marked differences between the two methods have been found. The first is that at low frequencies, the amplitude of a wave generated by the electron beam has only a weak dependence on frequency, whereas the wave amplitude for grid excitation exhibits a strong monotonic dependence on frequency, decreasing linearly toward zero with decreasing frequency (a multigrid excitation would be expected to exhibit an even stronger dependence on frequency). The second difference is that the grid excitation exhibits strong direct coupling in and near the excitation region, whereas the beam excitation exhibits no detectable direct coupling.

Although our theoretical model treats explicitly here the case where the plasma density in the excitation region periodically increases, theory also applies to the opposite case where the density is periodically decreased due to the particles collection, such as occurs very strongly for example, for grid excitation in a single ended Q machine. Since this new technique of waves excitation produces in all respects very small perturbations, it seems that the linear theory is completely adequate for giving a realistic description of the excitation process, as opposed to the case of grid excitation where non linear effects must be taken into account.

Acknowledgment : It is a pleasure for us to acknowledge the expert technological help of Mr ROUILLE who has designed and built the electron beam device as well as contributed in many other ways to the successful completion of this preliminary phase of our experimental studies. This work has been supported by Ecole Polytechnique, the Centre National de la Recherche Scientifique and the Direction des Recherches et Moyens d'Essais.

- REFERENCES -

- 1 - L. LANDAU - J. Phys. USSR 10, 25 (1946)  
W.E. DRUMMOND - Rev. Sci. Instr. 34, 779 (1963)  
R.W. GOULD - Phys. Rev. 136, A 991 (1964)  
M.R. FEIX - Phys. Letters. 9, 123 (1964)  
H. DERFLER, in Proceedings of the Seventh International Conference on Phenomena in Ionized Gases, B. Perovich and D. Toshich, Eds. (Gradevinska Knjiga, Beograd, Yugoslavia, 1966) Vol. II, p. 282.  
T.C. SIMONEN, SUIPR Rep. n° 100, Stanford University, Stanford, California (1968).  
J.L. HIRSHFIELD, J.H. JACOB - Phys. Fluids 11, 411 (1968)  
J.L. HIRSHFIELD, J.H. JACOB, D.E. BALDWIN - Phys. Fluids 14, 615 (1971)
- 2 - I. ALEXEFF, W.D. JONES - Phys. Rev. Lett. 15, 286 (1965)  
G. JOYCE, K. LONNGREN, I. ALEXEFF, W.D. JONES, Phys. Fluids 12, 2592 (1969)

Ion-Acoustic Collisionless Shocks In a Q-Machine\*

by

V. Vanek and T.C. Marshall  
Columbia University, New York, N.Y. 10027

Abstract

Ion-acoustic shocks have been observed in a single ended Q-device, operating at low plasma density, subsequent to microwave heating of the electrons. The microwave source, tuned to electron gyroresonance, can increase the electron/ion temperature ratio to  $\sim 13$  without ionization. The shock is produced by electrically gating a fine-mesh grid immersed in the plasma; the initial downstream/upstream density ratio is  $\sim 7$ . A step-discontinuity in density is observed first to broaden, and then to steepen into a shock having Mach number  $\sim 1.5$  (referred to the ion-acoustic wave speed of the unperturbed plasma). The shock width is less than 10% of the ion-ion collisional mean free path. No shock is formed for  $1 < T_e/T_i < 5$ , as theory predicts. The experimental results can be correlated with ion-acoustic shock numerical simulations.

Text

We report an experimental study of the development of an ion-acoustic collisionless shock generated by an initial density discontinuity in the plasma of a single-ended Q-machine. The shock was prepared first by greatly increasing the temperature of the electrons in the Q-machine using a microwave source tuned near the electron gyroresonance frequency; subsequently, a fine-meshed grid was opened electrically to permit the plasma to expand along the magnetic field lines into a region where the background plasma density was much lower (by a factor of seven). Previous experimental work<sup>1</sup> has described ion-acoustic shocks produced by accelerating one plasma into another, where rather small density discontinuities were produced.

Theories of collisionless shocks have been developed by

Moiseev and Sagdeev<sup>2</sup>; numerical simulations have been carried out by Sakanaka et al<sup>3</sup>. Our experimental work has been guided by the latter study, which uses the one-dimensional Vlasov-Poisson equations. Ion-acoustic shocks occur when the electron/ion temperature ratio is  $T_e/T_i \geq 5$ ; they are characterized by a rather low Mach number,  $1 \leq M \leq 1.5$ , which is sensitive to the size of the density-step causing the shock (the Mach number is the ratio of the shock speed to the ion-acoustic wave speed,  $[(T_e + 3T_i)/M_i]^{1/2}$  in the unperturbed plasma). In Fig. 1, we show a numerical simulation of a one-dimensional shock produced from a density-step of 7,  $T_e/T_i = 13$  (these are the approximate conditions of our experiment). We note that the expansion wave which follows the shock is not obvious in the ion flux calculations; we display the ion flux because our detector measures ion flux, not density. However, the actual location of the shock does not depend upon our measuring  $n_i$  or  $\Gamma_i$ .

The plasma was generated in a conventional single-ended Q-machine (Fig. 2a); the plasma density, determined by a double-probe, was  $\leq 10^{10} \text{ cm}^{-3}$ . The plasma is about 3 cm in diameter and 60 cm long, and is immersed in a uniform magnetic field (inhomogeneity  $\leq 1\%$ ) of  $\sim 3000$  G. Under our operating conditions, plasma flows away from the hot ionizer<sup>4</sup> with  $T_i \sim 2250^\circ \text{K}$  and a drift speed  $\sim 8 \times 10^4 \text{ cm/sec}$ .

When the shock is to be generated by electrically gating the grid, a 500  $\mu\text{sec}$  pulse of microwave power is injected into the stainless steel vacuum chamber of the machine, for purposes of gyroresonant electron heating. The power level could be increased up to  $\sim 200\text{w}$ . The microwaves are not coupled tightly to the plasma column; this avoids the problem of ionization at points of high microwave field strength. Heat is transported rapidly in the electron gas compared with the ion motion but the ions should remain at essentially the ionizer temperature due to the very long electron-ion equilibration time. The electron temperature was determined by measuring the wave speed of a low amplitude ion-acoustic wave pulse (duration, 20  $\mu\text{sec}$ ) transmitted between two grids in the machine. The maximum electron temperature achieved in the machine without ionization was  $\sim 2.7 \text{ eV}$ , which is approximately the same as reported in a similar microwave experiment<sup>5</sup>.

The spatial density discontinuity is maintained using a fine mesh grid (40 x 40 wires/cm; open area = 80%) immersed in the plasma and biased at -10 volts. At  $t = 0$ , the grid bias is changed to  $\sim -3$  volts, where the grid transmits  $\sim 80\%$  of the upstream plasma density; subsequently, the grid is very near the plasma potential and no electric fields occur between the wires and the plasma<sup>4</sup>. This is the type of initial condition considered by the theory<sup>3</sup>. The grid is basically a shutter-mechanism, and it was not possible to change the initial ratio of upstream-to-downstream density very much ( $n_0/n_{\infty} = 7$ ).

The evolution of the density discontinuity is shown in Fig. 2b where the signal is the ion current collected by a moveable, cold, flat, negatively biased (-20v) plate terminating the plasma column. The signal is proportional to the flux of ions ( $\Gamma_i$ ) moving parallel to the magnetic field at that point. The density step at first spreads, and then the leading part of the density rise steepens and forms a shock. This evolution is expected theoretically, and the shock ultimately formed by either a density ramp or step is the same<sup>6</sup>. In the particular case of Fig. 2b, we note that the qualitative features of the signal appear similar to those of Fig. 1 for  $\Gamma_i$ , and the measured Mach number of 1.5 is in good agreement with the calculated value of 1.35. The shock maintains its profile unchanged for as much as 20 cm distance from the grid.

It is also clear that the waves which follow an ion-acoustic shock for a small density step<sup>1</sup> do not occur here, as theory predicts<sup>3</sup>. Increasing the plasma density causes the shock to disappear completely for  $n \sim 10^{11} \text{ cm}^{-3}$ , and there is evidence that the shock will not form when the background cesium vapor pressure in the machine is high, possibly due to charge exchange collisions. The shock thickness is  $\sim 1$  cm which, although somewhat larger than expected theoretically ( $\sim 3$  mm), is still very thin compared with the ion-ion collisional mean free path ( $\sim 10$  cm at  $n \sim 10^{10} \text{ cm}^{-3}$ ); prior work<sup>7</sup> on shock waves in Q-devices has examined the collision-dominated case. Such experimental complications as the magnetic field, electrode effects, and the finite radial extent of the plasma, are not in the theory and may influence the comparison of certain details of the shock.

In Fig. 3 we show how the microwave heating affects the

evolution of the density discontinuity. The case corresponding to no heating ( $T_e/T_i \sim 1$ ) corresponds to a self-similar expansion of the plasma in which the ion free streaming is only slightly perturbed by the electron pressure gradient<sup>4</sup>. As the electron temperature increases, the plasma front accelerates and steepens, but there is no shock even at  $T_e/T_i \sim 5$ . For  $T_e/T_i = 10$  and 13, the wave forms a shock having  $M > 1$ . These results are also in good agreement with the theoretical predictions<sup>3</sup>.

#### Acknowledgment

The authors are grateful to Dr. P.H. Sakanaka for providing the data used to prepare Fig. 1.

- \* This research was supported by the National Science Foundation, Grant GK-26326.

#### References

- <sup>1</sup> R.J. Taylor, D.R. Baker, and H. Ikezi, Phys. Rev. Lett. 24, 206 (1970).
- <sup>2</sup> S.S. Moiseev and R.F. Sagdeev, J. Nucl. Energy Pt.C. 5, 43 (1963).
- <sup>3</sup> P.H. Sakanaka, C.K. Chu, and T.C. Marshall, Phys. Fluids 14, 611 (1971).
- <sup>4</sup> P. Korn, T.C. Marshall, and S.P. Schlesinger, Phys. Fluids 13, 517 (1970).
- <sup>5</sup> J. Soures and M.J. Lubin, Phys. Fluids 13, 1648 (1970).
- <sup>6</sup> P.H. Sakanaka, "Numerical Studies of Ion-Acoustic Collisionless Shocks and Solitary Waves," Plasma Laboratory Report No. 52, Columbia University, New York (unpublished).



- 7 H.K. Andersen, N. D'Angelo, P. Michelsen, and P. Nielsen, *Physics Fluids* 11, 606 (1968).

Figure Captions

Fig. 1 Numerical simulation of a collisionless ion-acoustic shock using the method of ref. 3;  $T_e/T_i = 13$ ;  $n_o/n_e = 7$ ; time in units of  $\omega_{pi}^{-1}$  ( $\omega_{pi}$  = ion plasma frequency); distance in units of the ion Debye distance; the initial density step has a small ramp to avoid extremely high field values. The initial ion kinetics are described by a drifted Maxwellian having drift speed equal to twice the ion thermal speed; the electrons are isothermal. The computed Mach number here is 1.35.

Fig. 2a Schematic of the Q-machine

2b Formation of the shock, time measured from opening of the grid and gating of microwave signal.  $T_e/T_i = 13$ ; the Mach number of the shock is  $\approx 1.5$ .

Fig. 3 Ion flux signal vs. time and microwave heating at  $x = 10$  cm from the grid. Curve (1): no microwave heating,  $T_e/T_i = 1$ ; (2) 20w,  $T_e/T_i = 2$ ; (3) 40w,  $T_e/T_i = 5.5$ ; (4) 80w,  $T_e/T_i = 10$ ; (5) 130w,  $T_e/T_i = 13$ . Cases (4) and (5) correspond to Mach 1.4 and 1.5 shocks respectively.

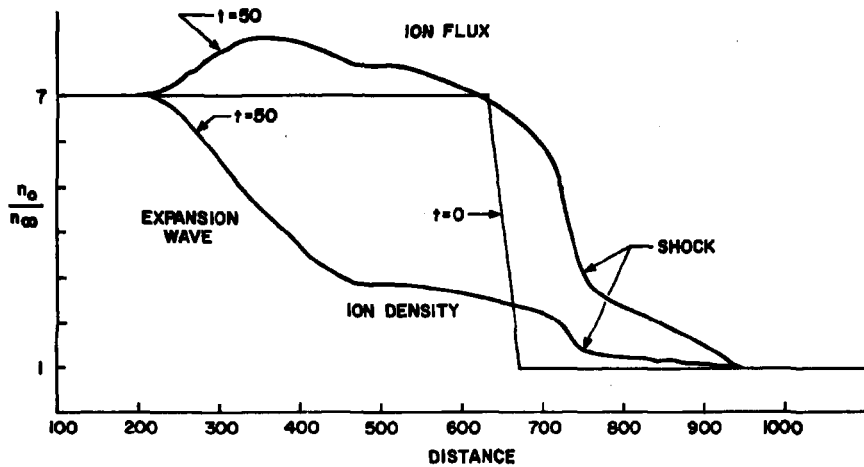


FIG. 1

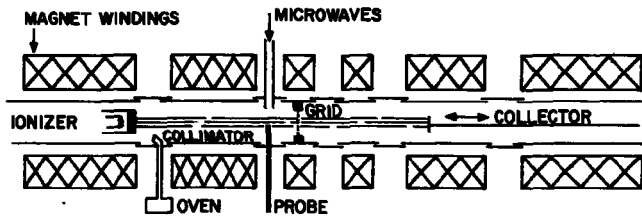


FIG. 2a

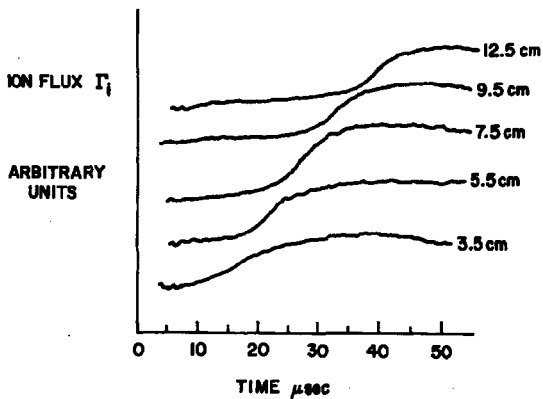


FIG. 2b

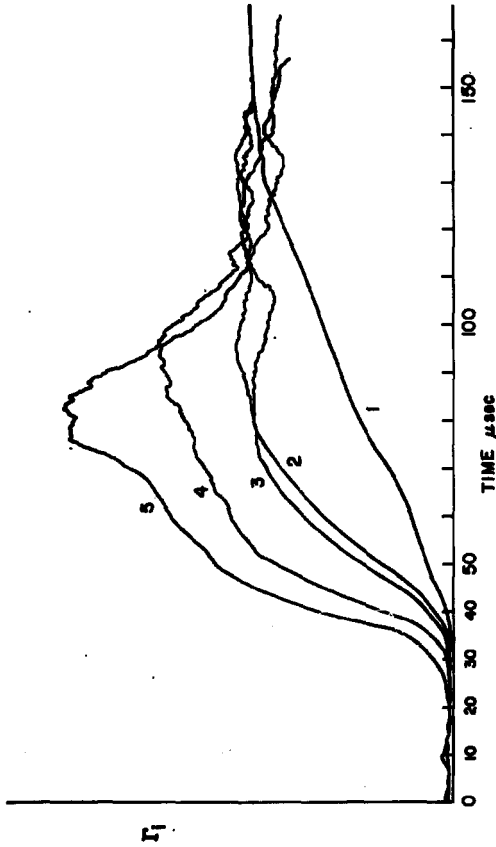


FIG. 3

Observation of the Propagation and Damping of Small  
Amplitude Electron and Ion Waves in Thermally  
Ionized Collisionless Alkali Metal Plasma

by

R.N. Franklin\*, S.M. Hamberger, G. Lampis and G.J. Smith\*  
UKAEA Culham Laboratory, Abingdon, Berkshire, England

Abstract

This paper presents experimental data on the dispersion of small amplitude electrostatic waves propagating in low density, magnetized, collisionless, sodium plasma produced by surface ionization on hot tungsten. From such measurements the electron and ion number densities, and the electron temperature have been determined, and information on the ion distribution function in a single-ended Q-machine has been obtained.

Electron Plasma Waves

Malmberg and Wharton<sup>1</sup> using a magnetized hot electron duoplasmatron plasma established, from measurements of both the real and imaginary parts of the propagation constant, and from independent measurements of the electron density and distribution function, the validity of Landau's dispersion equation, when corrected for finite plasma effects, for electron plasma waves. It was also verified, for heavily damped waves, by Derfler and Simonen<sup>2</sup> in experiments in an effectively infinite, unmagnetized, thermal plasma. Barrett, Jones and Franklin<sup>3</sup>, working in a thermally ionized, strongly magnetized, caesium plasma column showed that measurements of the real part of the dispersion of electron plasma waves could give accurate determinations of the electron number

density over a wide range of densities. However, electron temperatures determined from the real part of the dispersion indicated that  $T_e \sim 1.5 T_{hp}$ , where  $T_{hp}$ , the temperature of the ionizing hot plate, was determined with an optical pyrometer. This result was in disagreement with Langmuir probe measurements which showed  $T_e = T_{hp}$ . This discrepancy has now been resolved by measurements of the Landau damping of electron plasma waves. Within the limits of experimental uncertainty ( $\sim \pm 100^\circ K$ )  $T_e = T_{hp}$ , which agrees with probe measurements made by Buzzi, Doucet and Gresillon<sup>4</sup>.

The present experiments were performed in the strongly magnetized ( $B_z$  2-4 kG) sodium plasma column of the single-ended Culham Q-machine ARIADNE. Operation with an electron rich sheath at the hot plate, and the cold tantalum end plate floating, produced plasma with a low level of noise. Fig.1 shows typical radial variations in the plasma number density, floating potential and noise in the frequency range 0-50 KHz. It will be noted that over the area of the ionizing plate the plasma density is almost constant and drops rapidly beyond its edges. Axial number densities were in the range  $1 \times 10^7 \leq n \leq 7 \times 10^7 \text{ cm}^{-3}$  with a variation of  $\leq 1\%$  as measured by a Langmuir probe drawing saturation ion current, and confirmed by examining the variations in the wavelengths and damping rates of electron plasma waves propagating along the plasma column. The 25 mm diameter hot plate temperature was varied in the range 2200-2600 $^\circ K$  and was uniform to  $\sim \pm 30^\circ K$ .

The arrangement used to measure simultaneously the wavelength and spatial attenuation of a wave is shown in Fig.2. Waves were excited by applying high frequency signals, 100% square wave modulated at 1 KHz, to a single wire r.f. probe immersed in the plasma and matched to the signal generator close to its tip. Resulting fluctuations were detected on a similar receiving probe which was axially movable. The real part of the dispersion characteristic was determined from the interference between the received signal and a reference signal taken from the signal generator. The imaginary part was obtained from the detected signal recorded after passing through a logarithmic amplifier. Fig.3 shows some typical experimental data. Most of the trace clearly demonstrates the exponential damping of the wave with distance from the transmitter. However, when the receiving probe was close to the transmitting probe, direct coupling between them caused the system to act as an interferometer leading to the oscillation in received amplitude with the same wavelength as the wave. When the detecting probe was close to the end plate it detected standing electron plasma waves with half the wavelength of the propagating waves caused by reflection.

From data such as shown in Fig.3, curves for both the real and imaginary parts of the dispersion can be plotted as shown in Figs.4 and 5 respectively. The solid lines are theoretical curves which include effects due to finite geometry and assume that the electron distribution function is a complete Maxwellian and that the radial density profile is uniform. Fig.4 is plotted in normalized form:  $(\omega/\omega_{pe})^2$  versus  $ka$ , where  $k = 2\pi/\lambda$  and  $a$  is the

column radius. From this curve the electron number density can be determined with an accuracy of  $\sim \pm 2\%$  as described in ref.3.

Fig.5 shows  $k_i/k_r$ , the ratio of the imaginary to real parts of the propagation constant, plotted against the phase velocity  $v_\phi$  of the wave for two different hot plate temperatures. The solid lines are the best fit theoretical lines for Landau damping through the experimental points. The corresponding electron temperatures  $T_e$  are  $2500^\circ\text{K}$  and  $2800^\circ\text{K}$  for hot plate temperatures  $T_{hp} = 2350^\circ\text{K}$  and  $2600^\circ\text{K}$  respectively, measured with an optical pyrometer. The agreement is closer than the uncertainties in the pyrometric measurement due to the unknown hot-plate emissivity, window transmissions, etc.

Notice that in Fig.5 the measured values of  $k_i/k_r$  have a minimum  $\sim 10^{-3}$ . This corresponds to an effective collision frequency  $\nu$  where  $\nu/\omega \sim 10^{-3}$ , as seen from Fig.6 where the data for  $T_e = 2500^\circ\text{K}$  have been re-plotted and curves for different values of  $\nu/\omega$  are included. The theoretical methods used in calculating these curves are discussed in ref.5. The precise nature of the collisions has yet to be explored, but their frequency is consistent with electron-neutral sodium collisions if the Na vapour pressure is  $\sim 10^{-3}$  torr.

The range over which damping could be measured was limited for large values of  $k_i/k_r$  by the direct coupling between the probes, and by the presence of standing waves in the column for small values. Reliable damping measurements were made in the range  $10^{-1} \lesssim k_i/k_r \lesssim 10^{-3}$ , which, provided only Landau damping was responsible, corresponds to a range of phase velocities  $2.2 \lesssim \frac{v_\phi}{v_{Te}} \lesssim 3.5$  where  $v_{Te} = \sqrt{\frac{2kT_e}{m}}$ .

Finally, over the range of phase velocities investigated, the high frequency dispersion properties of the plasma were found to be independent of the direction of propagation of the wave, showing that the electron distribution function is essentially a complete Maxwellian.

### Ion Acoustic Waves

When the plasma density is low and the hot plate temperature is high, there is an electron rich sheath present at the hot plate<sup>4,5</sup>. This has been shown, both theoretically and experimentally<sup>4,5</sup> to produce an ion velocity distribution approximating to a Maxwellian truncated for velocities below some value which depends on the precise sheath conditions.

The dispersion relation for ion acoustic waves can be found by solving the appropriate expression for the plasma dielectric permittivity:

$$\epsilon(\omega, k) = 1 - \frac{\omega_{pe}^2}{k^2 v_{Te}^2} Z'(-u, \frac{u}{kv_{Te}}) - \frac{2 \omega_{pi}^2}{k^2 v_{Ti}^2} Z'(u, \frac{u}{kv_{Ti}}) \frac{1}{\text{erfc } u} = 0$$

where  $Z'(u, \zeta)$  is the derivative of the incomplete plasma dispersion function

$$Z(u, \zeta) = \frac{1}{\sqrt{\pi}} \int_u^{\infty} \frac{\exp(-x^2) dx}{x - \zeta}$$

and  $u$  is the truncation velocity normalized to the ion thermal velocity

$$v_{Ti} = \sqrt{\frac{2kT_i}{M}}$$

$\zeta$  is a normalized phase velocity.

This equation has been solved numerically<sup>7</sup> and shows the features expected of ion acoustic waves propagating on an ion beam: a fast positive energy wave  $s^+$  and a slow negative energy wave  $s^-$ .

Measurements of the real part of the dispersion of the fast wave were made in the same way as for electron plasma waves, and are shown by solid dots in Fig. 7. Only the positive energy wave was observed to be excited directly with a single wire probe. Propagation was observed up to  $\sim 4 u_{pi}$  showing that the waves were much less heavily damped than if the ions had a full Maxwellian distribution. However, both the positive and negative energy ion acoustic waves have been observed in the non-linear decay of a large amplitude electron plasma wave into another electron wave and an ion acoustic wave<sup>8</sup>. Waves excited in this way are shown by open circles in Fig. 7. The solid lines are theoretical curves for  $u = 2.0$ , the value which best fits the data. It should be noted that any change in  $u$  not only changes the slopes of the theoretical lines, but also their separation. The observed threshold for the decay into  $s^+$  is consistent with their theoretical damping  $\gamma/\omega = 0.04$ .

### Conclusions

It has been shown that by careful measurements of the dispersion of electron plasma waves the electron number density and electron temperature can be accurately determined. The electrons have essentially a complete Maxwellian distribution in a single ended Q-machine, and within the limits of experimental uncertainty their temperature is that of the hot plate.

The dispersion of ion acoustic waves propagating in a single ended Q-machine has been shown to be consistent with the ions having a truncated Maxwellian distribution function with the same temperature.

We are happy to acknowledge the excellent technical assistance of Mr W.J. McKay.

The research was supported jointly by the UKAEA and the Science Research Council.



References

- \* Also at Dept. of Engineering Science, Oxford University.
- <sup>1</sup> J.H. Malmberg and C.B. Wharton, *Phys. Rev. Letts.*, 17, 175 (1966); with  
W.E. Drummond, Proc. Int. Conf. Controlled Fusion, (1965)  
Paper CN21/116.
- <sup>2</sup> H. Derfler and T.C. Simonen, *Phys. Rev. Letts.*, 17, 172 (1966).
- <sup>3</sup> P.J. Barrett, H.G. Jones and R.N. Franklin, *Plasma Phys.*, 10, 911 (1968).
- <sup>4</sup> J.M. Buzzi, H.J. Doucet and D. Gresillon, *Phys. Fluids*, 13, 3041 (1970).
- <sup>6</sup> R.N. Franklin, *Plasma Physics*, 10, 805 (1968).
- <sup>6</sup> M. Hashmi, A.J. Van Der Houven Van Oordt and J.-G. Wegrowe, *Nuclear Fusion*, 10, 163 (1970).
- <sup>7</sup> R.N. Franklin, Proc. Xth Int. Conf. on Phenomena in Ionized Gases, Oxford (1971), p.269.
- <sup>8</sup> R.N. Franklin, G.J. Smith, S.M. Hamberger and G. Lampis, Proc. Xth Int. Conf. on Phenomena in Ionized Gases, Oxford (1971), p.324; (to be published in *Phys. Rev. Letts.*).
- <sup>9</sup> S.A. Andersen, V.O. Jensen, P. Michelsen and P. Nielsen, *Phys. Fluids*, 14, 728 (1971)

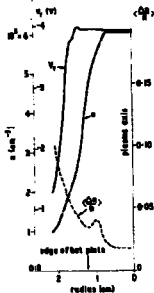


Fig. 1  
Radial variations in the  
electron number density  
 $n$ , plasma floating potential  
 $V_f$  and plasma noise  
 $\langle \frac{\Delta n}{n} \rangle$  in band 0-50 KHz

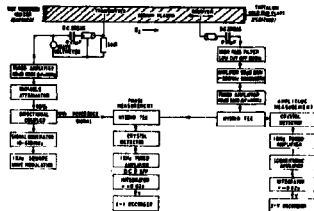


Fig. 2  
Arrangement used to measure wave-  
length and spatial attenuation of  
electron plasma waves

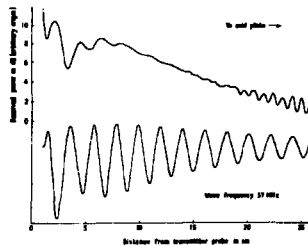


Fig. 3  
Typical experimental data showing  
spatial attenuation (top)  
and wavelength (bottom)

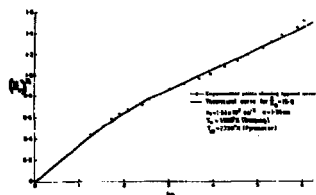


Fig. 4  
Experimental and theoretical dispersion of electron plasma waves

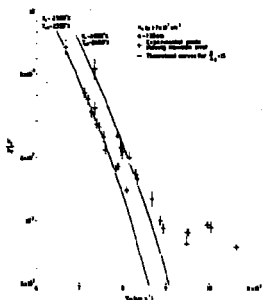


Fig. 5  
Experimental measurements compared with theoretical Landau damping of electron plasma waves

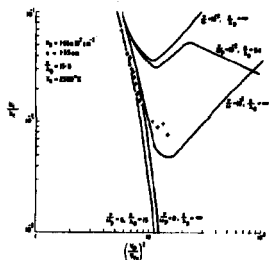


Fig. 6  
Experimental and theoretical damping of electron plasma waves including collisions

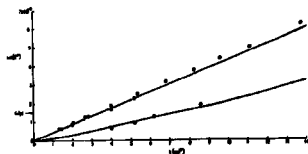


Fig. 7  
Dispersion of ion acoustic waves:  
● linear excitation, ○ non-linear excitation. Theoretical curves for  $u = 2.0$

SPATIAL AND TEMPORAL H.F.  
PLASMA RESPONSE TO AN EXTERNALLY APPLIED PULSE

P. Demulière, M. Guillemot, J. Olivair, F. Parceval, A. Quemeneur

**ASSOCIATION EURATOM-CEA**  
Département de la Physique du Plasma et de la Fusion Contrôlée  
Centre d'Etudes Nucléaires  
Boîte Postale n° 6 - 92 Fontenay-aux-Roses (France)

ABSTRACT.

The response of electrons in a collisionless plasma to a fast small amplitude voltage pulse is investigated theoretically and experimentally. The response, proportionnal to the excitation, is pseudo-periodic after a delay equal to  $V_{gmax} z / V_{gmax}$ ,  $V_{gmax}$  being the maximum group velocity of the induced waves and  $z$  the distance between the emitter and the receiver. The amplitude of the signal decreases and its pseudo period increases as  $z$  is increased.

INTRODUCTION.

It is known [1] that solitary waves in a cold collisionless plasma arise from two effects : dispersion of linear waves and non-linearity. A recent experiment [2] has been performed on this subject for an electron plasma. The aim of this paper is to consider a small initial signal in order to neglect the non linear mechanisms and permit analysis of the dispersion effects alone.

The phenomena can be simply described. The pulse generates a wave train which propagates along the column. Due to the dispersion of the medium the various components of the wave spectrum move at different velocities. It results a change in the pulse shape which is analyzed.

THEORY

In a one component collisionless plasma, a voltage pulse

$\Phi_{\text{ext}}(z,t)$  is applied

$$\Phi_{\text{ext}}(z,t) = \Phi_0 \mathcal{S}(\omega_0 t) \mathcal{S}(k_0 z) \quad (1)$$

Using a Fourier Laplace transformation method the plasma response can be written :

$$\Phi_T(k,\omega) = \frac{\Phi_{\text{ext}}(k,\omega)}{\mathcal{E}(\omega,k)} \quad (2)$$

then

$$\Phi_T(k,\omega) = \frac{\Phi_0}{\omega_0 k_0 \mathcal{E}(\omega,k)} \quad (3)$$

where  $\mathcal{E}(\omega,k)$  is the dielectric constant.

The inversion of formula (3) leads to the solution, e.g.

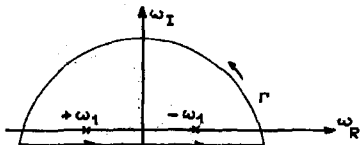
$$\Phi(z,t) = \frac{\Phi_0}{2\pi \omega_0 k_0} \int_{-\infty}^{+\infty} dk \frac{1}{2\pi} \int_{\gamma}^{\infty} \frac{e^{j\omega t - jkz}}{\mathcal{E}(\omega,k)} d\omega \quad (4)$$

For a uniform radially finite plasma, neglecting thermal effects,  $\mathcal{E}(\omega,k)$  is written :

$$\mathcal{E}(\omega,k) = 1 - \frac{\omega_p^2}{\omega^2} + \frac{k_{\perp}^2}{k^2} \quad (\omega < \omega_p)$$

where  $k_{\perp}$  is the transverse wave number.

Under these conditions the integrant of (4) has two poles  $\omega_1 = \omega(k) = \frac{\pm \omega_p}{\sqrt{1 + k_{\perp}^2/k^2}}$  laying on the real axis. The integration path can be modified according to fig. 1



Writing :

$$\frac{1}{\mathcal{E}(\omega,k)} = \frac{1}{1 + \frac{k_{\perp}^2}{k^2}} \left[ 1 + \frac{\frac{\omega_p^2}{\omega^2} \frac{1}{1 + \frac{k_{\perp}^2}{k^2}}}{1 - \frac{\omega_p^2}{\omega^2} \frac{1}{1 + \frac{k_{\perp}^2}{k^2}}} \right] \quad (5)$$

We check that (4) satisfies Jordan's lemma, then the contribution of  $\Gamma$  to the integral is null.

Using a Taylor's expansion of  $\mathcal{E}(\omega, k)$

$$\mathcal{E}(\omega, k) = \mathcal{E}(\omega(k), k) + (\omega - \omega(k)) \left( \frac{\partial \mathcal{E}}{\partial \omega} \right)_{\omega=\omega(k)} + \dots \quad (6)$$

we can write

$$\phi(z, t) = \frac{\phi_0}{2\pi \omega_0 k_0} \int_{-\infty}^{+\infty} \frac{dk}{2\pi} \int_C \frac{\exp i\omega t - ikz}{[\omega - \omega(k)] \left( \frac{\partial \mathcal{E}}{\partial \omega} \right)_{\omega=\omega(k)}} d\omega \quad (7)$$

a first integration of (4) following the C contour gives

$$\phi(z, t) = \phi_0 S(\omega_0 t) S(k_0 z) + \frac{\phi_0 \omega_p}{\omega_0 k_0} \frac{1}{2\pi} \int_0^{\infty} \cos \left[ \frac{\omega_p t}{\sqrt{1 + \frac{k_1^2}{k^2}}} - kz \right] \frac{dk}{\left(1 + \frac{k_1^2}{k^2}\right)^{3/2}} \quad (8)$$

Remark :

By using an approximation on  $\omega(k)$  valid for  $\frac{k}{k_1} \ll 1$

$$\omega(k) = \frac{\omega_p}{\sqrt{1 + \frac{k_1^2}{k^2}}} \approx \frac{k \omega_p}{k_1} \left( 1 - \frac{1}{2} \frac{k_1^2}{k^2} \right)$$

and by neglecting the self consistent field (7) leads to :

$$\phi(z, t) = \frac{\phi_0}{\pi \omega_0 k_0} \int_0^{\infty} \cos \left[ k \left( \frac{\omega_p t}{k_1} - z \right) - \frac{k^3 \omega_p t}{2 k_1^3} \right] dk \quad (9)$$

the solution of which is :

$$\phi(z, t) = \frac{\phi_0 \omega_p}{\omega_0 k_0} \left( \frac{3 \omega_p t}{2 k_1^3} \right)^{1/3} \text{Ai} \left[ - \left( \frac{3 \omega_p t}{2 k_1^3} \right)^{-1/3} \left( \frac{\omega_p t}{k_1} - z \right) \right] \quad (10)$$

where  $\text{Ai}(z, t)$  is the Airy function.

By a numerical calculation of (8) (fig. II a) or by looking at (10) (fig. III a) it appears that the response, proportional to the excitation  $\phi_0$ , is pseudo periodic after a delay given by  $\tau = \frac{z}{v_g \max}$ ,  $v_g \max = \frac{\omega_p}{k_1}$  being the maximum group velocity of the waves (given by the slope at the origin of the linear dispersion curve). The amplitude of the signal decreases and its pseudo period increases as the distance between the emitter and the receiver is increased.

The numerical calculation of (8) makes appear precursors which

have no physical reality. This calculation is needful for short distance between emitter and receiver ; on the other hand, approximate result (10) seems to be a good approximation for large distance (fig. III).

## EXPERIMENT

### 1) Experimental set up

The experiments are carried out in an argon plasma which diffuses along the vacuum chamber parallel to an uniform magnetic field of 1.5 Kg. For typical conditions the electron temperature is 2 eV and the electron density is  $10^7$  el/cm<sup>3</sup>. A Langmuir probe, immersed in the plasma, is connected to a generator which delivers a voltage pulse (amplitude  $\leq 1.5$  V, width  $\approx 2 \cdot 10^{-9}$  s, rise time  $\approx 10^{-9}$  s, recurrence frequency = 1MHz). The signal is detected by a longitudinally movable probe. In order to improve the detection an electronic averaging technic is used.

### 2) Average technique for high frequency signal detection

A technique to improve the signal/noise ratio is the use of an averaging method. By making N repetitions of the signal, the signal/noise ratio is increased by a factor  $\sqrt{N}$ . This does not lead to any difficulties as long as frequency is lower than approximately 1 MHz. For higher frequencies it is necessary to change the frequency range. The H.F. signal is transformed by a sampling oscilloscope into a L.F. one. The block diagram of the system is shown on fig. 4. The Y output of the sampling oscilloscope is connected to the corresponding input of a sampling memory device. The X L.F. sampling output drives the beginning of each cycle. Thus the signal is memorized, repeated and averaged. Fig. 5 illustrates typical results of such a method : a small amplitude signal immersed in a large noise is observed as much as the number of repetitions is increased. The observation of plasma response for low level of the exciting pulse has been shown with this method.

### 3) Results

Fig. (II b) and (III b) show experimental results. The upper trace of (II a) show the excitation pulse and the lower trace the received signal. Using a compensating delay circuit the origin of the two traces has been adjusted and the observed delay is entirely due to passage through the plasma. The corresponding propagation time (for instance  $\tau = 57,10^{-9}$  s) agrees with the value of the parameters  $\frac{k_{\perp} z}{\omega_p} = 53,10^{-9}$  s) deduced from the linear dispersion relation. Fig. (II a) and (III a) are the corresponding theoretical curve using respectively equation (8) and (10). Qualitatively the results agree.

We have also checked the linearity of the amplitude of  $\Phi(z,t)$  with  $\Phi_0$ .

Fig. (VI) shows the Fourier spectrum of the received signal at the same position than Fig. (II a). The discontinuous observed spectrum is connected with the technique of measuring modulation at 1 MHz of the signal). The various components lay well on the linear dispersion curve (Frequencies below 30 MHz cannot exist in the column:  $\lambda > 30 \text{ MHz} > L$  column; frequencies above 120 MHz are Landau damped) and then it confirms the theoretical model.

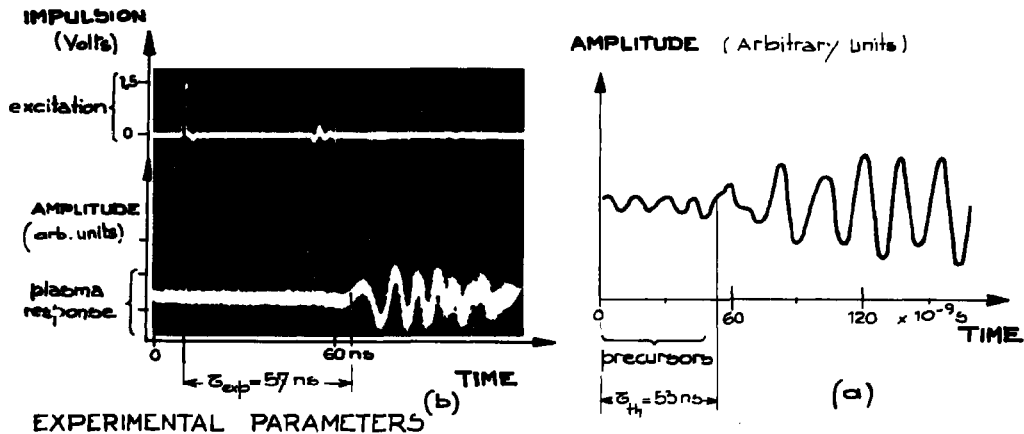
The authors conclude that, under these experimental conditions ( $\Phi_0 < 1,5$  V) the observed signal is due mainly to the dispersive properties of the medium and not to the non-linearity.

#### REFERENCES.

- [1] A.A. VEDENOV, E.P. VELIKHOV, R.Z. SAGDEEV, Nuclear Fusion 82 (1961)
- [2] H. IKEZI, P.J. BARRETT, R.B. WHITE and A.Y. WONG (submitted for publication)



Fig. 2. DETECTED SIGNAL AND CORRESPONDING THEORETICAL FUNCTION



EXPERIMENTAL PARAMETERS

Argon plasma

$$B_0 \approx 1.5 \text{ kG}$$

$$n_0 = 2 \cdot 10^{18} \text{ el / cm}^3$$

$$T_e = 2 \text{ eV}$$

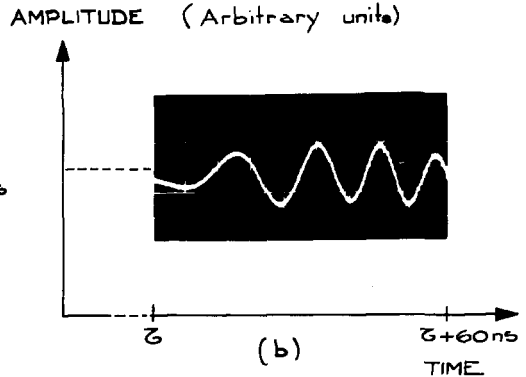
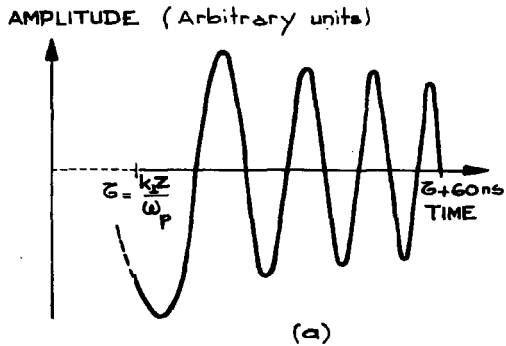
$$Z = 15 \text{ cm (distance between the emitter and the receiver probe)}$$

$$\text{Voltage probe} \begin{cases} \text{Rise and fall times} \approx 10^{-9} \text{ s} \\ \text{Amplitude} \approx 1.5 \text{ v} \end{cases}$$

$$\tau_{th} = \frac{k_1 Z}{\omega_p} = 53 \text{ ns}$$

$$\tau_{exp} = 57 \text{ ns}$$

Fig. 3 - DETECTED SIGNAL AND CORRESPONDING AIRY FUNCTION



157

EXPERIMENTAL PARAMETERS

Argon plasma

$B_0 \approx 1.5 \text{ kG}$

$n_0 \approx 2 \cdot 10^{18} \text{ el/cm}^3$

$T_e \approx 2 \text{ eV}$

$Z = 45 \text{ cm}$  (distance between the emitter and the receiver probe)

Voltage probe

$\left\{ \begin{array}{l} \text{Rise and fall times} \approx 10^{-9} \text{ s} \\ \text{Amplitude} \approx 1.5 \text{ v} \end{array} \right.$

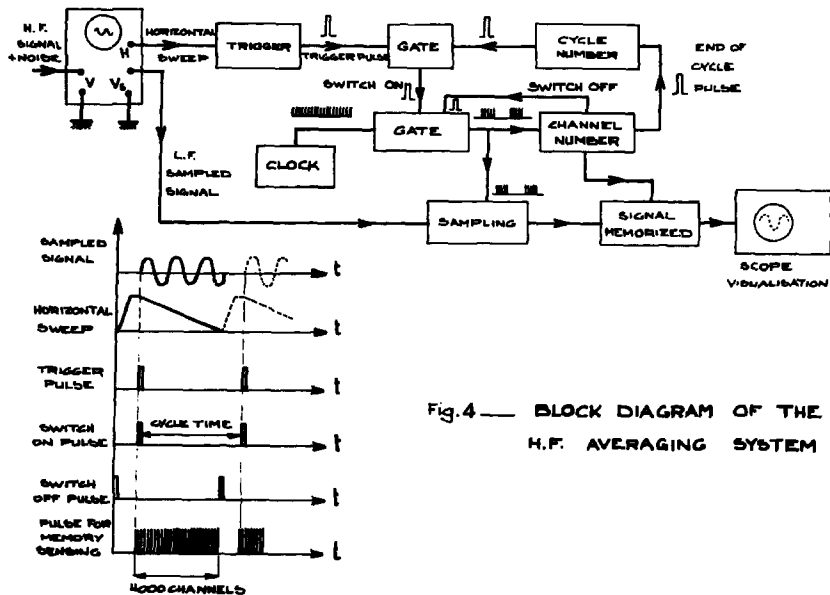
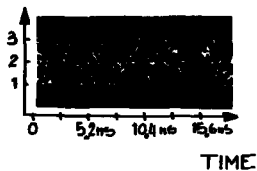


Fig.4 — BLOCK DIAGRAM OF THE  
H.F. AVERAGING SYSTEM



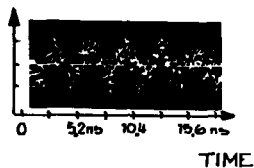
FIG. 5 - H.F. SIGNAL AVERAGING

AMPLITUDE (arbitrary units)



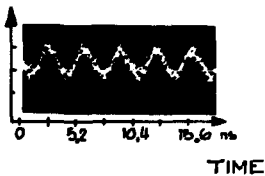
300 MHz H.F.  
NOISY SIGNAL

AMPLITUDE



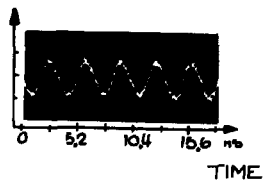
AVERAGED SIGNAL  
AFTER 10 CYCLES

AMPLITUDE



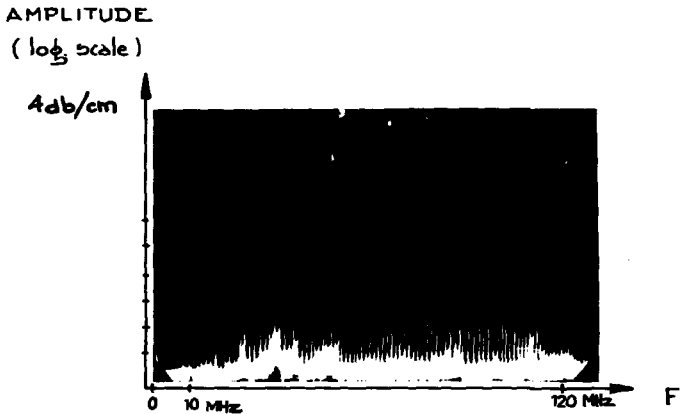
AVERAGED SIGNAL  
AFTER 100 CYCLES

AMPLITUDE



AVERAGED SIGNAL  
AFTER 500 CYCLES

Fig 6. FOURIER SPECTRUM OF THE RECEIVED SIGNAL



## EXPERIMENTAL PARAMETERS

Argon plasma  $n_0 \approx 2 \cdot 10^{18} \text{ el/cm}^3$

$B_0 \approx 1.5 \text{ kG}$   $T_e \approx 2 \text{ eV}$

$Z = 15 \text{ cm}$  (distance between the emitter and the receiver)

Voltage pulse: {

- Rise and fall times  $\approx 10^{-9} \text{ s}$
- Amplitude  $\approx 1.5 \text{ v}$
- Recurrence  $\approx 10^6 \text{ Hz}$

Ion-Acoustic Resonances in Bounded Plasmas and

Comparison with Refined Fluid Theory

R.R.Weynants, A.H.Messiaen, P.E.Vandenplas

Laboratoire de Physique des Plasmas - Laboratorium voor Plasmafysica  
*Ecole Royale Militaire* - *Koninklijke Militaire School*  
30, Avenue de la Renaissance - 30, Renaissanceaan  
1040 - Bruxelles - 1040 Brussel

Abstract

An extensive series of measurements is reported on ion-acoustic resonances in cylindrical plasmas. The results allow the identification of the noise components in a number of previous experiments. This furthermore increases the body of experimental evidence which can be compared with the theoretical predictions of our refined fluid model which takes non-neutrality into account in the neighbourhood of the transonic region.

I. Introduction

We report a series of experiments in the cylindrical plasma of a positive column dealing with the excitation of radial ion-acoustic resonances, i.e. the cut-offs of axially propagation modes. The theoretical difficulties linked to the radial drift-velocity due to the inhomogeneity of a real plasma are

well known /1/, but they can be overcome by not imposing a priori the condition of wave quasi-neutrality /2/ in such a drifting plasma .

Ion-acoustic standing waves have often been invoked to explain the low frequency components detected in the noise of positive columns /3/ or found to be parametrically excited in non-linear experiments /4/. The following factors greatly hamper the interpretation of these results:

1. Because of the uncontrolled excitation, a positive identification of the azimuthal dependence of the modes is difficult.

2. The noise in the positive column of most gases (Xe, Ne, Ar.-) is, to a large extent due to moving striations and occasionally to the ion-acoustic principal mode (i.e. the axisymmetric plane mode whose propagation properties are those of an unbounded medium).

3. In the non-linear experiments one should also add relaxation oscillations.

As a result, one should turn to controlled excitation. Our experiments are partly motivated by an apparent lack of convincing evidence for the existence of cut-off modes. Indeed, Jones and Little's results /5/ only occasionally hinted at cut-off, while, most of the time, they launched moving striations (M.S.) and the principal mode (P.M.) because higher order ion-acoustic modes are difficult to excite. Another reason for failure is the possibility of locking /6/ between the incident signal and the forementioned strong noise components; this is why a very quiescent plasma is required. The other motivation is of course to assemble a body of experimental facts that can be compared with our refined theory /2/. We tried to combine several favorable conditions : quiescent plasmas, excitation devices providing an axial wave number  $k_y$  approaching zero, so as to avoid the excitation of M.S. and P.M. in the appropriate frequency domain. Since the latter two modes are axisymmetric, a dipolar excitation is very interesting, although it does not always prove to be effective. Results are obtained in Hg, Xe and Ar over rather wide temperature and pressure ranges and they compare well with theory /2/. We should add that Alexandrov et al. /7/ recently obtained



results close to ours in a one-dimensional plasma capacitor.

## II. Experimental Set-Up

Several excitation set-ups yielding results which are in mutual agreement have been used, namely a probe system, magnetic coils and a non-linear electron temperature resonance experiment.

1. The probe system (previously reported in /8/, Fig.1) consists of two wires (10 cm in length) parallel to the axis and symmetrically immersed in a plasma column of radius 1.5 cm. The excitation can be in phase (mostly axisymmetric excitation) or in phase opposition (mostly dipolar excitation). The resonance phenomena are detected either by an external antenna system having the same symmetry as the excitation or by a photosensitive device, using coherent detection whenever necessary.

2. A system of dipolar magnetic coils is also used. It consists of two 8 cm long coils, symmetrically placed at the outside of the column and fed by phase opposite r.f. current to yield a magnetic induction of a few G. Two pick-up antennas are placed outside symmetrically with respect to the plane defined by the coil axes.

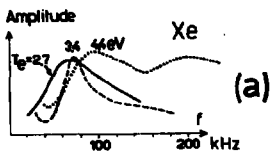
3. In the non-linear electron temperature resonance experiment, a 7.6mm i.d. tube ( $p=2 \times 10^{-3}$  Torr in Hg) is inserted across a rectangular waveguide (TE<sub>10</sub> mode,  $f_c = \omega/2\pi = 2.7$  GHz). The incident signal ( $P_{in} = 4$  to 8 W) is modulated at low frequency  $f_1$  (0-1 MHz) and the plasma density is adjusted on an electron temperature resonance /9/ (also called Tonks-Dattner resonance). The high-frequency is therefore just a means for bringing the low-frequency signal inside the plasma by non-linear demodulation of the resonant high-frequency signal. The plasma response at  $f_1$  is monitored by a pick-up antenna, by a photo device or in the modulation of the reflected microwave signal and furthermore coherently detected.

### III. Results

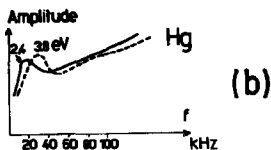
1. The probe system is effective for the excitation of radial axisymmetric modes. Broad peaks conforming to the predictions of the theory /2/ are observed in Hg, Xe and Ar; they are insensitive to density changes and have the correct mass and temperature dependence. The d.c. wire potential greatly influences the amplitude of the pick-up signal and is mostly maintained around plasma potential or up to some 20 V below, the a.c. signal amounting to a few V. Typical axisymmetric results are shown in Fig 1a. Contrarily to our earlier belief /8/, the probe system is not very effective in exciting dipolar modes. Indeed, our improved apparatus shows that symmetric components and harmonics are easily excited, apparently caused by non-linear sheath effects and asymmetry. The symmetric resonances then also yield a dipolar response. The spectra reported in /8/ are thus a mixture of predominant symmetric and less accentuated dipolar modes. Pure dipolar results are, however, obtained with the magnetic coil system which is free of the above inconveniences (Fig.1b).

2. Special attention is also paid to the noise spectra in view of a comparison with previous work /3/. The noise spectrum in Hg at  $2 \times 10^{-3}$  Torr ( $a = 1.45$  cm,  $T_e = 2.3$  eV) has its most prominent component at 42 kHz in agreement with Crawford's results. We interpret this noise frequency as the eigenvalue corresponding to the fundamental axisymmetric mode, that, upon excitation, occurs at a slightly higher frequency. We should also add that, still in Hg, a noise component occurs near the frequency of the excited dipolar resonance in that section of the tube where the wire system imposes some degree of dipolarity. We should stress, however, that Hg around  $10^{-3}$  Torr provides the only case where we can link the observed noise to radial ion acoustic waves and, thus, to the excited resonances. In Xe, Ar and Ne, we mostly found moving striation-noise with highly defined frequencies and occasionally much broader principal mode-noise. They were identified by showing that their measured  $\omega$  and  $k$  could be located on the dispersion curves experimentally found by launching waves with forward and backward characteristics by means of a magnetic coil system /5/.

3. The spectra obtained from the non-linear electron temperature resonance experiments in Hg are a mixture of symmetric and dipolar modes since the

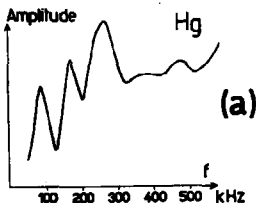


Plasma response picked-up by photo device with symmetric probe excitation (amplitude in arbitrary units,  $d = 2.9$  cm).

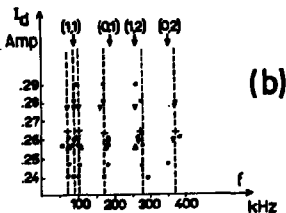


Plasma response picked-up by antennas with dipolar magnetic excitation (*idem*).

Fig.1.



Typical plasma response picked-up by antenna with non-linear temperature resonance excitation. (Amplitude in arbitrary units,  $d = 7.8$  mm,  $T_e = 3$  eV).



Resumé of the resonance frequencies as observed in a number of runs when the density is adjusted around the top of the first temperature resonance. ( $I_d$  is the discharge current,  $a = 7.8$  mm,  $T_e = 3$  eV).

Fig.2.

azimuthal dependence of the excitation is not very well defined. A typical signal picked-up by the antenna is displayed in Fig.2, where we also give a resumé of the observed frequencies in a number of runs for working conditions around the top of the first Tonks-Dattner resonance. ( $I_d$  is the discharge current). The electron temperature is about 3 eV. The arrows mark the theoretical locations (see below) of the resonances ( $m, n$ ) where  $m$  indicates the azimuthal dependence and  $n$  the order of the resonance. Occasionally, we also observe a relaxation oscillation around 100 kHz, i.e. with a period of the order of the ionization or loss rate and due to changes in the plasma background induced by the high power level /10/. When it occurs, one also finds a peak at the frequency difference between the fundamental axisymmetric mode and this relaxation frequency.

#### IV. Discussion

1. Our results can be fully explained by the uniform plasma model with a node of perturbed velocity at the wall, which as shown in /2/ leads to "valid" results for a positive column plasma. The fact that this crude model furnishes nearly the same results as a more realistic one is due to two strong but competing effects: on the one hand, the streaming of the plasma which reduces the frequency and on the other the confinement of the oscillations within the plasma core bounded by the "transonic" region which increases the frequency. It was also shown that the damping of the resonances is very pronounced and mainly due to the velocity gradient. A typical comparison between theory and experiment is shown in Fig.3, the tube diameter being 2.9 cm.

2. Comparison between noise and excited resonances allows us to identify the azimuthal dependence of the modes observed in the noise. This has allowed us to positively identify the fundamental peak observed by Crawford as being an axisymmetric one. Similar comparisons can lead to an explanation by the same theory (see /11/) of the results of Alexeff et al. /3/, Markhudarov et al./3/, Alexandrov et al./7/, Assussen et al./4/ and Tzoar et al./4/. Such a comparison is shown in Fig.4 for Hg. The ordinate is the product of resonance frequency by diameter which allows a comparison between results obtai-

ned with different tubes.

3. The non-linear technique demonstrates that the modulation of a resonant microwave signal by a well-chosen lower frequency is an efficient way of coupling energy from the outside into the ion-acoustic resonances. The comparisons made under 1 and 2 add credit to the identification made in Fig.2 where the theoretical figures are relative to a temperature of 35.000°K. We plan to also use the method in resonantly sustained magnetized plasmas to investigate the influence of a magnetic field on the resonances.

The following conclusions emerge : Ion-acoustic resonances are generally very broad and damped and, when sought in the noise, are very often masked by the much stronger moving striations. Our experimental results, obtained with different excitation methods permit the identification of the noise components in a number of previous experiments. As such they permit to considerably increase the range of experimental evidence which can be used for comparison with theory.

#### References

- 1/ B.Bertotti, A.Cavaliere, and P.Giupponi, *Phys.Fluids* 9, 265 (1966).  
A.Cavaliere, F.Englemann, and A.Sestero, *Phys.Fluids* 11, 158 (1968).  
E.Rosa and J.A.Allen, *J.Plasma Phys.* 4, 195 (1970).
- 2/ R.R.Weynants, A.M.Messiaen, and P.E.Vandenplas, *Proc. 13th. Int. Conf. on Phenomena in Ionized Gases*, Oxford, 306 (1971).
- 3/ I.Alexeff and R.V.Meidigh, *Phys.Rev.* 129, 516 (1963).  
F.W.Crawford, *Phys.Rev.Letters* 6, 663 (1961).  
H.Tanaka, A.Hirose, and M.Kogamei, *Phys.Rev.* 161, 94 (1967).  
E.M.Barkhudarov, B.P.Zhuzhniya, and V.P.Korkhondzhiya, *Sov.Phys-Tech.Phys.* 13, 1345 (1969).
- 4/ R.A.Stern and N.Tzouar, *Phys.Rev.Letters* 17, 903 (1966).  
O.Demokan, H.Hsuan, K.E. Longren and R.A.Stern, *J.Appl. Phys.* 41, 2122 (1970).  
J.Amussen and Q.H.Las, *Appl.Phys.Letters* 15, 183 (1969).  
G.Lisitano, S.Bernabei and E.Sindoni, *Phys.Letters* 29A, 613 (1969).
- 5/ F.F.Little and H.G. Jones, *Proc.Phys.Soc.* 85, 979 (1965).  
F.J.Barrett and F.F. Little, *Phys.Rev.Letters* 14, 356 (1965).
- 6/ B.E.Keen and W.H.Fletcher, *J.Phys.D: Appl.Phys.* 3, 1868 (1970).
- 7/ A.F.Alexandrov, A.A.Kuzovnikov, V.S.Smiridkina, V.V.Tarasova, *Proc.9th Int. Conf. on Phenomena in Ionized Gases*, Bucharest, 505 (1969).

- /8/ A.M.Messiaen, R.R.Weynants, P.E.Vandenplas, Proc.Int.Conf.on Phys.Quies. Plasmas, Edit.Ecole Polytechnique Paris, 107 (1969).  
 /9/ A.M.Messiaen, P.E.Vandenplas, and J-L Monfort, Phys.Letters 29A, 573 (1969).  
 /10/ C.W.Mendel and R.A.Stern, J.Appl.Phys. 41, 734 (1970).  
 /11/ R.R.Weynants, Doctor dissertation (to be submitted).

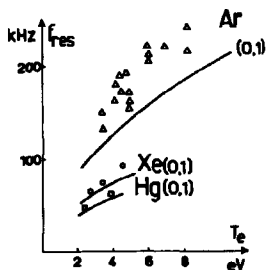
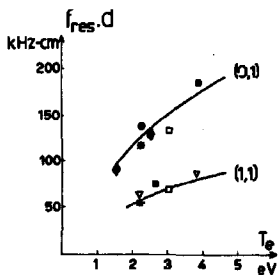


Fig.3.

Comparison of the experimental resonance frequencies with theory for the first symmetrical mode.



Hg

- probe excitation
  - ▼ coil excitation
  - non-linear excitation
  - noise
  - ◆ noise Crawford
  - Alexandrov (with correction from slab to cylinder)
- } this work

Fig.4.

Typical comparison for Hg of resonance frequencies observed in this and other investigations. The ordinate is the product of the resonance frequency by the tube diameter. The lines correspond to the theory.

Ion-Acoustic Instability of a Two-Temperature,  
Collisional, Fully-Ionized Plasma

by

T. D. Rognlien and S. A. Self

Institute for Plasma Research, Stanford University  
Stanford, California

Abstract

From a perturbation analysis of the fluid equations for a homogeneous unmagnetized plasma it is shown that long wavelength ion waves are unstable when  $T_e > T_i$ . The additional destabilizing effect of a current is also investigated.

Introduction

A plasma wave whose wavelength is small compared to the species mean free paths is described by collisionless kinetic theory. For electrostatic ion waves such treatments indicate stability, even for a two-temperature plasma.<sup>1-4</sup> These ion waves are Landau damped by electrons and ions, the latter predominating except when  $T_i \ll T_e$ . In the presence of a relative electron-ion drift (current), instability arises when Landau amplification by the electrons offsets Landau damping by the ions. When the wavelength is longer than the mean free path a fluid treatment is appropriate in which resonant particle effects are placed by transport effects.

For a weakly-ionized magnetoplasma, with  $T_i \ll T_e$ , the current and gradient-driven ion-acoustic and drift instabilities have been treated by Self<sup>5</sup> from the first two moment equations (continuity and momentum transfer), neglecting viscosity. In this case the destabilizing effect of drift is affected through electron-neutral collisions (resistance) and offsets ion-neutral collisional damping.

Fluid treatments have also been developed for fully-ionized collisional plasmas to describe gradient-driven drift instabilities in Q-devices. In the

two-moment (isothermal) theory of Hendel et al,<sup>6</sup> the destabilizing effect of drift is effected through electron-ion collisions (resistance) and offsets the damping due to ion-ion collisions (ion viscosity). The inclusion of third moment (energy) equations in a non-isothermal theory by Tsai et al<sup>7</sup> modifies the results somewhat. The latter treatment has been extended by Tsai et al,<sup>8</sup> to include the additional destabilizing effect of a current. It may be noted that for a fully-ionized plasma, unlike a weakly-ionized one, the destabilizing effect of current is not realized in a two-moment treatment neglecting electron viscosity, because of an exact cancellation of terms involving the drift. Furthermore, these treatments<sup>6-8</sup> do not reveal ion-acoustic modes because ion motion parallel to  $B_0$  is neglected.

Recently, Coppi and Mazzucato<sup>9</sup> have discussed the current and gradient-driven ion-acoustic and drift instabilities of a fully-ionized plasma from the three moment equations in connection with the anomalous resistivity observed in stellarators with a weak applied electric field  $E_0$ . The onset of anomalous resistivity is associated with the threshold of instability in current-driven ion-acoustic modes propagating parallel to  $B_0$  and  $E_0$ . Under these conditions the effects of  $B_0$  and the transverse gradients are negligible and their results apply to a uniform unmagnetized plasma. They calculate a threshold electron drift velocity as a function of wavelength and the plasma parameters.

In examining this analysis for the case of a uniform unmagnetized plasma, we have found that if certain terms, in particular the electron-ion collisional heat transfer, neglected by Coppi and Mazzucato, are included, the threshold drift velocity and growth rate may be quite different from the values they calculate. More especially we find that when  $T_i/T_e \leq 1$ , the system is unstable to long wavelength ion-acoustic modes even in the absence of any destabilizing currents or gradients. Thus the temperature difference alone can drive a resistive-type ion wave instability in a plasma which on a collisionless basis is stable.

### Theory

The fluid equations (i.e. continuity, momentum transfer and heat transfer) for an unmagnetized fully-ionized plasma may be written in the one-dimensional case for either species:

$$\partial n/\partial t + \partial(nv)/\partial x = 0, \quad (1)$$

$$mndv/dt = -\partial(nT)/\partial x + (4/3)\eta \partial^2 v/\partial x^2 + \sigma nE + R, \quad (2)$$

$$(3/2)nT/dt + nT\partial v/\partial x = -\partial q/\partial x + (4/3)\eta(\partial v/\partial x)^2 + Q. \quad (3)$$



The notation is that of Braginskii,<sup>10</sup> except where noted.

In Eq. (2) the charge  $\sigma = -e$  for electrons and  $\sigma = Ze$  for ions. The collision terms  $R_e = -R_i$  comprise frictional and thermal force components:

$$R_e = -C_{er} n_e n_e v_e (v_e - v_i) - C_{et} n_e (\partial T_e / \partial z),$$

where  $v_e (=v_{e1}) = (4/3)(2\pi)^{1/2} (1n\Lambda) Z n_e^3 (T_e^3 m_e)^{-1/2}$ , and  $C_{er} = 0.51$ ,  $C_{et} = 0.71$ . The viscosities are given by  $\eta_e = C_{e\eta} n_e T_e / v_e$  with  $C_{e\eta} = 0.73$ , and

$$\eta_i = C_{i\eta} n_i T_i / v_i \text{ with } C_{i\eta} = 0.96, \text{ where } v_i (=v_{i1}) = (4/3)(\pi)^{1/2} (1n\Lambda) Z^3 n_e^3 (T_i^3 m_i)^{-1/2}.$$

In Eq. (3) the electron heat flux is  $q_e = C_{et} n_e T_e (v_e - v_i) - \chi_e (\partial T_e / \partial z)$ , where the thermal conductivity is  $\chi_e = C_{e\chi} n_e T_e / m_e v_e$  with  $C_{e\chi} = 3.16$ . The ion heat flux is  $q_i = -\chi_i (\partial T_i / \partial z)$ , where the thermal conductivity is  $\chi_i = C_{i\chi} n_i T_i / m_i v_i$  with  $C_{i\chi} = 3.9$ . The heat acquired by electrons through collisions is  $Q_e = -R_e (v_e - v_i) - Q_\Delta$ , where  $Q_\Delta = 3(m_e / m_i) n_e v_e (T_e - T_i)$ . The heat acquired by ions is  $Q_i = Q_\Delta$ . The heat generated by viscosity is of second order in the velocity gradients and will be neglected.

The values quoted for the numerical coefficients of electron thermal force ( $C_{et}$ ), resistance ( $C_{er}$ ), viscosity ( $C_{e\eta}$ ) and thermal conductivity ( $C_{e\chi}$ ) are for  $Z = 1$ ; values for  $Z > 1$  are tabulated by Braginskii.<sup>10</sup>

We consider a homogeneous, neutral ( $Zn_{i0} = n_{e0}$ ) steady state, including an electron drift velocity  $v_{e0}$  relative to the fixed ion frame. Strictly, a homogeneous steady state with different temperatures or a current, neglecting other heat sources and sinks, is not possible in the presence of collisions. So, as usual, we neglect collisions in the steady state but include them in the perturbed equations. The variables  $n_e, n_i, v_e, T_e, T_i$  are perturbed in the form  $n_e = n_{e0} + n_{e1} \exp i(\omega t - kz)$ . We also assume neutrality,  $Zn_{i1} = n_{e1}$  and ignore Poisson's equation, so that the results are valid for low frequencies ( $\omega \ll \omega_{pi}$ ) and long wavelengths  $k\lambda_{De} \ll 1$ .

The continuity equations (1) yield to first order:

$$\begin{aligned} v_{e1} &= [(\omega - kv_{e0})/k](n_1/n_0), \\ v_{i1} &= (\omega/k)(n_1/n_0). \end{aligned} \quad (4)$$

On adding the momentum transfer equations for electrons and ions, the electric field and collision terms cancel. Neglecting electron inertia, in view of the restriction to low frequencies, and eliminating the velocities using Eq. (4), we have to first order:

$$\left\{ -\omega^2 + i \frac{4}{3} \frac{\omega v_{e0}^2}{n_e} \left[ 2^{1/2} C_{i\eta} n_i T_i^{5/2} / Z^2 + \frac{C_{e\eta} Z}{n_e} \left( 1 - \frac{kV}{\omega R_n} \right) \right] + \frac{(\cdot R_T)}{n_e^2} k^2 \right\} \left( \frac{n_1}{n_0} \right) + \left\{ \frac{R_T k^2}{n_e^2} \right\} \left( \frac{T_{i1}}{T_{i0}} \right) + \left\{ \frac{2k^2}{n_e^2} \right\} \left( \frac{T_{e1}}{T_{e0}} \right) = 0. \quad (5)$$

Here  $W = \omega/v_e$  is the normalized frequency,  $K = k(T_{e0}/m_e)^{1/2}/v_e = k\lambda_e$  is the normalized wavenumber,  $\lambda_e$  being the electron mean free path,  $R_m^2 = n_1/n_0$  is the mass ratio,  $R_T = T_{10}/T_{e0}$  is the temperature ratio and  $V = v_{e0}/(T_{e0}/m_e)^{1/2}$  is the normalized drift velocity.

In an isothermal theory based on two moment equations, the dispersion relation is just the coefficient of  $(n_1/n_0)$  in Eq. (5) equated to zero. This exhibits viscous damping due to ions and electrons analogous to Landau damping in the collisionless case. It also shows a destabilizing effect due to electron viscosity when  $(KV/W) > 0$ . For instability  $v_{e0}/(\omega/k) \geq 1 + 2^{1/2}(C_{1\eta}/C_{e\eta})R_m^{5/2}/Z^{3/2}$  where the phase velocity  $(\omega/k) = [(ZT_{e0} + T_1)/n_1]^{1/2}$ .

To first order the electron energy equation yields, using Eq. (4):

$$\left\{ -1 \left( W - \frac{KV}{R_m} \right) + 6 \frac{(1-R_T)}{R_m^2} \right\} \left( \frac{n_1}{n_0} \right) + \left\{ \frac{-3R_T}{R_m^2} \right\} \left( \frac{T_{11}}{T_{10}} \right) + \left\{ 1 \frac{3}{2} \left( W - \frac{KV}{R_m} \right) + \frac{3}{2} \frac{C_{e\eta} V^2}{R_m^2} + C_{e\kappa} K^2 - \frac{3}{2} \frac{(1-3R_T)}{R_m^2} \right\} \left( \frac{T_{e1}}{T_{e0}} \right) = 0. \quad (6)$$

Similarly the ion energy equation yields:

$$\left\{ -1W - \frac{6Z(1-R_T)}{R_m^2 R_T} \right\} \left( \frac{n_1}{n_0} \right) + \left\{ 1 \frac{3}{2} W + 2^{1/2} \frac{C_{1\eta} R_T^{5/2} K^2}{R_m^2} + \frac{3R_T}{R_m^2} \right\} \left( \frac{T_{11}}{T_{10}} \right) + \left\{ \frac{3}{2} \frac{Z(1-3R_T)}{R_m^2 R_T} \right\} \left( \frac{T_{e1}}{T_{e0}} \right) = 0. \quad (7)$$

The eliminant of Eqs. (5)-(7) is the dispersion relation, which is quartic in  $W$ . Numerical investigation shows that for real  $K$  there are two highly damped roots ( $W_1 > 0$ ), corresponding to electron and ion temperature waves and a pair of roots with  $W/K \sim \pm R_m^{-1}$  corresponding to ion waves propagating in either direction. The latter may be stable ( $W_1 > 0$ ) or unstable ( $W_1 < 0$ ) depending on the parameter values.

When the wavelength is not too large ( $R_m^2 \gg R_m^{-2}$ ) and for  $R_T \leq 1$ , the ion wave roots may be approximated by:

$$(W_1/K) \approx \pm (Z + 5 R_m/3)^{1/2}/R_m, \quad (8)$$

i.e.  $(\omega_1/k) \approx \pm [(Z T_{e0} + (5/3) T_{10})/n_1]^{1/2}$ , and

$$W_1 \approx \frac{2^{3/2}}{3} \frac{R_T^{5/2}}{R_m^2} C_{1\eta} K^2 + \frac{2}{3} \frac{R_T}{R_m^2} C_{e\eta} K^2 \left( 1 - \frac{KV}{W_1 R_m} \right) + \frac{2^{3/2}}{9} \frac{R_T^{7/2} C_{1\eta} K^2}{Z^2 R_m (Z+5R_m/3)} + \frac{R_T}{2R_m^2 C_{e\kappa}} \left( 1 - \frac{KV}{W_1 R_m} \right) - \frac{2Z(1-4R_m/3)}{R_m^2 (Z+5R_m/3)}. \quad (9)$$

Discussion

In Eq. (9) the terms are respectively the contributions of ion viscosity, electron viscosity, ion thermal conductivity, electron thermal conductivity and collisional energy transfer ( $q_{\Delta}$ ). The first four terms are all stabilizing (when  $V = 0$ ) but the last is destabilizing for  $R_T < 3/4$ . Drift is coupled via the electron viscosity and thermal conductivity, in a destabilizing sense when  $KV/W R_m > 0$  i.e. for the wave with phase velocity in the sense of  $v_{e0}$ . The ion terms tend to zero as  $T_1 \rightarrow 0$  and are proportional to  $R_m^{-1}$ , while the electron and collisional energy transfer terms are proportional to  $R_m^{-2}$ . The first three terms contain a factor  $K^2$ , so that the last two terms, which do not, dominate for long wavelengths.

Considering first the case  $V = 0$ , it is clear that for long wavelengths and  $R_T$  small enough, the destabilizing effect of the collisional energy transfer can overcome the stabilizing effects, principally that of electron thermal conduction. Figure 1 shows the real  $K$  contour mapped into the  $W$  plane for the ion wave root for  $R_m^2 = 1837$ , corresponding to hydrogen, and for various temperature ratios  $R_T$ . These results were computed from the full dispersion relation and agree approximately with those given by Eqs. (8) and (9) in their range of validity. The map is symmetric about  $W_r = 0$ . Since there is a branch point at the origin ( $W=0, K=0$ ), the system lies on the boundary between convective and absolute instability. Except when  $R_T \leq 0.1$ , instability is confined to the region  $0 < |K| \leq 1$ , under which conditions the fluid treatment is valid. From Eq. (9) one finds instability for:

$$K^2 < \frac{3W^3}{2} \left\{ \frac{2(1-4R_T/3) - (2+5R_T/3)/2 C_{eK}}{(2^{1/2} R_m R_T^{5/2} C_{e1} + 2^3 C_{e1}) (2+5R_T/3) + (2^{1/2}/3) R_m R_T^{7/2} C_{e1}} \right\}. \quad (10)$$

The maximum growth rate occurs for  $R_T \ll 1$  and is of order  $(-\omega_1)_{\max} \sim (n_e/n_i)^{1/2} v_{e1}$ . This is comparable with the characteristic rate of energy transfer by collisions between electrons and ions.

With drift, for  $K^2 \gg R_m^{-2}$ , instability occurs when the electron viscosity and electron thermal conduction terms balance the stabilizing effects, principally ion viscosity and ion thermal conduction, together with the effect of collisional energy exchange, which may be stabilizing or destabilizing according as  $R_T \gtrless 3/4$ . From Eq. (9) we find instability for velocities satisfying:

$$\frac{v_{e0}}{[(\pi T_{e0} + \pi T_{i0}/3) n_1]^{1/2}} > 1 + \frac{\{ 2^{3/2} R_{iT}^{5/2} [(z + 5R_{iT}/3) C_{\parallel} + R_{iT} C_{\perp} / 3] k^2 - 6z^3 (1 - 4R_{iT}/3) \}}{z^3 (z + 5R_{iT}/3) [(3/2c_{ex}) + 2c_{e\parallel}] k^2} \quad (11)$$

If we neglect electron viscosity (last term in denominator) and collisional energy exchange (last term in numerator), Eq. (11) reduces to Eq. (53) of Reference 9, apart from notation. It is clear that the threshold velocity is sensitive to the inclusion of the collisional energy exchange, and, as was shown above, may be zero, corresponding to instability driven purely by the temperature difference. Figure 2 shows the real  $K$  contour mapped into the  $W$  plane without drift and with a drift of  $V = 4$  for the case of hydrogen ( $n_m^2 = 1837$ ) and for  $R_{iT} = (1/2)$  and  $(1/10)$ . These results were computed from the full dispersion relation. It is seen that drift destabilizes the wave with phase velocity in the sense of the drift and stabilizes the wave with phase velocity in the opposite sense. For the case  $R_{iT} = (1/10)$  the drift of  $V = 4$  roughly doubles the maximum growth rate predicted in the absence of drift.

Because the free energy driving the instability derives from the non-equilibrium of the two-temperature plasma, it is clear that the instability must result (nonlinearly) in a decrease in the relaxation time to equilibrium below the purely collisional value, or, if the temperature difference is maintained, in an increase in the energy coupling between electrons and ions above the collisional value. Such effects may be important in plasmas which are large enough to be collisional, when they are heated by steady or high frequency electric fields. Since, in the latter case the absorption of high frequency power is density dependent, the excitation of low frequency density fluctuations can react back on the heating process.

Since in many naturally occurring and laboratory plasmas, the electron temperature tends to be significantly higher than the ion temperature because of the mechanisms by which the plasma is maintained or heated, it seems likely that, provided the plasma is larger than an electron mean free path, low frequency, long wavelength ion waves will spontaneously occur. This may explain the low level of low frequency turbulence commonly observed in ionospheric and laboratory discharge plasmas which appears to be independent of the presence of other known destabilizing influences such as currents, beams or gradients transverse to a magnetic field.

There are also possible implications for the solar wind. Cupperman<sup>11</sup> has shown that the observed profiles of density and temperatures can only be explained by the two-species fluid equations if one assumes a heat transfer between electrons and protons some 30 times the collisional value. It has

been suggested that such an enhanced transport is due to turbulence in Alfvén waves originating at the sun. An alternative possibility raised by the present work is that the solar wind is unstable to low frequency ion waves and such turbulence accounts for the enhanced transport.

Useful discussions with Dr. F. W. Crawford are gratefully acknowledged. This work was supported by the National Aeronautics and Space Administration.

#### References

1. B. D. Fried and R. W. Gould, *Phys. Fluids* 4, 139 (1961).
2. J. D. Jukes, *J. Nucl. Energy* C3, 140 (1961).
3. T. E. Stringer, *J. Nucl. Energy* 06, 267 (1964).
4. I. B. Bernstein and R. M. Kulsrud, *Phys. Fluids* 3, 937 (1960).
5. S. A. Self, *J. Plasma Physics* 4, 693 (1970).
6. H. W. Hendel, B. Coppi, F. Perkins and P. A. Politzer, *Phys. Rev. Letters* 18, 439 (1967).
7. S. T. Tsei, F. W. Perkins and T. H. Stix, *Phys. Fluids* 13, 2108 (1970).
8. S. T. Tsei, R. F. Ellis and F. W. Perkins, *Phys. Fluids* (to be published).
9. B. Coppi and E. Mazzucato, *Phys. Fluids* 14, 134 (1971).
10. S. I. Braginskii, in Reviews of Plasma Physics, edited by M. A. Leontovich (Consultants Bureau, New York, 1965) Vol. I, p. 205.
11. S. Cuperman and A. Harten, *Astrophysical Journal* 162, 315 (1970); 163, 383 (1971).

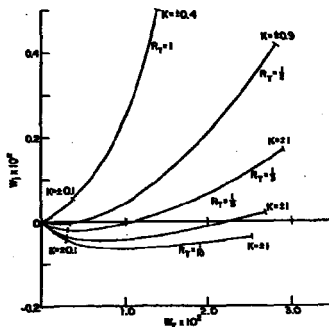


FIG. 1. Map of the real  $K(= k\lambda_e)$  contour into the complex  $W(= \omega/\nu_{ei})$  plane for a hydrogen plasma ( $R_m^2 = 1837$ ) and various temperature ratios  $R_T(= T_1/T_e)$ , showing instability for long wavelengths ( $K^2 \ll 1$ ) when  $R_T \leq 1$ .

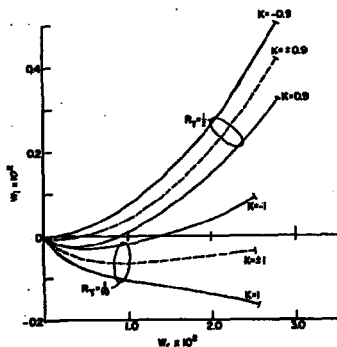


FIG. 2. Map of the real  $K(= k\lambda_e)$  contour into the complex  $W(= \omega/\nu_{ei})$  plane for a hydrogen plasma ( $R_m^2 = 1837$ ) for  $R_T(= T_1/T_e) = (1/2)$  and  $(1/10)$ . The broken curves are for zero drift while the solid curves are for a drift of  $V(= v_{e0}/(T_e/n_1)^{1/2}) = 4$ .

WAKE BEHIND A BODY IN MOTION IN A PLASMA,  
PARALLEL TO THE MAGNETIC FIELD. THEORETICAL SOLUTION

J.P.M. SCHMITT

Laboratoire de Physique des Milieux Ionisés  
Ecole Polytechnique, Paris - France  
(Equipe de Recherche associée au C.N.R.S.)

ABSTRACT

In this paper we extend the original work of Al'Pert et al. [1], for the wake behind a body in motion in a plasma, to include the effects of a parallel ion temperature and of the electric field. In addition, we consider the effects produced when the cross-sectional area of the body is made to vary periodically in time. It is found that the spatial oscillations are damped by the thermal motion of the ions, and that the spatial period of the wake is shorter than that given by the purely ballistic treatment of Al'Pert et al. The electric field leads to a coupling of the wake with parallel ion acoustic waves and with perpendicular ionic Bernstein modes, which we study in the linear approximation. The modulation of the cross-sectional area produces "magneto ballistic pseudo waves" which propagate along the ion trajectories.

I. INTRODUCTION

The plasma perturbation associated with a body in motion relative to a plasma has received considerable attention for numerous reasons, including the problem of interpreting results from probes in a streaming plasma, and the effects of the wake of a satellite on waves, [2]. A fundamental work on the subject was done by Al'Pert et al. [1]. They predict in the particular case of a body moving parallel to the magnetic field in a collisionless plasma, a remarkable wake, very long and pronounced, with a periodic structure having a spatial period equal to the distance travelled by the body during an ion gyroperiod. All these results were obtained from a purely ballistic theory which neglects the effects of collisions, the parallel ionic temperature and the electric field. In this paper we neglect collisions also; however, we consider the effects of the other two perturbations. First we discuss the basic assumptions and useful approximations for the problem (Sec II). We then describe the zero-order solution for the wake problem, given by the ballistic approximation, including the damping effects of the ionic thermal motion. (Sec III). After this, we describe the solution of the linearized problem, using a new approximation to estimate the coupling of the

wake with the ionic Bernstein waves. (Sec IV). Finally, we discuss the results and give our conclusions. (Sec V).

## II. BASIC ASSUMPTIONS .

We will assume that 1) there are no collisions. This is valid when the ionic collision frequency  $\nu_i$  is much less than the ionic gyrofrequency  $\Omega/2\pi$ . (For the treatment with collisions reader should refer to [3,4]) ; 2) the electrons follow the Boltzmann law in so far as the velocity of the body  $v_p$ , is much less than the electron thermal velocity; 3) There is no important ion deflection on the edge of the body [5,6]. The body is assumed to act only as a particle absorber. This is valid for a body at the floating potential when the Debye Length  $\Lambda$  is much less than the body size ; 4) The equilibrium density  $n_0$  and the magnetic field  $B_0$  are uniform ; 5) The perpendicular ionic distribution function is Maxwellian with a temperature  $T_i$  and a corresponding thermal velocity  $v_0 = \sqrt{\frac{2k T_i}{m_i}}$  and mean Larmor radius  $\rho_i = v_0 / \Omega$  ; 6) The body is flat with its plane perpendicular to the streaming direction. Whatever is the body shape, it can be reduced to its projected area  $S$  in a mean plane (which will be the plane  $z = 0$ ), providing the body thickness is much less than  $L = 2 \pi v_p / \Omega$ .

Even with the above assumptions, the resolution of the Vlasov equations for the ionic distribution function  $f_i(x, v, t)$  and the potential  $V(x, t)$  is still too complicated, and requires others assumptions. The most drastic is the ballistic approximation : 7) The self consistent electric field is negligible and the electrons are assumed to provide complete neutrality. Another assumption frequently used is the linear approximation [1,7] ; 8) The perturbation and the related electric field are assumed to be weak. This is strictly valid only in the far wake where the perturbation is damped but, anyway this approximation is less strong than the ballistic approximation.

## III. THE BALLISTIC APPROXIMATION .

Using the assumptions 1) to 7) the Vlasov system reduces to the linear equation

$$\frac{\partial f_i}{\partial t} + v \frac{\partial f_i}{\partial x} + \frac{q_i}{m_i} v A B_0 \frac{\partial f_i}{\partial v} = 0 \quad (1)$$



The equilibrium ionic distribution function in the body reference frame, is given by

$$f_{io}(v) = \frac{n_0}{\pi v_0^2} \exp - \frac{v_z^2 + v_\perp^2}{v_0^2} f_{io}(v_z) \quad (2)$$

where  $f_{io}(v_z)$  is the normalized parallel ionic distribution function drifting with a velocity  $v_p$ . The boundary conditions, given in the  $z = 0$  plane, are :

$$\begin{aligned} \text{Outside S} \quad & f_i(v) = f_{io}(v) \\ \text{Inside S} \quad & \begin{cases} f_i(v_z < 0) = f_{io}(v) \\ f_i(v_z \geq 0) = T f_{io}(v) \end{cases} \quad (3) \end{aligned}$$

where  $T$  is the transparency of the body - Generally  $T = 0$ , but in order to represent a body the cross section of which is modulated at a frequency  $\omega_0$ , we take a model in which  $T = 1 - \cos \omega_0 t$

For  $z > 0$  the resulting density  $n$  and ionic flux  $j$  can be expressed as :

$$n(x, y, z, t) = n_0 \left[ 1 - \int_0^z H_B(x, y, z, v_z) \cos \omega_0 \left( t - \frac{z}{v_z} \right) f_{oi}(v_z) dv_z \right] \quad (5)$$

$$j(x, y, z, t) = n_0 \left[ v_p - \int_0^z H_B(x, y, z, v_z) \cos \omega_0 \left( t - \frac{z}{v_z} \right) f_{oi}(v_z) v_z dv_z \right] \quad (6)$$

where  $H_B(x, y, z, v_z) = \iint_0^R H(x - x', y - y', z, v_z) dx' dy'$

$$H(x, y, z, v_z) = \frac{\exp - \frac{x^2 + y^2}{4 \rho_i^2 \sin^2(z/2v_z)}}{4 \pi \rho_i^2 \sin^2(z/2v_z)}$$

For  $\omega_0 = 0$  and neglecting the parallel ionic velocity spread,  $n$  and  $j$  are periodic functions of  $z$  with a period  $L = 2\pi v_p / \Omega$ . In the case of a disk of radius  $R$ , the density along the axis is given by

$$n(z) = n_0 \exp - \frac{R^2}{4 \rho_i^2 \sin^2(\pi z/L)} \quad (7)$$

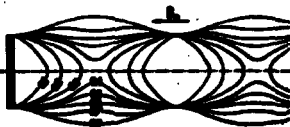


FIG. 1

Isodensities in the wake of a disk computed for  $R = 1.4 \rho_i$ . The densities are normalized to the equilibrium density.

Figure 1 shows the calculated structure of a wake for a monoenergetic ion stream. Note that the density as a function of  $z$  along a field line oscillates in opposite phase whether the field line crosses or not the body.

The parallel ionic velocity spread provides through the integration on  $v_z$  in (5) and (6) a damping of the spatial oscillations.  $f_{i0}(v_z)$  in a Q machine with a low density ( $n_0 \leq 10^{16} \text{cm}^{-3}$ ) is a truncated Maxwellian [8,9,10]. We studied the damping of the wake oscillations for this case and for  $\omega_0 = 0$ . Exact numerical calculations and approximate analytical calculations give the same results. The pseudo period of oscillation is given by the cut-off velocity, (and not the mean velocity  $v_p$  which is a little greater.) The oscillations are damped as  $1/z$ . The very far wake is a cylindrical hole. (But collisions should be taken into account at such a distance).

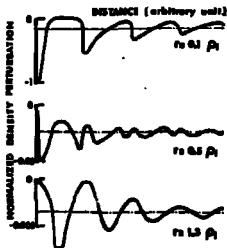


FIG. 2

Perturbed density versus the distance in the wake behind a very small body ( $R \ll \rho_1$ ). Three curves are given for various distances  $r$  from the wake axis. The parallel distribution function used in this case was  $f_{i0}(v_z) \sim \exp -v_z^2/v_0^2 Y(v_z - 2v_0)$  where  $Y$  is the step function.

When in  $f_{i0}(v_z)$ , the velocity spread  $\Delta v$  is much less than  $v_p$ , an approximate law can be obtained from Eq.(6) giving the amplitude of the flux maxima as a function of their order  $k$  along a given field line.

$$j(x,y, (k + \frac{1}{2}) L) = \alpha(x,y) + \beta(x,y) \left( \frac{\Delta v}{v_p} \right)^2 (2k + 1)^2 \quad (8)$$

where  $\alpha$  and  $\beta$  depend only of the geometry of the body. Note that this relation is valid only when  $k\Delta v \ll v_p$ .

When  $\omega_0 \neq 0$ , the modulation of the body transparency progresses in the plasma stream along the ion trajectories as a three dimensional pseudo wave which is comparable to one-dimensional pseudo-waves [11,12]. In a given position behind the body, the density and the ionic flux are modulated in time. We find that the modulation amplitude is at a maximum where the density is at a minimum in the steady wake, and vice versa. When  $\omega_0 \ll \Omega_p$ ,

the amplitude of the density modulation and the perturbed density in a steady wake are similar, in particular they have both the same damping as a function of  $x$ . For intermediate values of  $\omega_0$  ( $\omega_0 \approx \Omega/10$ ), the spatial oscillations of the pseudo wave amplitude are a little less damped than the density oscillations of the steady wake.

#### IV. INFLUENCE OF THE ELECTRIC FIELD

The above results are obtained using the ballistic approximation, which gives only a zero-order solution of the wake problem. This solution will now be modified in accordance with the assumptions 1) to 6) and B) taking into account the first-order effects of the electric field. The formal resolution of the linearized Vlasov equations by means of a Fourier transform has been already done [1,7]. However, the inverse transform is practically impossible. It has been demonstrated also, that the parallel effects of the electric field are connected with the excitation of parallel ionic waves by the moving body [1]. Doing similar calculations, we have found that the coupling of the wake with parallel ionic waves can be regarded as negligible (less than 2 % of difference on the density Fourier transform) as long as  $v_p > 2v_\phi$ , where  $v_\phi$  is the ionic wave phase velocity.

To estimate the perpendicular effects of the electric field, it is interesting to look at the problem from a vantage point within the plasma reference frame. At time  $t = 0$  the body passes by the plasma, creating a cylindrical hole which we will assume to be infinitely long, provided that  $R \ll L$ . Then the plasma relaxes from this initial state. In the ballistic approximation, the hole will oscillate at the ionic gyrofrequency with no damping. This explains the spatial oscillations of the wake in the body reference frame. In our treatment of the problem, we solve the linearized Vlasov equations with the initial condition for the perturbed ion distribution function  $f_{11}(x, v, t = 0) = n_0(x) f_{10}(v)$ , which has cylindrical symmetry. The equilibrium function  $f_{10}(v)$  is assumed to be Maxwellian. A Hankel Laplace transform ( $x \rightarrow k_\perp$ ,  $t \rightarrow m$ ) yields the perturbed ionic density.

$$n(k_\perp, m) = \frac{n(k_\perp) \Gamma(\omega/\Omega) k_\perp^2 \rho_\perp^2 / 2}{1 + \frac{1 + m/\Omega \Gamma(m/\Omega) k_\perp^2 \rho_\perp^2 / 2}{1 + \Lambda^2 k_\perp^2 / 2}} \quad (9)$$

where 
$$\left\{ \begin{aligned} T(a, b) &= \frac{e^{-b}}{a} (I_0(b) + 2 \frac{2a}{N^2 - a^2} \text{IN}(b)) ; \\ n(k_{\perp}) &= \int_0^{\infty} J_0(k_{\perp} r) n(r) r dr. \end{aligned} \right. \quad (10)$$

$n(k_{\perp}, \omega)$  is given by a ratio in which the numerator is the pure ballistic solution of the same problem and the denominator the dispersion function for ionic Bernstein waves [13]. The singularities of  $n(k_{\perp}, \omega)$  for a given real  $k_{\perp}$  are an infinity of single real poles which are near  $\Omega$  and its harmonics. The variations of the positions of the poles as a function of  $k_{\perp}$  are given in figure 3.

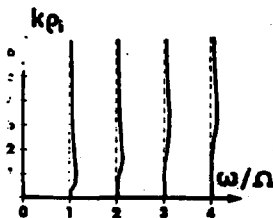


FIG. 3.

Dispersion curves of the ionic Bernstein waves. This case is for  $T_0 = T_1$  and  $\Lambda = \pi/3$

The summation of the poles residues and the Hankel inverse integration has to be done numerically. We computed the evolution of the axial density in an initially Gaussian shaped hole, as a function of time for two typical cases : a body of three millimeters radius in a Q machine and a large satellite in the ionosphere (altitude about 500 km).

In figures 4 and 5 we note that the coupling of the relaxation of the hole with Bernstein waves not only shifts the oscillations frequency to a mean value  $\Omega'$  larger than  $\Omega$ , but also produces distortion and damping of the oscillations. For a disk in a Q machine plasma, as shown in figure 4 ( $R \approx \pi > \Lambda$ ), the oscillations are not very distorted and the frequency  $\Omega'$  is about  $1,16 \Omega$ , which corresponds closely to the maximum of the dispersion curves of ionic Bernstein waves in the first pass-band (indicated by an arrow in figure 3). For a satellite in the ionosphere, the parameters are typically related as  $\pi > R \gg \Lambda$ . The oscillations of the waves seem to be

more distorted and damped than in the previous case. Thus, the coupling with Bernstein waves can make the density on the wake axis overcome the equilibrium density. We note, however, that the frequency is not very much shifted.

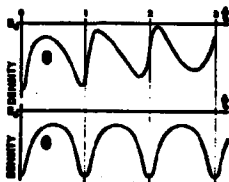


FIG. 4

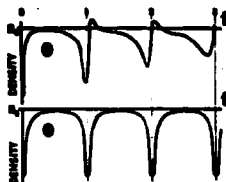


FIG. 5

Axial density as a function of time in a hole the profile of which was Gaussian at time  $t = 0$ . The time is normalized to the ion gyroperiod and the density unit is arbitrary. Curves 1 are calculated in the linear approximation and curves 2 in the ballistic approximation. Figure 4 is for  $T_e = T_i$ ,  $R = \rho_i$  and  $\Lambda = \rho_i/10$ . Figure 5 is for  $T_e = T_i$ ,  $R = 0.3 \rho_i$ , and  $\Lambda = 0.08 \rho_i$ .

#### V. SUMMARY AND CONCLUSIONS .

In the wake problem for a body in motion parallel to the magnetic field, in a collisionless plasma, the ballistic approximation gives a zero-order to the ion dynamics which is qualitatively good. The periodic wake predicted by Al'Pert et al. is diffused as a consequence of the parallel ion velocity spread and the self consistent electric field. The wake damping given by the parallel ion thermal motion is studied in the ballistic approximation. The damping is an increasing function of the parallel ion temperature.

The electric field effects are studied in a linear approximation. We show that there is a coupling of the wake with the ionic Bernstein modes which modifies the ballistic wake by shifting the spatial period to a smaller value, by distorting the oscillations and by increasing the damping. All these effects are more or less important according to the plasma parameters, and each case has to be computed.

The propagation of the signal given by the modulation of the transparency of the body is, in the first approximation, described by the ballis-

tic approximation. The calculated pseudowave has an amplitude which is a function of space in a same manner as the perturbed density in the steady wake behind a similar solid body, provided that the modulation frequency is much less than the ionic gyro frequency. Under the same condition, the self consistent electric field have the same consequences on the pseudo wave than on the steady wake.

- REFERENCES -

- [1] Y.L. Al'Pert, A.V. Gurevitch, and L.P. Piteevskij, Space Physics with artificial satellites, Consultant Bureau, New York, (1965)
- [2] J.M. De Leeuw, Rarefield Gas Dynamics, suppl. 4, 11, (C.L. Brundi éditeur), Académic Press, New-York, 1561, (1967).
- [3] F. Albini, and S. Rand, Phys. Fluids, 1, 480, (1958).
- [4] Y.S. Pan, and R. Vaglio Laurin, AIAA J., 5, 10, 1801, (1967).
- [5] L. Krauss, and K.M. Watson, Phys. Fluids, 1, 480, (1958)
- [6] S.D. Heeter, and A. Gonin, AIAA J., 8, 6, 1090, (1970)
- [7] M.I. Boudko : Geomagnetism I Aeronomia, 6, 1008, (1961)
- [8] J.M. Buzzi, H.J. Doucet, and D. Gressillon, Phys. Fluids, 13, 12, 3041, (1970)
- [9] M. HASMI, A.J. Van der Hooven, Van der Dordt, and J.V. Wegrove, Nuclear fusion, 6, 225, (1966)
- [10] S.A. Anderson, V.D. Jensen, P. Michelsen, Phys. Letters A, 31A, 7, 395, (1970)
- [11] K. Loongreen, D. Montgomery, I. Alexeff, and W.D. Jones, Phys. Letters, 25A, 629, (1967)
- [12] J.L. Hirschfield, and J.H. Jacob, Phys. Fluids, 11, 411, (1968)
- [13] I.B. Bernstein, Phys. Rev., 102, 10, (1958)

WAKE BEHIND AN OBSTACLE IN A SINGLE-ENDED Q-MACHINE AND  
ITS USE AS A DIAGNOSTIC OF THE ION DISTRIBUTION FUNCTION

J.P.M. SCHMITT

Laboratoire de Physique des Milieux Ionisés  
Ecole Polytechnique, Paris - France  
(Equipe de Recherche associée au C.N.R.S.)

---

ABSTRACT

The wake behind different obstacles immersed in the plasma flow of a single-ended Q-machine is investigated. This experiment is shown to be a simulation of the flight of a polar satellite through the ionosphere. The obstacles experimented with (disk, blade, probe) are thick in the streaming direction to ensure their electrical neutrality towards the Cesium ions. The measurements agree very well with the theory; in particular the coupling of the wake with ionic Bernstein modes is demonstrated. The excitation of pseudo waves by means of a small probe is described for frequencies below the ion gyro frequency. The wave amplitude variations as a function of space is compared to the density in the steady wake. This experiment is used as a diagnostic of the ion distribution function; the measurement of the perpendicular ion temperature and of the ion mean velocity are shown to be good.

I. INTRODUCTION

The plasma of a single-ended Q-machine is well adapted to check the theory given in the previous paper, "Wake behind a body in motion in a plasma, parallel to the magnetic field". (Same proceedings). Here the body is resting in a plasma stream, the wake is stationary in the Cesium plasma column. The same kind of experiments was done recently by J. WALDES and T.C. MARSHALL [1] and by BOGATCHENKO and al. [2]. The paper [1] contains only preliminary results. The paper [2] presents good observations of the steady-state wake of a disk, taking into account the damping effect of the ion parallel temperature.

In the present paper we first describe the experimental set up (sec.II) and show briefly why this experiment can be regarded as the simulation of the wake of a satellite in the ionosphere (sec.III). We then report

our observations of the structure of the steady-state wake with regard to its spatial period and damping (sec.IV). The propagation of a three dimensional magneto pseudo wave emitted from a probe is studied and the spatial variations of the amplitude is compared to the results of the former section (sec.V). Some of these experiments can be used as diagnostic methods to measure the first moments of the ionic distribution function. These diagnostics are tested and discussed (sec.VI). Finally, we summarize and comment on the results (sec.VII).

## II. DESCRIPTION OF THE EXPERIMENTAL SET UP

The experiments were carried out in the same single-ended Q-machine described [3], using the low-density range ( $10^7 \leq n_0 \leq 5.10^8 \text{ cm}^{-3}$ ). The equilibrium in such a machine is now very well known [3,4] and, in particular, we were able to measure the ion drift velocity using several methods : Electrostatic analyser coupled either with (1) a probe measurement of the plasma potential [3], or (2) with charge-exchange [4], (3) Coupled parallel and perpendicular electrostatic analysers ; (4) Flux measurement coupled with density measurement with a cavity. It is found that all these methods give the same value for the drift velocity  $v_p$  and give results in agreement with the sheath theory [3].

The obstacles are immersed in the center of the plasma column ( $\beta \approx 3\text{cm}$ ). The obstacle shapes used were a disk, a blade, and a small cylindrical probe parallel to the magnetic field. When very thin obstacles were used, we observed a complex wake, varying with the obstacle polarization which resulted from ion deflection by the edges of the obstacle. Thus, we used thick obstacles (about 2 mm) biased slightly negatively ( $-2\text{V}$ ), which was found to eliminate this effect (see. Figure 1.).



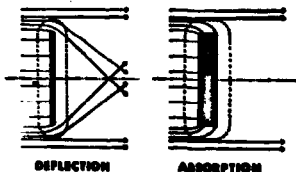


FIGURE . 1

This drawing shows how a thick obstacle collects all the streaming ions which enter the sheath around the edges. For thin obstacles the sheaths produce deflection, leading to complex wake structure.

A small probe can be biased with a modulated negative voltage, giving rise to a modulation of its cross section as a result of the change of the sheath thickness. This provides a mean of excitation of the magneto pseudo waves.

Our measurements were performed with a thin probe which could be precisely displaced along the magnetic field. The ion current collected by the probe was for experimental conditions, equal to the ion flux on the projected probe area. The ion flux modulation associated with the pseudo wave was detected using a filter and autocorrelation techniques.

### III. SIMULATION OF THE IONOSPHERE IN A Q-MACHINE

In the following table we give the important ratios for the wake problem, both for a Q-machine ( $n_0 = 10^8 \text{ cm}^{-3}$ ) and for the ionosphere (altitude 500 km).

|   | Q-MACHINE | IONOSPHERE |
|---|-----------|------------|
| Ion collision frequency / ion gyrofrequency     | 0,01      | 0,01       |
| Mobile velocity / electron thermal velocity     | 0,01      | 0,03       |
| Ion parallel thermal velocity / mobile velocity | 0,3       | 0,2        |
| Mobile radius / ion Larmor radius               | 0,2 - 1   | 0,05 - 0,5 |
| Debye length / ion Larmor radius                | 0,1       | 0,001      |
| Ion wave phase velocity / mobile velocity       | 0,4       | 0,2        |

The comparison between these ratios shows that a Cesium plasma is a good medium in which to simulate satellite motion along the earth's magnetic field. The scales are about 1/2000 for the perpendicular distances, 1/1000 for the parallel distances and 150/1 for the time. Note that the only large difference is the ratios of the Debye lengths to the ion Larmor radii. This will not, however, affect the ballistic solution only the effects of the self-consistent electric field.

#### IV. STEADY-STATE WAKE EXPERIMENTS

Behind a small disk (5 mm  $\beta$ ) the ionic current on a probe was measured along the axis as a function of the distance. The results plotted in Figure 2 shows a periodic structure. The slight increase of the mean density along the wake axis is attributed to collisions ( $n_0 = 2 \cdot 10^8 \text{ cm}^{-3}$ ); for higher densities, this effect becomes stronger as shown in figure 3 ( $n_0 = 10^9 \text{ cm}^{-3}$ ).

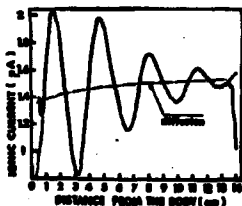


Figure 2

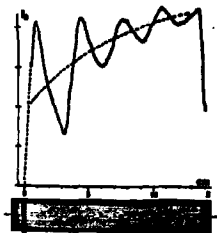


Figure 3

Ionic current to a probe, behind a disk (5 mm  $\beta$ ), measured on the wake axis as a function of distance. Figure 2 :  $n_0 = 2 \cdot 10^8 \text{ cm}^{-3}$ . Figure 3 :  $n_0 = 10^9 \text{ cm}^{-3}$ .

For a given plasma, the spatial period  $L$  was verified to be inversely proportional to  $B_0$  (Figure 4), as theoretically predicted in the preceding paper.

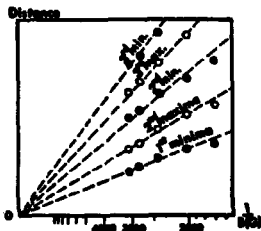


FIGURE 4

Distance from the body of the wake maxima and minima as a function of the inverse of the magnetic field.

In this experiment  $B_0$  and  $L$  are measured and values for  $v_p$  are calculated using both the purely ballistic theory ( $v_p = \Omega L / 2\pi$ ) and accounting for the coupling with the Bernstein waves ( $v_p = \Omega' L / 2\pi$ ). In figure 5 these results are compared with the values. It appears that the spatial period of the wake is appreciably shorter than the one predicted by the ballistic theory, but is in good agreement when the calculated correction due to the electric field effect is taken into account.

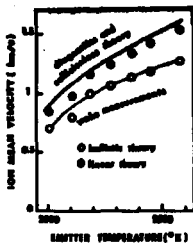


FIGURE 5

Variations of the ion mean velocity  $v_p$  as a function of the emitter temperature  $T_k$ . The actual values were obtained by four different methods. The values calculated from the measurement of the wake spatial period are plotted taking into account or not the coupling with ionic Bernstein waves.

The damping effect of the ion parallel temperature  $T_{i//}$  is well exhibited when the wake structure is studied for various emitter temperatures, as shown in Figure 6. It is known that when  $T_k$  decreases,  $v_p$  decreases while the ion parallel velocity spread increases. In figure 5,  $B_0$  is constant and the increase of the damping with  $T_{i//}$  is evident.

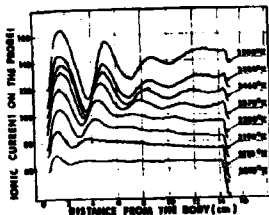


FIGURE 6

Variations of the axial wake structure for various emitter temperatures, showing the damping effect of the parallel ion temperature.

### V. THREE DIMENSIONAL PSEUDO WAVES

The first step is the comparison between the steady-state wake density variations and those of the modulated signal amplitudes. In figure 7, as predicted, the two axial structures are shown to oscillate  $180^\circ$  out of phase in space ; also, the pseudo wave is more weakly damped.

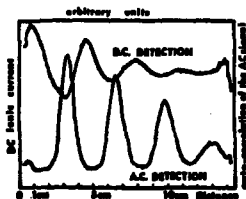


FIGURE 7

Comparison between the D.C. ionic current and the A.C. signal amplitude detected with auto-correlation on the axis of a small probe which is biased with a modulated voltage (frequency 3000 Hz)

We checked to see if the antenna was exciting both pseudo waves and ion acoustic waves. Using a tone burst a pulse of a few oscillations would separate at a certain distance which depended on the different velocities of the pseudo wave ( $\sim v_p$ ) and of the fast and slow ionic waves. No important ionic wave was excited. For example, in typical conditions, (modulations frequency 15 kHz ; ion gyro frequency 40 kHz ; ion plasma frequency 80 kHz), it is at the 4<sup>th</sup> maximum (10 cm behind the antenna) that we observed a rise of a weak faster signal which was identified as the fast ionic wave.

When the wake is modulated, synchronous detection permits sensitive measurements of the structure of the edge of the wake. As predicted by the

theory, Figure 8 shows that the amplitude is oscillating in distance at the edge in the sense opposite to that on the axis of the wake.

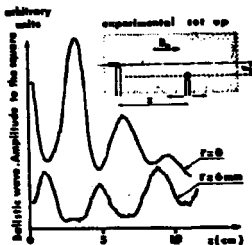


FIGURE 8

A three dimensional pseudo wave excited by a small probe. The variation of its amplitude versus the distance along the axis, and at two ion Larmor radii from the axis, are compared and seen to be 180° out of phase, as predicted by theory.

#### VI Q-MACHINE DIAGNOSTICS

It was theoretically possible to deduce from the wake measurements the ionic mean velocity as well as the ion parallel and perpendicular temperatures. The mean velocity  $v_p$  is obtained from the measurement of the length of periodicity and the results are shown in Figure 5. The correction  $\Omega^2/\Omega$  coming from the theory does not vary very much for a Q-machine. ( $1,14 \leq \Omega^2/\Omega < 1,17$ ). Taking the average value  $\Omega^2/\Omega = 1,16$ , we can expect an accuracy of about 5% for the measurement of  $v_p$ . The same measurement with the magneto pseudo wave, however, is often easier, as the detection is more sensitive. In addition, the smaller obstacle used with the synchronous detection perturbs the plasma less.

The measurement of  $T_{\perp p}$  is connected with the damping of the wake. As long as the damping is weak, Eq.(8) given in the theoretical paper is valid. The ratio  $\Delta v/v_p$ , which we deduced from the amplitudes of the first minimum, was roughly in agreement with electrostatic analyser measurements ( $\Delta v/v_p \approx 0,2$ ). Since the wake damping can be drastically affected by the collisions and the electric field, however it gives only an indication rather than a precise value for  $T_{\perp p}$ .

The measurement of  $T_{ii}$  is more precise. Assuming that  $T_{ii} \approx 0$ , Eq. (7) gives for the density maximum on the axis of a disk of radius  $R$ ,

$$n_{\max} = n_0 \exp - \frac{q^2 R^2 B_0^2}{8 m_i k T_{ii}}$$

For a disk of radius 3 mm, the density at the first maximum was measured for various values of  $B_0$  as shown in Figure 9.

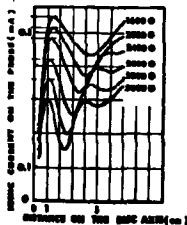


FIGURE 9

Ionic flux variations along a disk axis ( $R = 3$  mm) for various values of the magnetic field.

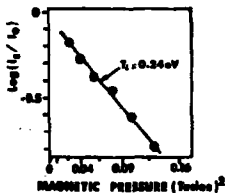


FIGURE 10

Logarithm of the current at the first maximum versus the magnetic field to the square.

The  $\text{Log}(n_{\max}/n_0)$  should be a linear function of  $B_0^2$ , which is verified in figure 10. From the slope we can calculate that  $kT_{ii} = 0,24$  eV, when the emitter temperature was  $kT_k = 0,22$  eV. This agrees with theory which predicts that both temperatures should be equal.

#### VII SUMMARY AND CONCLUSIONS

A single-ended Q-machine in the low density range ( $n_0 < 10^6 \text{ cm}^{-3}$ ) provides a good simulation for the wake problem of a satellite in the earth's atmosphere when the satellite motion is parallel to the magnetic field. These experiments show that the wake structure is fairly well explained by the ballistic approximation. Precise measurements, however show that there is a small corrective effect due to a coupling with ionic Bernstein

modes. The participation of quasi-free-streaming ions was also observed in the propagation of a pseudo wave excited by a modulated potential on a small probe. From the measurement of the wake of an obstacle in a Q-machine, we can calculate an approximate value for the parallel ionic temperature ; however, accurate measurements (errors of less than 10 %) of the ion mean velocity and of the perpendicular ion temperature are possible from such measurements.

- REFERENCES -

- [1] J. WALDES , T.C. MARSHALL, bull of the A.P.S., II, 15,11, 1448, (1970)
- [2] I.A. BOGATCHENKO, A.V. GUREVITCH, R.A. SALIMOV, J.I. EIDELMAN, S, 11 1540, (1970)
- [3] J.M. BUZZI, H.J. DOUCET, D. GRESILLON, Phys Fluids, 13, 12, 3041, (1970)
- [4] S.A. ANDERSEN, V.O. JENSEN, P. MICHELSEN, Phys Letter A, 31 A, 7, 395, (1970)

Current-Driven Collisional Drift Instability in a Q-Machine Plasma: Wave Induced Losses and Anomalous Resistivity.

by

R.F. Ellis<sup>†</sup>) and R.W. Motley

Princeton Plasma Physics Laboratory, Princeton N.J.

Abstract

We have continued experiments on the current-driven collisional drift instability in a cesium plasma created in a double-ended Q-machine (Plasma Radius = 2 cm, Length = 110 cm,  $T = 2500^{\circ}\text{K}$ ,  $n = 10^{10-3} \times 10^{11} \text{ cm}^{-3}$ ). Onset of this large amplitude instability ( $\bar{n}/n_0 \sim 10\%$ ) is well defined and occurs at a critical current which varies with plasma parameters. Concomitant with onset the average plasma density decreases by 10 - 30%. These wave induced losses are consistent with calculations using a linearized two fluid theory, including electron temperature oscillations and electron heat flow. The calculations employ the measured wave parameters, especially the amplitude and phase of the fluctuating density and fluctuating potential. These results are additional proof that electron temperature oscillations are necessary to describe this instability. Measurements of plasma resistivity indicate that for  $n_0 > 10^{11} \text{ cm}^{-3}$ , where sheath resistance effects are negligible, there is no anomalous plasma resistivity attributable to this mode.

A. Wave Induced Losses

The establishment of a causal relationship between plasma instabilities and anomalous plasma transport is of considerable importance for plasma confinement studies. In this paper we report on wave induced plasma loss produced by the current-driven collisional drift mode. Previous work (1) dealt with

<sup>†</sup>) Present Address: Max-Planck-Institut für Plasmaphysik, Garching



an identification of this mode on the basis of a comparison of many mode features with a linear two fluid theory which included the effects of electron heat flow and electron temperature fluctuations (2). Indeed, it was shown that the inclusion of electron temperature fluctuations was of primary importance in describing the instability; the present work strongly reinforces that conclusion.

The experiments were performed in a cesium plasma produced in a double-ended Q-machine with the following parameters: Plasma Length = 110 cm, Plasma Radius = 2 cm,  $T = 2500^\circ\text{K}$ ,  $n_0 = 10^{10}$  to  $3 \times 10^{11} \text{ cm}^{-3}$ ,  $1/n_0 (dn_0/dr) \sim -1 \text{ cm}^{-1}$ . Axial currents in the range 20 - 200 ma were driven through the plasma and onset of instability occurred at a well defined critical current which was a function of plasma parameters. The instability was detected by Langmuir probes as a coherent, single mode oscillation of probe ion saturation current and floating potential. The oscillation was of large amplitude ( $\bar{n}/n_0 \sim 10$  to  $30 \%$ ), low frequency, and was radially localized in the region of maximum density gradient. Concomitant with the onset of instability there occurred a large decrease (10 -  $30 \%$ ) in the average density of the plasma column, as shown in Fig. 1. The transition from the stable to the unstable state is produced by a very small change in the axial current, so that the instability can essentially be "turned on" without grossly changing the plasma parameters. The density decrease with onset can thus be directly attributed to the appearance of the instability. Moreover, this feature of instability control allows us to study the plasma in detail, both before and after onset, and thereby to relate the density decrease to the measured oscillation features. This requires a simple model of the loss process, which follows.

The expected radial ion flux for a coherent single mode collisional drift wave can be calculated with the result (3)

$$j_r(r) = \frac{1}{2} \frac{cm}{Br} |\tilde{n}(r)| |\tilde{\phi}_s(r)| \sin \theta \hat{r} \quad (1)$$

where  $m$  is the azimuthal mode number,  $\tilde{n}$  is the fluctuating density,  $\tilde{\phi}_s$  is the fluctuating space potential and  $\theta$  is the angle by which  $\tilde{n}$  leads  $\tilde{\phi}_s$  in the non-rotating plasma rest frame (4). Using this flux we estimate the steady state wave induced ion loss as

$$\overline{\Phi}_W = j_r(R_{\max}) A(R_{\max}) \quad (2)$$

where  $R_{\max}$  is the radius of maximum wave amplitude and  $A(R_{\max}) = 2\pi R_{\max} \times \text{Machine Length}$ . Assuming that the non-wave losses (represented by the ion confinement time  $\tau$ ) occur at the same rate both before and after wave onset we can write:

$$\text{Before Onset:} \quad \overline{\Phi}_{IW} = n_o^b V_p / \tau$$

$$\text{After Onset:} \quad \overline{\Phi}_{IW} = n_o^a V_p / \tau + \overline{\Phi}_W$$

where  $\overline{\Phi}_{IW}$  is the steady state ion input flux from the endplates (measured with a negatively biased collecting plate inserted across the plasma column),  $V_p$  is the plasma volume, and  $n_o^b$  ( $n_o^a$ ) is the average density before (after) wave onset. This equation yields

$$\frac{\Delta n_o}{n_o} \equiv \frac{n_o^a - n_o^b}{n_o^b} = \frac{\overline{\Phi}_W}{\overline{\Phi}_{IW}} \quad (3)$$

To test this relation we have measured  $\Delta n_o/n_o$ ,  $\overline{\Phi}_{IW}$ , and the various plasma and wave parameters for a wide range of conditions. In particular, the amplitude and phase of the fluctuating density ( $\tilde{n}$ ) and floating potential ( $\tilde{\phi}_f$ ) were recorded with a Langmuir probe, care being taken to avoid instrumental errors in these quantities (4). Note, however, from eq. (1) that it is the space potential ( $\tilde{\phi}_s$ ) which is required and in the presence of electron temperature fluctuations ( $\tilde{T}$ ) probe floating potential is not the same as space potential. For a cesium plasma the relation between the two fluctuating quantities can be calculated

$$\frac{e \tilde{\phi}_f}{kT_e} = \frac{e \tilde{\phi}_s}{kT_e} - 5 \frac{\tilde{T}}{T_e} \quad (4)$$

Using eq. (4) and the theory of Ref. 6 it is possible to calculate the relations among  $\tilde{n}$ ,  $\tilde{\theta}_s$  and  $\tilde{\theta}_p$  given the measured plasma parameters. These relations are then used to calculate  $\theta$  and  $|\tilde{\theta}_s|$  from the measured fluctuations. The final results are given in Fig. 2 which shows  $\Delta n_o/n_o$  versus  $\tilde{\theta}_W/\tilde{\theta}_{IN}$  for various modes with a range of density from  $2 \times 10^{10}$  to  $2 \times 10^{11} \text{ cm}^{-3}$  and azimuthal mode number from  $m = 2$  to  $m = 5$ . Considering the simplicity of the model the two quantities are in excellent agreement.

An important point must be made with respect to the sign of the phase angle  $\theta$ . Eq. (1) predicts a radially outward flux, and thus a density decrease, only if  $\theta$  is a positive angle. If we were to interpret probe floating potential as space potential (i.e. ignore temperature fluctuations) then we would identify  $\theta$  with the measured phase angle between fluctuating density and fluctuating floating potential. As described in Ref. 1 this measured phase angle is negative i.e.  $\tilde{n}$  lags  $\tilde{\theta}_p$  in the plasma rest frame. Therefore, the neglect of electron temperature fluctuations would lead us to conclude from eq. (1) that the radial flux was inward, in direct contradiction to the experiment.

To summarize, the data presented demonstrate that the measured wave induced losses can be accounted for by the measured wave parameters provided these parameters are used in conjunction with the temperature fluctuation theory of the current-driven drift mode.

### B. Anomalous Resistivity

A recent paper (5) has attributed low electric field anomalous resistivity in stellarators to the current-driven drift mode and another recent work (6) has reported a 5% increase of plasma resistivity with onset of the current-driven collisional drift mode in a Q machine plasma.

In the present experiment plasma resistivity in the presence of the current-driven drift mode has also been measured, using exter-

nal current-voltage (I-V) characteristics of the plasma. With this method the measured resistance is the sum of the plasma resistance  $R_p$  and the sheath resistance  $R_s$ , which is contributed by the sheaths at the two endplates. In the electron sheath regime  $R_s$  is given by

$$R_s \approx \frac{2 k T_e}{\sqrt{\pi} n_0 e \sqrt{A_p}}$$

where  $A_p$  is the cross sectional area of the endplates and  $V_e = (kT/m_e)^{1/2}$ .  $R_s$  is inversely proportional to the density and can be quite large at low densities. The density dependence of  $R_s$  is important because the onset of the current-driven mode invariably causes a significant density decrease (see part A) which is reflected as an increase in  $R_s$  and thus an increase in the total measured resistance. Therefore, to study the change in  $R_p$  with wave onset it is necessary to operate at high densities where  $R_s$  is small and cannot significantly affect the results. Figure 3. shows a typical I-V characteristic at a density of  $2 \times 10^{11} \text{ cm}^{-3}$  for which such changes of  $R_s$  due to wave induced losses are negligible. The plasma resistance at zero current (position a-stable plasma) agrees with the classical value. As the current is increased the resistance decreases slightly, indicative of ohmic heating. At a current of 140 ma (position b) the abrupt onset of an  $m = 2$  current-driven drift mode occurs with  $\tilde{n}/n_0 \approx .12$  and  $U_0^+) = .02 V_e$ . In the vicinity of onset there is no detectable change in the plasma resistance. For  $n_0 > 10^{11} \text{ cm}^{-3}$  we have investigated this effect for varying magnetic fields and mode numbers, for values of  $\tilde{n}/n_0$  to 0.25 and for  $U_0$  up to 5% of  $V_e$ . In all cases no increase in resistivity was observed with mode onset, demonstrating that at these densities any anomalous resistivity caused by the current-driven collisional drift mode is very small.

---

+)  $U_0 = I/n_0 A_p$

References

1. R.F. Ellis and R.W. Motley, Bull. Am. Phys. Soc. 14, 1055 (1969) and Bull. Am. Phys. Soc. 15, 1438 (1970)
2. S.T. Tsai, F.W. Perkins and T.W. Stix, Phys. Fluids 13, 2108 (1970)
3. H.W. Hendel, T.K. Chu, and P.A. Politzer, Phys. Fluids 11, 2426 (1968)
4. R.W. Motley and R.F. Ellis, Phys. Fluids 14, 886 (1971)
5. B. Coppi and E. Mazzucato, Phys. Fluids 14, 134 (1971)
6. T.C. Simonen, T.K. Chu and H.W. Hendel, Bull. Am. Phys. Soc. 15, 532 (1970)

Figure Captions

1. Radial ion saturation current ( $J_+$ ) profiles before and after the onset of a  $m = 2$  current-driven drift mode at  $B = 3.3$  kG.
2. Relative density decrease  $\Delta n_0/n_0$  with onset of current-driven modes, versus  $\bar{\Phi}_W/\bar{\Phi}_{IN}$ . Solid line is theoretical curve.
3. Current-voltage characteristic of plasma at  $n_0 = 2 \times 10^{11} \text{ cm}^{-3}$ ,  $B = 5.76$  kG.  $\tilde{n}_a$  ( $\tilde{n}_b$ ) is fluctuating density recorded with a Langmuir probe at position a (position b) of the characteristic; horizontal sweep .5 ms/cm.

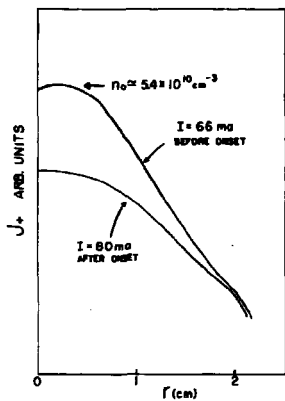


Figure 1

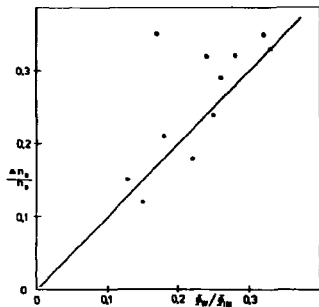


Figure 2

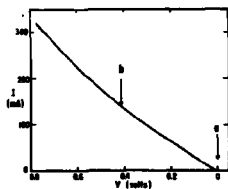


Figure 3

Effects of Parallel Wavelength on Collisional Drift Instability\*

by

L. G. Schlitt and H. W. Hendel<sup>†</sup>

Plasma Physics Laboratory, Princeton University, Princeton, N. J. 08540

Abstract

The dependence of the collisional drift instability on parallel wavelength has been studied in potassium Q-machine plasmas. The parallel wavelength is determined by the length of the plasma column ( $\lambda_{||} \approx 2L$ ), which can be varied ( $L = 15$  to  $130$  cm). The instability is driven by the expansion, limited by resistivity, of the electron fluid parallel to the magnetic field. Stabilization at both long and short parallel wavelength ( $\lambda_{||} \geq 200$  and  $\lambda_{||} \leq 100$  cm respectively) by ion viscosity has been demonstrated. Stabilization of individual modes at high magnetic field and short parallel wavelength ( $B/k_{||} \approx 1$  kG-cm,  $\lambda_{||} \approx 100$  cm) due to ion motion parallel to the magnetic field has also been observed. These results are consistent with the predictions of a two-fluid, slab model theory which includes electron temperature fluctuations in addition to the effects mentioned above.

Introduction

The effects of parallel wavelength on the collisional drift instability

---

\*This work was supported by U.S. Atomic Energy Commission Contract AT(30-1)-1238.

†On leave from RCA.

in potassium plasmas have been studied on the Princeton Q-1 device. This study has led to the prediction and observation of four general stability characteristics of the drift wave.

### Theory

Previous two-fluid, slab model theories used to describe the collisional drift wave have included the effects of parallel resistivity, finite ion larmor radius, ion viscosity,<sup>1</sup> and thermal conductivity.<sup>2</sup> However, for parallel wavelengths of 100 cm or less under typical conditions, ion motion parallel to the magnetic field must be included in the theory. The resulting dispersion relation can be written in the form:

$$D(\omega, k) = D_0(\omega, k) + D_1(\omega, k) = 0$$

where  $D_1(\omega, k)$  contains all of the terms which result from the inclusion of ion motion parallel to the magnetic field.

$$D_0(\omega, k) = b\omega^3 + [bR\omega_s + i\omega_1 + i\omega_1(R + 4.03b)]\omega^2 \\ - [iR\omega_s\omega_1(1 - 4.03b) - iR\omega_s\omega_1 + \omega_1\omega_1(R + 4.03) + 1.08\omega_1^2(R+b)]\omega \\ + [1.08R\omega_s\omega_1^2(1-b) - 3.03R\omega_s\omega_1\omega_1 - 1.08i\omega_1\omega_1^2(R+1)]$$

$$D_1(\omega, k) = \frac{\omega_s^2}{Q} [\omega_s\omega(R + 2.14) + \omega_s\omega_s(1.95R + 0.81) + 1.08i\omega_1^2(R + 1)]$$

$$Q = i\omega - \frac{4\omega_1}{b}$$

The various quantities appearing in  $D(\omega, k)$  are defined as follows

$$b = \frac{k_{\perp}^2 T_i}{M \Omega^2}$$

$$\Omega = \frac{eB}{Mc}$$

$$\omega_1 = \frac{1}{4} b^2 v_{i1}$$

$$R = T_i / T_e$$

$$\omega_1 = \frac{k_{\perp}^2 T_e}{n_e v_{e1}}$$

$$\omega_s = k_y v_d = \frac{-k_y T_e}{M \Omega} \frac{1}{n_e} \frac{dn_e}{dx}$$

$$\omega_s^2 = \frac{T_i k_{\perp}^2}{M}$$



$$v_{ii} = 2.84 \frac{e^2 n_0}{M^2 T_i} \lambda_n \Lambda$$

$$v_{ei} = 1.69 \frac{e^2 n_0}{M^2 T_e} \lambda_n \Lambda$$

The predictions of this dispersion relation are presented in Fig. 1, which displays the ratio of magnetic field strength to perpendicular wave-number  $B/k_{\perp}$  at onset of instability as function of parallel wavelength  $\lambda_{\parallel}$ . These marginal stability curves separate the plasma parameter space into stable and unstable regions. The solid line is the marginal stability curve for the complete theory including ion parallel motion and the dashed line neglects ion parallel motion. Although the exact shape and location of the marginal stability curve in the  $B/k_{\perp}$  versus  $\lambda_{\parallel}$  plane depends upon the values of other plasma parameters such as density and density gradient scale length, the general shape of the curve is retained and therefore predicts four general stability characteristics of the collisional drift wave:

1) low field stability - for any  $\lambda_{\parallel}$ , the plasma is stable for sufficiently small  $B/k_{\perp}$ ; 2) long parallel wavelength stability - for any  $B/k_{\perp}$  the plasma is stable for sufficiently large  $\lambda_{\parallel}$ ; 3) short parallel wavelength stability - for any  $B/k_{\perp}$  the plasma is stable for sufficiently small  $\lambda_{\parallel}$ , in fact, there exists a critical  $\lambda_{\parallel}$  below which the plasma is stable for all  $B/k_{\perp}$ ; and 4) high field stability - for any  $\lambda_{\parallel}$ , individual modes are stable for sufficiently large  $B/k_{\perp}$ . The first three characteristics are predicted by previous theories and result from the balance between the destabilizing effects of parallel resistivity and thermal conductivity and the stabilizing effects of ion viscosity. The fourth characteristic, high field stability of individual modes, results from the inclusion of ion parallel motion and is due to ion viscosity and the collisional coupling of ion parallel motion to electron heat flow. Because of the  $1/k_{\perp}$  dependence in the ordinate of Fig. 1, high field stability applies only to individual modes of oscillation as illustrated in Fig. 2, which displays marginal

stability curves for the first seven azimuthal modes. Unless  $\lambda_{||}$  is sufficiently close to the critical parallel wavelength, the plasma is unstable for all magnetic fields higher than that necessary to destabilize the  $m = 1$  mode. However, if  $\lambda_{||}$  is sufficiently close to the critical parallel wavelength there will be intervals in magnetic field, between the appearance of successive azimuthal modes, where the plasma is stable.

#### Experiment

The Q-1 device, whose features and operation have been described previously,<sup>1</sup> was modified to permit the variation of the plasma column length. The heated tungsten end-plate assemblies were mounted on vacuum bellows and supported by tracks inside the vacuum vessel so that the column length could be varied while the experiment was in progress. With both end plates operating under "electron-rich" conditions, the parallel wavelength was measured from axial oscillation amplitude profiles for a wide range of column lengths and densities. The parallel wavelength was found to be 2.5 times the column length with an uncertainty of 20% for all cases.

Marginal stability curves were determined experimentally by setting the column length and increasing (or decreasing) the magnetic field until the  $m = 1$  mode became unstable. The plasma density and density gradient were measured in the stable regime near onset. As in previous work<sup>1,2</sup> the magnetic field was scaled by a factor of 1.5.

Figure 3(a) shows an experimental marginal stability curve. The density was constant,  $n_0 = 2.5 \times 10^{10} \text{ cm}^{-3}$ , however,  $|\nabla n_0/n_0|$  increased as  $\lambda_{||}$  was decreased. The experimental apparatus does not permit independent control of these parameters, but the theoretical curve shown includes the variation of  $\nabla n_0/n_0$ . The error brackets indicate the total uncertainty in the measured values of  $\lambda_{||}$  and  $B/k_1$ . The uncertainty between adjacent data points is about 1/3 of the error indicated by the brackets. This

figure demonstrates three of the four stability characteristics of the drift wave:

1. Low field stability - the plasma is stable at all parallel wavelengths for  $B/k_{\perp} < 0.35$ .

2. Short parallel wavelength stability - as  $\lambda_{\parallel}$  decreases  $(B/k_{\perp})_{\text{crit}}$  increases until the critical parallel wavelength  $\lambda_{\parallel \text{crit}} = 60$  cm is reached. For shorter  $\lambda_{\parallel}$ , the plasma is stable for all values of  $B/k_{\perp}$ .

3. High field stability of individual modes - the four points  $(B/k_{\perp})_{\text{crit}} \geq 0.8$  are points at which the  $m = 1$  mode is stabilized by ion parallel motion for large values of  $B/k_{\perp}$ . The stabilization of the  $m = 1$  mode could not be followed to  $(B/k_{\perp})_{\text{crit}} > 1.0$  because of the destabilization of the  $m = 2$  mode.

Figure 3(b) is similar to Fig. 3(a) except that  $n_0 = 2 \times 10^{11} \text{ cm}^{-3}$  and  $V_{n0}/n_0$  is nearly constant ( $-1.8 \text{ cm}^{-1}$ ). The comments regarding experimental uncertainty, low field, short parallel wavelength, and high field stabilization, made for Fig. 3(a), apply to this figure as well, except for the quantitative differences. In addition to the three stability characteristics demonstrated by Fig. 3(a), this figure demonstrates the remaining stability characteristic of the drift wave, long parallel wavelength stability. As the parallel wavelength was increased from  $\lambda_{\parallel} = 230$  cm to 330 cm, the stability parameter increased from  $(B/k_{\perp})_{\text{crit}} = 0.5$  to 0.6.

Figure 4 shows the oscillation amplitude  $n_1$  as a function of magnetic field  $B$  for various column lengths  $L$ . This figure emphasizes the region of stability between the stabilization of the  $m = 1$  mode by ion parallel motion ( $B < 4.7$  kG) and the destabilization of the  $m = 2$  mode ( $B > 4.7$  kG). This region of stability appears at  $L = 32$  cm and widens to 1 kG at  $L = 29$  cm,  $L_{\text{crit}} = 28.5$  cm. In addition to emphasizing high field stabilization of the  $m = 1$  mode this figure also demonstrates low field and short parallel

wavelength stabilization.

Summary

A two-fluid, slab model theory has predicted four observed stability characteristics of the collisional drift wave: 1) low field stability; 2) long parallel wavelength stability; 3) short parallel wavelength stability; and 4) high field stability of individual modes.

References

1. H. W. Hendel, T. K. Chu, and P. A. Politzer; *Phys. Fluids* 11, 2426 (1968).
2. S. T. Tsai, F. W. Perkins, and T. H. Stix, *Phys. Fluids* 13, 2108 (1970); R. Gravier, G. Laval, R. Pellat, C. Renaud, in Proceedings of Conference on Physics of Quiescent Plasmas (Ecole Polytechnique, Paris, France, 1970), Pt. II, p. 1.
3. R. W. Motley, Princeton University Plasma Physics Laboratory Report, MATT-Q-27, 98 (1969); R. F. Ellis, Doctoral Thesis, Princeton University (1970).

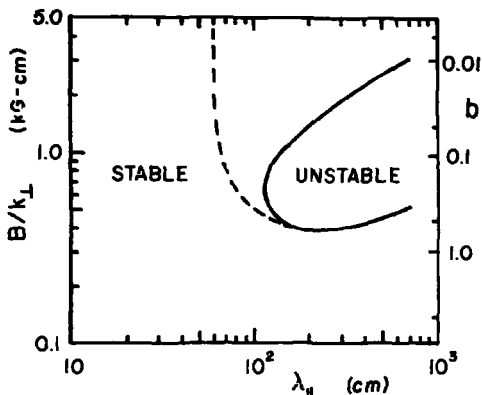


Fig. 1. Marginal stability curves ( $B/k_{1,crit}$  vs.  $\lambda_{||}$ ).  $n_0 = 5 \times 10^{10} \text{ cm}^{-3}$ ,  $k_x = k_y$ ,  $V_{th0}/n_0 = -1 \text{ cm}^{-1}$ ,  $T_i = T_e = 2650^\circ \text{K}$ . Solid line from complete dispersion relation. Dashed line neglects ion parallel motion.

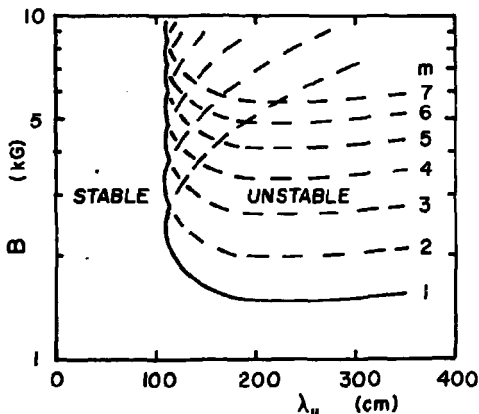


Fig. 2. Marginal stability curve (solid line). Dashed lines are marginal stability curves for azimuthal modes  $m = 1$  to 7. Conditions as Fig. 1.

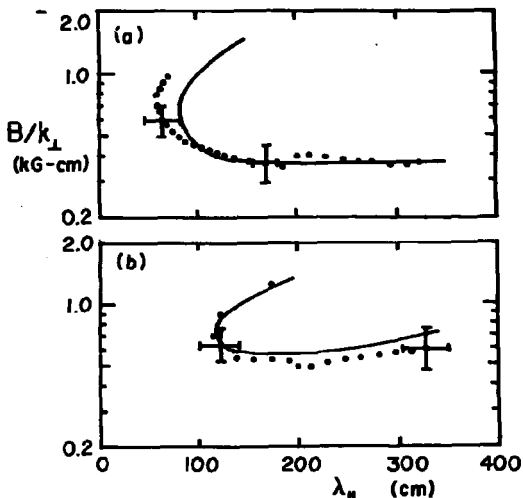


Fig. 3. Marginal stability curves.  $B/k_{\perp}$  scaled by 1.5,  $k_{\perp} = 2.5$  k,  $T_i = T_e = 2650^{\circ}\text{K}$ . (a)  $n_e = 2.5 \times 10^{10} \text{cm}^{-3}$ ,  $V_{n_e}/n_e$  from  $-1.4$  to  $-2.7 \text{cm}^{-1}$ . (b)  $n_e = 2.0 \times 10^{11} \text{cm}^{-3}$ ,  $V_{n_e}/n_e = -1.8 \text{cm}^{-1}$ .

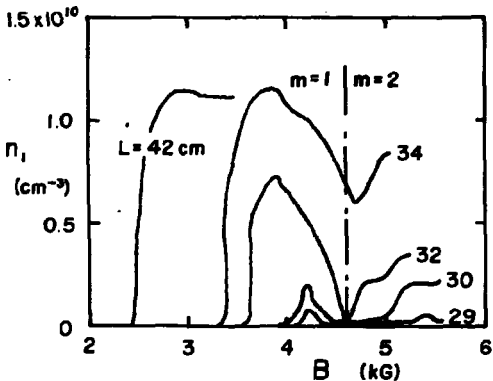


Fig. 4. Instability amplitude  $n_1$  versus  $B$  with  $L$  as parameter.  $n_e = 5 \times 10^{10} \text{cm}^{-3}$ ,  $V_{n_e}/n_e = -1.8 \text{cm}^{-1}$ .  $m = 1$  mode to left of vertical line,  $m = 2$  mode to right.  $L_{\text{crit}} = 28.5$  cm.

NUMERICAL INVESTIGATION OF THE EFFECT OF HEAT TRANSPORT ON  
COLLISIONAL DRIFT WAVES.

P. Brossier, P. Deschamps, R. Gravier, R. Pellat, C. Renaud.

**ASSOCIATION EURATOM-CEA**

Département de la Physique du Plasma et de la Fusion Contrôlée  
Centre d'Etudes Nucléaires  
Boîte Postale n° 6 - 92 Fontenay-aux-Roses (France)

ABSTRACT

A detailed numerical investigation of the linear dispersion relation for pressure gradient driven drift instabilities is reported here for the collisional plasma. Besides effects related to the finite thermal conductivity coefficients for both ions and electrons, correction terms have been included in the equation a) for low magnetic field regime, i.e. when  $\Omega_e k \ll \nu_i$ , b) for heat exchange between the ion and electron fluids which may become important for ions and electrons with different temperature.

The influence of the magnetic field B on growth rate and frequency shows the evolution of the fluctuation spectrum into a turbulent one and deviation from the 1/B dependance. Correction due to finite  $\nu_i/\Omega_{ei}$  are stabilizing, heat exchange is important only at large densities (for instance  $> 10^{11} \text{cm}^{-3}$ ). Comparison with available experimental data shows that high azimuthal and parallel wave numbers are more stable than expected from the linear theory.

Pressure gradient driven oscillations were shown to grow unstable under the influence of electron-ion collision [1,2,3]. Ion viscosity reduces the instability domain i.e.. The mode are more easily stabilised as the ion-ion collision frequency increa-

ses. For instance, when the density increases the minimum ion larmor radius  $a_1$  to stabilize the mode increases. Later a more accurate description of the influence of the collisions was derived [4,5], when heat transport from both electrons and ions was included, allowing for electron and ion temperature fluctuations. In the mean time, the difficulty of analytically solving for normal modes increased and help of numerical technique was required. We present here results of a numerical investigation of the collisional drift wave dispersion relation for conditions in the range of Q-machine operation.

The dispersion relation used here, derived in a slab geometry, includes the ion viscosity and heat transport features mentioned above. Using the notations we defined in ref. 4, it can be schematically written as

$$(\bar{\omega} + 1)V = iz H_E \left\{ (\omega \bar{\omega} - 1)(1 + H_I) + (1 + \bar{\omega})V \right\}$$

with  $V = b(\bar{\omega} - \frac{3}{10} i\alpha)$

$$H_E = 0.98 \frac{\bar{\omega} - 1.07 iz}{\bar{\omega} - 2.96 iz}$$

$$H_I = \frac{V + \frac{1}{2}b}{\frac{3}{2}\bar{\omega} - 2i\alpha}, \quad \bar{\omega} = \tau_i/\tau_e$$

where  $V$ ,  $H_E$  and  $H_I$  arise respectively from the ion viscosity, electron and ion heat conductivity contributions.

When isothermal fluctuations are considered and no heat transport is involved, the expressions for  $H_E$  and  $H_I$  are

$H_E = 1$ ,  $H_I = 0$ . The comparison between isothermal and adiabatic fluctuations arises from the computations. The effect is shown on fig. 1, where contours of constant growth rate are plotted for both cases. The isothermal case looks more unstable for long wavelengths and more stable for short wavelengths. Although the exact numerical values depend on the value of the viscosity coefficient which comes into the parameter  $\nu_i/\epsilon \cdot \nu \tau_i$  ( $\epsilon = \nabla n/n$ ), the qualitative results are the same. For long wavelengths where most experiments operate ( $\epsilon \sim 10^{-1}$ ,  $\lambda_H \sim 1-2 m$ )



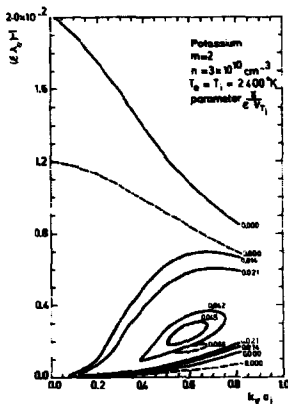


fig.1. NON-ISOTHERMAL DRIFT DISSIPATIVE INSTABILITY  
 — non-isothermal  
 - - - isothermal

for the non-isothermal case the stability is recovered below a critical field ( $B_{crit}$ ) larger than expected from the isothermal theory.

The transport coefficients used here have been published by Braginskii in ref.[6]. They include correction terms in  $(v/\Omega_c)^2$ . Since the marginal stability field  $B_{crit}$  scales with density as  $n^{1/2}$  (in the limit  $k_y \rightarrow 0, b \rightarrow 0$ ), the correction terms scale as  $n$  at marginal stability. The ion transport coefficients are thus modified at larger densities. The modification appears to be important whenever the normalized ion

collision frequency  $v_i/\epsilon \cdot v_{Ti}$  exceeds 1 (for  $k_y \sim \epsilon$ ). In the dispersion relation printed above,  $V$  now reads

$$V^+ = b(\bar{\omega} - \frac{3}{10} i\alpha(1+S_1) - (S_3 + d_3))$$

and  $H_1$  reads

$$H_1^+ = \frac{V^+ - \frac{1}{2}b}{\frac{3}{2}\bar{\omega} - 2i\alpha(1+S_1) - \frac{5}{2}(S_\lambda + d_\lambda)}$$

where a)  $S_1, S_3, S_\lambda$  and  $S_\lambda$  are respectively first order corrections in  $(v_i/\Omega_{ci})^2$  to Braginskii's ion viscosity coefficients  $\eta_\parallel, \eta_\perp$  and perpendicular and transverse ion heat conductivity coefficient  $\chi_\perp, \chi_\parallel$  [7].

b)  $d_3, d_\lambda$  are first order corrections to  $\frac{dn_3}{dr}, \frac{d\chi_\lambda}{dr}$

Such a dispersion relation  $D(k_y/\epsilon, k_\perp a_i, \omega, \gamma) = 0$  is displayed on a double plot on fig. 2, when  $v_i/\epsilon \cdot v_{Ti} = 0.21$  (which obtains for instance for  $n = 3.0 \times 10^{10} \text{ cm}^{-3}$ ,  $T_i = 2400 \text{ K}$ ,  $\epsilon = -1 \text{ cm}^{-1}$ ). The ratio  $K_x/K_y$  is chosen to fit an  $m = 2$  azimuthal mode.

With the corrections included a) the maximum growth rate goes down, b) the stability is improved at any parallel wavelength and obtains for larger field. This increase in stability is observed for any azimuthal mode as shown on fig.3 where the growth rate is plot-

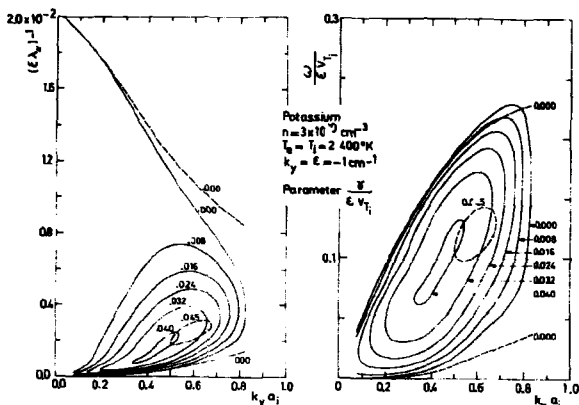


Fig.2. INFLUENCE OF THE CORRECTION TO THE TRANSPORT COEFFICIENT ON THE RESISTIVE DRIFT INSTABILITY DISPERSION RELATION.

— corrected  
 - - - uncorrected

ted against the magnetic field. It does show that  $\nu_i/\Omega_{ci}$  correction vanishes at large field.

Figure 4 shows too that, as B increases, higher azimuthal modes appear with higher growth rate. The frequency for these modes are plotted on fig. 4 and are all located in the same frequency range, From fig.3 and 4 at large field one expects to observe a large number of azimuthal modes of comparable growth rate at frequencies between 0 and a few tenths of  $\epsilon \cdot V_{Ti}$  , For each individual mode the frequency 1/B dependance is observed only at large field. It is almost independant of B around the maximum growth rate and increases with B near marginal stability.

From the linear theory the correlated part of the radial flux ( $\tilde{n} \cdot \tilde{v}_r$ ) may be estimated, by taking  $v_r = \frac{EY}{B}$  . This quantity is proportional to  $|\tilde{\psi}|^2$  , where  $\tilde{\psi}$  is the amplitude of the fluctuating potential. The proportionality coefficient  $\langle \tilde{n} \cdot \tilde{v}_r \rangle / \langle \psi^2 \rangle$  for conditions of figs,3 and 4 is presented on fig. 5. From figs,3 and 5 the simple assumption that  $\tilde{\psi}$  follows  $\tilde{\gamma}$  would lead to the

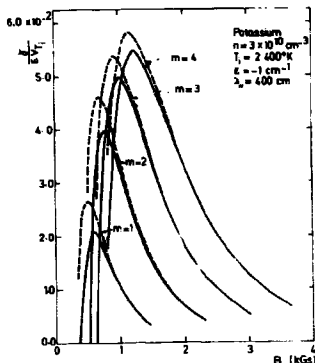


Fig.3. INFLUENCE OF THE CORRECTION TO TRANSPORT COEFFICIENTS ON THE RESISTIVE DRIFT INSTABILITY GROWTH RATE

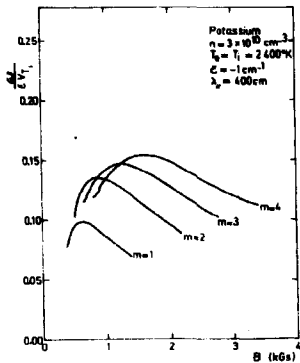


Fig.4. FREQUENCY FOR VARIOUS AZIMUTHAL MODES

conclusion that high magnetic field would bring increased radial transport from higher modes. Actually the amplitude for large azimuthal mode number drops presumably due to non-linear and/or boundaries effects. Another example of high mode limitation in actual experiments, at least in Q-machines, is shown for parallel wave numbers on fig.6. Two different parallel wave modes ( $\lambda = L =$  machine length;  $\lambda = 2L$ ) can exist with comparable growth rate. Since waves are standing in a symmetric double ended machine the higher wavenumber ( $\lambda = L$ ) should exhibit a node around the center of the machine. Such a wave structure has not been reported so far.

Heat exchange between the electron and the ion fluid has been ignored. This term is proportional to  $V_{ii}(\tau_i - \tau_e)$  which contributes to first order, even for equal equilibrium temperatures  $T_{i0} = T_{e0}$ . It can become important for dense cold plasmas and/or unequal ion and electron temperature. The effect for a dense equitemperature plasma (fig.7) shows slightly destabilizing for the short wavelength branch. Beyond the case of dense cold plasma this effect can prove important for partially ionized gases where

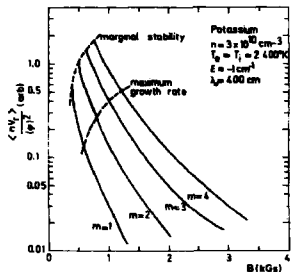


fig. 5. RADIAL TRANSPORT COEFFICIENT FOR VARIOUS AZIMUTHAL MODES

collisional drift wave have been reported, [8].

The dispersion relation including correction terms printed above has been computed for the parameters published in [9] by Hendel. Two cases are considered a) for ion temperature equal to the plate temperature, b) for ion temperature above the plate temperature as might be the case due to the voltage drop

in the sheath. The improvement of stability (fig. 8) over previous theory is not enough to account for the discrepancy with the experimental results. There still is a factor  $\sim 1.5$  on the critical field for the wavelength actually measured or a factor  $\sim 3$  on the wavelength for the critical field observed in the experiment.

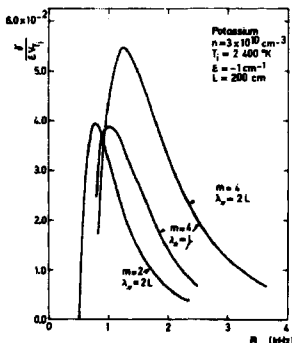


fig. 8. GROWTH RATE AS A FUNCTION OF PERPENDICULAR AND PARALLEL WAVELENGTH

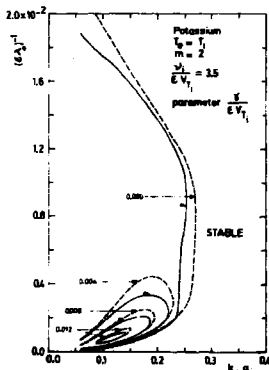


Fig. 7. INFLUENCE OF HEAT EXCHANGE BETWEEN IONS AND ELECTRONS ON RESISTIVE DRIFT WAVES  
 - - - heat exchange  
 — no exchange



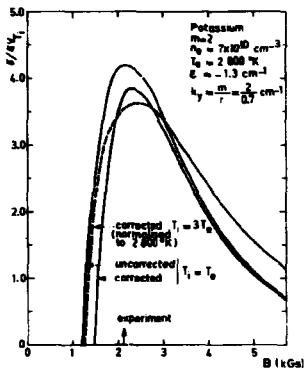


fig. 8. INFLUENCE OF THE CORRECTION TO THE TRANSPORT COEFFICIENT ON GROWTH RATE  
 ———  $k_y a_i > 1$

The computation of the collisional drift wave dispersion relation in an infinite plasma has been performed for non isothermal fluctuations when corrections to the ion transport coefficients and heat exchange between ion and electrons are considered. It yields the frequency and the growth rate for perpendicular and parallel wave numbers. The effect of the magnetic field on the azimuthal modes and on the frequency is shown. The  $1/B$ -dependance of the frequency can only be used for identification of drift wave at large field.

Agreement of this dispersion relation with existing experiments is improved. However the remaining discrepancies might question the adhequacy of the linear theory to accurately explain the observations in actual machines where end effects, radial dependances and non-linear phenomena are present.

#### REFERENCES

- [1] A.B. MIKHAILOVSKII , O.P. FOGUTSE, Dokl. Akad. Nauk, SSSR, 156, 64, (1964).
- [2] F.F. CHEN, Phys. Fluids, 8, 1323 (1965)
- [3] G. LAVAL, R. PELLAT  
 Proceedings conf. on Phys. of Quiescent Plasmas, Frascati 1967, Part I, p. 111.

- [4] R. GRAVIER, G. LAVAL, R. PELLAT, C. RENAUD  
Proceedings Int. Conf. on phys. of Quiescent Plasmas,  
Paris 1969, Part II, p. 1
- [5] S.T.TSAI, F.W. PERKINS, T.H. STIX  
Phys. Fluids, 13, 2108 (1970)
- [6] S.I. BRAGIINSKI in Reviews of Plasma Physics, edited by  
M.A. Leontovich (Consultant Bureau, New-York, 1965) Vol. I,  
P. 205.
- [7] S.I. BRAGIINSKI, in Reviews of Plasma Physics, edited by  
M.A. Leontovich (Consultant Bureau, New-York, 1965) p. 250,  
253.
- [8] M. BERNARD, G. BRIFFOD, R. FRANCK, M. GREGOIRE, J. WEISSE  
Proceedings 3rd Int. Conf. on Plasma Phys. and Controlled  
Nuclear Fusion Research, Novosibirsk, 1968, p. 715.
- [9] H.W. HENDEL, T.K. CHU, P.A. POLITZER, Phys. Fluids, 11  
2426 (1968)  
and T.K. CHU, H.W. HENDEL, L.G. SCHLITT, T.C. SIMONEN,  
T.H. STIX, Proceedings Int. Conf. on Phys. of Quiescent  
Plasmas, Paris, 1969, Part II, p. 57.

MEASUREMENTS OF TEMPERATURE WAVES IN CONNECTION  
WITH A DRIFT-TYPE INSTABILITY

by

W. Friz, G.L.J. Müller<sup>+</sup> and R.S. Palmer

Aerospace Research Laboratories, WPAFB, Ohio 45433

Abstract

Experimental investigations were made to substantiate the existence of electron temperature fluctuations accompanying a drift-type instability in a Q-device as predicted in an experimental study by R.W. Motley and R.F. Ellis and in a theory promoted by S. Tsai, F.W. Perkins and T.H. Stix. These fluctuations violate the isothermal assumptions of previous drift wave theories. As it appears their most evident effect is on the phase relations between density and potential fluctuations. Results of measurements and a discussion of the applied diagnostic techniques are presented. The temperature fluctuations are in all measured cases much smaller than the density and potential fluctuations, their normalized value being  $2 \cdot 10^{-2} \leq T/T_0 \leq 7 \cdot 10^{-2}$ . With increasing plasma density the phase lag of the temperature waves increases, whereas their amplitudes decrease monotonically.

Introduction

In recent works<sup>1,2</sup> on density driven drift waves it has been pointed out that the experimental results do not follow in all details the predictions of the generally accepted isothermal theories<sup>3,4</sup>. In particular, there are discrepancies between the measured and the theoretically predicted phase angles for density and potential fluctuations which would lead to irreconcilable consequences for the wave induced radial losses. Apparently the problem arises from the equalization of the space and floating potential  $\tilde{\phi}_s = \tilde{\phi}_f$ , an identity valid only under isothermal plasma conditions. However, when fluctuations of the plasma

<sup>+</sup> Ohio State University Research Foundation, Columbus, Ohio.  
On leave from the Max-Planck-Institut für Plasmaphysik,  
Garching, Federal Republic of Germany



electron temperature  $\tilde{T}$  are involved, a relation between  $\tilde{\phi}_s$ ,  $\tilde{\phi}_f$  and  $\tilde{T}$  can be derived from the Langmuir probe theory

$$\frac{e\tilde{\phi}_s}{kT_o} = \frac{e\tilde{\phi}_f}{kT_o} + \frac{\tilde{T}}{T_o} \ln \left( \frac{u_e}{\alpha u_i} \right) \quad (1)$$

Equation (1) shows that  $\tilde{\phi}_s$  is not in phase with  $\tilde{\phi}_f$ , in general, and may eliminate the discrepancies mentioned earlier as pointed out by Motley and Ellis<sup>1</sup>.

Here we present experimental results showing electron temperature fluctuations  $\tilde{T}$  accompanying the density and floating potential fluctuations  $\tilde{n}$  and  $\tilde{\phi}_f$  of a drift-type instability in the ARL Q-device in single ended operation. The plasma column was 260 and 111 cm long and had a diameter of 3.5 cm. The machine was operated with Caesium at plasma densities  $n_o > 10^{10} \text{ cm}^{-3}$  and at magnetic field strengths of  $1 \leq B \leq 3 \text{ kG}$ . A detailed description of the experimental apparatus and the features of the instability is given elsewhere<sup>5,6</sup>. Measurements of potential, density and temperature fluctuations were made using shielded Langmuir probes, .125 mm in diameter and 3 mm long. They were located near the maxima of  $\tilde{n}/n_o$  and  $e\tilde{\phi}_f/kT_o$  and close to the peak density gradient  $\nabla n_o$  in a plane 56 cm from the ionizer and at different azimuthal positions.

#### Experimental Method

An electronic sampling method was used to measure the fluctuations of plasma density, potential of the unbiased probe, and the electron temperature in phase and amplitude. The a.c. probe signals were sampled during each instability period, phase locked to the instability, and with a gate time much smaller than the oscillation period (Figure 1). The d.c. and a.c. plasma

densities were derived from ion saturation probe currents. A. c. potentials of a floating probe were measured with a shielded probe and a high impedance input ( $R > 10^9 \Omega$ ).

As a basis for the electron temperature measurements, the well known Langmuir relation

$$-\frac{e}{kT} = \frac{d \ln I_e}{d\phi} = \frac{1}{I_e} \cdot \frac{dI_e}{d\phi} \quad (2)$$

was used where:  $I_e$  is electron current,  $\phi$  the probe voltage,  $T$  the electron temperature. By switching the d.c. probe bias between two potentials, one in the ion saturation current region and the other in the electron portion of the probe characteristic, (Fig. 2) the electron current

$$I_e = I_{pr} - I_{sat} \quad (3)$$

was controlled. The slope of the probe characteristic  $dI_{pr}/d\phi$  ( $I_e \approx I_{pr}$ ), which was assumed equal to  $dI_e/d\phi$ , was measured by a probe current modulation<sup>7</sup> which was induced by a small superimposed a.c. signal on the probe bias (Fig. 2) with an amplitude  $u \ll kT/e$  and with a frequency

$\Omega \ll \omega$ . Measurements were taken in a range with  $|I_e| \leq 3 |I_{sat}|$  where

Determination of Electron Temperature

Periodic sampling:



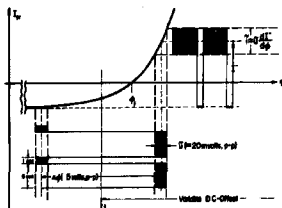
Linear modulation:

$$\phi = \phi_0(t) + u \sin \Omega t \quad \Omega \ll \omega; u \ll kT/e$$

$$\frac{dI_e}{dt} = \left( \frac{dI_e}{d\phi} \right) \cdot \frac{d\phi}{dt} = \left( -T + \frac{e}{kT} \right) \frac{du(t)}{dt}$$

$$\left[ \frac{1}{T} \cdot \frac{dI_e}{du} = \frac{1}{T} \left( -T + \frac{e}{kT} \right) \right] \frac{1}{\Omega}$$

Fig. 1



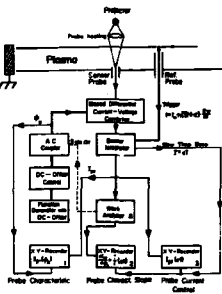
BIAS VOLTAGE RELATIONS

Fig. 2

the probe characteristic has a very good exponential behavior. By continuously tuning the d.c. offset of the probe d.c. bias, the electron probe current  $I_e$  is held constant, therefore the slope  $dI_e/d\phi$ , in equation (1), becomes proportional to  $1/T$ . Deviations in probe characteristic slope, sampled over an instability period and at a fixed  $I_e$ , allowed measurements of variations in  $T$  in both phase and amplitude over the same period.

### Diagnostic Apparatus

The schematic of the diagnostic apparatus used in these experiments is shown in Fig. 3. The left side shows the probe bias arrangement. The probe current signals are fed to a Box Car Integrator which performs the sample and hold function. The d.c. output of the box car integrator delivers phase locked probe currents to both recorders 1 and 3. Recorder 1 plotted phase locked probe characteristics ( $I_{pr}$  vs  $\phi$ ) while recorder number 3 monitored the constant probe current control ( $I_e$ ). Recorder number 2 plots the probe characteristic slope by measuring the low frequency probe current modulation. The time base of the box car integrator is triggered by the instability signal of a separate reference probe.



Temperatures West, Diagnostic and Control Circuits

Fig. 3

The fluctuations in the probe floating potential  $\tilde{\phi}_+$  were also recorded with this circuitry (Fig. 3), only in this case a floating input amplifier was used instead of the current to voltage converter shown in that schematic.

Experimental Results

Fig. 4 shows in the upper part typical traces of the fluctuations of the floating probe and the ion saturation current. The lower part of figure 5 shows probe characteristics for three instability phase points.

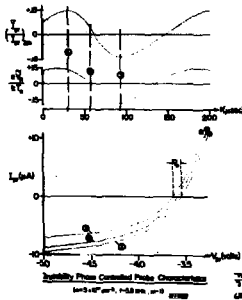


Fig. 4

Fig. 5 shows typical results of a set of recordings of density, floating probe potential and electron temperature fluctuations vs the stretched time resulting from the sampling technique.

Many runs of this type were recorded in a range of plasma densities  $10^{10} \leq n_0 \leq 1.5 \cdot 10^{11} \text{ cm}^{-3}$ , magnetic fields  $1 < B < 3 \text{ kG}$  and for column lengths of 260 and 111 cm.

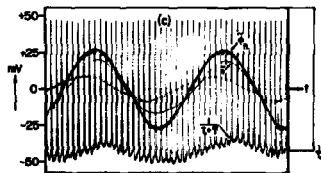


Fig. 5

Results of these measurements showed temperature fluctuations in the range of  $2 \cdot 10^{-2} \leq \tilde{T}/T_0 \leq 7 \cdot 10^{-2}$  which were found to be much smaller than the density and floating potential fluctuations  $\tilde{n}/n_0 \approx e\tilde{\phi}_f/kT_0$ .

Fig. 6 shows the phase relations between potential and density fluctuations vs  $n$ . The lower half of Fig. 6 shows the measured phase differences between the density oscillation and the potential oscillation of the floating probe, with the floating potential oscillations always leading in phase. The upper half of this figure shows the phase of the density oscillation in regard to the phase of the space potential, which

was calculated from equation(1) using the measured values of phase and amplitude of floating potential and temperature fluctuations. These results show that the density oscillations are mostly leading the space potential oscillations as is postulated in linear drift-wave theory. Experimental results of the electron temperature oscillations in phase and amplitude vs the plasma density are presented in Fig. 7. The amplitudes decrease and the phase lag w.r.t.space potential increases with increasing plasma density.

These preliminary measurements allow the following conclusions: 1) from the Langmuir probes in conjunction with a sampling technique, fluctuations of the plasma electron temperature, in phase and amplitude, were measured in the presence of density and potential oscillations of a drift type instability. 2) The density oscillations were found to be lagging in phase in regard to the potential oscillations of the floating probe but mostly leading in phase in regard to the space potential oscillations calculated in connection with temperature fluctuations. 3) The measured electron temperature fluctuations decrease in amplitude and increase in phase lag in regard to floating potential with increasing density.

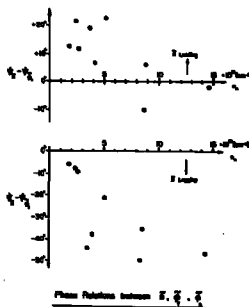


Fig. 6

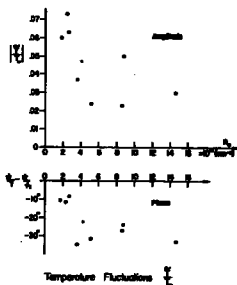


Fig. 7

References

1. R.W. Motley and R.F. Ellis, *Phys.Fluids* 14, 886 (1970).
2. S. Tsai, F.W. Perkins and Th.H. Stix, *Phys.Fluids* 13, 2108 (1970).
3. H.W. Hendel, T.K. Chu, and P.A. Politzer, *Phys. Fluids* 11, 2426 (1968).
4. R.E. Bowberg and A.Y. Wong, *Phys.Fluids* 13, 661 (1970).
5. W. Friz, G.S.J. Müller, J.C. Corbin, R.S. Palmer, Europe Conference Contr.Fusion and Plasma Phys., Rome, Italy 1970, Proc. 149.
6. G.L.J. Müller, J.C. Corbin, R.S. Palmer, *Bull. Am. Phys. Soc. Proc. II*, 15, 1464 (1970).
7. R.H. Sloane and E.I.R. MacGregor, *Phil.Mag.* 18, 193 (1934).

Dynamic Stabilization of Transverse Kelvin-Helmholtz Instability\*

by

Y. C. Lee<sup>†</sup> and T. K. Chu

Plasma Physics Laboratory, Princeton University, Princeton, N.J. 08540

Abstract

The transverse Kelvin-Helmholtz instability is driven by non-uniform  $\underline{E} \times \underline{B}$  motion of a plasma. An a. c. electric field near ion cyclotron frequency, applied across the shear layer resulting from the nonuniform d. c. electric field, can be used to stabilize the transverse Kelvin-Helmholtz instability. The stabilizing effect is shown to arise from high-frequency excursion of ions near the shear layer.

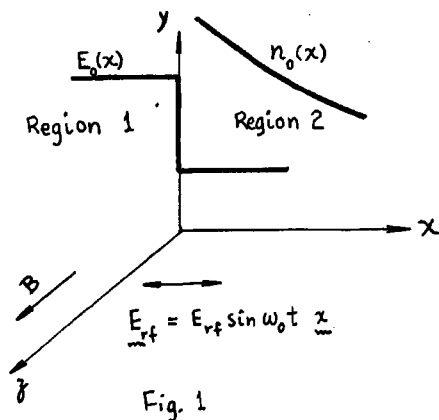
---

\* This work was supported by U.S. Atomic Energy Commission Contract AT(30-1)-1238.

<sup>†</sup> Present address, University of California at Los Angeles, Los Angeles, California.

A cylindrical plasma column confined by uniform axial magnetic field and possessing a radial electric field rotates with the  $\underline{E} \times \underline{B}$  frequency. If the electric field does not vary linearly with radius, the plasma rotates nonuniformly and velocity shear exists between radially adjacent layers. When adjacent layers mix, the directed kinetic energy decreases and the Kelvin-Helmholtz mode thus may become unstable<sup>1</sup>.

A transverse a. c. electric field, near ion cyclotron frequency, is used in the present model to dynamically stabilise the low-frequency Kelvin-Helmholtz mode. We select a two-region plasma, Fig. 1. At equilibrium, there exists a discontinuity in  $E_0(x)$  so that a velocity shear exists in the  $x$  direction.





To follow the relative motion of electrons and ions due to the applied field of frequency  $\omega_0$ , we define the following transformations of particle displacement and velocity:

$$\underline{\rho}_\alpha = \underline{x}_\alpha + \underline{\epsilon}_\alpha \sin \omega_0 t \quad (1)$$

$$\underline{u}_\alpha = \underline{v}_\alpha + \omega_0 \underline{\epsilon}_\alpha \cos \omega_0 t \quad (2)$$

$$\alpha = i, e$$

and

$$\phi_{k_y, \alpha}^n(\underline{\rho}_{\alpha, x}, t) = \int d\rho_{\alpha, y} dt \phi(\rho_{\alpha, x}, \rho_{\alpha, y}, t) \exp[-ik_y \rho_{\alpha, y} + i(\omega + n\omega_0)t] \quad (3)$$

of the function  $\phi(\rho_{\alpha, x}, \rho_{\alpha, y}, t)$ . It follows that a function  $f$  in both the electron and ion frames is related by

$$f_{k_y, e}^n = \sum_p J_p(\epsilon_x \frac{d}{dx} + k_y \epsilon_y) f_{k_y, i}^{n-p} \quad (3)$$

$$f_{k_y, i}^n = \sum_p J_{-p}(\epsilon_x \frac{d}{dx} + k_y \epsilon_y) f_{k_y, e}^{n-p} \quad (4)$$

$$\underline{\epsilon} = \underline{\epsilon}_e - \underline{\epsilon}_i \quad (5)$$

where  $J_p$  is the Bessel function of order  $p$ .

The dispersion relation<sup>2, 3, 4</sup> is, therefore

$$\nabla^2 \phi_i^n = L_i^n \phi_i^n - \sum_p J_{-p} L_e^{n-p} \phi_e^{n-p} \quad (7)$$

where

$$L_i^n = \frac{\omega_{pi}^2}{(\bar{\omega} + n\omega_0)^2 - \Omega_{ci}^2} \left[ \frac{n'_0}{n_0} \frac{k_y \Omega_{ci}}{\bar{\omega} + n\omega_0} - k_y^2 + \frac{1}{n_0} \frac{d}{dx} n_0 \frac{d}{dx} - \frac{(\omega'_n)_i}{n_0 (\bar{\omega} + n\omega_0)} \right] \quad (8)$$

$$L_e^n = \frac{\omega_{pe}^2}{(\bar{\omega} + n\omega_0)^2 - \Omega_{ce}^2} \left[ \frac{n'_0}{n_0} \frac{k_y \Omega_{ce}}{\bar{\omega} + n\omega_0} \right] \quad (9)$$

and  $\omega_{p\alpha}^2 = 4\pi e^2 n_\alpha / m_\alpha$ ,  $\bar{\omega} = \omega + k_y U$ ,  $U = \frac{cE_0}{B}$ ,  $\Omega_{c\alpha} = \frac{eB}{cm_\alpha}$ , where

prime denotes differentiation with respect to  $x$ . In obtaining Eqs. (8) and (9) for the Kelvin-Helmholtz mode, we have neglected finite Larmor radius effect and terms smaller by a factor of  $(\frac{\omega}{\Omega_{ci}})^2$ . We have also

assumed  $k_{||} = 0$  and no collision and wave-particle resonance effects.

For  $(\bar{\omega}) \ll \omega_0 \sim \Omega_{ci}$  and small high-frequency field so that

$k_y \epsilon \ll 1$ , Eq. (7) gives

$$\nabla_x^2 \phi_i^0 = L_i^0 \phi_i^0 - L_e^0 \phi_e^0 - \frac{1}{4} \left( \frac{d}{dx} + k_y \epsilon_y \right)^2 L_e^0 \phi_e^0 \quad (10)$$

$$\nabla_x^2 \phi_i^{\pm 1} = L_i^{\pm 1} \phi_i^{\pm 1} - L_e^{\pm 1} \phi_e^{\pm 1} \pm \frac{1}{2} \left( \epsilon_x \frac{d}{dx} + k_y \epsilon_y \right) L_e^0 \phi_e^0 \quad (11)$$

where  $\phi_i^{\pm 1}$  are associated with frequencies  $(\bar{\omega} \pm n\omega_0)$ .

For the two-region model in Fig. 1, the differential equations

governing  $\phi_i^0$  and  $\phi_i^{\pm 1}$  reduce to

$$\left( \frac{d^2}{dx^2} - k_y^2 \right) \phi_i^0 = 0 \quad (12)$$

$$\left( \frac{d^2}{dx^2} - k_y^2 \right) \phi_i^{\pm 1} \approx 0 \quad (13)$$

The boundary condition is

$$\frac{\phi_1^n}{\bar{\omega} + n\omega_0} \quad \text{continuous across interface} \quad (14)$$

The solutions to Eqs. (12) and (13) are

$$\phi_{11}^0 = A\bar{\omega}_1 \exp(k_y x) \quad \left. \vphantom{\phi_{11}^0} \right\} \quad x < 0 \quad (15)$$

$$\phi_{11}^{\pm 1} = B^{\pm} \exp(k_y x) \quad (16)$$

$$\phi_{12}^0 = A\bar{\omega}_2 \exp(-k_y x) \quad \left. \vphantom{\phi_{12}^0} \right\} \quad x > 0 \quad (17)$$

$$\phi_{12}^{\pm 1} \approx B^{\pm} \exp(-k_y x) \quad (18)$$

Multiplying Eqs. (10) and (11) by  $\bar{\omega}$ , integrating across the interface, we obtain the following dispersion relation when  $\omega_0$  is close to  $\Omega_{ci}$ ,

$$\bar{\omega}_1^2 + \bar{\omega}_2^2 = \omega_\alpha \omega + \omega_\alpha \frac{1}{2} k_y (U_1 + U_2) + \beta \omega_\alpha k_y (U_2 - U_1) \quad (19)$$

where

$$\omega_\alpha = k_y^2 \epsilon_x^2 \Omega_{ci} \left[ -\frac{2\kappa_n}{k_y} - \frac{\Delta n_0}{n_0} \right] + k_y^2 \epsilon_y^2 \Omega_{ci} \frac{\Delta n_0}{n_0} \quad (20)$$

$$\omega_\alpha \beta = i k_y^2 \epsilon_x \epsilon_y \Omega_{ci} \frac{\Delta n_0}{n_0} \quad (21)$$

and  $-\kappa_n = n'_0/n_0$ ,  $\Delta n_0 =$  density change across the shear-layer interface.

The stability criterion is

$$\left[ \omega_\alpha + 4\beta k_y (U_2 - U_1) \right]^2 > (16\beta^2 + 4) k_y^2 (U_2 - U_1)^2 \quad (22)$$

Thus, for sufficiently large a.c. electric field strength, the high-frequency excursion of ions near the shear layer dynamically stabilises the transverse Kelvin-Helmholtz mode. For laboratory plasmas of

$k_y (U_2 - U_1) \approx 10 \text{ kHz}$ ,  $\Omega_{ci} \approx 250 \text{ kHz}$ , then  $k_y^2 \frac{c^2}{x^2} \sim 0.4$ , i. e., the ion excursion is of the order, or a fraction of, the inverse of the instability wavenumber.

<sup>1</sup> S. Chandrasekhar, Hydrodynamic and Hydromagnetic Stability, Oxford University Press, London, 1961.

<sup>2</sup> M. N. Rosenbluth and A. Simon, Physics of Fluids 8, 1300 (1965).

<sup>3</sup> T. E. Stringer and G. Schmidt, Plasma Physics 9, 53 (1967).

<sup>4</sup> F. W. Perkins and D. L. Jassby, Physics of Fluids 14, 102 (1971).

PASSIVE FEEDBACK CONTROL OF A DRIFT-TYPE  
INSTABILITY IN A Q-MACHINE PLASMA COLUMN

by

G. L. J. Muller\* and R. S. Palmer

Aerospace Research Laboratories, WPAFB, Ohio 45433

Abstract

A passive feedback instability control method, consisting of a tunable series resonance circuit connected with a feedback probe and driven by the plasma instability energy itself, was applied to a  $m = 1$  "drift-type" instability of a single ended Q-machine plasma. Phase and amplitude of the feedback drive current is controlled by varying the resonance circuit characteristics. Measurements were made of the oscillation amplification, partial suppression, and the equilibrium plasma density changes caused by instability induced plasma losses. The passive control mechanism can be described by the stationary solution of the "Van der Pol" differential equation for non-linear oscillation phenomena. The efficiency of the oscillation control was found to be small in this experiment because only a single feedback loop is applied. Suggestions are discussed to improve the stabilization efficiency of this passive feedback method.

Introduction

Feedback plasma stabilization methods have recently received some attention<sup>1</sup> and were applied with success to various instabilities in different plasma devices<sup>2,3</sup>. This paper describes the results of a passive feedback control experiment where the feedback energy is supplied by the internal energy of the plasma instability. A part of the plasma instability energy is coupled from the plasma, by means of a probe, into an L-C series resonance circuit and fed back into the plasma by the same probe. The feedback drive current is controlled, in its phase and amplitude, by varying the eigenfrequency, in regard to the instability frequency, and the ohmic impedance of the resonance circuit.

\* Ohio State University Research Foundation, Columbus, Ohio.  
On leave from the Institut für Plasmaphysik, 8046  
Garching near München, Germany

We applied this passive feedback control method to a "drift-type" instability of a Q-machine plasma column and investigated the characteristics of this stabilization mechanism and its plasma response. The single ended Q-machine was operated with Cesium, at plasma densities in the range of  $1 \times 10^{11} \text{ cm}^{-3}$ , at magnetic fields of about 2 Kilogauss, and at a plasma column length of 265 cm. Details about the characteristics of the instability<sup>4</sup> and its control by virtue of a d.c. electric field<sup>5,6</sup> and of an active feedback method<sup>6,7</sup> were reported elsewhere.

Partial suppression and amplification of the instability and the change of the instability induced plasma losses were measured as a function of the externally controlled phase and the amount of the instability driven feedback current. Most measurements were performed with a d.c. floating feedback probe at the position in the plasma column where highest instability amplitudes were observed.

### Experimental Method

We applied a phase sensitive method to measure the plasma oscillations and the equilibrium density as a function of the feedback characteristics.

Figure 1 shows the applied diagnostic method. The feedback loop on the left side was periodically gated by a chopper driven by a square wave signal of 135 Hz. The plane feedback probe, 1 cm. x 4 cm., was placed in a radial position of peak

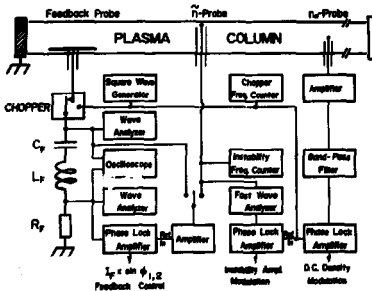


Figure 1

density and potential oscillations.

Feedback voltage and current signals were controlled and monitored by wave analyzers and a multi-channel oscilloscope. One phase lock amplifier delivered directly the feedback drive signal  $I_f \sin \phi$ , where the phase  $\phi$  can be referred to the feedback probe potential or the density oscillations, dependent on whether the reference input of the phase lock amplifier is connected with the feedback or density oscillation measuring probe.

The feedback controlled density oscillations and the d.c. density were measured with two small shielded probes of the same size, (2 mm long and .2 mm diam.), at axial positions near the machine half length. These signals were measured phase locked to the chopper drive signal. The density oscillation measuring probe was shifted  $90^\circ$  azimuthally in reference to the feedback probe in order to prevent direct coupling disturbances between both probes. D.c. and a.c. plasma density measurements were derived from the ion saturation current of probes biased at 15 volts negative. All measurements were performed using the mode = 1 instability with a frequency of about 8 KHz.

### Results

Measurements of the amount and phase of the feedback loop current and the feedback controlled instability amplitude are shown in Figure 2. Here the feedback characteristics are measured at various impedances  $F_f$  vs. the inductivity  $L_f$  of the external resonance

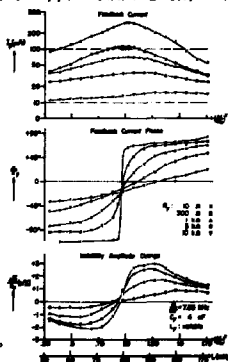


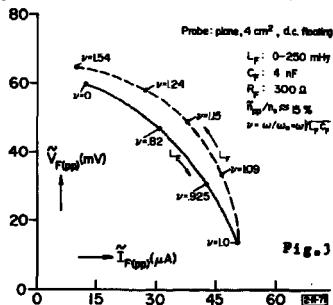
Figure 2

circuit. One recognizes the typical feedback behavior in the families of curves in the middle and the bottom of this figure. Positive marked phases  $\phi_F$  correspond to an inductive resonance circuit behavior and to a lagging of the feedback current in regard to the feedback drive voltage. This case leads to a destabilization, while a leading in phase results in an instability amplitude reduction. The instability amplitude change around the resonance ( $\omega/\omega_F = 1$ ) is mainly caused by a fast change of the feedback current phase vs.  $\omega/\omega_F$ . A reduction of the feedback control, far outside the resonance, is caused mainly by the reduction of the feedback current when the resonance frequency  $\omega_F$  deviates more and more from the instability frequency  $\omega$ .

The feedback circuit current-voltage characteristic shown in Figure 3 represents the instability control of the passive feedback loop itself.

In this diagram, the a.c. feedback probe voltage (the probe is at d.c. floating potential) is directly recorded vs. the a.c. current in the feedback loop, when the circuit resonance frequency  $\omega/\omega_F$  was varied. In the lower branch, with  $\gamma = \omega/\omega_F < 1$ , we have a stabilizing effect to the plasma oscillations, while in the upper branch, with  $\gamma > 1$ , the resonance circuit is inductive,  $L_F$  is dominant and both the feedback loop voltage and current are amplified.

An experimental result on the influence of instability



Feedback Circuit Current-Voltage Characteristic  
(Ca.  $n=1 \times 10^7 \text{ cm}^{-3}$ ,  $B=2 \text{ kG}$ ,  $l=280 \text{ cm}$ ,  $f=7.7 \text{ kHz}$ )



control to the radial containment of the plasma column is shown in Figure 4. Here the change  $\Delta n_0$  of the equilibrium density in the center of the column is directly recorded vs.  $I_F \sin \phi$ , while the feedback loop eigenfrequency is varied in a wide range

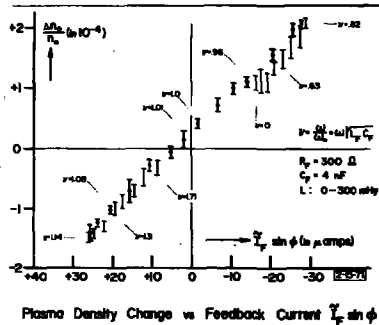


Figure 4

by changing the circuit inductance  $L_F$  step by step at a fixed capacitance  $C_F$ . Both signals in Figure 4 were derived from the phase lock technique.

Discussion

The expressions shown in Figure 5 represent an analysis of the probe-plasma passive feedback loop where  $R_t$  is the total complex impedance of the loop,  $R_{p1}$  is the plasma impedance, and  $R_{pr}$  is the probe resistance at floating potential. From these equations, one can express a

$$R_t = R \left[ 1 + \frac{(\omega^2 \omega_c^2 - 1)^2}{\omega^2 \tau^2} \right]^{1/2} \exp \{ i\phi \}$$

relation for the feedback oscillation density  $\tilde{n}_2$ . At resonance of the feedback circuit with the instability frequency,

with:  $\phi = \arctan \left[ \frac{\omega^2 \omega_c^2 - 1}{\omega \tau} \right]$

$$\omega_r = (C_p L_F)^{-1/2}, \quad \tau = RC_p$$

$$R = R_w + R_{pr} + R_p$$

$\frac{\omega_r}{\omega_c} = 1$ , the internal plasma feedback signal  $\tilde{n}_2$  is about  $180^\circ$  out of phase in reference to the instability signal  $\tilde{n}_1$ . The impedance of the total feedback

$$R_w = 6.53 \times 10^8 \frac{\Delta n_A}{T^{3/2}} \times \frac{L_F^2}{R^2} \text{ (ohm)}$$

$$(R_w)_{V_n} = 3.45 \times 10^9 \frac{I_T}{R_A} \left| \frac{V_n}{\sigma V} \right|$$

Figure 5

loop has a minimum when  $R_t = R$  and the feedback current is maximum under this condition.  $\tilde{n}_2$  is leading or lagging in phase, in regard to the instability signal  $\tilde{n}_1$ , dependent on whether  $\omega/\omega_F > 1$  (capacitive circuit) or  $\omega/\omega_F < 1$  (inductive circuit).

Recently, it was shown that the "Van der Pol" theory of non-linear oscillation phenomena is able to describe successfully the plasma instability feedback control mechanism<sup>2,3</sup>. According to this theory, the oscillation control is given by:

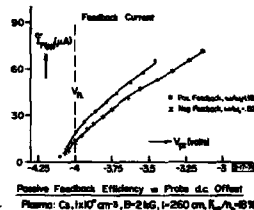
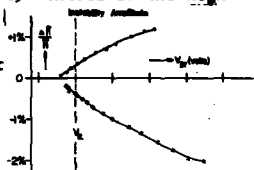
$$\left( \frac{\tilde{n}_1}{\tilde{n}_{10}} \right) \left\{ \left( \frac{\tilde{n}_1}{\tilde{n}_{10}} \right)^2 - 1 \right\} = \frac{\omega}{\omega_I} \frac{\tilde{n}_2}{\tilde{n}_{10}} \sin \phi$$

where  $n_1$  and  $n_{10}$  are the feedback controlled and the natural instability saturation amplitudes,  $\phi$  the phase of the feedback signal in regard to the instability signal, and  $\omega_I$  the instability growth rate. The right side of this equation is the feedback oscillation control parameter, which is  $> 0$  for destabilization and  $< 0$  for stabilization dependent on whether the feedback oscillations are leading or lagging in phase in regard to the instability oscillations. For a comparison to our circuit, it follows that a predominantly capacitive resonance circuit  $\omega/\omega_F < 1$  corresponds to a negative or stabilizing feedback loop, while an inductive circuit  $\omega/\omega_F > 1$  results in a positive or destabilizing feedback.

In our earlier experiments where we applied, to the same instability, an active feedback control technique, we found a plasma density reduction varying with the squared instability amplitude. The linear behavior of  $\Delta n_0$  vs.  $I_F \sin \phi$  in Figure 5 can be understood as a result of the weak oscillation control in this passive feedback experiment.

Feedback Efficiency

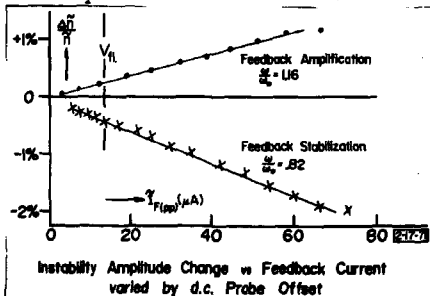
One reason for the weak instability control is the high probe-plasma coupling impedance. The probe-sheath a.c. impedance is high at d.c. floating potential but can be reduced considerably by applying a positive d.c. bias to the feedback probe. Figures 6 and 7 show the experimental behavior of a d.c. biased feedback loop for typical feedback parameters. These measurements were performed under conditions of a relatively small feedback current (by use of  $R_F = 1K$  ) and of resonance circuit



Positive Feedback Efficiency = Probe d.c. Offset  
 Plasma:  $C_1, 1.1 \times 10^{-7} \text{ cm}^{-3}$ ,  $B = 2 \text{ kG}$ ,  $f = 260 \text{ cm}^{-1}$ ,  $\eta_p = 0.8\%$

Figure 6

eigenfrequencies for optimal oscillation amplification and suppression. Figure 6 shows in the lower half, the feedback currents and in the upper half the corresponding feedback instability amplitude vs. the externally applied d.c. probe bias varied positively and negatively with respect to floating potential  $V_{F1}$ . The feedback current  $I_F$  increases considerably with a



Instability Amplitude Change vs Feedback Current varied by d.c. Probe Offset

Figure 7

amount of the feedback current as shown in Figure 7.

positively growing bias and improves the instability control. In both cases of positive and negative applied feedback, the controlled instability amplitudes vary linearly with the

The feedback efficiency is small in this single feedback loop experiment. The reasons of the limited feedback control efficiency and several proposals to improve the power of this passive plasma stabilization method are discussed. Future work has to answer the question whether the passive instability control method can ever be made powerful enough to quench out completely a plasma instability because of inevitable energy losses in the plasma, plasma boundary sheaths, and the external circuit. However, its application, under optimal conditions, would reduce the power requirement for an auxiliary or additional active feedback necessary for complete suppression of an instability.

#### References

1. T.K.Chu and H.W. Hendel, AIP Conference Proceedings No 1 Feedback and Dynamic Control of Plasmas, American Institute of Physics, New York, 1970.
2. B.E. Keen, Phys Rev. Letters 24, 259, (1970)
3. G.L.J. Müller, J.C. Corbin, and P.S. Palmer, AIP Conference Proceedings, No 1, p. 129 (1970)
4. G.L.J. Müller, W. Friz and P.S. Palmer, APL 70-0080, (1970) Aerospace Research Laboratories, WPAFB, Ohio.
5. W. Friz, G. Müller, J.C. Corbin, and P.S. Palmer, IV European Conference on Controlled Fusion and Plasma Physics, Rome, Italy (1970) Proc. p.149
6. G.L.J. Müller, J.C. Corbin and P.S. Palmer, APS Meeting Washington, D.C., Nov 1970, Proc. II, 15, 1464 (1970)
7. G.L.J. Müller, APS Meeting, Washington, D.C., Nov 1970, Bull. Am. Phys. Soc. II, 15, 1488 (1970).

Experimental Frequencies and Growth Rates of a  
Drift-Dissipative Instability in a Continuous r.f. Plasma

by

B.E. Keen and M.W. Alcock

U.K.A.E.A. Research Group, Culham Laboratory, Abingdon, England.

Abstract

Results are presented for a low frequency self-excited oscillation in an inhomogeneous r.f. collisional plasma. These waves occurred mainly as  $m = +1$  azimuthal propagating modes, and as standing waves in the axial direction with approximately half a wavelength in the tube. The frequency ' $\omega$ ' was dependent on the tube length, the axial magnetic field, and the gas neutral pressure, and measurements have been made when varying these parameters.

The initial growth rates have been measured under various conditions, by using a method of dynamic stabilisation to suppress the instability, and analysing the subsequent return of the oscillation. Comparison of the results obtained with a previous theory of the drift-dissipation instability shows reasonably good agreement.

Introduction

Lately, there has been considerable theoretical and experimental work on the low frequency drift instabilities occurring in plasmas. These micro-instabilities are driven unstable by the plasma density gradient in both collisionless and collisional plasmas. Their importance derives from the probable correlation between the anomalously high diffusion of plasma across

a containing magnetic field and the presence of these finite amplitude waves in the plasma.

Previous attempts to measure drift instability characteristics and compare them with theory have suffered from some or all of the following difficulties:-

- (a) In most reported observations on drift waves, large radial electric fields  $E_r$ , have existed in the plasma column, as well as the radial density gradient. This radial electric field taken together with the axial magnetic field, leads to an azimuthal drift of plasma. This drift causes a plasma rotation, and consequently leads to a Doppler shift of the instability frequency measured in the laboratory frame of reference. This rotation frequency is usually the same order of magnitude as the predicted instability frequency<sup>1,2,3</sup> and can lead to complications in comparison with theory. Also, it has been shown that a rotationally convected drift instability<sup>4</sup> can be sustained in a collisional plasma.
- (b) Most theories with which the experimental results are compared are linearised theories, whereas most experiments have been performed on self-excited oscillations which are amplitude limited by non-linear mechanisms, and thus, the results have been obtained in the non-linear, large amplitude regime.
- (c) Few experiments have obtained direct measurement of the initial growth rate of the drift instability. When values are obtained of this parameter direct comparison can be made with linearised theories.

This paper reports experiments on a low frequency self oscillatory wave in an r.f. collisional discharge, in which the radial electric field was extremely small ( $0 \pm 10\text{mV/cm}$ ). Experiments were performed using a dynamic stabilisation technique<sup>5</sup> to reduce the instability to a very small amplitude

( $n'/n_0 \leq 1\%$ ), and so experiments could be performed in the small amplitude, linear regime. Further, the initial growth rate ( $\gamma$ ) was measured as the instability returned to its non-linear saturation amplitude.

### Theory

The stability of an inhomogeneous plasma column in a uniform magnetic field, in which both electron-neutral ( $\nu_e$ ) and ion-neutral ( $\nu_i$ ) collision frequencies were included, has been considered by Timofeev<sup>6</sup>, and further extended by Alcock and Keen<sup>7</sup>. The plasma behaviour was described by using the 'two fluid' equations of motion, taken together with the equations of continuity of each species. These equations were considered in 'slab' geometry, in which the uniform magnetic field, B, was taken in the 'z' direction, the density gradient, ( $\frac{dn}{dr}$ ), was in the 'x' (radial) direction, and propagation was mainly in the 'y' (azimuthal) direction, with wavenumber  $k_y$ . Wave propagation oblique to the magnetic field was considered (wavenumbers  $k_x, k_z \ll k_y$ ), and density,  $n'$ , and potential perturbations,  $\phi'$ , of the form  $\exp-i(\omega t - \vec{k} \cdot \vec{r})$  were assumed. The electron velocity was eliminated between the linearised electron equation of motion, and equation of continuity to obtain a relationship for the electron density perturbation,  $n'_e$  :-

$$\frac{n'_e}{n_0} = \frac{[k_z^2 - i \beta k_y \kappa (1 - \beta k_x/k_y)]}{(k_z^2 D_e - i\omega)} \frac{e\phi'}{m_e} \quad \dots(1)$$

where  $\beta = \nu_e/\Omega_e$ ,  $\Omega_e = eB/mc$ ,  $\kappa = \frac{1}{n_0} \left(\frac{\partial n_0}{\partial r}\right)$  and  $D_e = T_e/m_e \nu_e$ .

Similarly, an expression may be obtained for the ion density perturbation,  $n'_i$ , in which ion temperature  $T_i$  is assumed to be small ( $T_i \ll T_e$ ).

$$\frac{n'_i}{n_0} = \left[ (i k_x \kappa - k_z^2)(\omega + i\nu_i)/\Omega_i - k_y \kappa \right] \frac{e\phi'}{M_i \Omega_i} \quad \dots(2)$$

where  $\Omega_i = eB/M_i$  and  $k_z^2 = (k_x^2 + k_y^2)$ .

If the condition of quasi-neutrality is assumed, then  $n'_e$ ,  $n'_i$  and  $\phi'$  can be eliminated between Eqs. (1) and (2), in the low frequency approximation to give the following dispersion relationship:-

$$\omega^2 + \omega [x\omega_g/(1+x^2) + i k_z^2 D_e + \nu_i + \omega_g/(1+x^2)] - k_z^2 D_e \nu_i + x\omega^*\omega_g/(1+x^2) + i\omega_g\omega^*/(1+x^2) = 0 \quad \dots(3)$$

where  $\omega^* = k_y c T_e/eB$ ,  $\omega_g = k_z^2 \Omega_e \Omega_i/k_z^2 \nu_e$  and  $x = \kappa k_x/k_z$ . This dispersion equation has been obtained in the approximations: (1)  $\omega \ll \Omega_i$ , (2)  $\nu_e \ll \Omega_e$  and (3)  $\nu_i \ll \Omega_i$  and these approximations are reasonably well satisfied experimentally. Eq. (3) can be solved numerically under the appropriate conditions for the  $R_e(\omega)$  and the growth rate  $\Upsilon = \text{Im}(\omega)$ , as a function of the variable parameters, magnetic field, axial wavenumber and neutral pressure.

#### Experiment and Results

The plasma was produced by an r.f. discharge between a plate and a grid at one end of the discharge tube (~ 5 cm diam.), and the plasma diffused through this grid into an electric field free region = 180 cm in length. Plasmas were formed in this way in both  $H_2$  and He gas, and were contained in a uniform axial magnetic field. Peak densities in the range  $10^8 - 10^{10} \text{ cm}^{-3}$  (depending upon r.f. power) were measured on a double probe and the density gradient was measured by traversing the double probe across a radius of the plasma and typical values of  $\kappa = 0.40 \text{ cm}^{-1}$  in  $H_2$  and  $\kappa = 0.70 \text{ cm}^{-1}$  in He were obtained. The electron temperature measured on the same probe gave values in the range 3-8 eV depending upon the neutral gas and r.f. power.

The floating potential of the plasma was measured on a high impedance digital voltmeter as a function of radius and was found to vary less than 1.0 mV across the radius. This, taken with variations in electron temperature  $T_e$  across the radius, gave a radial electric field,  $E_r = 0 \pm 0.01 \text{ V/cm}$ .



Consequently, any plasma rotation due to this field should be small and can be ignored.

The electron-neutral collision frequency was obtained by measuring the change in the 'Q' factor of a resonant microwave cavity coaxial with the glass discharge tube<sup>7</sup>. It has been shown<sup>8</sup> that  $\nu_e = (\pi f_0^2 / \Delta f) (1/Q - 1/Q_0)$ , where  $Q_0$  is the Q value of the empty cavity and Q its plasma loaded value,  $f_0$  the resonant frequency and  $\Delta f$  the change in frequency value with the plasma present. A cylindrical cavity operating in the  $TM_{010}$  mode was used on the outside of the glass tube and its 'Q' value change was measured as a function of neutral pressure 'p' in the discharge tube. A linear relationship between p and (1/Q) resulted, thus indicating that the electron-neutral collision frequency was the measured quantity. Values of

(a)  $\nu_e/p = (0.70 \pm 0.15) \times 10^9 \text{ (sec torr)}^{-1}$  for  $H_2$  plasma, and

(b)  $\nu_e/p = (0.80 \pm 0.15) \times 10^9 \text{ (sec torr)}^{-1}$  for He plasma

were obtained.

On simple hard-sphere kinetic theory considerations<sup>7</sup> values of the ion-neutral collision frequencies  $\nu_i$  were computed and gave

(a)  $\nu_i/p = (2.5 \pm 0.15) \times 10^7 \text{ (sec torr)}^{-1}$  for  $H_2$  plasma, and

(b)  $\nu_i/p = (2.0 \pm 0.15) \times 10^7 \text{ (sec torr)}^{-1}$  for He plasma.

The instability was observed on various floating and ion-biased probes distributed along and around the plasma column. The mode number of the wave was found by amplitude and phase measurements from probes around the azimuth. It was found to be mainly an  $m = +1$  propagating wave. A longitudinally moving single probe was used to measure the axial phase and amplitude, and in this way it was found to be a standing wave in the axial direction, with a wavelength of twice the tube length. By varying the tube length, at constant neutral pressure, and magnetic field length, the frequency variation was obtained. A typical dispersion relationship obtained in this way is shown in Fig 1(a) for He and (b) for  $H_2$ . Further results were obtained by varying

the magnetic field at constant neutral pressure and the tube length, and typical values are shown in Fig. 2(a) for He and (b) for H<sub>2</sub>.

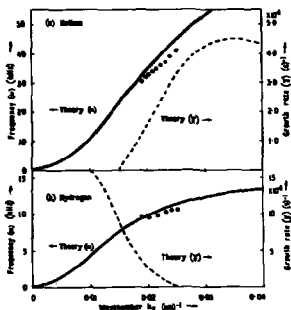


Fig. 1

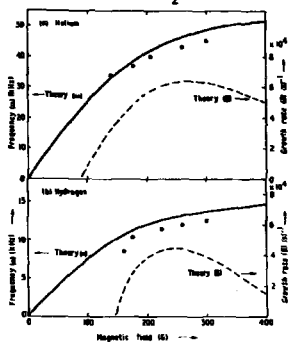


Fig. 2

Further results are shown in Figs. 3(a) for He and Fig. 4(a) for H<sub>2</sub> of the frequency as the neutral pressure is varied at a constant magnetic field and tube length.

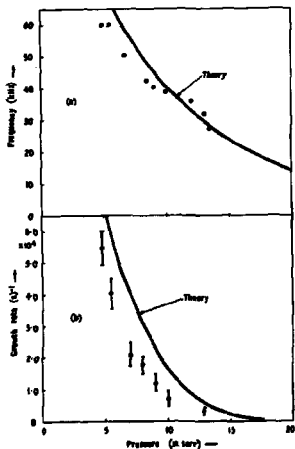


Fig. 3

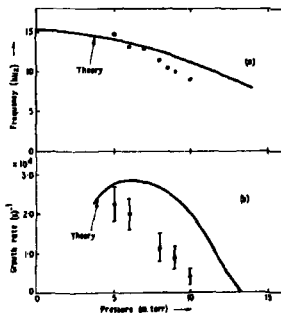


Fig. 4

The initial growth rate of the instability was directly measured by using a method of dynamic stabilisation<sup>5</sup> to suppress the instability or reduce it to a small amplitude. The instability was then allowed to recover to its large amplitude saturation level, and the resulting instability signal photographically stored. A typical signal obtained in this way is shown in Fig. 5. Analysis of photographs of this type enabled a measure of the initial growth rate to be obtained under different conditions. Plots of relative amplitude ( $a/a_0$ ) as a function of time are shown for the growing part of the signal in Fig. 6 at different neutral pressure values in helium for (a)  $p = 10$  mtorr, (b)  $p = 9$  mtorr and (c)  $p = 7$  mtorr.

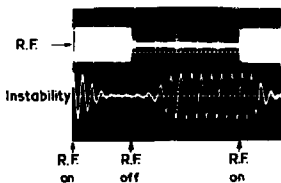


Fig. 5

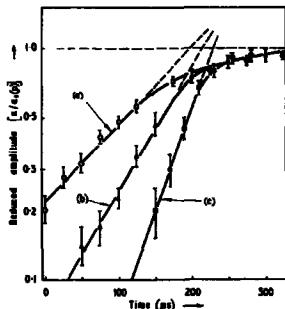


Fig. 6

The growth rates obtained in this way, as a function of neutral pressure are shown in Fig. 3(b) for He and in Fig. 4(b) for  $H_2^+$ .

#### Comparison and Conclusions

The theoretical variation of the frequency,  $\omega$ , and the growth rate,  $\gamma$ , for the drift dissipative instability as a function of the externally variable parameters tube length ( $\propto k_z$ ), magnetic field and neutral pressure can be computed from the dispersion relationship in Eq. (3). Values obtained from this equation for the parameter values appropriate to each particular case are shown marked in Figs. 1(a), 1(b), 2(a), 2(b), 3(a), 3(b), 4(a) and 4(b). In each case, the agreement between theory and experiment for the frequency, ' $\omega$ ' is good. In the case of the growth rate, the agreement is not so good. However,

In the theoretical calculation, the growth rate values are subject to much larger error than the real frequency ( $\text{Re}(w)$ ) values. In spite of this, the variation of  $\gamma$  with neutral pressures, Figs. 3(b) and 4(b), appears to be of the correct form.

In conclusion, experimental results have been obtained on the frequency and the growth rate of a low frequency instability in a continuous r.f. plasma in both helium and hydrogen plasmas, as a function of certain physical parameters ( $B$ ,  $p$  and  $k_z$ ). Comparison with the simple theory (in slab geometry) of the drift-dissipative instability shows reasonably good agreement and therefore it is inferred that the observed instability is, indeed, the drift-dissipative instability.

#### References

- 1 Hendel, H.W., Chu, T.K. and Politzer, P.A. (1968) Phys. Fluids 11, 2426.
- 2 Enriques, L., Levine, A.M. and Righetti, G.B. (1968) Plasma Phys. 10, 641.
- 3 Rowberg, R.E. and Wong, A.Y. (1970) Phys. Fluids 13, 661.
- 4 Aldridge, R.V. and Keen, B.E. (1970) Plasma Phys. 12, 1.
- 5 Alcock, M.W. and Keen, B.E. (1971) Phys. Rev. Letts. 26, 1426.
- 6 Timofeev, A.V.T. (1964) Sov. Phys. (Tech. Phys.) 9, 882.
- 7 Alcock, M.W. and Keen, B.E. (1971) Phys. Rev. (A) 3, 1087.
- 8 Buchsbaum, S.J. and Brown, S.C. (1957) Phys. Rev. 106, 196.

RESONANT CHARACTERISTICS OF COLLISIONLESS DRIFT-WAVES IN HYDROGEN  
PLASMA - COMPARISON BETWEEN EXPERIMENTAL RESULTS AND LINEAR THEORY

R. Beissier, P. Brossier, P. Deschamps, R. Gravier  
R. Pellat, C. Renaud,

**ASSOCIATION EURATOM-CEA**

Département de la Physique du Plasma et de la Fusion Contrôlée  
Centre d'Etudes Nucléaires  
Boîte Postale n° 6 - 92 Fontenay-aux-Roses (France)

ABSTRACT

Spontaneous collisionless drift-waves driven by a pressure gradient perpendicular to the confining magnetic field are observed in the low- $\beta$  plasma of the ODE device.

The experiment was designed specifically to study this instability, characterized by very long parallel wavelengths, which results from the resonant coupling between the wave and the electrons. A double ended device produce a 5.4 m long collisionless hydrogen plasma confined by a uniform magnetic field  $B_0 \approx 5$  kGs.

Detailed measurements of the unstable modes have been performed by correlation techniques using a 10 MHz bandwidth real time correlator. The experimental dispersion curves are compared with the computed solutions of the linear dispersion relation. The agreement between theoretical and experimental parallel wavelengths is better than a factor 2 when  $B_0$  increases from 1.5 to 3 kGs.

To change the reflecting conditions for resonant electrons two mirror coils have been located at each end of the column. The subsequent variation of  $\omega$  and  $\lambda_{||}$  for drift modes demonstrates the importance of end effects on the selection of the unstable parallel wavelengths.

## I - INTRODUCTION

Pressure gradient driven drift-waves have been identified in the collisionless hydrogen plasma of ODE device and detailed measurements have been reported recently [1]. They have shown that resonant drift-waves with parallel phase velocity close to the electron thermal velocity can grow spontaneously in a long enough plasma column. Those drift-instabilities propagate in the electron diamagnetic velocity direction; they are stationary in both the radial and parallel (to  $B_0$ ) directions, with a node of amplitude in the middle plane; parallel wavelengths are equal to or larger than the column length. This paper deals with a more detailed comparison of the experimental results with the linear theory, when the magnetic field and/or the reflecting conditions are modified.

## II - EXPERIMENTAL SET UP AND PLASMA PARAMETERS.

The ODE plasma column is created by two  $E_0 \times B_0$  discharges 8.8 m apart (fig.1). In the  $L = 5.4$  m long central chamber the collisionless hydrogen plasma has the following characteristics, on the axis:  $n_0 = 10^{10} \text{ cm}^{-3}$ ,  $T_e = 10-14 \text{ eV}$ ,  $T_i = 1 - 2 \text{ eV}$ , plasma diameter = 3 cm, base pressure =  $10^{-6}$  torr. Both  $n_0$  and  $T_e$  exhibit a radial Gaussian profile with  $\nabla n_0/n_0 \approx \nabla T_e/T_e \approx 1 \text{ cm}^{-1}$ .  $n_0$  varies less than 8% over the machine length. A radial inward electric field  $E_0$  induces a uniform rotation of the plasma column. The flute-like mode associated with this rotation has been described in ref. 1. Its frequency (40 to 50 kHz in the laboratory frame) represents the plasma rotation frequency and is used to correct the drift-mode frequencies for Doppler shift. Two coils located at each end of the main chamber can create two steep magnetic mirrors; the mirror ratio ( $R = 1.4$ ) allows the reflection of electron with  $v_{\parallel} / v_{\perp} < 0.6$ .

The wave characteristics are measured with continuously moving probes in the  $r, \theta, z$  directions. Measurement along the  $z$ -direction is performed by a probe moveable over 3 m at any radius, supplemented by 10 fixed probes which can be aligned on

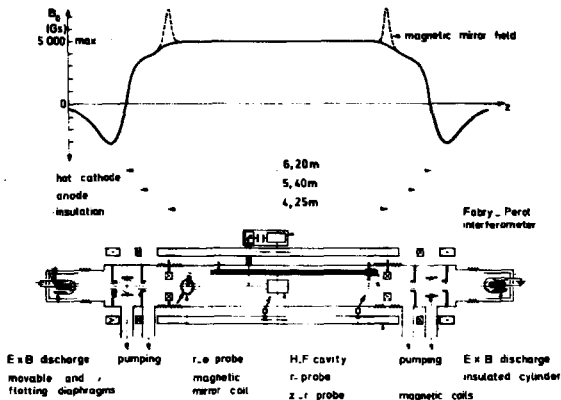


Fig.1. ODE DEVICE

the same line of force. A 10 MHz-200 channels real time correlator is used to measure the auto- and cross-correlation functions of probe signals. The Fourier transforms of these functions yield the power density of the density fluctuations as well as the azimuthal wave number  $m = k_y r$  versus the real part of the frequency  $f_R$  (here after called the "azimuthal dispersion relation") [2][6].

### III-EXPERIMENTAL RESULTS AND COMPARISON WITH THE LINEAR THEORY

The density fluctuations spectrum shows several peaks located in the density gradient and identified as collisionless drift instabilities. The wave characteristics (amplitude, frequency and wavelengths) have been measured for several values of  $B_0$ , from 1.35 kGs to 3 kGs. A typical result of correlation technique analysis is shown on fig. 2; on the lower part the density fluctuations spectrum  $n_1/n_0$  is plotted for  $B_0 = 2.5$  kGs; the upper part shows the azimuthal dispersion curves obtained for 3 values of  $B_0$ , as indicated. The real part of the frequency  $f_R$  and amplitude variations of density fluctuations  $n_1/n_0 \sim f$  each mode versus  $B_0$  are shown on fig. 3. The normalized perturbed potential  $\alpha\phi/kT_e$

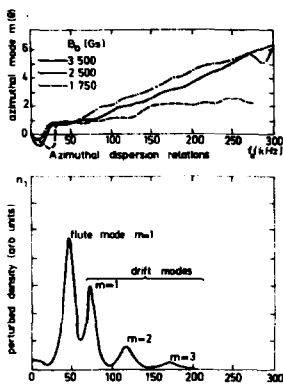


Fig.2. Density fluctuations spectrum. ( $B_0=2500$  Gauss) (kHz)

DENSITY FLUCTUATIONS SPECTRUM AND AZIMUTHAL DISPERSION RELATIONS OBTAINED BY CORRELATIONS TECHNIQUE ANALYSIS

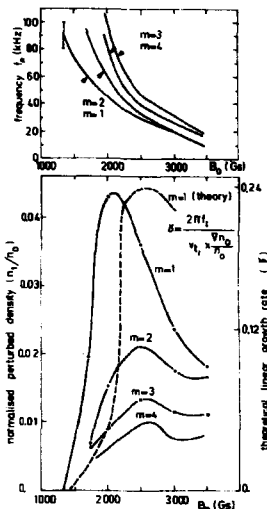


Fig.3. FREQUENCY AND DENSITY FLUCTUATIONS OF DRIFT MODES VERSUS MAGNETIC FIELD IN THE PLASMA REFERENCE SYSTEM.  $n_0 = 10^{18} \text{ cm}^{-3}$

shows the same behaviour as  $n_1/n_0$ ; at the maximum amplitude of the  $m=1$  mode  $e\phi/kT_e \sim 0.1$  and  $n_1/n_0 \sim 0.04$ .

The parallel amplitude measurements of the  $m=1$  mode are plotted on figure [4]. For lower values of  $B_0$  the amplitude vanishes in the middle of the column and is maximum near the ends. The parallel wavelength obtained from these data increase with  $B_0$ ; for  $B_0 \geq 3$  kGs,  $\lambda_{\parallel}$  is larger than twice the column length. The resonant character of the collisionless drift instability is emphasized by the values of the parallel phase velocity to electron thermal velocity ratio in the explored range of magnetic field:  $0.25 \leq v_{\parallel} / v_{the} \leq 0.55$ .

These results show the importance of the boundary conditions at the end of the column; in the zero-field region, some particles get reflected, but the efficiency of reflection for the resonant electrons is unknown and may vary with  $B_0$ , with subsequent effects on the parallel wavelengths quantification. In order to ensure the efficiency of the reflection process for reso-



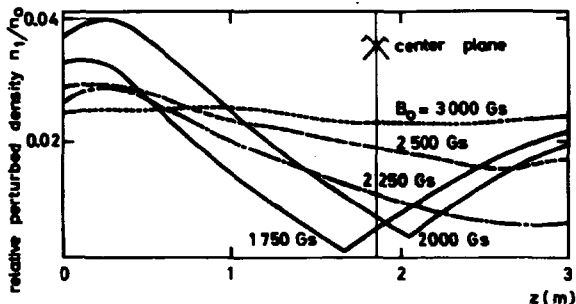


Fig. 4. AMPLITUDE OF THE  $m=1$  MODE IN  $z$  DIRECTION VERSUS MAGNETIC FIELD  $B_0$

ant electrons the two symmetric magnetic mirror coils have been used. Those trapped electrons can thus be coupled to the wave during a time long enough compared to the growth rate of the instability. The plasma density is adjusted to remain constant during the mirrors application, which does not perturb the equilibrium of the plasma column. The application of the mirror field has the expected effect of the parallel wavelengths (Fig. 6)

which are then quantified to the distance between the two mirrors. For  $B_0=2kGs$  the most unstable modes have the same wavelength. The density fluctuations spectrum changes with mirror field on (Fig. 5) and the unstable frequencies are shifted to slightly higher values. In any case the parallel phase velocity adjusts itself in such a way as to remain slightly smaller than the electron thermal velocity. A new  $m = 3$  mode appears which was marginally stable without mirrors. Increasing further the mirror ratio  $R$  has no further effect on the unstable frequencies but their amplitude decreases. These results are gathered in

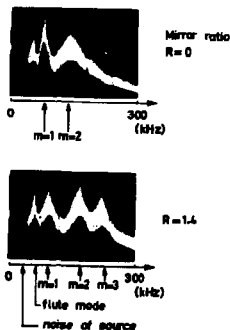


Fig. 5. EFFECT OF THE ELECTRONS MIRROR TRAPPING ON THE DRIFT WAVES SPECTRUM  
 $B_0=2250$  Gs,  $n_0=10^{10} \text{ cm}^{-3}$ ,  $T_e=100000^\circ K$

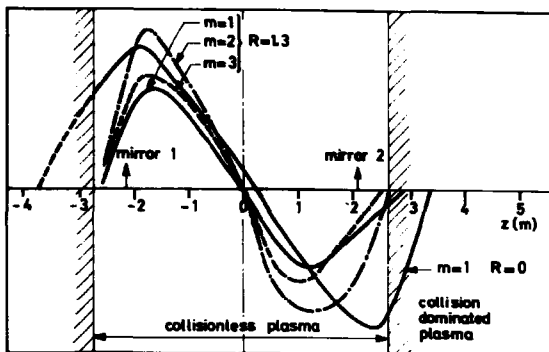


Fig.6.EFFECT OF MAGNETIC MIRRORS ON PARALLEL WAVELENGTHS OF DRIFT MODES. ( $B_0=2000$  Gs)

the Table I.

This table and the figure 7 give also a comparison of the measured parallel wavelengths with the solutions of the plane dispersion relation [3]. The experimental parameters (density, electron to ion temperature ratio, temperature gradient and radial wavenumber) have been introduced into the computation [4], which gives the instability growth rate  $\gamma = \frac{2\pi \times F_1}{0.15 \times \frac{V_{Te}}{V_e}}$  for each frequency and wave number ( $F_1$  is the imaginary part of the frequency) It should be noted that the electron temperature

|                             |                          | Mirror ratio | m=1     | m=2    | m=3   | Observations                                      |
|-----------------------------|--------------------------|--------------|---------|--------|-------|---|
| linear theory- (slab model) | $\lambda_{\parallel}(m)$ |              | 12 - 14 | 6 - 10 | 5 - 9 | $T_e/T_i = 5$<br>$\frac{V_{Te}/V_e}{n_0/V_e} = 1$ |
| EXPERIMENT                  | $\lambda_{\parallel}(m)$ | R=0          | 8 - 9   | 8 - 9  |       |   |
|                             | $\lambda_{\parallel}(m)$ | R=1.3        | 5 - 6   | 5 - 6  | 5 - 6 |   |
|                             | $V_e/v_{Te}$             | R=0          | 0.23    | 0.30   |       |   |
|                             | $V_e/v_{Te}$             | R=1.3        | 0.20    | 0.25   | 0.30  |   |

TABLE.1. INFLUENCE OF MAGNETIC MIRRORS ON RESONANT DRIFT WAVES  $B_0 = 2000$  Gs

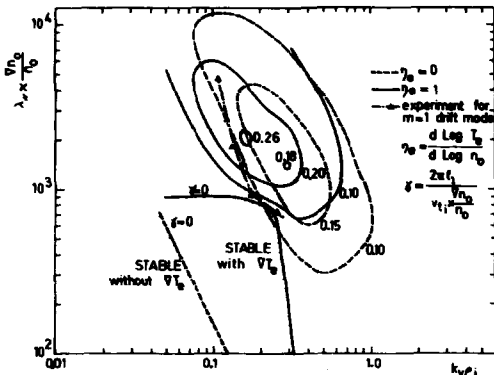


Fig. 7. MAP OF CONSTANT LINEAR GROW RATE  $\gamma$  FOR  $T_e/T_i=5$ ,  $k_x/k_y=1.4$   
INFLUENCE OF  $\nabla T_e$  AND EXPERIMENTAL RESULTS FOR  $m=1$  DRIFT MODE

gradient has a strong stabilizing effect in the large transverse wavelengths ( $k_y \rho_i \lesssim 0.3$ ) but modifies only slightly the maximum growth rate of the instability. At lower values of  $B_0$ , the experimental points sit near the marginal stability curve. When

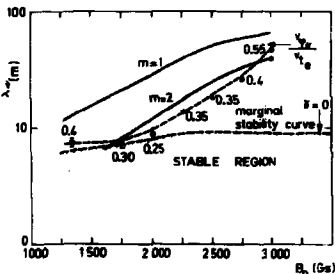


Fig. 8. PARALLEL WAVELENGTHS AND PHASE VELOCITIES OF DRIFT WAVES

--- Measured for  $m=1$   
 — Linear theory (slab model) deduced from the real values of measured frequencies with experimental parameters:  $T_e/T_i=5$

$$\gamma_e = \frac{d \text{Log } T_e}{d \text{Log } n_0} = 1$$

$$\nu_0/\nu_0 = 1 \text{ cm}^{-1}$$

$B_0$  increases the measured frequency and wavenumber are such that the growth rate approaches its maximum value. We also note that the variations of the calculated values of  $\gamma$  and of the measured values of  $\frac{\nu_{\parallel}}{\nu_0}$  are similar for the  $m=1$  mode (fig. 3)

The measured and computed parallel wavelengths are plotted on fig. 8, for the  $m=1$  and  $m=2$  modes. The agreement between the experimental results and the theory is better for the  $m=2$  mode than for the  $m=1$  mode, as it could be expected from the use of a plane-slab model. As indicated on fig. 8,

the measured values of  $\sqrt{v_{\phi}}/\sqrt{v_{thm}}$  show that the parallel phase velocity is lower than but near the electron thermal velocity.

#### IV - CONCLUSIONS

The values of the different ratios  $m_e/m_i$ ,  $T_e/T_i$  and  $L(\nabla n_e/n_e)$  in the ODE plasma are more favorable to the spontaneous onset of collisionless drift instabilities than the corresponding parameters which can be obtained in alkali plasma [5]. Indeed the hydrogen plasma permits the study of drift-waves with maximum growth rate for wavelengths equal to the device length. The linear theory of collisionless drift instabilities in the resonant region where  $\sqrt{v_{\phi}} \lesssim \sqrt{v_{thm}}$  has been checked by the experimental results. The importance of the parallel wavelengths measurements for accurate check of the theoretical model has been shown. The magnetic mirrors change the wavelengths it is possible to observe in the experimental set-up. Their effect emphasizes the coupling between the electrons and the wave, although it has not been proved that the trapped particles are responsible for the wave growth.

It is a pleasure to thank M. P. Blanc and M. M. Occhionorelli for help in calculations and experimentation.

#### REFERENCES

- [1] P. Brossier, P. Deschamps, R. Gravier, R. Pellat, C. Renaud Phys. Rev. Letters, 26, 124, 1971.
- [2] M. Bernard, G. Briffod, R. Frank, M. Gregoire and J. Weisse in Proc. Third Int. Conf. Plasma Physics and Cont. Nucl. Fusion Novosibirsk, USSR 1968, Vol. 1 p. 715.
- [3] L.V. Mikhailovskaya and A.B. MikhaYlovskii, Sov. Phys. Techn Phys., 8, 896, 1964.  
W.A. Krall and M.W. Rosenbluth, Phys. Fluids, 8, 1488, 1965.
- [4] P. Brossier, Report EUR-CEA 565, 1970
- [5] P.A. Politzer, Bull. Amer. Phys. Soc. 13; 1547, 1968 and 14, 1055, 1969.  
P.E. Stott, P.F. Little and J. Burt, in Proc. Int. Conf. Quiescent Plasmas, Paris, 1968.
- [6] R. Beissier, Thesis Report EUR-CEA in print.

Experimental Measurement of Drift Waves in  
a Strongly Sheared Magnetic Field

by

P. E. Stott and J. Burt

UKAEA Research Group, Culham Laboratory, Abingdon, Berkshire, U.K.

Abstract

Collisionless drift waves have been studied in a column of thermally ionized lithium plasma with a variable shear magnetic field. When the shear is zero or weak, the drift waves are unstable and have typical peak amplitudes  $\bar{n}/n_0 \sim 0.1$ . The measured cross-field diffusion coefficient is comparable to  $D_{\text{Bohm}}$  and is approximately three orders of magnitude larger than the value calculated for classical collisional diffusion. As the shear is increased in magnitude the drift waves are stabilized and the diffusion coefficient is reduced by two orders of magnitude.

Introduction

The stability of a low- $\beta$ , magnetically confined plasma may be seriously weakened by drift waves. These are fundamental modes of plasma oscillation which are driven unstable by a spatial inhomogeneity of the plasma density or temperature. These modes are therefore expected to persist in confinement systems from which all other mechanisms which support instabilities have been eliminated. The drift waves are manifest as low frequency oscillations of the plasma density and potential, and lead to plasma losses across the confining magnetic field at a rate comparable to that given empirically by Bohm.

According to linear theory, the growth of drift waves in a collisionless plasma is due to a resonant particle interaction with the electrons, whereas the ions provide a damping mechanism. The ion damping is however usually insufficient to ensure complete stability except for modes with very short parallel wavelengths.

The most promising method of stabilizing drift waves in a fusion plasma appears to be by means of strong magnetic shear. This requires the confining magnetic field to be strongly twisted in a way so that the pitch angle increases as one moves outwards from the plasma centre. Such a field configuration is produced by the helical multipolar winding of a stellarator confinement system. The drift waves should be stabilized if the shear is sufficiently strong, as was demonstrated for the collisional drift instability by Chen<sup>1</sup>.

We have investigated the stabilization of collisionless drift waves in a stellarator field geometry. The stabilizing shear was produced by an  $l=3$  helical multipolar winding surrounding the plasma column. A straight system was chosen for these experiments since in a toroidal device it would not be possible to vary the shear over a wide range of values without disturbing the basic toroidal equilibrium.

#### Experimental Details

The essential features of the experimental apparatus (STAMP) are shown in Fig.1. Lithium or sodium plasmas are produced by thermally ionizing a beam of neutral atoms directed onto a rhenium plate (diameter 7.5 cm) heated to over 2000°K. The basic principles of such a Q-machine are well known and the detailed design of the sources used on STAMP has been reported previously<sup>2</sup>. Two identical sources which can be moved axially produce a plasma whose length may be varied between 40 and 400 cm. The axial magnetic field is variable up to 4000 G and at that field lithium ions have a Larmor radius of 0.3 mm. The periodicity of the  $l=3$  helical winding is 80 cm and the maximum current is 48,000 A.

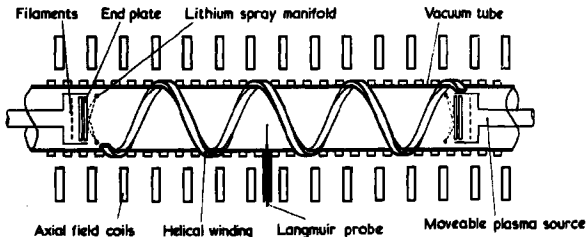


Fig.1

Schematic of the STAMP experiment. For clarity, only one of the six helical conductors is indicated

Computations of the helical magnetic fields are in good agreement with measurements using an electron beam to trace out field lines onto a fluorescent screen. The magnetic field lines lie on a nested set of trefoil shaped cylinders. The rotational transform  $\frac{1}{2}$  has a nearly parabolic radial dependence and at the separatrix the transform per winding period is  $2\pi$ . It is convenient to express the magnetic shear in terms of the shear length

$$L_s = [(1/80)r \, dt/dr]^{-1}$$

which varies roughly as the inverse square of the radius and is about 7 cm at the separatrix.

Matching the trefoil shaped magnetic surfaces onto the circular endplates presents a difficult problem since there are no magnetic circularisers. In order to avoid complicated  $\underline{E} \times \underline{B}$  drifts in the plasma the equipotentials of the endplate sheaths must be made coincident with the magnetic trefoils. This is particularly important for unambiguous measurements of diffusion losses due to drift waves. The end plate temperature has been made uniform to within 1°K by using a double plate construction heated by a rotating spiral filament<sup>3</sup>. The profile of the neutral lithium spray is more difficult to control and a system which involves spraying the lithium through small holes in the endplate itself is being developed.

#### Drift Wave Stabilization

The plasma density profile  $n_0(r)$  and the density fluctuation amplitude  $\tilde{n}_1(r)$  were measured with single spherical Langmuir probes biased to collect ion saturation current (Fig.2). The same probes were used with a high impedance 'boot strap' amplifier to

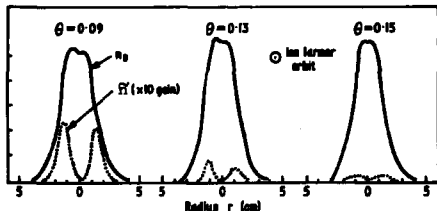


Fig.2  
Profiles of density  $n_0$  and fluctuation amplitude  $\tilde{n}_1$  for various values of the shear  $\theta = \Delta/L_s$

measure the potential fluctuations  $\phi_1(r)$ . The peak relative amplitude of the density and potential oscillations occurred close to the steepest part of the density gradient and  $\tilde{n}/n_0 = e\tilde{\phi}/kT_e \leq 20\%$ . Similar oscillations had been identified previously as collisionless drift waves<sup>3</sup>. Collisions of electrons with ions ( $\lambda_{ei} \approx 10^3$  cm) or with neutrals ( $\lambda_{en} \gg 10^3$  cm for a typical base pressure of  $10^{-7}$  torr) were too infrequent in this plasma to generate collisional

drift waves. Clearly defined azimuthal modes were identified with mode numbers  $m$  in good agreement with the fastest growing modes predicted by linear theory, i.e.  $k_{\perp} \rho_i = m \rho_i / r = 1$ . For the stabilization experiments, the plasma radius and magnetic field were increased so that  $\rho_i / r \ll 1$  and the frequency spectrum of the instability revealed a mixture of many modes with large values of  $m$ .

Several theoretical estimates of the critical shear needed to stabilize the collisionless drift waves have been published. Krall and Rosenbluth<sup>4</sup> considered a slab model with a localized density gradient producing a potential well which was examined for stability of the normal modes. The stability criterion

$$\theta = \kappa / L_B \geq (1/2) \rho_i / \Delta$$

was obtained. With increasing shear the radial extent of the region of instability may shrink to such a small extent that these normal modes are not localized. Rutherford and Frieman<sup>5</sup> considered a wave packet of the normal modes which grew initially as a local perturbation before convecting into a stable region where it was ultimately damped. Since the critical amplitude of such a wave packet was undefined, the choice of stability criterion was somewhat arbitrary but to restrict the growth to a single e-folding factor required  $\theta \geq (m_e / m_i)^{1/2}$ . A more recent analysis by Pearlstein and Berk<sup>6</sup> has shown that normal modes may occur even in the limit of high shear  $\theta \geq (1/2) \rho_i / \Delta$  and these modes are stable only if  $\theta \geq (m_e / m_i)^{1/2}$ .

Experimentally as the shear was increased, the relative amplitude  $\tilde{n}/n_0$  fell and became effectively zero for  $\theta \geq 0.15$  (Fig.3).

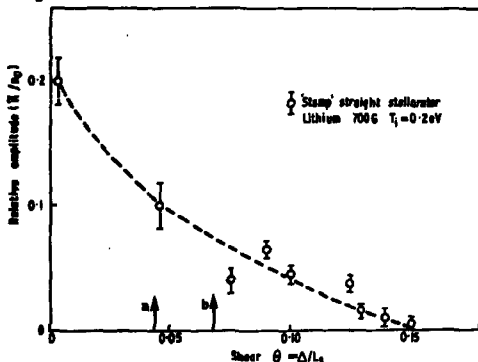


Fig.3

Variation of the instability amplitude  $\tilde{n}/n_0$  with  $\theta$ . The theoretical stability criteria are indicated by arrows. (a)  $\theta > (m_e / m_i)^{1/2}$ ; (b)  $\theta > (\rho_i / \Delta)$



This value exceeds the theoretical estimate of Krall and Rosenbluth by a factor of 2, which is surprisingly close agreement in view of the theoretical approximation. The theory assumed a slab model with uniform shear whilst the experiment was cylindrical and the shear was non-uniform both radially and azimuthally. In addition the linear growth rate of the drift waves may have been enhanced due to finite length effects. The experimental results were all in the regime  $(1/2/2)\rho_i/k > (m_e/m_i)^{1/2}$ , and the wave packet regime was not tested. Machine developments are in hand to extend the range of measurements.

### Diffusion Measurements

The most important manifestation of the drift instability is the effect on the plasma containment. The radial particle flux transported by the wave is:  $j_r = (1/rB) \partial(\tilde{n}\tilde{\phi})/\partial\psi$  where the correlation function  $\langle \tilde{n}\tilde{\phi} \rangle$  was measured using two probes as a function of the azimuthal angle  $\psi$ . An outwardly directed plasma flux was measured with a maximum close to the radius where  $K$  was a minimum. Good agreement was obtained with the total flux measured on a particle collector surrounding the outside of the column. The collected flux fell sharply when the shear was increased. In a uniform field, (i.e.  $\theta=0$ ) the radial diffusion coefficient  $D_{\perp}$  was nearly inversely proportional to the field strength  $B_z$  and was of the order of  $D_{Bohm} = ckT_e/16 eB$ . This was roughly two orders of magnitude larger than the diffusion coefficient for binary collisions. An accurate calculation of  $D_{\perp}$  in the sheared field was complicated by the presence of convective cells in this particular instance, but values calculated from the mean density gradient showed a clear improvement as  $\theta$  was increased (Fig.4).

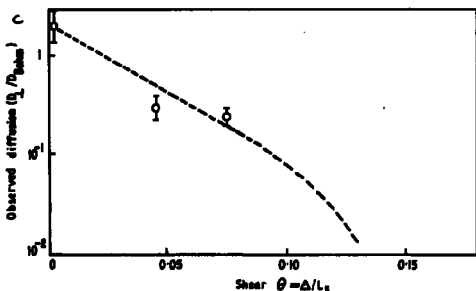


Fig. 4

Variation of the normalized diffusion coefficient  $D_{\perp}/D_{Bohm}$  with shear. The broken line is taken from probe measurements of  $\langle \tilde{n}\tilde{\phi} \rangle$ . The points indicate independent measurements with a particle collector surrounding the plasma

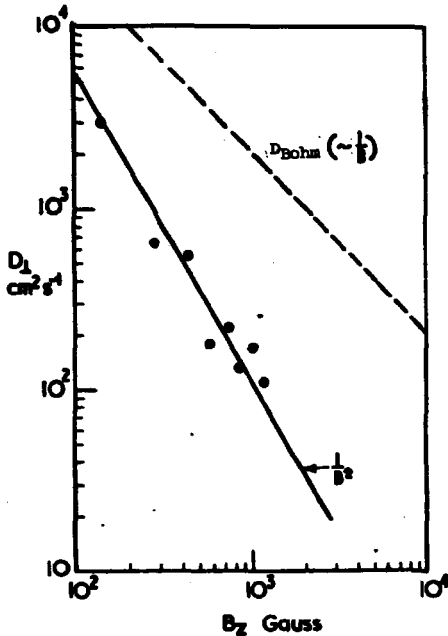


Fig.5  
Variation of  $D_1$  with magnetic field  $B_z$  at constant  $l$  and separatrix radius in a partially stabilized plasma

The particle collector surrounding the column was used to measure  $D_1$  as a function of the main magnetic field  $B_z$  in a partly stabilized plasma. The rotational transform  $l$  and separatrix radius were kept constant by corresponding changes in the helical winding current. The results plotted in Fig.5 show that  $D_1 \sim B^{-2}$ . The maximum value of  $\delta \sim 0.07$  and the amplitude of the drift waves was typically  $\delta/n_0 \sim 0.04$ .

### Conclusions

Strong magnetic shear has been shown to be effective in stabilizing collisionless drift waves. All modes appeared to be suppressed for values of shear not too much in excess of theoretically estimated values. Stabilization of the drift waves was accompanied by a reduction in the cross field diffusion coefficient  $D_{\perp}$  of about two orders of magnitude. In a partly stabilized plasma  $D_{\perp} \sim B^{-2}$  was measured.

### Acknowledgements

It is a pleasure to acknowledge stimulating discussions concerning the diffusion flux measurements with Dr K. Young and the excellent technical support of G. Gigy, R. Dyer and I. Hammond.

### References

- 1 P.F. Chen, Int. Conf. on Physics of Quiescent Plasmas, Frascati, (1967)
- 2 J. Burt, P.F. Little, and P.E. Stott, Plasma Phys., 11, 789, (1969); also Culham Laboratory Report CLM-R 98  
J. Burt and P.E. Stott. Culham Laboratory Report CLM-R 110
- 3 P.E. Stott, P.F. Little and J. Burt., In Proc. of the 3rd European Conf. on Controlled Fusion and Plasma Physics, Utrecht, The Netherlands, June, 1969, Wolters-Noordhoff Publishing, Groningen, The Netherlands, (1969)
- 4 N.A. Krall and N.M. Rosenbluth, Phys. Fluids, 8, (1965) 1488
- 5 P.H. Rutherford and E.A. Frieman, Phys. Fluids, 10, (1967) 1007
- 6 L.D. Pearlstein, and H.L. Berk, Phys. Rev. Letters, 23, (1969) 220

HIGH FREQUENCY FLUCTUATIONS IN THE DENSITY GRADIENT  
OF AN ALCALI PLASMA.

P. Brossier, P. Deschamps, R. Gravier, C. Renaud.

**ASSOCIATION EURATOM-CEA**  
Département de la Physique du Plasma et de la Fusion Contrôlée  
Centre d'Etudes Nucléaires  
Boîte Postale n° 6 - 92 Fontenay-aux-Roses (France)

ABSTRACT

A study has been made of the drift wave modes present in the EPAL Q-machine. This double ended device produces a potassium plasma with density variable from  $10^8$  up to  $10^{10}\text{cm}^{-3}$ , length of 200 cm, magnetic field up to 10 000 gauss and temperature (of end plates) of  $2200^\circ\text{K}$ . Measurements have been made on azimuthal modes of  $m = 1$  up to  $m = 10$ , which are seen to be localized in the density gradient where the electric field is weak. The spectrum can be monochromatic and the higher modes can be above the ion cyclotron frequency. Evolution of this spectrum into a turbulent spectrum (amplitude  $\propto \omega^2$ ) is obtained by increasing the magnetic field.

The results reported here have been obtained on the EPAL Q-machine at low density, weak magnetic field for which unstable drift waves localized in the density gradient have been observed.

The 2 m long plasma column is formed by contact ionization of potassium beam on two hot plate assemblies (in a homogeneous magnetic field B). Each hot plate, 10 cm O.D., has a thicker central part of 5 cm O.D. onto which the plasma is formed. The temperature at the center reaches  $2200^\circ\text{K}$ , decreases about 5 %

across the central disk and then drops sharply to  $\sim 1000$  \*K at the outer edge.

Profiles of plasma density and floating potential are displayed on Fig. 1 along with low frequency density fluctuations. This shows that the noise associated with the density gradient is rather well separated from the region where a

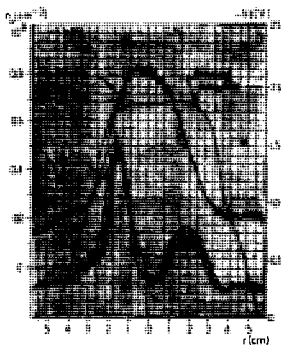


FIG. 1. PROFILES OF FLOATING POTENTIAL DENSITY AND FLUCTUATING DENSITY  $n_e$ , 7700°K 520Gs

a large inward electric field is present. The evolution of the noise spectrum with the magnetic field is shown on fig. 2 for a density in the range  $5-10 \times 10^8 \text{cm}^{-3}$  for mean free path shorter than the machine length. The individual peaks have been identified as  $m = 1, 2$  and 3 azimuthal modes propagating in the direction of the electron diamagnetic drift.

As the field increases one observes, in addition to a frequency shift proportional to  $B^{-1/2}$ , that highest modes are more easily excited. At 800 gauss, the amplitude of  $m = 2$  passes that of the  $m = 1$  mode which is larger at

600 gauss. As the field increases further to 1500 gauss the peaks merge into a turbulent spectrum with a maximum of amplitude around the  $m = 2$  frequency. This behaviour is expected from the linear theory of collisional drift waves in the high field regime, i.e. when the magnetic field is higher than the maximum growth rate field. In this range an increase in magnetic field destabilizes successively increasing azimuthal mode numbers with successively larger linear growth rate, at about the same frequency [1]. The amplitude does not follow the linear growth rate but decays roughly as  $r^2$ . On the other hand in the lower magnetic field regime, the waves are stabilized through the ion viscosity whenever the parameter  $b V_i / E V_{Ti}$  is large enough ( $b = \frac{1}{2} (\kappa_1 \alpha_i)^2$ ,  $\alpha_i$  ion larmor radius,  $E = \frac{1}{n} \frac{dn}{dr}$ ,  $V_i$  ion collision frequency,  $V_{Ti}$  ion thermal velocity). An increase in density will have the same

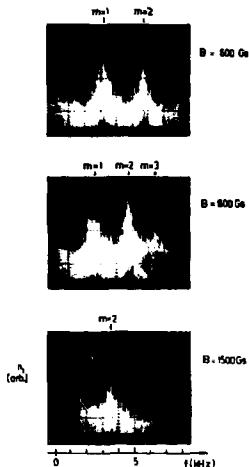


FIG. 2. EVOLUTION OF THE INSTABILITY SPECTRUM FOR HIGH MAGNETIC FIELD

connected to two probes either azimuthally or longitudinally separated. Longitudinal measurement indicate in any case that the parallel wavelength is larger than twice the machine length with a standing wave structure. Frequency spectrum and azimuthal mode measurements show that higher mode numbers appear out of the noise level as the field is decreased. They all are harmonic of a fundamental frequency (4.5 kHz) slightly lower than the  $m = 1$  mode frequency 4.7 kHz. In the laboratory frame the frequencies vary proportional to  $B^{-1/2}$  and can be higher than the ion cyclotron frequency  $f_{ci}$  for higher modes at low frequency.

Azimuthal mode number can

stabilizing effect as decreasing  $B$ . Observations in this density and magnetic field regime, and comparison with the collisional theory have been reported in [2].

For low density plasmas, the value of  $b$  above which stability should be recovered can get so large that the theory, derived in the limit  $b \ll 1$ , no longer holds. At  $n_e \approx 10^8 \text{ cm}^{-3}$ , for mean free path longer than the machine length and for magnetic field down to a few hundred gauss, results are indicated on fig. 3 where the frequency (in the laboratory frame) and mode information is obtained by Fourier analyzing the cross correlation output of a 10 MHz correlator connected to two probes either azimuthally or longitudinally separated.

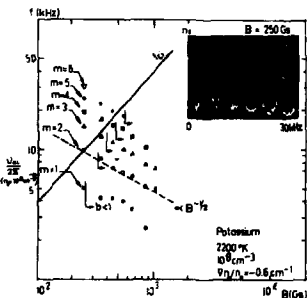
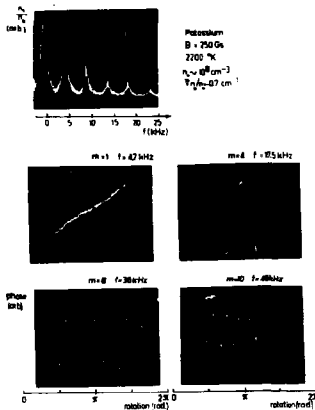


FIG. 3. MAGNETIC FIELD DEPENDENCE OF THE FREQUENCIES AND MODES OF THE DRIFT INSTABILITY

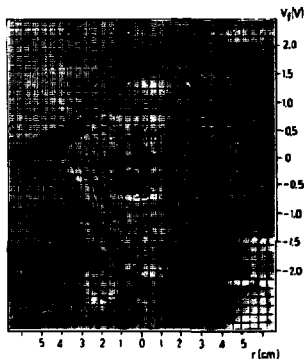


..FIG. 4. IDENTIFICATION OF AZIMUTHAL MODES.

also be measured by a lock-in phase detector connected to a probe continuously movable in the azimuthal direction. Recordings of the phase signal  $\Psi$  (in the range  $-\pi/2, +\pi/2$  with the sign of  $\sin \Psi$ ) plotted against the probe rotation are displayed on fig.4 for 250 gauss. All azimuthal modes up to 6 identified with the correlator technique can be recovered. For higher order harmonics, when no peak can be singled out of the noise, the phase measurements indicate that even higher mode structure is present in the fluctuations. Thus, for 250 gauss, up to  $m=10$  at 46 kHz, has been demonstrated, along with a rapid decrease of

the amplitude of successive modes as  $m^{-2}$ .

In order to correct the measured frequencies for the Doppler shift due to the inward electric field, an attempt has been made to modify externally the radial electric field. The plasma sources were biased positively with respect to the chamber wall, changes in the plasma potential were observed. The resulting modification of the floating potential profile when the bias voltage varies from 0 to 4 volts is shown on fig. 5. The outer profile is affected first. At 4 volts the inner profile is essentially flat whereas



..FIG.5. FLOATING POTENTIAL PROFILES AS A FUNCTION OF THE BIAS VOLTAGE.

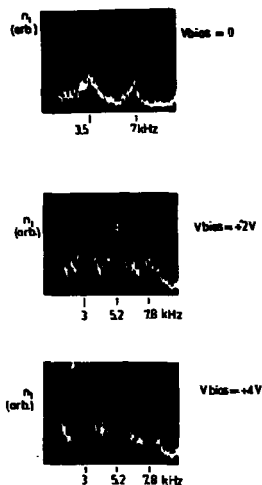


FIG. 6. FREQUENCY AND AMPLITUDE DEPENDANCE ON THE RADIAL ELECTRIC FIELD. POTASSIUM 2200°K,  $10^{18} \text{cm}^{-3}$  50 Gs.

the electron mean free path is of the order or longer than the machine length, has been investigated and results are shown on fig. 7. The unstable frequencies are slightly shifted towards the origin as the density increases. This is the same as computed for collisional drift wave in the  $B > B(\gamma_{\text{max}})$  regime for  $b < 1$  and short mean free path, which is not the case here. Conversely collisionless drift wave should be insensitive to density change (when the affect of Debye length is negligib..), A possibility is that electrons are trapped

the outer profile is almost symmetric to the no-bias case with respect to the  $V = 0$  axis. The density and fluctuations radial profiles are unaffected. The change in the fluctuation spectrum for 0, 2 and 4 bias voltages is shown on fig. 6 at 510 gauss. Although little change is observed after the bias voltage reaches 2 volts, the total frequency shift from zero to 4 volts when the floating potential profile reverses is  $\sim 0.5$  kHz per mode. Should this quantity scale as  $1/B$  this shift is not enough to bring the higher mode frequencies below  $f_{ci}$ ; for the low field measurement as seen from fig. 3.

Influence of the density on the instability spectrum when

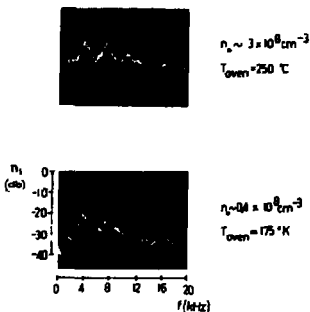


FIG. 7. INFLUENCE OF THE DENSITY ON THE FREQUENCY OF LOWER MODES. POTASSIUM 2300°K 50 Gs.



between the sheaths at the hot plate, long enough to experience collisions. This result suggests that even for a Q-machine shorter than the mean free path destabilization of drift wave occurs through particle collisions rather than through particle wave interaction as would be the case in a collisionless plasma.

From these observations we conclude that the collisional drift instability can be carried over to a regime characterized by large ion orbit and long mean free path (compared to the machine length) high azimuthal mode numbers are present in the fluctuations. External modification of the radial electric field into the plasma, yields an upper limit for the Doppler shift. The observed frequencies can be higher than the ion cyclotron frequency in the plasma frame.

It is a pleasure to thank Mr. R. Boissier for his help in correlation measurements and Mr. A. Bouron for his technical assistance.

#### REFERENCES

- [1] P. Brossier, P. Deschamps, R. Gravier, R. Pellat, C. Renaud, This conference, Numerical investigation ... of collisional drift waves.
- [2] H.W. Hendel, T.K. Chu, P.A. Politzer, Phys. Fluids, II, 2426 (1968).

Interpretation of Dispersion Relations for Bounded Systems

by

T. D. Rogulien and S. A. Self

Institute for Plasma Research, Stanford University  
Stanford, California

Abstract

A treatment is given of the problem of constructing normal modes for an arbitrarily bounded system from roots of the linear dispersion relation  $D(\omega, \underline{k}) = 0$  for the corresponding infinite or periodically bounded system. The implications of the results for the interpretation of experiments on plasma waves and instabilities on finite cylinders is discussed, with particular reference to the effects of end-plate damping on collisional drift waves in Q-machines.

Introduction

Linear perturbation analyses of plasmas are commonly performed as an initial value problem for an infinite (unbounded) or periodically bounded system. For perturbations  $\propto \exp i(\omega t - \underline{k} \cdot \underline{r})$ , waves and instabilities are categorized in terms of the roots of the dispersion relation  $D(\omega, \underline{k}) = 0$  with complex  $\omega$  and real  $\underline{k}$ . In interpreting such theories for experimental systems, which are necessarily bounded (though not in general periodically), it is often assumed that the system must be described in terms of such roots with real  $\underline{k}$ , without enquiring properly into the effect of boundaries.

In this paper we give a prescription for constructing normal mode solutions for a certain class of bounded systems from the roots of  $D(\omega, \underline{k}) = 0$  for the corresponding infinite system. The boundaries are characterized by complex reflection coefficients for the dominant wave roots  $\underline{k}(\omega)$  of  $D = 0$ , where in general both  $\underline{k}$  and  $\omega$  are complex. The treatment is restricted to fluid-type analyses for systems of general cylindrical form. The theory is

applied to the interpretation of collisional drift waves in Q-machines to take account of the effects of end-plate damping. A more detailed account of this work is given in an unpublished report.<sup>1</sup>

### Theory

Consider a system of general cylindrical form, uniform along  $x$  between boundaries  $x_1, x_2$  ( $x_1 < x_2$ ). A linear perturbation analysis by Fourier (space) - Laplace (time) transformation of the corresponding unbounded problem is assumed to yield a dispersion relation  $D(\omega, k) = 0$  for perturbations  $\propto \exp i(\omega t - kx)$  for a given transverse eigenmode ( $k_{\perp}$  fixed). Initially, for simplicity, we assume  $D$  is quadratic in  $k$ , and that the two roots  $k^{\pm}(\omega)$  correspond to waves excited by a source of frequency  $\omega = \omega_r + i\omega_i$  on the positive ( $k^+$ ) and negative ( $k^-$ ) sides. Following Briggs<sup>2</sup> the roots are identified by the requirement  $k_1^- > 0$  and  $k_1^+ < 0$  as  $\omega_i \rightarrow -\infty$ .

The solution to the bounded problem, for any wave variable  $\psi$  is then written

$$\psi = \psi^+ + \psi^- = \psi^+ \exp i(\omega t - k^+ x) + \psi^- \exp i(\omega t - k^- x), \quad (1)$$

where the complex amplitudes are written  $\psi^{\pm} = |\psi^{\pm}| \exp i\theta^{\pm}$ . The wave  $\psi^+$  is regarded as excited at  $x_1$  by reflection of the wave  $\psi^-$  and, likewise,  $\psi^-$  is excited at  $x_2$  by reflection of  $\psi^+$ .

We define the (time-independent) complex reflection coefficients  $\rho_1, \rho_2$  as the ratios of the amplitudes of the reflected to incident waves:

$$\rho_1 \equiv |\rho_1| \exp \pm i\theta_1 \equiv \frac{\psi^+(x_1)}{\psi^-(x_1)} = \frac{|\psi^+|}{|\psi^-|} \exp i[-(k^+ - k^-)x_1 + (\theta^+ - \theta^-)], \quad (2a)$$

$$\rho_2 \equiv |\rho_2| \exp \pm i\theta_2 \equiv \frac{\psi^-(x_2)}{\psi^+(x_2)} = \frac{|\psi^-|}{|\psi^+|} \exp i[(k^+ - k^-)x_2 - (\theta^+ - \theta^-)], \quad (2b)$$

where  $0 \leq |\rho_{1,2}| \leq 1$  and  $-\pi < \theta_{1,2} \leq \pi$ .

Here we have assumed that the phase of the reflected wave is given, either from physical arguments or by experiment, as leading or lagging the incident wave by a certain angle  $|\theta|$ , and adopt the convention that  $\theta > 0$  when the reflected wave leads and  $\theta < 0$  when it lags. In order to preserve this convention, irrespective of the sign of  $\omega_r$ , the alternate signs are introduced in Eqs. (2), and should be taken as + or - according as  $\omega_r \gtrless 0$ .

Elimination of  $\psi^+/\psi^-$  between Eqs. (2) yields

$$(k^+ - k^-)L = [2n\pi \pm (\theta_1 + \theta_2)] - i[\log|\rho_1| |\rho_2|], \quad (3)$$

where  $L = (x_2 - x_1)$  is the system length,  $n = 0, \pm 1, \pm 2$  etc., and the

term  $(\theta_1 + \theta_2)$  takes the same sign as  $\omega_r$ . Thus specifying the reflection coefficients  $\rho_1, \rho_2$  together with the system length quantizes the difference between the roots  $k^+(\omega), k^-(\omega)$  of the infinite dispersion relation to a discrete set of (generally complex) values. The physical content of Eq. (3) is just that the total phase shift around the loop must be an integral multiple of  $2\pi$ , and that the loop gain must be unity.

The (complex) frequencies  $\omega_n$  of these axial eigenmodes must satisfy both Eq. (3) and the infinite system dispersion relation. Writing the latter in the form

$$a(\omega)k^2 + b(\omega)k + c(\omega) = 0 \quad (4)$$

$$\text{we have } (k^+ - k^-) = \pm [b^2(\omega) - 4a(\omega)c(\omega)]^{1/2}/a(\omega). \quad (5)$$

The frequencies  $\omega_n$  of the axial modes are then given by eliminating  $(k^+ - k^-)$  between Eqs. (3) and (5) and solving for  $\omega$ .

The asymptotic time response of the system is governed by the mode whose  $\omega_n$  lies lowest in the complex- $\omega$  plane, provided this lies below the lowest relevant branch point of  $k(\omega)$  in the sense of Briggs.<sup>2</sup>

It is useful to express the total solution in the form

$$\psi_n(t, z) = Y_n(z) \cos[\omega_n t + \chi_n(z)] \exp - \omega_n t \quad (6)$$

where  $Y_n$  and  $\chi_n$  are real functions of  $z$ , because in practice it is the amplitude  $Y_n$  and phase  $\chi_n$  of the total wave which can be measured as functions of  $z$ . Moreover, a measurement of  $Y(z)$  and  $\chi(z)$  allows one to determine the reflection coefficient as in a transmission line impedance measurement. Taking the origin at the centre, we find

$$[Y(z)]^2 = \left\{ \begin{aligned} &|\rho_1| \exp 2 k_1^+ z + |\rho_2| \exp 2 k_1^- z \\ &+ 2 |\rho_1|^{1/2} |\rho_2|^{1/2} \exp (k_1^+ + k_1^-) z \cos [2\phi - (k_r^+ - k_r^-) z] \end{aligned} \right\} \quad (7)$$

$$\tan \chi(z) = \frac{[|\rho_1|^{1/2} \exp k_1^+ z \sin(\phi - k_r^+ z) - |\rho_2|^{1/2} \exp k_1^- z \sin(\phi + k_r^- z)]}{[|\rho_1|^{1/2} \exp k_1^+ z \cos(\phi - k_r^+ z) + |\rho_2|^{1/2} \exp k_1^- z \cos(\phi + k_r^- z)]} \quad (8)$$

where  $2\phi = (\theta^+ - \theta^-) = \pi \pm (\theta_1 - \theta_2)/2$ .

Certain general deductions can be made as follows. For reciprocal systems, i.e. D involving only even powers of  $k$  so that  $k^+ = -k^-$ , the axial modes are pure standing waves composed of real  $k$  travelling waves only when the terminations are lossless i.e. purely reactive ( $|\rho_1| = |\rho_2| = 1$ ). With dissipation ( $|\rho_1|, |\rho_2| < 1$ ), the modes are partial standing waves composed of complex  $k$  waves growing spatially towards either end. The effect of lossy terminations is stabilizing, i.e. it reduces the temporal growth rate or increases the damping rate compared with lossless terminations. For non-reciprocal systems, i.e. D involving odd powers of  $k$  as occurs with an axial

current, the modes are partial standing waves even for lossless terminations. In this case the spatial growth of one component wave balances the spatial damping of the other.

Application to Collisional Drift Waves

The dispersion relation for isothermal collisional drift waves in a fully-ionized plasma neglecting ion parallel motion may be written:<sup>3,4</sup>

$$w^2 + \left\{ 1 - 1 \left[ \frac{(1+b)k^2}{b v_e} + C_1 b v_i \right] \right\} w - \left\{ 2 \frac{C_1 b v_i K^2}{v_e} - 1 \left[ \frac{(1-b)k^2}{b v_e} - C_1 b v_i \right] \right\} = 0 \quad (9)$$

where  $w = \omega/\omega_D$ ;  $\omega_D = k_y v_D$ ;  $v_D = \frac{-T\chi}{eB}$ ;  $\chi = (1/n)(\partial n/\partial x)$ ;  $T_e = T_i = T$ ;

$$b = \frac{k_x^2 T}{n_i \omega_{ci}^2}; K^2 = \frac{k_x^2 T}{\omega_D^2 m_e}; v_i = \frac{v_{i1}}{\omega_D}; v_e = \frac{C_r v_{e1}}{\omega_D}.$$

Here  $v_{e1}, v_{i1}$  are the collision frequencies as defined by Braginskii<sup>5</sup> and the coefficient of electron parallel resistivity  $C_r = 0.513$ . The coefficient of ion viscosity  $C_1$  is given as (3/10) by Braginskii but was taken as (1/4) in Refs. 3 and 4. With  $C_1 = 1/4$ , Eq. (9) is the dispersion relation of Rowberg and Wong. That of Hendl et al differs slightly in terms involving  $b$ , which is necessarily small compared to unity for fluid theory.

In applying this theory to the cylindrical geometry of the Q-machine,  $k_y$  is real and determined experimentally by identifying it with  $m/a$  where  $m$  is the azimuthal mode number and  $a$  is the radius at which the azimuthally traveling wave has its maximum amplitude. Also  $k_x$  is determined from the radial wave profile to give  $k_x^2 = k_x^2 + k_y^2$ .

Rowberg and Wong, working with ion rich sheaths, observed temporally damped waves under conditions that Eq. (9) predicts temporally growing waves for real values of  $\lambda_{\parallel} \approx 3.6 L$  apparently indicated by the axial profile. They attributed this to end plate damping which they calculated as a decrement  $\omega_{1D}$  to be subtracted from the growth rate calculated for real  $k_{\parallel}$ . However, it is clear from the present work that end-plate damping is not compatible with a pure standing wave.

Figure 1a shows curves of temporal growth rate  $\omega_i$  versus magnetic field  $B$ , calculated from Eq. (9) for the conditions of Rowberg and Wong's experiment for the first axial mode with  $m = 2$ . The values of  $|\rho| (=|\rho_1|=|\rho_2|)$  have been varied keeping the phase angle  $\theta (= \theta_1 = \theta_2)$  fixed at  $\pi/1.8$ , to give  $\lambda_{\parallel} \approx 3.6L$  when  $|\rho| = 1$  as taken by Rowberg and Wong. It is seen that reducing  $|\rho|$  reduces the growth rate and leads to damping, but it is clear that no single



$|\rho| < 1$  curve matches the experimental results. The  $|\rho| = 0.3$  curve matches at low B but has the wrong shape at large B. On the other hand, Rowberg and Wong's procedure of subtracting a constant damping decrement  $\omega_{1D} \approx 1.4 \times 10^3$  sec<sup>-1</sup> from the theoretical curve for real  $k_{\parallel}$  ( $|\rho| = 1$ ) does lead to a reasonable match with the experiment. However, in the experiment  $\lambda_{\parallel}$  is sufficiently small that the effect of ion parallel motion is important, especially at higher B, so we should not expect agreement with a theory neglecting ion parallel motion.

Including ion parallel motion in the isothermal theory leads to the dispersion relation:

$$w^3 + \alpha_2 w^2 + \alpha_1 w + \alpha_0 = 0 \quad (10)$$

where

$$\begin{aligned} \alpha_2 &\equiv 1 - i \left[ \frac{(1+b)K^2}{bv_e} + 5C_1 bv_i \right] \\ \alpha_1 &\equiv - \left[ \left( \frac{b}{6} + 6 \right) \frac{K^2 C_1 bv_i}{v_e} + 4(C_1 bv_i)^2 \right] + i \left[ \frac{(1-b)K^2}{b} \frac{K^2}{v_e} - 5C_1 bv_i \right] \\ \alpha_0 &\equiv \left[ \frac{4C_1 v_i (1-b)K^2}{v_e} - 4(C_1 bv_i)^2 \right] \\ &\quad + i \left[ \left( \frac{3C_1 bv_i}{v_e} + 2 \frac{m_e}{m_i} \right) C_1 bv_i K^2 + 2 \frac{m_e}{m_i} \frac{(1-b)}{bv_e} K^4 \right]. \end{aligned}$$

Figure 1b shows the growth rate as a function of B calculated from Eq. (10) for various values of  $|\rho|$  for the same conditions as Fig. 1. Comparing Figs. 1a and 1b it is seen that the inclusion of ion parallel motion reduces the growth rate appreciably, especially at large B. As a result there is now much better agreement between the experimental damping curve and a theoretical one taking account of end-plate damping through a reflection coefficient  $|\rho| < 1$ . The best match occurs for  $|\rho| \approx 0.6$ . The relatively poor match for low B is probably due to the fact that  $b(\propto B^{-2})$  is not particularly small.

Figure 2 shows the amplitude and phase of the lowest axial mode for various values of  $|\rho|$ . For  $|\rho| = 0.6$  the phase shift over the central region accessible to measurements is no more than  $6^\circ$ . Now, in stating that the observed axial mode was a standing wave, Rowberg and Wong placed no experimental limit on how small the phase shift was. However, it seems probable that a phase shift of  $6^\circ$  went undetected, especially in view of the fact that the phase varies rapidly with azimuth ( $m$  times the angle), so that detection of a small axial shift presupposes a rather precise tracking of the probe along a field line.

Discussion

When  $D(\omega, k)$  is of order  $\beta > 2$  in  $k$ , the various roots  $k(\omega)$  can all be identified as waves excited on the + or - sides of an excitation point. Usually  $\beta$  is even and there will be  $\beta/2$  pairs of roots  $k^\pm$  corresponding to waves excited on either side for each wave type. We may then write the total solution as a sum of the  $\beta$  waves with complex coefficients determined by a set of reflection coefficients between the various waves. In practice this procedure is hardly tractable. Fortunately, in most cases of practical interest, one pair of waves is dominant, the others being strongly attenuated and excited only very locally to the terminations. In this case we may follow the usual practice established in transmission line measurements, and lump the effect of the evanescent waves into the reflection coefficient for the dominant waves and proceed as in the case for  $\beta = 2$ .

The construction of axial eigenmodes for a finite length system from the dominant roots  $k^\pm(\omega)$  of the infinite system dispersion relation depends upon the characterization of the terminations by complex reflection coefficients for these waves. This enabled us to describe the finite system behavior in general terms; in particular the stabilizing effect of end losses and the partial standing wave structure of the modes for systems with end loss and/or a non-reciprocal dispersion relation. However, if the theory is to have utility for specific systems, one must have a method for determining the reflection coefficient either by calculation or measurement.

Unfortunately, in many plasma experiments using discharge columns, the boundaries are ill-defined and the boundary conditions difficult to specify in terms precise enough for calculations. For a Q-machine, for which there are approximate theories for the physical processes at the hot end-plates, the situation is better. However, since there are sheaths at the end-plates, it is strictly not possible to regard the plasma between the plates as a section of a uniform infinite system. There is also a more fundamental problem in using a fluid description for a bounded system in that a fluid description breaks down close to a boundary. When the magnetic field is normal to the boundary the fluid equations fail within a mean free path,  $\lambda$ , of the boundary, while if  $B$  is parallel to the surface it fails within a distance  $\lambda$  or the gyro-radius,  $\rho$ , whichever is the smaller. Consequently, it is difficult, in general, to calculate the reflection coefficients for the dominant waves  $k^\pm(\omega)$  from a knowledge of the physical processes at the boundaries.

For these reasons it is more satisfactory to regard the reflection coefficient as an experimentally determined quantity. The effect of sheaths



and the failure of the fluid description are lumped together with those of possible localized surface waves and higher modes (for  $\beta > 2$ ) into an effective reflection coefficient measured at distances from the boundary greater than the mean free path (or gyro radius) and sheath thickness. This standpoint is analogous to transmission line practice where, although the reflection coefficient can be calculated in principle for arbitrary terminations, in practice it is usually much simpler to measure it.

When the system is stable, the reflection coefficient may be measured as a function of frequency by externally exciting waves in a chosen transverse eigenmode and measuring the amplitude and phase of the partial standing wave as a function of position from the termination. When the system is unstable, such measurements may be made on the (nonlinearly limited) self-excited modes. If two or more modes are excited at different frequencies, the separate patterns may be isolated by frequency filtering.

#### References

1. T. D. Rognlien and S. A. Self, Institute for Plasma Research, Report No. 423, Stanford University (May 1971).
2. R. J. Briggs, Electron-Stream Interaction with Plasmas (M.I.T. Press, Cambridge, Mass., 1964).
3. H. W. Kendel, T. K. Chu and P. A. Politzer, Phys. Fluids 11, 2426 (1968).
4. R. W. Rowberg and A. Y. Wong, Phys. Fluids 13, 661 (1970).
5. S. I. Braginskii, in Reviews of Plasma Physics, edited by M. A. Leontovich (Consultants Bureau, New York, 1965) Vol. I. p. 205.

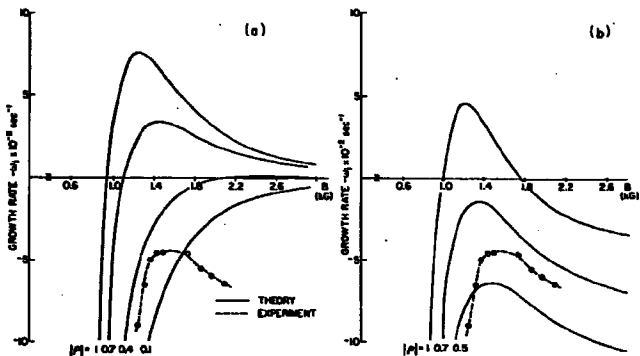


FIG. 1. Growth rates as a function of magnetic field calculated from (a): Eq. (9) which neglects ion parallel motion; and (b): Eq. (10) which includes ion parallel motion, for various end-plate reflection coefficients. Parameters are from Rowberg and Wong's experiment:

$$\begin{aligned}
 m_i &= 39.1 \text{ AMU}; \quad n = 6.7 \times 10^{10} \text{ cm}^{-3}; \quad T = 0.19 \text{ eV}; \quad m = 2; \quad k_y = k_x = 1.43 \text{ cm}^{-1}; \\
 \chi &= -0.80 \text{ cm}^{-1}; \quad v_{e1} = 2.0 \times 10^7 \text{ sec}^{-1}; \quad v_{i1} = 5.2 \times 10^4 \text{ sec}^{-1}.
 \end{aligned}$$

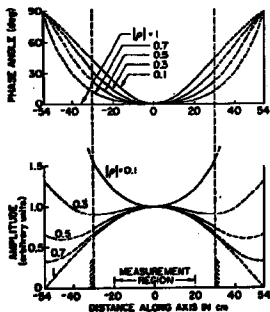


FIG. 2. Amplitude and phase of the axial mode as a function of position for various reflection coefficients  $|\rho|$  keeping the phase  $\theta$  constant at  $\pi/1.8$ .

AMPLITUDE OF ELECTRON PLASMA WAVE ECHOES

M. Guillemot, J. Olivain, F. Perceval, A. Quemeneur

ASSOCIATION EURATOM-CEA

Département de la Physique du Plasma et de la Fusion Contrôlée  
Centre d'Etudes Nucléaires

Boîte Postale n° 6 - 92 Fontenay-aux-Roses (France)

and G. Matthieussent

Laboratoire de Physique des Plasmas - Faculté des Sciences

91 - ORSAY (France)

ABSTRACT

New experimental results of spatial plasma wave echoes are presented. They especially show :

- the observed echoes are dominated by collective effects.
- the dissymmetric role played by the two emitters on the amplitude and on the profile of the echo .
- the decay of the amplitude of the echo under the influence of a homogeneous noise (plasma noise) and an inhomogeneous noise (random noise generator).

I - INTRODUCTION

Plasma wave echoes have been predicted by mean of a perturbation expansion of Vlasov and Poisson equation [1] . This theory, as well as the effects of diffusion of particles in velocity space on echoes amplitude [2] have been demonstrated experimentally for electron plasma [3] [4] and ion acoustic waves [5]. The perturbation theory does not predict satisfactorily the amplitude dependance of the echo . The aim of this paper is to bring experimental evidence of these features pointed out by a previous theory [6] which accounts for the self consistent fields of the waves and the echo. On the basis of [2] , this theory has been completed in order to include diffusion in velo-

city space which affects the echo amplitude.

## II - THEORY

If two plasma waves of frequency  $\omega_1$  and  $\omega_2$  are continuously excited at  $x = 0$  and  $x = \ell$  by externally applied potentials  $\Phi_1$  and  $\Phi_2$ , provided that the Landau damping lengths are small compared to  $\ell$ , echoes of frequency  $\omega_{m,n}$  will appear at distances  $\ell_{m,n}$  from the point where the first wave is excited.

$$\omega_{m,n} = n\omega_2 - m\omega_1 \quad \ell_{m,n} = \frac{n\omega_2}{\omega_{m,n}} \quad (1)$$

( $m$  and  $n$  are integers defining the  $(m, n)$  echo).

Gould and O'Neil theory's [1] predicts a peak echo amplitude  $E_{m,n}$  of the form

$$E_{m,n} \sim \Phi_1^m \Phi_2^n \ell^n \quad (2)$$

The condition of validity of such a theory may be written as

$$\left( \frac{e\Phi}{m\nu_p^2} \right) \frac{k_r}{k_i} \ell k_r < 1 \quad (3)$$

where  $\nu_p$  is the phase velocity of the wave,  $k_r$  and  $k_i$  the real and imaginary part of the wave number.

Diffusion of plasma electrons in velocity space reduces the amplitude of the echo [2]. Homogeneous diffusion due to Coulomb collisions and due to fluctuations reduce the amplitude of a resonant echo ( $m = 1, n = 2$ )

$\omega_1 = \omega_2 = \omega_{1,2} = \omega$   
by the scaling factor [2].

$$\exp \left[ -D_2(\nu_p) \frac{2}{3} \frac{\ell^3 k_r^5}{\omega^3} \right] \quad (4)$$

where  $D_2(\nu_p)$  is the value of the diffusion coefficient for the phase velocity of the wave. Noise injected in the plasma at the position  $x = \ell_1$ , in a band centered about the resonant echo frequency produces inhomogeneous diffusion. The echo amplitude is reduced by the scaling factor [2]

$$\exp \left[ - \left( \frac{e}{m} \right)^2 \frac{\Delta |E(\omega)|^2}{\Delta f} \frac{\ell_1^2 k_r^5}{2k_1 \omega^3} \right] \quad (5)$$

where  $\frac{\Delta |E(\omega)|^2}{\Delta f}$  is the spectral density of the noise. Good agreement between theory and experiments [3,4] is found as long as condition (3) holds.

Experimental conditions in which (3) is violated are easily produced in the case of electron plasma waves [3, fig 5,6], [7]. A more accurate theory [6], taking into account the self consistent fields of the plasma, points out new non linear aspects of the echo behaviour :

i, the saturation and decrease of the echo amplitude when either the power on the second emitter, or the distance between the emitters is increased,

i i, the dissymmetric role played by the emitters on the echo amplitude,

i i i, the saturation amplitudes of the echoes of the (1, n) serie of the same magnitude.

In such a theory the peak echo amplitude is

$$E_{1,n} \sim \Phi_1 \int_0^\infty dv \frac{df^0(v)}{dv} J_n(\omega_1 \Phi_2 \ell h(v, \omega_2)) g(v, \omega_1) k(v, \omega_3) \quad (6)$$

where  $J_n$  is the  $n^{\text{th}}$  order Bessel function of first kind,  $g(v, \omega_1)$   $h_1(v, \omega_2)$ ,  $k(v, \omega_3)$  account for the self consistent fields of the waves and of the echo and  $f^0(v)$  the unperturbed velocity distribution function. As expected linearization of (6) with respect to the Bessel function argument gives the echo amplitude found previously. For a resonant echo (1,2) the peak echo amplitude can be written as

$$E_{1,2} \sim \Phi_1 J_2(\omega_1 \Phi_2 \ell h(v_p, \omega_1)) \quad (7)$$

where the integral in (6) has been evaluated at the phase velocity of the primary waves and of the echo.

If the self consistent fields of the plasma are not included in the non-linear echo theory and the unperturbed distribu-

tion function is Maxwellian, for low values of the product  $\Phi_2 \ell$ , the main contribution to the integral (6) comes from low velocity electrons and yields a peak echo amplitude varying as

$$E_{1,n} \sim \Phi_1 (\Phi_2 \ell)^{2/3}$$

Such a theoretical result has been checked by numerical calculation and remains valid until the echo saturates.

To fit the experimental results we had to include diffusion in velocity space. A rigorous treatment of such collisional effect is not yet available for the spatial case as it is for the temporal case [8]; we, therefore, follow O'Neil's argument [2], the amplitude of a resonant echo may be obtained by making the product of the peak echo amplitude (7) by the appropriate scaling factor (4) or (5).

### III - EXPERIMENT

Experiments were performed on a diffusive argon plasma column [9]; the plasma produced in a P.I.G. discharge drifts into an uniform magnetic field parallel to the column axis. For the data reported, the plasma column is 65 cm long and has a density of  $2.10^8$  electrons per  $\text{cm}^3$ . The magnetic field, 1.2 kGs is large enough to be considered as infinite. The electron temperature is about 2 eV and the background pressure  $10^{-6}$  mm Hg. Under such conditions the mean free path for electron-ion collisions is of the order of 300 m and for electron neutral collisions is about  $10^3$  m.

The Landau damped waves are launched and the echo detected by probes which can be moved longitudinally. Two of them are used as emitters and connected to generators operating at angular frequency  $\omega_1$  and  $\omega_2$ . The signal at  $\omega_1$  is chopped in order to use coherent detection. The third probe is connected through a low-noise broad band receiver to a spectrum analyzer whose linear output drives a coherent detector operating at the first emitter chopping frequency. Linear detection is used throughout the experiment.

A typical measured dispersion relation for a plasma wave is plotted fig. 1 and compared with the wave number in the decay of several (1,1) echoes. This result shows that the observed echoes can be interpreted as dominated by collective effects [3, 10]

To check the dependence of the peak echo amplitude on the amplitude of each primary wave a third order ( $m = 1, n = 2$ ) quasi resonant echo was used ; in order to reject the electromagnetic signal which would appear at the frequency of the resonant echo ,the frequencies of the two primary waves are choosen slightly different, the resulting echo is called a quasi resonant echo. Fig. 2 and 3 show that, as expected from both theory (2), (7), the peak echo amplitude is proportionnal to  $\Phi_1$ , and  $\Phi_2^2$  for low amplitude of the waves, i.e when inequality (3) holds, At larger amplitude of the waves, the peak echo amplitude saturates and then decreases as the amplitude of the second wave increases ; however it still remains linear on the first wave amplitude. The dependence on  $\Phi_2$ , namely  $J_2(\omega_1 \Phi_2 \ell h(\omega_p, \omega_2))$  is drawn in order to fit the maximum peak echo amplitude  $\hat{E}_{12}$ . According to the fact that  $\Phi_2 \ell$  enters the expression for the echo amplitude as the argument of a Bessel function which depends on velocity, formula (7) is approximative ; the exact dependence on  $\Phi_2 \ell$  would result on an integration over velocity as shown on expression (6).

The radial profile of the echo is in agreement with its theoretical shape [11] as long as (3) holds. Fig.4 shows the radial profile of the echo for different value of  $\Phi_2$ . Such a result is in agreement with a theory taking into account both saturation and finite geometry effects.

If the distance between emitters is varied, the resulting damping of the echo can be attributed to the non linear dependence on  $\Phi_2 \ell$  described by Coste and Peyraud and to electron diffusion in velocity space, Therefore care must be taken in measuring the collisional damping. For a fixed value of  $\Phi_1$ , and for the value of  $\Phi_2 \ell$  which produces the maximum peak echo amplitude  $\hat{E}_{12}$ , we study the influence of homogeneous diffusion in velocity space by increasing the distance between emitters. If the plasma

was not subjected to fluctuations, this maximum would be a constant. In the presence of fluctuations, a diffusion takes place in velocity space leading to (fig. 5).

$$\hat{E}_{1,2} \sim \exp - \frac{\ell^3}{\ell_0^3}$$

This decay of the amplitude has been found in another plasma wave echo experiment [4]. The use of a theory which accounts for the echo saturation phenomena allows us to confirm such a result on larger distances. However the measured value of  $\ell_0, \ell_0 = 0.2\text{m}$ ; is too small to attribute such a diffusion process to electron ion encounters which give  $\ell_0 \simeq 6\text{ m}$ . The diffusion must therefore be due to background noise : the density fluctuations in the plasma column are of the order of 10 %.

The influence of inhomogeneous diffusion was studied. A third probe inserted between the two emitters is connected to a random noise generator. The high frequency noise is launched in the plasma in a 10MHz band around the quasi resonant echo frequency. Fig. (6) shows the decrease of the quasi resonant echo amplitude as a function of the integrated noise power. In agreement with the theoretical prediction of formula (5) the logarithm of the echo amplitude decreases linearly with the noise power. A shift of the peak echo amplitude towards the emitters is observed and remains quantitatively unexplained.

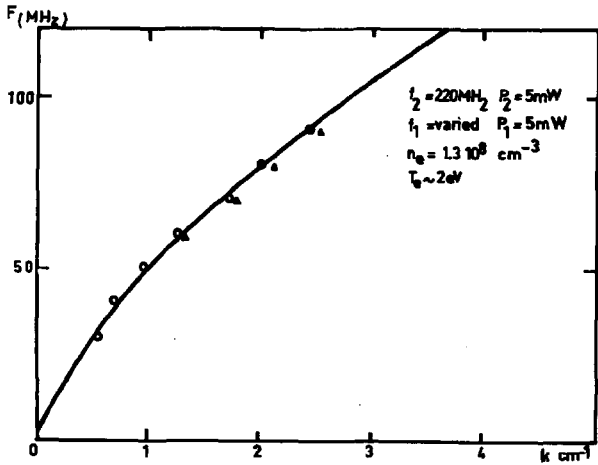
#### IV - SUMMARY

The dependence of the peak echo amplitude on the amplitude of the two primary waves, chiefly the saturation and decrease with the second wave amplitude, the influence of homogeneous and inhomogeneous diffusion in velocity space are verified in the case of a quasi-resonant echo. The saturation effect can be used as a tool to measure the amplitude of a wave injected in the plasma, the collisional damping, as described in [2,4] to measure diffusion coefficient in velocity space.

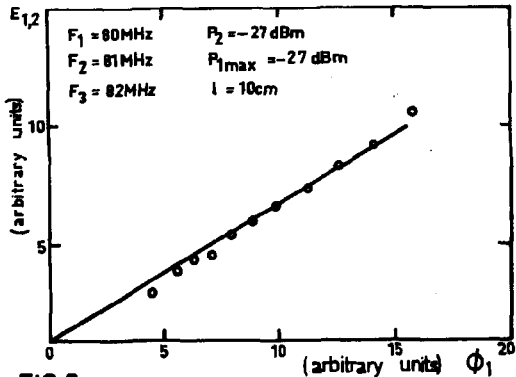


REFERENCES

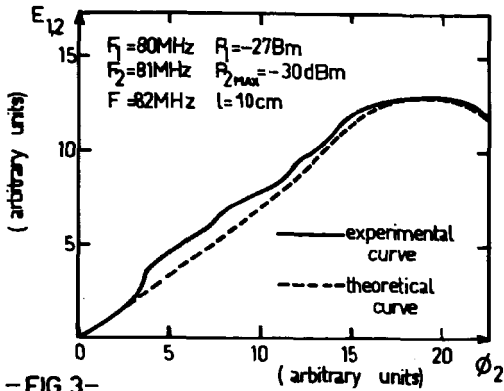
- [1] T.M. O'NEIL, R.W. GOULD, Phys. Fluids 11, 134 (1968)
- [2] T.M. O'NEIL, Phys. Fluids 11; 2420 (1968)
- [3] J.H. MALMBERG, C.B. WHARTON, R.W. GOULD and T.M. O'NEIL  
Phys. Fluids 11, 1147 (1968)
- [4] T.H. JENSEN, J.H. MALMBERG, T.M. O'NEIL, Phys. Fluids 12,  
1728 (1969)
- [5] H. IKEZI, N. TAKAHASHI and K. NISHIKAWA, Phys. Fluids 12,  
853 (1969)  
A.Y. WONG and D.R. BAKER, Phys. Rev. 188, 326 (1969)
- [6] J. COSTE and J. PEYRAUD, J. Plasma Phys, 3, 603 (1969)
- [7] M. GUILLEMOT, P. LEPRINCE, G. MATTHIEUSSENT, J. OLIVAIN and  
F. PERCEVAL, C.R. Acad. Sci, B 270, 317 (1970)
- [8] Y. FURUTANI, J. COSTE, J. Plasma Physics 4, 843 (1970)
- [9] M. PERULLI, Thesis, EUR-CEA Report n° R 3639 (1968)
- [10] B.H. RIPIN, R.E. PECHACEK, Phys. Rev. Letters 24, 1330 (1970)
- [11] T.H. JENSEN, Phys. Fluids 13, 1778 (1970)



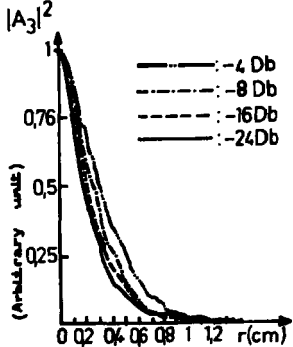
-FIG.1- PLASMA WAVE DISPERSION CURVE(°)  
AND WAVE NUMBER IN THE DECAY  
OF (1,1) ECHOES(△)



-FIG.2- QUASI RESONANT ECHO AMPLITUDE  
VERSUS FIRST EMITTER AMPLITUDE



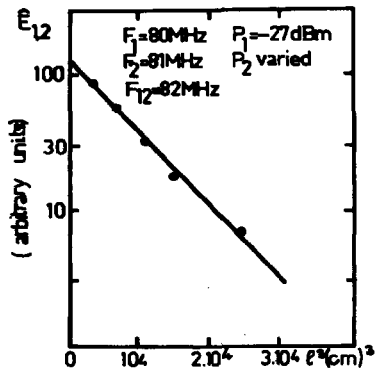
-FIG.3- QUASI RESONANT ECHO AMPLITUDE VERSUS SECOND EMITTER AMPLITUDE



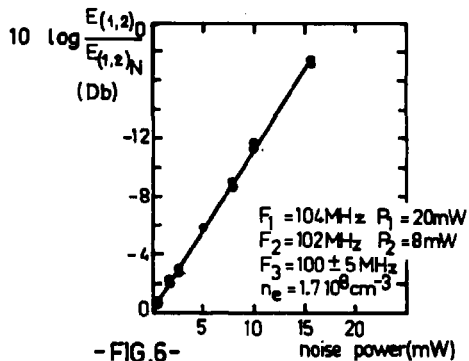
EXPERIMENTAL PROFILE OF A 12 RESONANT ECHO.

-FIG.4-

$n_0 = 10^8 \text{ el. cm}^{-3}$      $T_0 = 1 \text{ eV}$   
 $F_1 = 85\text{MHz}$      $F_2 = 87\text{MHz}$   
 $P_1 = 0.2\text{W} - 20\text{db}$      $P_2 = 60\text{mW} - 2\text{Db}$  (Saturation for -16Db)



-FIG.5-  
 MAXIMUM PEAK AMPLITUDE  
 OF A QUASI RESONANT  
 ECHO VERSUS  $n^3$



-FIG.6-  
 DAMPING OF THE ECHO  
 DUE TO A RANDOM NOISE  
 $E_{(1,2)0}$  ECHO AMPLITUDE WITHOUT NOISE  
 $E_{(1,2)N}$  ECHO AMPLITUDE WITH NOISE

Wave Growth in a Large Unmagnetized  
Electron-Beam-Plasma System

by

P.J. Barrett, D. Gresillon<sup>†</sup>, and A.Y. Wong

Department of Physics, University of California, Los Angeles, USA

Abstract

A large diameter electron beam is drawn into a quiet, collisionless, unmagnetized discharge plasma from a similar plasma. The relative beam density can be varied from 0 to 1 and the beam energy is typically in the range  $3 T_e$  to  $10 T_e$ . When the beam is modulated at frequencies comparable to the electron plasma frequency, growing waves are observed, from which the dispersion is obtained and compared with linear kinetic theory.

Introduction

There have been many experiments on the interaction between an electron beam and a plasma<sup>1</sup>. The electrons have usually been obtained by thermionic emission, with the consequent limitations of small dimensions, non-uniformity, low temperature, etc. Such features greatly affect the growth rate, both in the absence<sup>2</sup> and in the presence<sup>3</sup> of a magnetic field: they are avoided in the present experiment by using a separate plasma as the beam source. Section 2 deals with the experimental arrangement and the characteristics of the beam; Section 3 describes the dispersion measurements, and in Section 4 these are discussed and compared with linear kinetic theory.

### Experimental Arrangement

The Double-Plasma device<sup>4</sup> represented in Fig.1, comprises two independent quiet argon plasmas, 1 and 2, separated by a fine grid (40 lines/cm, diameter 25 cm) connected to the wall of Plasma 1. The plasma density is in the range  $10^8 - 10^9 \text{ cm}^{-3}$  and the electron temperature is about 1.5 eV. At the operating pressure of 0.1 to 0.25 microns, the mean free path for electron-neutral collisions is greater than the plasma dimensions and the electron distribution consequently has a high energy tail up to 30 eV due to the presence of primary discharge electrons. The movable plane probe p is a tantalum disc of diameter 7 mm, coated on the rear side and mounted at the end of a coaxial line. By coupling to p directly and also through a capacitor, we can obtain simultaneous measurements of the electron distribution function (by differentiating the Langmuir characteristic) and the high frequency signals around  $\omega_{pe}$ ; the latter are usually observed, however, with the probe floating.

The potential distribution along the axis is shown at the bottom of Fig.1. The plasma potentials are about 0.6 eV more positive than wall potential. When chamber 1 is biased negatively (typically in the range -4 to -20 eV) there is a flux of electrons into chamber 2, which is grounded. To compensate for this loss, electrons of low energy ( $\sim T_e$ ) are extracted by Plasma 1 from the extra filament c, otherwise the flux would be largely inhibited by space charge.

The effect of the extra filament c is demonstrated in Fig.2. The electron distribution function  $f(v)$  is measured close to the grid at five values of the current  $I_f$  in c. The right-hand-side of the main peak, at  $V \sim 0$ , represents the bulk of plasma electrons, whereas the beam appears as a bump at  $V \sim 7$  eV, which increases with  $I_f$  until it becomes as large as the plasma peak.

On entering chamber 2 the electron beam encounters a region of positive density gradient which reduces to  $n^{-1} (dn/dx) < 0.04 \text{ cm}^{-1}$  at  $x \sim 5$  cm, the region of interest; the plasma is uniform at  $x \gtrsim 8$  cm. In the radial direction there is a slight gradient in the plasma density  $n_0$  and a larger one in the beam: the latter has a width of 15 cm at half density which is much greater than typical values of the wavelength and the wave growth distance. For the measurements described below, the beam energy is in the range 4 to 20 eV, and the beam to plasma density ratio  $n_b/n_0$  is maintained at a few per cent or less.

### Dispersion Measurements

As a first step in the investigation of the beam-plasma interaction we have measured the dispersion relation of the electrostatic waves occurring at  $\omega \sim \omega_{pe}$ . With chamber 1 and the grid d-c coupled by a low inductance coil, the waves are excited by applying a small signal (<0.1 V) to the grid, thereby velocity-modulating the beam. The signal is itself modulated by the low frequency

reference signal of a lock-in amplifier and the waves are detected by the usual interferometric technique.

Fig.3 shows the output from the interferometer circuit at five different frequencies, where the plasma frequency (from the probe characteristic) is 225 MHz and the beam energy  $V_b = 8$  eV. As the distance  $x$  from the grid increases, spatial growth is first observed, followed by decay at  $x > 6$  cm attributable to non-linear effects<sup>6</sup>. The dispersion and growth rate from such data are plotted in Fig.4 in the form of a normalized ( $\omega, k$ ) diagram. The bars and dots representing the real part of the normalized wave number  $k_x \cdot v_b / \omega_p$  (where  $v_b$  is the beam velocity) indicate that the phase velocity of the waves is close to  $v_b$ . The dots and curve on the left-hand part of the diagram show that the wave growth (see upper scale for  $k_i/k_r$ ) occurs in a broad band of frequencies around  $\omega_p$ , with a maximum  $k_i/k_r \sim 0.1$  - the same behaviour is found at different values of the plasma density  $n_0$  throughout the range  $10^8 - 10^9$   $\text{cm}^{-3}$ .

### Theory and Discussion

The curves in Fig.4 were computed for an infinite, uniform, Maxwellian plasma, using the following dispersion relation from kinetic theory:

$$1 - \left(\frac{s}{f}\right)^2 \left[ (1-b) Z'(s) + \frac{b}{T} Z' \left( \frac{s-u}{T^{1/2}} \right) \right] = 0 \quad \dots (1)$$

where  $b = n_b / (n_0 + n_b)$

$$T = T_b / T_e \quad (T_e \text{ is the temperature of the plasma electrons})$$

$$f = \omega / \omega_0$$

$$\omega_0 = (\omega_{pe}^2 + \omega_{pb}^2)^{1/2} \quad (\omega_{pe} \text{ is the beam electron plasma frequency})$$

$$u = v_b / c_e$$

$$s = \omega / kc_e \quad (c_e^2 = 2 kT_e / m)$$

and  $Z'$  is the derivative of the plasma dispersion function. Equation (1) is written in a form suitable for spatial rather than temporal development of a wave, i.e.  $f$  is real and  $k$  complex. The complex solution  $s$  provides the real part of the wave number, namely

$$k_x v_b / n_c = u f \text{Re } s / |s|^2, \quad \dots (2)$$

and the growth rate

$$k_i / k_r = - \text{Im } s / \text{Re } s. \quad \dots (3)$$

The curves are computed with  $b = 0.01$ ,  $u = 3$  and  $T = 0.17$ : the low value of  $T$  reflects the effective cooling of the beam electrons when accelerated.

It should be noted that a fluid model<sup>5</sup> could appropriately have been used here since, even with  $b$  as low as 0.01 where the

beam is observed as a small bump on the tail of the distribution function, the dispersion relation is predicted<sup>7</sup> to be topologically close to the beam-type dispersion.

Without taking into account the effect of density gradient, we find agreement between experimental and theoretical growth rates to within a factor 2. In the case of the real part of the wave number, the agreement is much closer: the slight discrepancy is probably due to an over-estimate of  $v_b$ , since the beam velocity decreases slightly with distance and  $v_b$  is measured near the grid.

In conclusion, by adapting the Double-Plasma machine to produce an electron beam (hitherto this device has been used primarily for studies of ion phenomena), we have obtained a large diameter, fairly uniform electron beam of relatively high temperature, variable energy (up to tens of eV), with a wide range of relative density,  $n_p/n_0$ . As a preliminary to the more detailed studies described in the following paper in these Proceedings, we have measured linear dispersion properties of the system and found reasonable agreement with theory.

#### References

- \* Work supported by the National Science Foundation, Contract NSF GP-28509X.
- + CNRS and NATO Fellow, on leave from Ecole Polytechnique, Paris.
- <sup>1</sup> Ya.B. Fainberg, Czech. J. Phys. B., 18, 652 (1958).
- <sup>2</sup> G.D. Boyd, R.W. Gould and L.M. Field, Proceedings of the IRE, 49, 1906 (1961).
- <sup>3</sup> J.H. Malmberg and C.B. Wharton, Phys. Fluids, 12, 2600 (1969)
- <sup>4</sup> R.J. Taylor, H. Ikezi and K.R. MacKenzie, Proc. of the Int. Conf. on Physics of Quiescent Plasmas (Laboratoire PMI, Ecole Polytechnique, Paris, 1969), Pt. III, p.57.
- <sup>5</sup> P.J. Barrett, D. Gresillon and A.Y. Wong, to be presented at the 3rd Int. Conf. on Physics of Quiescent Plasmas, Sept.20-24, 1971, Elsinore, Denmark.
- <sup>6</sup> R.J. Briggs, 'Electron-Stream Interaction with Plasmas' (MIT Press, Cambridge, Mass., 1964); and F.W. Crawford, SU-IPR Report no.13 (Institute for Plasma Research, Stanford University, Stanford, Calif., 1965).
- <sup>7</sup> T.M. O'Neil and J.H. Malmberg, Phys. Fluids, 11, 1754 (1968); and S.A. Self, M.M. Shoucri and F.W. Crawford, J. of Applied Physics, 42, 704 (1971)



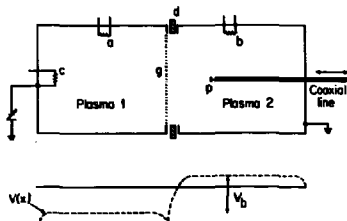


Fig. 1. D-P machine arranged for electron beam production and, below, potential distribution along axis. *a* and *b* are othode filaments for the two plasmas and extra filament *c* is used for the larger beam densities. *d* is an insulator and *g* is a fine grid (40 lines/cm, 25 cm diam). Probe *p* is a 7 mm disc insulated on the back surface.

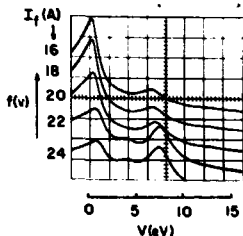


Fig. 2. Electron velocity distribution function at  $x = 1$  cm for different values of the current  $I_f$  through extra filament *c*. The beam is represented by broad bump at 7 eV.

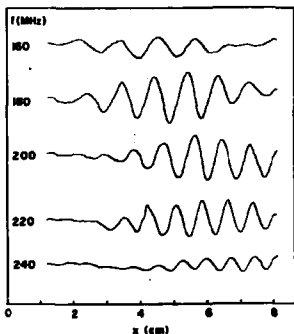


Fig. 3. Waveforms from interferometer circuit showing spatial growth and decay at different frequencies. Plasma frequency from probe characteristic is 225 MHz.

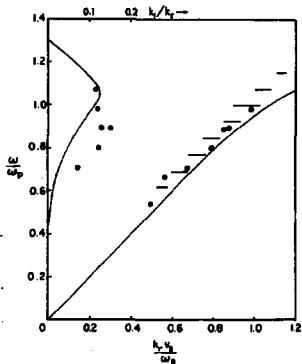


Fig. 4. Dispersion diagram: right-hand data for real part of  $k$ , and left-hand data for imaginary part. Bars represent  $k_r$  for 7 values of beam energy  $V_b$  ranging from 4.5 to 16 eV; dots correspond to  $k_i$  and  $k_r$  respectively, at  $V_b = 8$  eV. Curves are computed from kinetic theory for  $n_b/n_e = 0.01$ ,  $v_b/v_e = 3$ , and  $T_b/T_e = 0.17$ .

Measurement of Velocity Diffusion in an Electron Beam- Plasma Interaction\*

by

P. J. Barrett, D. Grésillon<sup>†</sup> and A. Y. Wong

Department of Physics, University of California, Los Angeles, U S A

Abstract

The interaction between a large diameter electron beam and a collisionless plasma is investigated experimentally in the absence of a magnetic field. The noise power grows spatially and then decays at the same rate. The beam is simultaneously scattered, forming a monotonically decreasing tail in the distribution function. By means of a lock-in technique, the beam particles are tracked through the interaction and observed to spread to both lower and higher energies; the velocity diffusion coefficient is thence determined.

Introduction

The deformation of the electron beam distribution function in a beam-plasma interaction has been described in quasilinear<sup>1</sup> and non-linear<sup>2</sup> theory. There have also been many experiments<sup>3</sup> on this phenomenon, usually with a strong magnetic field parallel to the beam. Several of the features expected from one-dimensional quasilinear theory have been investigated; for example, the growth and saturation of the noise<sup>4</sup>, including the character of the noise spectrum at saturation<sup>5</sup>, and the formation of a plateau in the distribution function<sup>6</sup>. According to quasilinear theory, the noise and beam behavior in the absence of a strong B field differs appreciably from the one-dimensional case<sup>7</sup>. Here we describe an experiment without a B field, in which a large diameter

electron beam interacts with a collisionless plasma, and present a method of measuring the velocity diffusion coefficient  $D$  which describes the spatial evolution of the beam distribution function.

Experimental conditions

The experiment is performed in the collisionless plasma of the Double-Plasma device<sup>8</sup> described in the previous paper<sup>9</sup> of these Proceedings, at plasma densities  $n_0 \sim 10^9 \text{ cm}^{-3}$ , relative beam densities  $n_b/n_0 \sim 10^{-2}$ , electron temperature  $T_0 \sim 1.5 \text{ eV}$  and beam energy  $V_b$  in the range 4 to 20 eV. The beam, with a diameter of 15 cm at half density, encounters a positive density gradient on entering the plasma, which reduces to  $n^{-1}(dn/dx) < 0.04 \text{ cm}^{-1}$  at  $x \sim 5 \text{ cm}$ , the region of interest. The electron flux is measured by means of an axially movable plane probe  $p$  of diameter 7 mm (20 Debye lengths), coated on the back surface and mounted at the end of a coaxial line.

An example of the observed noise spectrum is given in Fig. 1; absolute values of the noise power are not known since this requires knowledge of the high frequency coupling efficiency between plasma and receiver probe. The main peak is centered on  $\omega_p$  (determined from the probe characteristic) and has a width of about  $0.04\omega_p$ . In general the spectrum does not change shape with distance. By differentiating the probe characteristic, we obtain the distribution function  $f(v)$  at different distances from the grid, as shown in Fig. 2 (a) and (b). The corresponding noise power  $P$ , as a function of distance, is presented in Fig. 2 (c). As  $x$  increases it is observed that the beam remains constant as long as  $P$  is small, and then spreads in velocity at about the position where  $P$  is a maximum. The noise then decays, leaving  $f(v)$  with a monotonically decreasing tail.

Tracking of the beam electrons

In order to track the beam electrons as they stream through Plasma 1 and to discriminate between their development and that of the plasma electrons, we use the look-in detection system shown in Fig. 3. The beam energy is modulated by adding a small (0.7 V) 10 kHz square wave potential  $V_1$  to the dc bias voltage on chamber 1. The coherent current  $J_1(V)$  to the probe, due to the beam electrons, is then detected with the look-in amplifier. This represents the distribution function  $f_b(v)$  of the beam electrons since

$$J_1(V) = V_1(dJ_b/dV) = (e^2/m)V_1 f_b(v) \quad (1)$$

where  $J_b$  is the beam current density.

Fig. 4 (a) shows  $J_1(V)$  as a function of  $V$  for different positions of

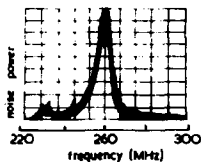


Fig. 1. Noise power spectrum for  $V_b = 10$  eV,  $n_b/n_o \sim 0.01$ .

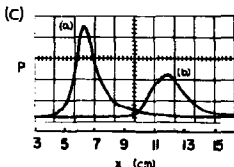
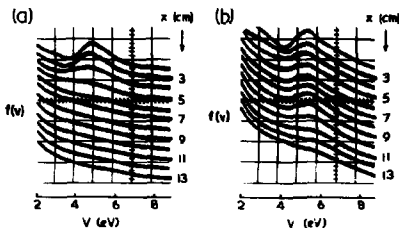


Fig. 2. (a), (b) Electron velocity distribution at different distances and (c) corresponding total noise power  $P$  (integrated over sweep width of spectrum analyzer) as a function of distance.

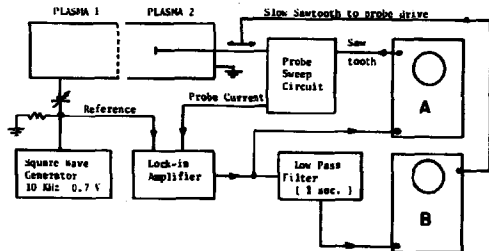


Fig. 3. Circuit for measuring the distribution function and flux of the tracked beam electrons as a function of distance. As the probe is swept through a selected portion of its characteristic, oscilloscope A displays contribution of original beam electrons to total distribution function, and oscilloscope B shows integral of this contribution over the selected voltage range, i.e. the beam flux.

the probe.  $V=0$  corresponds roughly to the plasma potential and the average beam energy is  $\approx 8$  eV. The distribution remains unchanged over the first 3 cm, starts to flatten in the region of positive slope at about  $x = 4$  cm and then continues to flatten and spread over an increasing range of energy. A shift to higher energy is observed between 5 and 6 cm, together with a slower shift to lower energies between 7 and 10 cm.

If the  $J_1(V)$  curves are now integrated over a given energy range we find, from Eq (1), a quantity proportional to the flux of those beam electrons which lie in this range. Range A at the top of Fig. 4 (a) spans the main part of the initial beam distribution, range B corresponds to the lower energies (down to the plasma potential) and range C to the higher energies. The spatial development of the corresponding fluxes  $J_A$ ,  $J_B$  and  $J_C$  are shown in Fig. 4 (b), together with the integrated noise power P. At the position of maximum noise, the downward step in  $J_A$  and corresponding upward steps in  $J_B$  and  $J_C$  indicate a diffusion of electrons from range A into ranges B and C. Apart from the initial decrease in  $J_A$  and  $J_B$  (probably due to the decreasing flux of energetic primary electrons from Plasma 1 as the solid angle subtended by the grid at the probe decreases), the total beam flux  $J_A + J_B + J_C$  is constant within 3% up to  $x = 12$  cm.

The flux of kinetic energy in the beam direction,  $K_{||} = \int \frac{1}{2} m v^2 f(v) v dv$ , can also be estimated, either from the area under the probe characteristic<sup>10</sup> or by the appropriate integration of the curves in Fig. 4 (a). Within the limits of experimental error, no loss of  $K_{||}$  is detected around the noise maximum. From energy conservation this sets an upper limit on the sum of the noise energy density  $\mathcal{E}$  and the kinetic energy  $K_{\perp}$  transferred from the axial to the perpendicular direction:  $(\mathcal{E} + K_{\perp})/K_{||} \leq 0.05$ .

#### Velocity diffusion coefficient

The data of Fig. 4 may be used to determine directly the velocity diffusion coefficient D for the beam distribution. This quantity is given by<sup>1</sup>

$$v \frac{\partial f_b(v, x)}{\partial x} = \frac{\partial}{\partial v} \left[ D \frac{\partial}{\partial v} f_b(v, x) \right], \quad (2)$$

$$\text{from which } D(v_0, x) = - \left[ \frac{\partial}{\partial x} \int_v^{\infty} v f_b dv \right] \left[ \frac{\partial f_b}{\partial v} \right]^{-1}_{v_0} \quad (3)$$

$$\text{or } D(v, x) = - 2(e/2m)^{3/2} \left[ \frac{\partial}{\partial x} \int_v^{\infty} f_b dv \right] \left[ v^2 \frac{\partial f_b}{\partial v} \right]^{-1} \quad (4)$$

where  $eV = \frac{1}{2} m v^2$ . When  $(\partial f/\partial v)_{v_0} = 0$  we obtain from Eq (2)

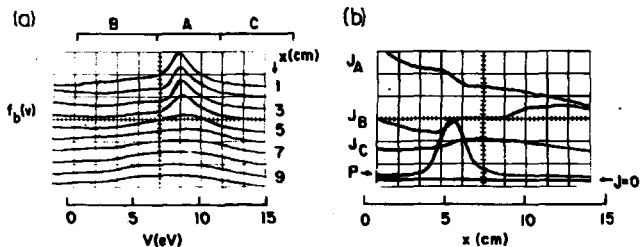


Fig. 4. (a) Velocity distribution function of the tracked beam electrons at different distances;

(b) total noise power  $P$  and beam flux  $J_A, J_B, J_C$  (corresponding to energy ranges A, B, C respectively).

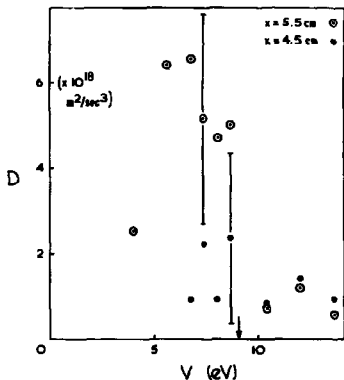


Fig. 5. Velocity diffusion coefficient  $D$ , measured from Fig. 4(a), at two distances  $x$ . Arrow on horizontal axis shows position of  $f_b(v)$  maximum.

$$D(v_0, x) = [v_0 \frac{\partial f_b}{\partial x}] \cdot [\frac{\partial^2 f_b}{\partial v^2}]^{-1} v_0, \quad (5)$$

which is a more suitable form of  $D(v_0, x)$  when  $V$  is very close to the beam energy.

By graphic integration and differentiation, (4) has been used to obtain approximate values of  $D(v_0)$  at  $x = 4.5$  cm (where  $P \sim 0.3 P_{\max}$ ) and  $x = 5.5$  cm (where  $P \sim P_{\max}$ ): these are plotted in Fig. 5. We find the following: (i) At both distances  $D(v_0, x)$  has a maximum value  $D_m$  at an energy somewhat less than the beam energy; (ii) the absolute value of  $D_m$  at the position of maximum noise,  $x = 5.5$  cm, is  $\sim 6 \times 10^{18} \text{ m}^2/\text{sec}^3$ ; (iii) the ratio of  $D_m(x=5.5)$  to  $D_m(x=4.5)$  is nearly equal to the ratio of  $P(x=5.5)$  to  $P(x=4.5)$ , i.e. 2.8 and 3.4 respectively; and (iv) at velocities greater than the beam velocity  $D(v_0)$  is not zero, unlike the case of a one-dimensional interaction<sup>1</sup>, and, also, the proportionality to  $P$  does not appear to be preserved.

#### Discussion

Although the waves in this experiment show a dispersion<sup>9</sup> of the beam type rather than the gentle-bump Landau type<sup>11</sup>, the observed broad noise spectrum, with its absence of amplitude-dependent side-bands, suggests that particle trapping is not significant. So we think that three-dimensional quasilinear theory is relevant here. The interaction may be considered as follows: The main growth of waves occurs in the beam direction, with a tendency to form a plateau in the distribution function. However, waves at a small angle to the beam are also unstable and their tendency to plateau formation connects the particles of the original plateau (i.e. those associated with the tendency to plateau formation in the beam direction) with regions of higher and lower velocities, thus smoothing out any step in the distribution function<sup>7b</sup>.

In conclusion, we have measured experimentally the velocity diffusion coefficient  $D$  in a particularly simple beam-plasma interaction. As expected on the basis of one-dimensional quasilinear theory, the maximum value of  $D$  occurs at a velocity smaller than  $v_0$ , and is proportional to the noise power. Furthermore, we have observed the following phenomena which are in accordance with three-dimensional quasilinear theory: (i) A well localized beam-noise interaction in which noise growth and decay rates are equal; (ii) large scattering of the beam by low level noise fluctuations; (iii) diffusion of the beam electrons to both low and high energies, producing (iv) an equilibrium distribution function which decreases smoothly and monotonically.

\* This work was supported by the National Science Foundation, contract NSF GP-28509X.

† CNRS and NATO Fellow, on leave from Ecole Polytechnique, Paris.

References

1. W. E. Drummond and D. Pines, Nuclear Fusion Suppl. Pt 3, 1049 (1962);  
W. E. Drummond, Phys. Fluids 7, 816 (1964).
2. V. D. Shapiro, Sov. Phys. JETP 17, 416 (1963).
3. Ya. B. Fainberg, Czech. J. Phys. B18, 652 (1968).
4. J. H. Malmberg and C. B. Wharton, Phys. Fluids 12, 2600 (1969).
5. C. Roberson, K. W. Gentle and P. Nielson, Phys. Rev. Letters 26, 226 (1971);  
V. Arunasalam, M. A. Heald and J. Sinnis, Phys. Fluids 14, 1194 (1971).
6. E. G. Shustin, V. P. Popovitch and I. F. Kharchenko, Proc. 8th Int. Conf. Phenomena in Ionized Gases (Springer Verlag, Vienna, 1968) p. 376; and R. Frank, *ibid*, p. 414.
7. I. B. Bernstein and F. Engelsmann, Phys. Fluids 2, 937 (1966); and R. Z. Sagdeev and A. A. Galeev, "Nonlinear Plasma Theory" (ed. by T. M. O'Neil and D. L. Book, Benjamin, New York, 1969) p. 51.
8. R. J. Taylor, H. Ikeai and K. R. Mackenzie, Proc. Int. Conf. Physics of Quiescent Plasmas (Laboratoire PMI, Ecole Polytechnique, Paris, 1969) Part III, p. 57.
9. P. J. Barrett, D. Gresillon and A. Y. Wong, "Wave growth in a large unmagnetized electron beam-plasma system", in Risø Report No. 250 (1971) 285-289.
10. Suggested by R. J. Taylor.
11. T. M. O'Neil and J. h. Malmberg, Phys. Fluids 11, 1754 (1968).



## Cross-field Current-driven Ion Acoustic Instability

by

F. J. Barrett, B. D. Fried, C. F. Kennel, and R. J. Taylor\*

Department of Physics, University of California, Los Angeles, California 90024

and J. M. Sellen

T. R. W. Systems, Redondo Beach, California 90278

### Abstract

This instability occurs when an ion beam (along  $x$ ) travels across a weak magnetic field  $B_z$  in a plasma with (i) beam velocity  $v_D$  greater than the ion acoustic velocity  $c_s$ , (ii)  $\omega \ll \omega_{ce}$  and (iii)  $1 \gg k_x/k_z \gg (m/M)^{1/2}$ ; the spatial growth rate  $k_y/k_x$  is enhanced by a factor  $k_x/k_z$  over the value at  $B_z = 0$ . Measurements of  $k_y/k_x$  in two different plasma configurations show good agreement with computed values when  $(k_x/k_z)(m/M)^{1/2}(v_D/c_s)$  is assumed to be  $\sim 1$ .

### Introduction

The theory of cross-field instabilities, i.e. those associated with the relative streaming of electrons and ions across a magnetic field, has been examined recently by several authors<sup>1-6</sup>. We report here two direct and distinct experimental observations of one class of such instabilities, namely ion acoustic waves propagating at large angles to the magnetic field  $B_z$  (i.e. with  $1 \gg k_x/k_z \gg (m/M)^{1/2}$ ) at frequencies well below the electron cyclotron frequency  $\omega_{ce}$ , wavelengths of the order of the electron gyroradius  $r_e$  and phase velocity close to the ion drift velocity  $v_D$ . Both of the experiments discussed here satisfy  $r_e \ll L \ll v_D/\omega_{ci}$  where  $L$  denotes the dimensions of the plasma,

so the conditions generally assumed in calculations on these cross-field instabilities (magnetised electrons but straight-line ion motion) are well satisfied.

This instability differs from the ion acoustic instability with  $B = 0$  (or  $\vec{k} \parallel \vec{B}$ ) in the following respect: Over the wide range of drift velocity between the ion acoustic velocity  $c_s$  and the electron thermal speed  $c_e = (2kT_e/m)^{1/2}$ , the maximum growth rate is enhanced by a factor  $k_x/k_z$  because the electron motion along  $B_z$ , when projected onto the direction of the wave number  $\vec{k}$ , corresponds to a reduced thermal velocity  $v_e = (k_x/k_z)c_e$  insofar as wave-particle resonance is concerned. Thus, for  $kr_e < 1$  and  $\omega < \omega_{ce}$ , the wave phase velocity can coincide with the velocity of maximum slope of the projected electron distribution function,  $f[\vec{v}_z \cdot \vec{k}/k]$ , even when  $v_D/c_e \ll 1$ , thus enhancing the growth rate which is proportional to this slope.

A further consequence of the magnetic constraint on the electron motion is that this instability, like the electron cyclotron drift instability at  $\omega \gtrsim \omega_{ce}^4$ , is relatively insensitive to  $T_e/T_i$ . For example, whereas the threshold value of  $v_D$  for growth rises from  $c_s$  to  $c_e$  as  $T_i/T_e$  varies from 0 to 1 in the  $B = 0$  case, the threshold remains of the order of  $c_s$  when  $B \neq 0$ , provided that  $k_x/k_z$  can be as small as  $(m/M)^{1/2}$ . Well above the threshold, i.e. for  $c_s \ll v_D \ll c_e$ , the instability can have an appreciable growth rate for larger  $k_x/k_z$  (of the order of  $(m/M)^{1/2}(v_D/c_s)$ ), even when  $T_i/T_e \approx 1$ .

### Theory

The dispersion relation for cross-field electrostatic waves in a homogeneous plasma, with an isotropic Maxwellian electron distribution (in the lab frame) and ions streaming with  $\vec{v}_D$  at a large angle to  $\vec{B}$ , is<sup>1,4</sup>

$$1 + (k^2/k_D^2) + (\omega/k_z c_e) \sum_{n=-\infty}^{\infty} \Gamma_n Z_n - (T_e/2T_i) Z'(\bar{\omega}/k\omega_{ci}) = 0 \quad (1)$$

where  $k_D = (4\pi ne^2/kT_e)^{1/2}$ ;  $\bar{\omega} = \omega - \vec{k} \cdot \vec{v}_D$  is the frequency in the ion rest frame;  $\Gamma_n = e^{-b} I_n(b)$  with  $b = \frac{1}{2}(k_x r_e)^2$ ,  $I_n$  being the modified Bessel function; and  $Z_n = Z[(\omega - n\omega_{ce})/k_z c_e]$ ,  $Z$  being the plasma dispersion function. In the limit  $k_x \rightarrow 0$ , this is just the dispersion relation studied by Forslund et al.<sup>4</sup> in the high frequency regime ( $\omega \gtrsim \omega_{ce}$ ). Here we consider instead the case  $\omega \ll \omega_{ce}$ ; then  $Z_n \approx -Z_{-n}$  and the sum in (1) reduces to the single term  $\Gamma_0 Z_0$ , giving a dispersion relation (also obtained by Aref'ev<sup>1</sup>)

$$2\eta = 2[1 - \Gamma_0 + k^2/k_D^2]/\Gamma_0 = Z'(\omega/k_z c_e) + (T_e/T_i \Gamma_0) Z'(\bar{\omega}/k\omega_{ci}) \quad (2)$$

which is similar to that for ion acoustic waves with  $B = 0$ . The only

differences are the factor  $\Gamma_0$  in the ion term; the replacement of the usual  $k^2/k_D^2$  by  $\eta$  (which reduces to  $k^2/k_D^2$  for  $k_x r_e \ll 1$ ); and, most important, the replacement of  $\omega/kc_e$  in the electron Z function by  $\omega/k_z c_e$  which leads to the aforementioned  $k/k_z$  enhancement of the growth rate. In the cold fluid limit ( $T_e, T_i \rightarrow 0$ ) both Z' functions may be approximated by their asymptotic forms, whereupon (2) reduces to the dispersion relation of Ashby and Paton<sup>6</sup> which has a structure similar to that for the usual two beam instability. However, for the regime studied here, the argument  $\omega/k_z c_e$  is not large and so a power series expansion for the electron Z' function is more appropriate than the asymptotic expansion. If  $T_e/T_i$  is large (as in the experiments described below), we can continue to use the asymptotic form for the ion Z' function and thus obtain a simple, explicit expression for the growth rate

$$(k_i/k_r) = (\pi/8)^{1/2} (m/M)^{1/2} (k/k_z) \Gamma_0 (1 + k^2/k_D^2)^{-3/2} \quad (3)$$

where  $k$  is the complex wave number  $k_r + ik_i$ . This equation clearly exhibits the  $(k/k_z)$  enhancement. For the experiments reported here, however, the parameter  $\omega/k_z c_e$  is typically  $\sim 1$ , so the full expression (2) has been used, with  $T_i/T_e \rightarrow 0$ . For given values of  $b, k/k_D$  and  $v_D/c_s$ , we choose  $k_z$  to maximise  $k_i/k_r$ . The resultant growth rates are larger than those observed experimentally by a factor  $\sim 2$ . If, on the other hand, we set  $k_z = \pi/L$  where  $L$  is the plasma length along  $B_z$ , the calculated growth rates are too small. As shown below, reasonable agreement is obtained by assuming that the parameter  $s = (k/k_z)(\pi/2M)^{1/2}$  has a fixed value.

#### Experimental arrangements

The instability has been directly observed in two different plasma configurations. Fig. 1 (a) shows a Double-Plasma device<sup>7</sup> in which two steady-state argon plasmas ( $\sim 10^8 \text{ cm}^{-3}$ ), separated by a fine negatively-biased grid

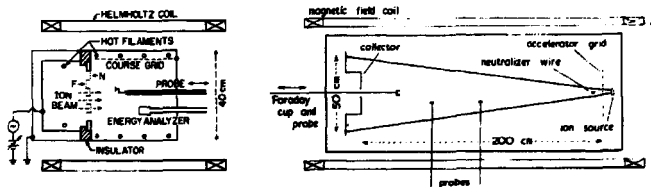


Fig. 1. (a) Double-Plasma device. (b) Streaming cesium plasma apparatus.

of diameter 27 cm, can be held at independent plasma potentials. An ion beam of this diameter can thus be extracted from the left-hand plasma into the larger right-hand plasma (diameter 40 cm), and velocity-modulated by adding a sinusoidal signal (typically a few millivolts, i.e.  $< 0.01 T_e$ ) to the left-hand chamber potential. For most of the measurements the separating grid was plane, but, in an attempt to impose a fixed value of  $k_x$ , a corrugated grid such as that shown in Fig. 1 (a) was also used. The ion beam is neutralised by electrons from grounded filaments in the right-hand chamber. A large clean coarse grid, also grounded (i.e. positive with respect to the plasma), helps to make  $T_e$  uniform and also reduces its value by removing more of the faster electrons; the presence of this grid is important since a variation in  $T_e$  of 30 %, for example, can change the growth rate by a factor 2.

A larger plasma, with different boundary conditions and a greater value of  $v_D/c_s$ , is obtained in the cesium plasma device<sup>8</sup> shown in Fig. 1 (b). Here an ion beam is formed by contact ionisation of cesium atoms in a hot porous tungsten plug. These are accelerated by a nearby plane tungsten grid and neutralised by electrons from a hot wire. Typically the beam energy is  $\sim 300$  eV ( $v_D \sim 2 \times 10^6$  cm/sec) and the density at the source is  $\sim 4 \times 10^9$  cm<sup>-3</sup>, diminishing to  $\sim 10^7$  cm<sup>-3</sup> two meters downstream due to the divergence of the beam. The collector plate at the far end is biased negatively to collect the beam ions, while the magnetized electrons form a stationary background fluid (they rapidly fill the plasma volume when the beam is switched on).

### Experimental results

Spatial growth rates from each device are presented in Fig. 2 as a function of the quantity  $b^{-1}(k_x) = 2/k_x^2 r_e^2 = (e^2 B_z^2 / mKT_e) k_x^{-2}$ , where  $k_x$  is varied at a given value of  $B_z$ . The upper points correspond to excited waves in the

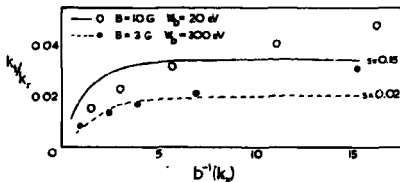


Fig. 2. Experimental and theoretical growth rate  $k_1/k_x$  versus  $b^{-1}(k_x) = (e^2 B_z^2 / mKT_e) k_x^{-2}$  for (a) waves excited in D-P device from 0.6 to 0.1 MHz, with  $n = 2 \times 10^8$  and  $T_e = 1.5$  eV; (b) plasma noise observed in Streaming Cesium Plasma device from 0.8 to 0.2 MHz, with  $n \approx 2 \times 10^8$  and  $T_e = 0.25$  eV.  $s = (k/k_x)(m/2M)^{1/2}$ .

Double-Plasma machine, whereas the lower set represent the naturally occurring noise growth in the Streaming Cesium Plasma device, measured with the aid of tuned filters. The corresponding theoretical curves, with  $s$  as a fitted parameter, show agreement to better than a factor 2.

In Fig. 3 the growth rate from the D-P machine is presented as a function of  $b^{-1}(B_z) = 2/k_x^2 r_o^2 = (e^2/mKT_o k_x^2) B_z^2$  at  $W_b = 80$  eV and two values of the frequency; waveforms obtained at a lower frequency and energy are included in the inset and show the rapid variation of  $k_x/k_r$  with  $B_z$  at low values of  $B_z$ .

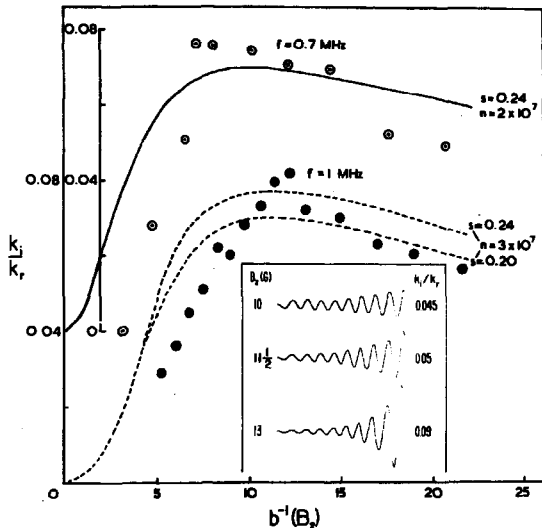


Fig. 3. Experimental and theoretical growth rate  $k_x/k_r$  versus  $b^{-1}(B_z) = (e^2/mKT_o k_x^2) B_z^2$  at two frequencies, with  $W_b = 80$  eV, for waves in D-P device; from probe data,  $n \sim 10^8$  cm<sup>-3</sup>. Solid curve,  $T_o(B_z) = 1.1 + 0.07 B_z$  eV; dashed curves,  $T_o(B_z) = 0.76 + 0.048 B_z$  eV. Inset shows interferometer waveforms at  $f = 0.5$  MHz and  $W_b = 40$  eV.

( $k_x/k_r > 0.5$ ). At high magnetic field there is a slight decrease of growth rate, rather than the asymptotic approach to a constant value expected for a given

$T_0$ : this reflects the observed increase of  $T_0$  with  $B_0$  (see Fig. 3), which has been included in the calculations. The main effect of the reduction in  $T_0$  from the solid to the dashed curves, is to shift the steep portion of the curve to the right. It should be noted that the fitted values of  $s$  imply very small values of  $k_z$  ( $\approx 0.01 \text{ cm}^{-1}$ ), which are difficult to determine experimentally: probe measurements simply indicate that  $\lambda_z$  is somewhat greater than twice the plasma dimension. Presumably the wave electric fields fall rapidly to zero in the sheaths at the plasma boundaries, but have long wavelengths along the magnetic field in the bulk of the plasma. Although growth rates are shown in Fig. 3 only for high values of  $f$  and  $W_0$ , similar behavior is observed throughout the parameter ranges investigated (0.2 - 1 MHz, 10-80 eV, with  $B_0$  varying from 0 to 40 gauss).

The following effects have also been noted: (1) In the D-P experiment an attempt was made to impose a comparatively large value of  $k_z$  on the wave by segmenting the grid as in Fig. 1(a). This leads to the effect shown in Fig. 4(a), that is, the waveform obtained with the probe facing an F (far) segment

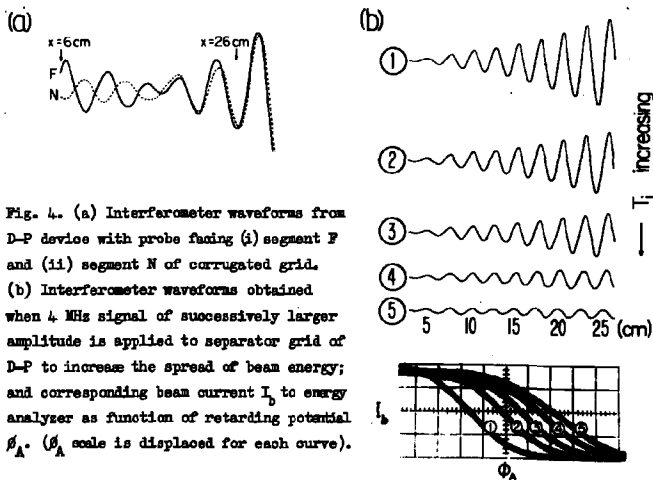


Fig. 4. (a) Interferometer waveforms from D-P device with probe facing (i) segment F and (ii) segment N of corrugated grid. (b) Interferometer waveforms obtained when 4 MHz signal of successively larger amplitude is applied to separator grid of D-P to increase the spread of beam energy; and corresponding beam current  $I_b$  to energy analyzer as function of retarding potential  $\phi_A$ . ( $\phi_A$  scale is displaced for each curve).

is initially out of phase with that obtained opposite an N (near) segment and no growth is observed; but at  $x \approx 20$  cm a sharp phase transition occurs in which the F and N waves phase-lock and begin to grow rapidly. It appears that at this point the initially dominant  $k_z$  imposed by the grid is swapped by a

fast-growing mode corresponding to the minimum  $k_z$  allowed by boundary conditions, magnetic field non-uniformity, etc. It is also found that the instability is insensitive to small changes in the direction of the magnetic field (up to about 10 degrees). (2) A reduction of the growth rate is observed in both devices when a high frequency modulation signal is applied to the beam, thereby increasing the beam temperature  $T_i$  to the point where the effect of ion Landau damping becomes important. This is demonstrated in Fig. 4 (b) where the change of  $(dI_b/d\beta_A)$  from curve 1 to curve 5 represents a change in energy width from 2.5 to 3.1 eV. (3) At the higher values of  $B_z$  both plasmas show increased turbulence and a corresponding increase in  $T_e$ .

#### Conclusions

In conclusion, we have observed the cross-field ion acoustic instability in two quite different plasma devices, finding good agreement between measured and calculated growth rates over a wide range of magnetic field and wave number; it has been necessary, however, to make  $k_x/k_z$  (which determines the maximum growth rate) a fitted parameter, since  $k_z$  is too small to be measured accurately. Because this instability occurs at comparatively low values of the drift velocity ( $v_D \ll c_0$ ) and is relatively insensitive to  $T_e/T_i$ , it may be responsible for anomalous transport and ion heating in collisionless shocks, neutral sheet phenomena (such as the tail of the magnetosphere), and other situations where there is a drift of ions relative to electrons across a magnetic field.

#### Acknowledgements

We are indebted to Mr. William Gould for assistance with the computations. This research was jointly supported by AFOSR, AEC, NSF, ONR, and TRW I.R.&D. program.

\* Present address: Massachusetts Institute of Technology, Cambridge, Mass.

#### References

1. V. I. Aref'ev, Soviet Phys.-Tech. Phys. 14, 1487 (1970).
2. H. V. Wong, Phys. Fluids 13, 757 (1970).
3. S. P. Gary and J. J. Sanderson, J. Plasma Phys. 4, 739 (1970).
4. D. Forslund, R. Morse and C. Nielson, Phys. Rev. Letters 25, 1266 (1970).
5. M. Lampe, W. Manheimer, J. E. McBride, J. H. Orens, R. Shanny and R. N. Sudan, Phys. Rev. Letters 26, 1221 (1971).
6. D. E. T. F. Ashby and A. Paton, Plasma Phys. 2, 359 (1967).
7. R. J. Taylor, Ph. D. thesis, U. C. L. A. (1970).
8. J. M. Sellen, W. Bernstein and R. F. Kemp, Rev. Sci. Instr. 36, 316 (1965).

LARGE AMPLITUDE WAVE INTERACTION WITH A PLASMA : TRAPPING EFFECTS

M. Guillemet, J. Olivain, F. Perceval, A. Quemeneur,

**ASSOCIATION EURATOM-CEA**

Département de la Physique du Plasma et de la Fusion Contrôlée  
Centre d'Etudes Nucléaires

Boîte Postale n° 6 - 92 Fontenay-aux-Roses (France)

SUMMARY

The deformation of the distribution function of an electron plasma under the influence of a large amplitude is measured. It is shown to be in good agreement with a non-linear spatial theory.

INTRODUCTION

The temporal evolution of a large amplitude weakly damped wave has been treated first by Al'tshul and Karpman [1]. They used the quasi-linear theory and found that the wave amplitude undergoes small oscillations around an undamped average value provided that the linear damping rate is smaller than the bounce frequency of trapped particles in the wave electrostatic potential.

Later O'Neil [2] used the exact equation of motion for resonant particles and obtained a similar result but he showed that the oscillations disappear by phase mixing after a time longer than the bounce period.

More recently Laval, Pellat and Roux (3-4), starting from Al'tshul and Karpman's theory, made a more accurate calculation keeping higher order terms. They found that wave damping still exists for any amplitude if the phase velocity is greater than the thermal velocity ( $v_{\text{phase}}/v_{\text{thermal}} \sim 4$ ). This result was clarified in ref.4 where it is shown that the distribution function was perturbed to a larger extent than was assumed in previous theories and that non resonant particles were responsible for the damping.

These theoretical treatments are done by averaging over



space coordinates. Experimentally, however, the wave is launched at  $X = 0$  and evolution of the wave as a function of  $X$  is observed. This more realistic problem has been solved especially by Jablon [5] and by Lee and Schmidt [6] using the preceding models. As expected they found that the wave oscillates in space with a characteristic length (bounce length)  $L_b = v_\phi \frac{2\pi}{k} \sqrt{\frac{m}{e\phi}} = v_\phi \frac{2\pi}{\omega}$  where  $v_\phi$  is the phase velocity,  $k$  the wave number,  $\phi$  the wave potential and  $\omega$  the bounce frequency. The first experimental observation of these effects was made by Malmberg, Wharton and O'Neil [7,8].

Nevertheless none of the experimental results gives precise data concerning the spatial evolution of the distribution function. Then, in collaboration with Laval, Pellat and Roux and using O'Neil's calculation technique we have tackled this problem.

#### THEORY

On a plasma column a large amplitude Langmuir wave is excited at  $X = 0$  and propagates along the  $X > 0$  direction with a very small damping. Some electrons (trapped electrons) oscillate back and forth in the troughs of the wave and neighboring electron trajectories (untrapped electrons) are also very much modified. This interaction creates a deformation of the instantaneous and time averaged distribution functions.

The Vlasov equation is exactly solved following particle trajectories.

The oscillating wave potential in the one dimension plasma is assumed to vary as

$$\phi(x,t) = \phi_0 Y(x) \cos(\omega t - kx)$$

where  $Y(x)$  is the Heaviside function,  $\phi_0$  is a constant and, therefore, the calculation is only valid for a weakly damped wave.

Let  $V_0$  be the initial velocity of a particle ( $x < 0$ ). Suppose  $V$  to be the velocity of a particle at time  $t$  and position  $X$ ; Liouville's theorem yields

$$F(X, V, t) = F_0[V_0(X, V, t)]$$

where  $V_0(X, V, t)$  is governed by the equation of motion of a particle in the potential  $\varphi(X, t)$ .

If we work in the wave frame, the equation of motion can be written

$$m \frac{d^2 x}{dt^2} = -e k \varphi_0 \sin kx$$

where :

$$x = X - \frac{\omega}{k} t$$

This equation can be exactly solved [3] in terms of elliptic functions. The solution depends on the value of the parameter  $\beta$  :

$$\beta = \sqrt{\frac{k^2 v^2}{4\omega^2} + \sin^2 \frac{kx_0}{2}} = \sqrt{\frac{k^2 v^2}{4\omega^2} + \sin^2 \frac{kx_0}{2}}$$

where  $v = V - \frac{\omega}{k}$ ,  $x_0 = -\frac{\omega}{k} t_0$  and  $t_0$  is the time when the particle begins to interact with the electric field ( $X = 0$ ).

Particles satisfying  $\beta < 1$  are trapped. Their position and velocity are given by

$$\begin{cases} \sin \frac{kx}{2} = \beta \operatorname{sn}(\alpha t + \psi, \beta) \\ v = \frac{2\omega}{k} \operatorname{cn}(\alpha t + \psi, \beta) \end{cases}$$

For particles satisfying  $\beta > 1$  (untrapped particles)

$$\begin{cases} x = \pm \frac{2}{k} \operatorname{am}(\alpha/\beta t + \psi, \frac{1}{\beta}) \\ v = \pm \frac{2\omega/\beta}{k} \operatorname{dn}(\alpha/\beta t + \psi, \frac{1}{\beta}) \end{cases}$$

where  $\psi$  is an integrating constant.

The inversion of these relations leads to transcendental equations and, then, the solution must be determined by a numerical calculation. In this way,  $F(X, V, t)$  can be obtained.

Results concerning an initially Maxwellian function are presented in fig. 1. They show the contribution of the trapped and of the untrapped particles to the instantaneous distribution function for various times. As expected the main deformation is located near the phase velocity of the wave and its width in energy is  $\Delta U \approx \frac{\omega}{\lambda} \phi_0$ . It is important to notice the significant contribution of the untrapped particles.

This instantaneous distribution function  $F(X, V, t)$  oscillates at the frequency  $\frac{\omega}{2\pi}$ . Then it is interesting to determine the Fourier components of  $F(X=X_1, V=V_1, t)$ , where  $X_1$  and  $V_1$  have given value (fig. II). Analysis is made using a numerical calculation [9]. The spectrum consists of harmonics of the wave frequency  $\frac{\omega}{2\pi}$ . Table I presents results obtained with  $\frac{X_1}{L_b} = 0.43$  and several values of  $\frac{V_1}{V_{th}}$ . The number of harmonics increases as  $\frac{V_1}{V_{th}}$  decreases, it is maximum for  $\frac{V_1}{V_{th}} = 5$  which corresponds to the phase velocity of the wave and, it decreases as  $\frac{V_1}{V_{th}}$  tends to zero.

TABLE I

| $\frac{V_1}{V_{th}}$ | $\eta_2 = \frac{\text{Fond. ampl.}}{\text{Harm. 2 ampl.}}$ | $\eta_3$ | $\eta_4$ | $\eta_5$ |
|----------------------|--|----------|----------|----------|
| 3                    | 0.35   | 0.11     | 0.02     | 0.005    |
| 4                    | 0.43   | 0.22     | 0.10     | 0.05     |
| 4.5                  | 0.44   | 0.43     | 0.36     | 0.27     |
| 5                    | 0.75   | 0.57     | 0.44     | 0.33     |
| 5.5                  | 0.59   | 0.30     | 0.16     | 0.09     |
| 6                    | 0.63   | 0.22     | 0.03     | 0.01     |
| 10                   | 0.08   | 0.005    | 0        | 0        |

Parameters

$$\frac{\omega}{kV_{th}} = 5 \quad \frac{X_1}{L_b} = 0.43 \quad \frac{\omega}{2\alpha} = 7.5$$

On the other hand (table II) we have checked that, as expected, the harmonic generation increases as  $\varphi_0$  is augmented

TABLE II

| $\frac{\omega}{2\alpha}$ | $\eta_2$ | $\eta_3$ | $\eta_4$ | $\eta_5$ |
|--------------------------|----------|----------|----------|----------|
| 3.5                      | 0.63     | 0.47     | 0.5      | 0.45     |
| 15                       | 0.1      | 0.017    | 0        | 0        |

Parameters

$$\frac{\omega}{kV_{th}} = 5, \quad X_1 = 0.93L_b \left( \frac{\omega}{2\alpha} = 3.5 \right), \quad \frac{V_1}{V_{th}} = 4$$

Fig. III shows the time averaged distribution function  $\langle F(X=X_1, V, t) \rangle_t$  which appears at various  $X_1$  positions. The deformation is centred in the neighborhood of the phase velocity of the wave and can create a bump in the high energy tail of the distribution. In addition many accidents may appear in the lower energy region, due to untrapped particles.

EXPERIMENT

The apparatus used for this experiment has been described previously [10]. For the present purpose it may be considered simply as a device that produces a 65 cm long uniform column of collisionless plasma ( $N_e \sim 3.10^8 \text{ cm}^{-3}$ ,  $T_e \sim 2 \text{ eV}$ ). The plasma is immersed in a strong longitudinal magnetic field. The unperturbed electron velocity distribution measured by a velocity analyzer located at one end of the column is a truncated Maxwellian,

A large amplitude plasma wave is launched at the position  $X = 0$  by means of a Langmuir probe. A second longitudinally movable

probe is used to detect the wave amplitude and to measure the wave number. The electrostatic multi-grid analyzer measures the total (time independent and oscillating) current and, by using an electronic differentiating technique, we deduce the corresponding distribution functions.

Our previous measurements concerning trapping effects have been described elsewhere [11]. We observe the appearance of sidebands; the wave and the sidebands were found to oscillate in space and confirmed those given by Wharton, Malmberg and O'Neil [8].

Up to now no complete results concerning the oscillating distribution function  $F(X = X_1, v, t)$  have been obtained. Using the averaging technique described in another paper [12], preliminary observations have been done. However it is impossible to conclude (ballistic terms and plasma potential oscillations affect the result).

Our experimental observation agree with the Fourier analysis of this function. For experimental simplicity the verification is performed on the oscillating current

$J_1(X=X_1, v=v_1, t) = q \int_{v_1}^{\infty} f(X=X_1, v, t) v dv$ , but this does not affect the result. Fig. IV shows Fourier analysis of  $J_1$  for two values of the parameter  $\frac{v_1}{v_{th}}$ . As predicted by theory the harmonic generation is greater for  $\frac{v_1}{v_{th}} = 2$  ( $\frac{\omega}{Kv_{th}} \sim 2$ ) than for  $\frac{v_1}{v_{th}} = 0$ . Nevertheless the detected signal is weak and does not permit to observe many harmonics. In addition we observe the generation of new harmonics as  $\varphi_0$  is increased.

Experimental observations of the averaged distribution function  $\langle F(X = X_1, v, t) \rangle_t$  have been made. Fig. V shows  $\langle F(X_1, v, t) \rangle_t$  at various positions  $X_1$ . On fig. VI we have shown the influence of the wave power on  $\langle F(X_1, v, t) \rangle_t$  for a fixed distance  $X_1$ . On the same diagram we have drawn corresponding theoretical curves in such a way that the two "plateau" fit. The curves correctly coincide as long as  $\varphi_0$  is not too large. In particular a bump can be observed. On both curves nevertheless we have never observed accidents for particles such as  $\frac{Kv}{\omega} < 1$

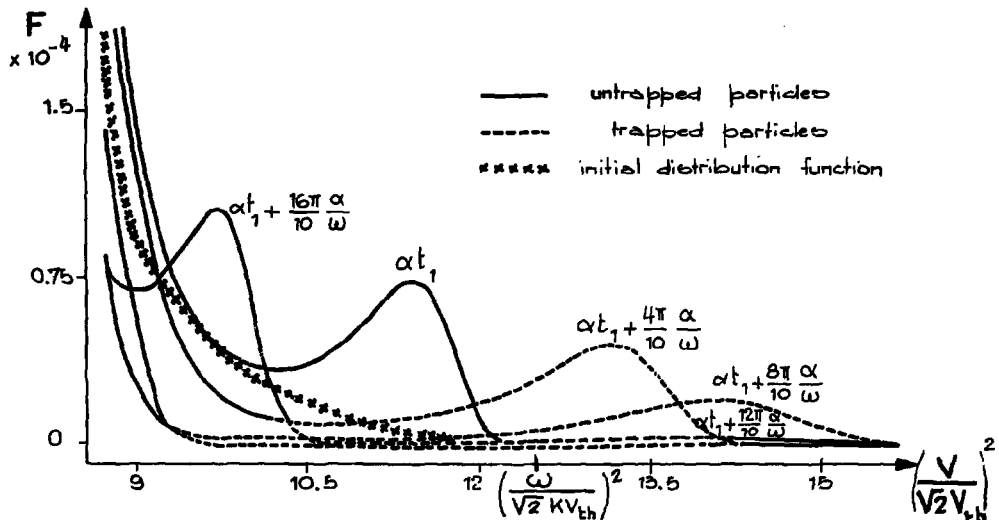
CONCLUSION

In conclusion the experimental observations reported here fairly agree with theory. They allow us to explain the deformation of the distribution function and especially to point out the active role played by the untrapped particles in the phenomena.

REFERENCES

- [1] L.M. Al'tshul and V.I. Karpman, Zh. Eksp. Teor. Fiz, 42, 515 (1965) , [Sov. Phys. JETP 22, 361 (1966)]
- [2] T.M. O'Neil, Phys. Fluids 8, 2255 (1965)
- [3] G. Laval, R. Pellat and A. Roux, Phys. Letters 29A, 159 (1969).
- [4] G. Laval, R. Pellat and A. Roux, Ninth International Conference on Phenomena in ionized gases, Bucharest (1969)
- [5] C. Jablon, EUR-CEA-FC Report 509, (1969).
- [6] A. Lee and C. Schmidt, Phys. Fluids, 13, 10,2546 (1970)
- [7] J.H. Malmberg, and C.B. Wharton, Phys. Rev. Letters, 19, 775 (1967)
- [8] C.B. Wharton, J.H. Malmberg and T.M. O'Neil, Phys. Fluids 11, 8. 1761 (1968)
- [9] F. Perceval, CEA Report R 3740 (1969)
- [10] J. Olivain, EUR-CEA, Report FC 602 (1971)
- [11] M. Guillemot, G. Matthieussent, J. Olivain, F. Perceval et A. Quemeneur, C.R. Acad. Sc. Paris, 272, (1971)
- [12] P. Demulière, M. Guillemot, J. Olivain, F. Perceval, and A. Quemeneur, Risø (1971)

- Fig 1- LARGE AMPLITUDE WAVE INTERACTION WITH A PLASMA  
THEORETICAL INSTANTANEOUS DISTRIBUTION FUNCTION AT VARIOUS MOMENTS



DIMENSIONLESS PARAMETERS:

$\omega / k V_{th} = 5$      $\omega / \alpha = 18$      $x / L_b = 0.4$

Where:  $\omega$ : wave pulsation

$k$ : wave number     $x$ : distance

$V_{th}$ : thermal velocity

$\alpha$ :  $\frac{1}{2\pi} k \sqrt{\frac{e\Phi}{m}}$  bounce frequency     $L_b = \frac{2\pi \omega}{\alpha k}$ : bounce length

FIG. II. INSTANTANENOUS DISTRIBUTION FUNCTIONS  $F(x-x_1, v-v_1, t)$  FOR SEVERAL VELOCITIES  $v_1$  AND ASSOCIATED FOURIER SPECTRUM

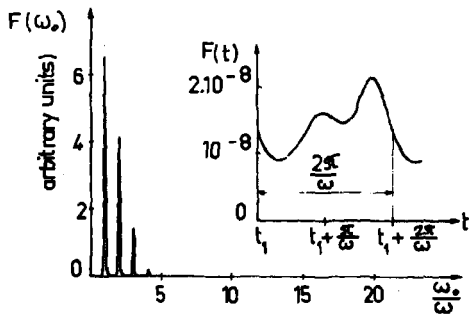
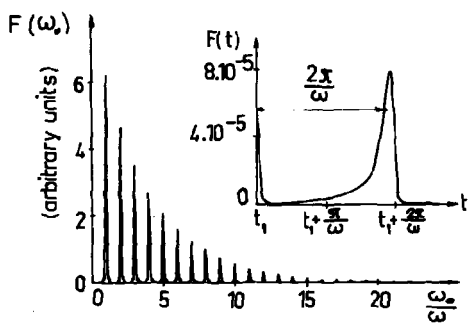
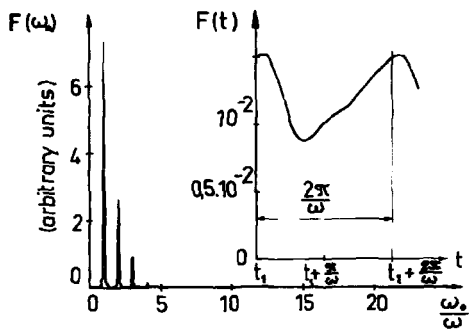
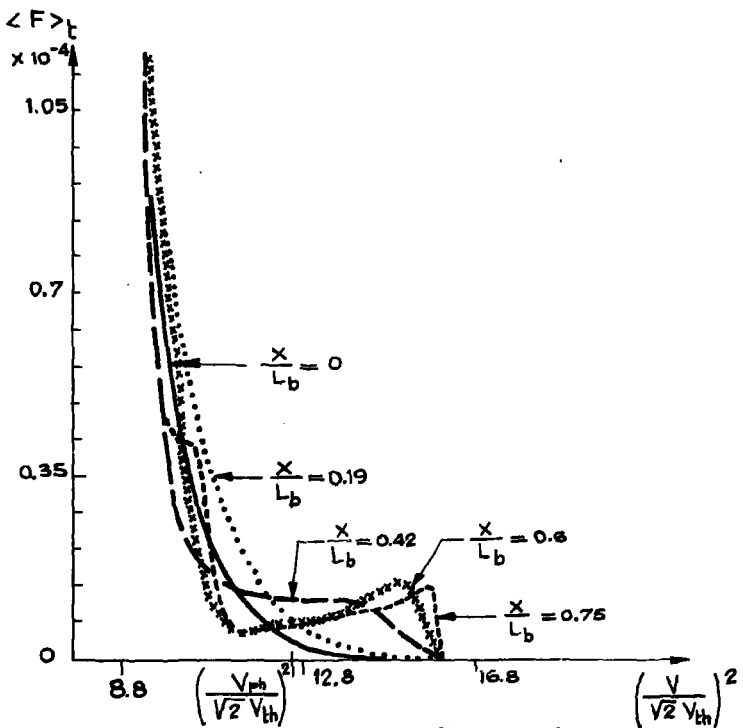




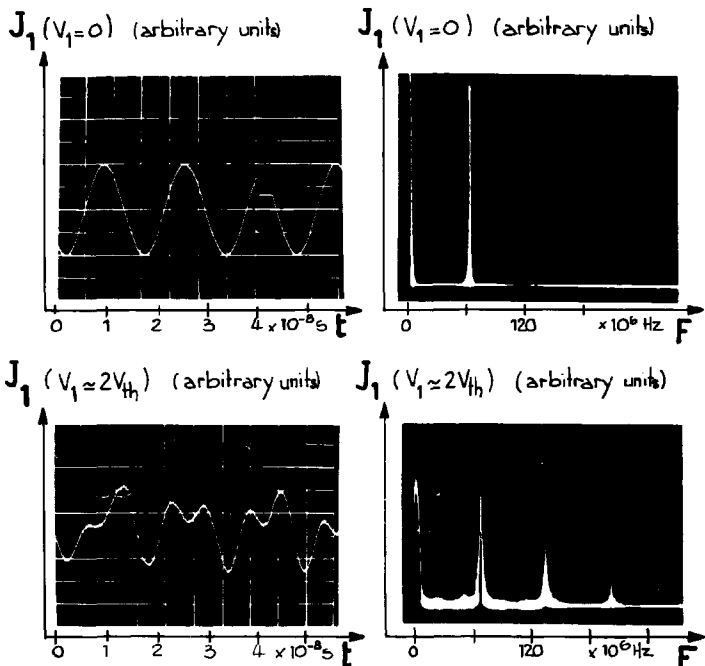
FIG. III. - LARGE AMPLITUDE WAVE INTERACTION WITH A PLASMA

Theoretical change of the time independent distribution function for several interacting lengths.



DIMENSIONLESS PARAMETERS:  $\frac{\omega}{kV_{th}} = 5$   $\frac{\omega}{\alpha} = 15$   
 where  $\omega$ : wave pulsation  $k$ : wave number  
 $x$ : distance  $V_{th}$ : Thermal velocity  
 $\alpha = \frac{1}{2\pi} k \sqrt{\frac{eE_0}{m}}$ : bounce frequency  $V_{ph} = \frac{\omega}{k}$   
 $L_b = \frac{2\pi}{\alpha} \frac{\omega}{k}$ : bounce length

Fig. IV - VARIATION OF THE OSCILLATING CURRENT HARMONIC GENERATION VS ANALYSE POTENTIAL



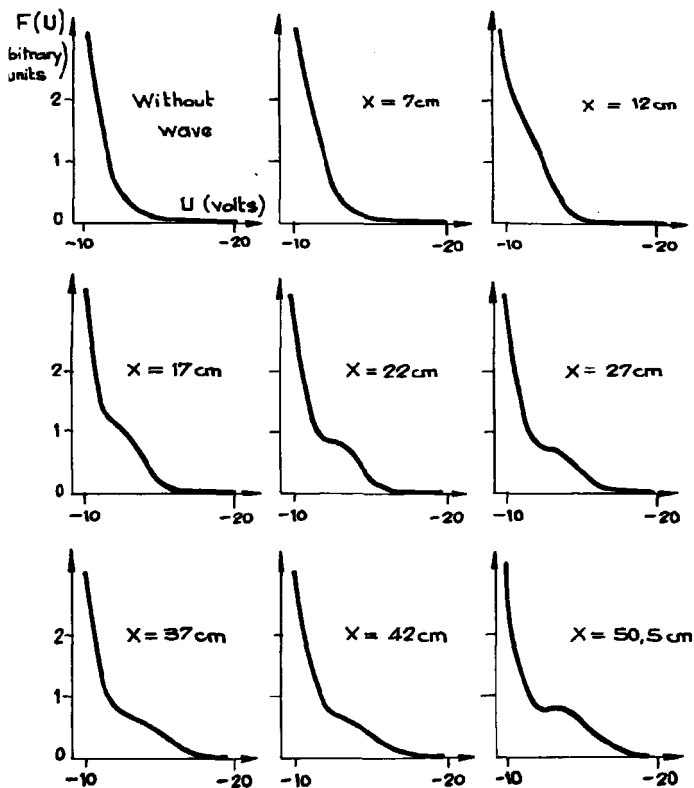
EXPERIMENTAL CONDITIONS :

$$J_1(V) = q \int_{V_1}^{\infty} F(V) dv$$

Argon plasma       $n_0 = 6.5 \times 10^8 \text{ e/cm}^3$        $T_e \approx 2\text{eV}$   
 $B_0 = 1.5 \text{ kG}$        $F = 60 \text{ MHz}$        $V_{th} \approx 2\text{V}$   
 $z$  : distance between the emitter and the receiver = 48 cm

# .FIG. V - LARGE AMPLITUDE WAVE INTERACTION WITH A PLASMA

Change of the time independent distribution function for several interacting lengths.



Experimental conditions:

Xénon

$T_e \approx 1,5\text{ eV}$

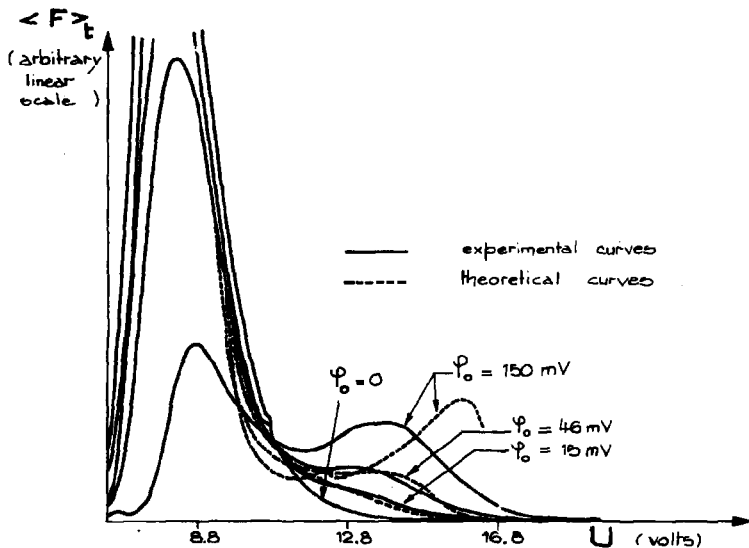
$n_e = 1,5 \cdot 10^8 \text{ cm}^{-3}$

$F = 40\text{ MHz}$

$\phi_0 = 50\text{ mV}$

$P_0 \sim 10^{-6} \text{ torr}$

Fig. VI — LARGE AMPLITUDE WAVE INTERACTION WITH A PLASMA  
 CHANGE OF THE TIME INDEPENDANT DISTRIBUTION FUNCTION FOR VARIOUS WAVE AMPLITUDES



EXPERIMENTAL CONDITIONS

$$n_e = 2.7 \cdot 10^7 \text{ cm}^{-3}$$

$$T_e = 1 \text{ eV}$$

$$\frac{\omega}{2\pi} = 50 \text{ MHz}$$

$$\lambda = 4.15 \text{ cm}$$

$$X = 27 \text{ cm}$$

$$B_0 = 1.5 \text{ kG}$$

EXCHANGE OF ENERGY BETWEEN LARGE-AMPLITUDE  
PLASMA WAVES AND THE ELECTRON ENERGY DISTRIBUTION

E.P. Barbian and B. Jurgens

FOM-Instituut voor Atoom- en Molecuulfysica, Amsterdam / Wgm., The Netherlands

EURATOM-FOM Association Contract

ABSTRACT

Particles trapped in a large amplitude electrostatic wave cause the growth of sidebands next to the excitation frequency. The displacement of the sidebands starts from a threshold value for the electric field and is proportional to the square root of the large wave amplitude.

If instead of one large monochromatic wave two waves with a small frequency difference are excited, the sidebands become broadened and show a discrete structure.

INTRODUCTION

Longitudinal electron plasma waves can be propagated in a plasma column below the electron plasma frequency. The density of the plasma can be chosen in the way that the phase velocity of the plasma waves  $v_p$  reaches a value several times the mean velocity of the Maxwellian-like electron energy distribution. In this density region ( $n \approx 10^8 \text{ cm}^{-3}$ ) the plasma is not dominated by Coulomb collisions.

The plasma waves interact with the electron distribution strongly at small amplitudes if the phase velocity reaches into the main bulk of the electrons ( $v_p/v_t \approx 3$ ). A very strong Landau damping is also observed for large wave amplitudes at much higher phase velocities, because then again a large number of particles becomes involved [1,2].

The electrons which become trapped in the propagating wave start to bounce in the potential trough of the wave to first approximation with a frequency  $\Omega = [qEk/m]^2$ , where E is the wave field amplitude and k the wave number [3]. The frequency of this oscillation is nearly constant during several periods at least for the particles at the bottom of the trough, which therefore move coherently and stream-like similar to a bunched beam of harmonic oscillators through the plasma. The observed growth of sidebands to the frequency at the large amplitude wave is theoretically explained by Kruer, Dawson and Sudan [4] as a kind of two-stream instability and is called a trapped particle instability or sideband instability. The broadening of the frequency spectrum and the existence of sidebands is also described by a theory of Eldridge [5], not involving an instability and assuming the driving wave to be always dominant in the spectrum.

A related fundamental non-linear phenomenon of more subtle kind is the plasma wave echo, as it was demonstrated by Mainberg, Wharton, Gould and O'Neil [6]. The plasma wave echo can be observed after the Landau damping of the macroscopic wave field and the accompanying density disturbances. Then the evolution of the undamped oscillations of the electron phase space distribution can be reversed and a macroscopic field can be reestablished.

The observation of sidebands and of echo phenomena is possible at moderate large wave amplitudes. The situation changes if very strong fields are applied to the plasma. Then low frequency instabilities are generated by the parametric action of the field. This causes a randomization of phases and a strong decay of wave fields. This effect may however be used for the purpose of electron heating [7].

#### APPARATUS

The experimental set-up consists out of a single-ended Q-machine of a length of 90 cm. Cesium is ionized at a plate of 2.2 cm diameter and the parameters were chosen to get an electron-rich sheath. The plasma is guided by a magnetic field of 1500 G and the density decreases in axial direction to a  $1/e$ -value after about the length of the apparatus. The dispersion for the waves is measured by an interferometer technique. The density region used was between  $10^7$  and  $10^8 \text{ cm}^{-3}$ . The large amplitude waves were excited by probes or by the collector plate.

## THE SIDEBAND INSTABILITY

In a computer experiment Kruer and Dawson [4] showed that the large amplitude wave decays strongly when the sideband amplitude becomes comparable in magnitude to the decaying wave and the unstable sideband modes saturate.

In Fig. 1 we find back this general characteristic. A 5 Volt sinusoidal signal was applied at  $z = 0$ . The upper signal shows the large amplitude wave. After a distance of about 20 cm a bouncing effect is superimposed on the decaying amplitude. The observed bouncing length is in agreement with the length  $L$

$$L = (du/dk)(1/\Omega) \quad (1)$$

calculated from the independently determined wave velocity  $du/dk$  and the bouncing frequency  $\Omega$ . On the lower curve in Fig. 1 the amplitude value (within 1 MHz band limits) of the red sideband is shown. Fluctuations near  $z = 60$  cm are due to standing wave effects in front of the end plate ( $z = 60$  cm).

The maximum amplitude of the red and blue sideband is separated from the excitation frequency by a frequency difference

$$\Omega = \frac{1}{2\pi} (ek/m)^{\frac{1}{2}} E_z^{\frac{1}{2}} \quad (2)$$

where  $E_z$  is the amplitude of the wave field in the plasma. The blue satellite is often influenced by Landau damping because waves with higher  $k$ -values reach into the main bulk of the distribution due to their smaller phase velocity.

In Fig. 2 the dependence on  $\sqrt{E}$  of the separation of a red sideband is shown. Similar observations had been reported by several authors [3,8]. The measured values in Fig. 2 were taken by an antenna placed 30 cm away from the exciting probe in the direction of the drifting ions. A maximum value of 20 MHz for  $\Omega$  was observed when a 35 MHz signal of 4 Volt was applied across a 50  $\Omega$  terminator at the probe. For greater amplitudes the sideband approaches a saturation level both for  $\Omega$  as well as for the amplitude of the sideband. This is mainly due to the strong decay of the large wave amplitude similar to the numerical results of Kruer and Dawson [4] and besides that, energy is fed into increasing amplitudes of low

frequency oscillations in the ion acoustic region. In this strong excitation region an additional broad frequency band of secondary waves is created in the whole region below the excitation frequency.

The field strength of a wave propagating along the plasma column can be estimated if the coupling factor between the probes and the plasma is known. This factor was determined to be  $5 \times 10^{-3}$  in power (37 dB) by measuring the attenuation of two identical probes when a small amplitude wave is transmitted through the plasma without damping between both probes. The power  $W$ , available for the plasma will be

$$W = 5 \times 10^{-3} \frac{1}{2} \frac{E^2}{R} \quad (3)$$

and is put into a volume of the plasma cross section 0 times the group velocity  $v_g$  of the wave and can be transferred for one half to the field energy. We get

$$\frac{1}{2} \frac{W}{0v_g} = \frac{1}{2} \epsilon_0 \frac{d}{d\omega} (\omega K) E_z^2 \quad (4)$$

where

$$K = 1 + p^2/k^2 - \frac{\omega_p^2}{\omega_0^2 + 3v_t^2 k^2} \quad (5)$$

represents the dispersion of the warm plasma column. For  $p = 1.65 \text{ cm}^{-1}$ ;  $k = 1.05 \text{ cm}^{-1}$ ;  $\omega_p = 410 \times 10^6 \text{ s}^{-1}$ ;  $\omega_0 = 220 \times 10^6 \text{ s}^{-1}$  and  $v_t = 3 \times 10^7 \text{ cm s}^{-1}$  we arrive at an equivalent for  $E_z$  of

$$E_z = 3.3 \times 10^{-2} \text{ V cm}^{-1} \text{ for } E = 1 \text{ V} \quad (6)$$

This value might be checked by calculating  $\Omega$  together with (2). We arrive at  $\Omega = 7.8 \text{ MHz}$  which is a reasonable value if we compare with Fig. 2.

#### THRESHOLD VALUE

By extrapolation of the linear dependence of the separation frequency versus  $\sqrt{E}$  in Fig. 2 we determine a threshold value of  $\sqrt{E} = 0.7$  or  $E = 0.84 \text{ Volt}$ . By the use of (6) we get an equivalent of  $3 \times 10^{-2} \text{ V cm}^{-1}$ .

To start with, we want to discuss this threshold value along the lines followed in the theoretical work of Kaw and Dawson [9], treating the case of a two-stream instability. Their result is restricted to excitation frequencies near to the plasma frequency and shows a strongly reduced threshold value



if the collision frequencies of the electrons  $\nu_e$  are taken into account. The threshold field should depend on  $\nu_e$  and the plasma frequency  $\omega_p$  like

$$E \geq 6^{\frac{1}{2}} \frac{m_e}{4} \left( \gamma \frac{T_e}{m_e} \right)^{\frac{1}{2}} \left( 1 + \frac{T_i}{T_e} \right)^{\frac{1}{2}} (\nu_e \omega_p)^{\frac{1}{2}} \quad (7)$$

If we take  $\nu_e = 2.1 \times 10^4 \text{ s}^{-1}$  from Spitzer's formula for  $n = 5.3 \times 10^7 \text{ cm}^{-3}$  and  $T = 2000 \text{ K}$ , use  $\gamma = 3$  and put  $T_e = T_i$  we arrive at

$$E_0 = 1.7 \times 10^{-2} \text{ V cm}^{-1}$$

which is about the value determined together with (6).

Though the use of (7) may only give a rough estimation, one can also follow the arguments of Perkins and Flick [10] and replace the collision frequency  $\nu_e$  in (7) by similar terms taking into account the inverse time needed for passage through an instability region or the time connected with randomization in connection with Landau-damping.

#### EXCITATION WITH TWO FREQUENCIES

Waves are now propagated in the reverse direction and interact with the electron distribution which was reflected back at the sheath of the floating collector plate. Then a striking difference in the sideband excitation can be obtained, depending on the case if one monochromatic wave or two waves of slightly different frequencies are used. The two excitation peaks, still visible at a distance of 40 cm away from the excitation region (upper curve) are 0.1 MHz apart from each other which results after 10 wavelengths in a phase difference of only 3%.

Fig. 3 demonstrates that in the case of a double frequency excitation the sidebands were obtained, but not in the case of the single frequency excitation (lower curve). Both curves were taken at the same plasma conditions. For excitation the collector plate was used which makes no difference with the excitation on a probe. The upper curve shows a red and a blue sideband and the separation is again proportional to  $\sqrt{E}$  and a threshold value is existing as well. In the case of monochromatic excitation the signal is broadened to several 100 kHz.

Fig. 4 shows the development of the sideband when different amplitudes are applied to the collector plate. The spectra are now composed out of equally spaced discrete peaks and have an envelope which has the typical shape of the sidebands. This is furthermore illustrated by Fig. 5, where the frequency difference between two excitation peaks was varied. The applied voltage is 5 Volt at  $f_0 = 30$  MHz. The waves were excited with a probe at some distance in front of the reflecting end plate.

We consider this discrete spectrum to be due to high order spatial wave echos. The selection rules given by Malmberg, Wharton, Gould and O'Neill [11]

$$f_3 = mf_2 - nf_1$$

for  $mf_2 > nf_1$  (where  $f_2, f_1$  belong to continuously excited waves and  $m, n$  are integers) are fulfilled in our case. The excitation of the two waves took place at the same probe and therefore the excitation of the "echo" peaks is symmetric.

Fig. 6 shows the spatial development of the excited spectrum when  $f_{01} = 29.8$  MHz and  $f_{02} = 30.2$  MHz. A 5 Volt amplitude was applied on a transmitter probe. Higher order peaks develop at greater distances from the excitation region, which is in general agreement with the spatial dependence of wave echos. Landau damping causes on the upper side of the spectrum a decrease of the higher order wave amplitudes.

#### ACKNOWLEDGEMENTS

The authors want to thank Dr. H.J. Hopman and Dr. J. Brownell for valuable discussions.

This work was performed as a part of the research program of the association agreement of Euratom and the "Stichting voor Fundamenteel Onderzoek der Materie" (FOM) with financial support from the "Nederlandse Organisatie voor Zuiver-Wetenschappelijk Onderzoek" (ZWO) and Euratom.

REFERENCES

- [1] J.M. Dawson and R. Shanny, *Phys.Fluids* 11, 1506 (1968).
- [2] T. Matitti, E.P. Barbian and B. Jurgens, Proc. 4th Europ.Conf. on Controlled Fusion and Plasma Phys., Rome (1970).
- [3] J.H. Malmberg, C.B. Wharton and T.M. O'Neil, *Phys.Fluids* 11, 1761 (1968).
- [4] W.L. Kruer, J.M. Dawson and R.N. Sudan, *Phys.Rev.Letters* 23, 838 (1969).  
W.L. Kruer and J.M. Dawson, MATT-768, June 1970.
- [5] O. Eldridge, *Phys.Fluids* 13, 738 (1970).
- [6] J.H. Malmberg, C.B. Wharton, R.W. Gould and T.M. O'Neil, *Phys.Fluids* 11, 1147 (1968).
- [7] E.P. Barbian, T. Matitti and B. Jurgens, Proc. 4th Europ.Conf. on Controlled Fusion and Plasma Phys., Rome (1970).
- [8] R.N. Franklin, G.J. Smith, S.M. Hamberger and G. Lampis, 4th Europ.Conf. on Controlled Fusion and Plasma Phys., Rome (1970).
- [9] P.K. Kaw and J.M. Dawson, *Phys.Fluids* 12, 2586 (1969).
- [10] F.W. Perkins and J. Flick, MATT-833, March 1971.
- [11] J.H. Malmberg, C.B. Wharton, R.W. Gould and T.M. O'Neil, *Phys.Fluids* 11, 1147 (1968).

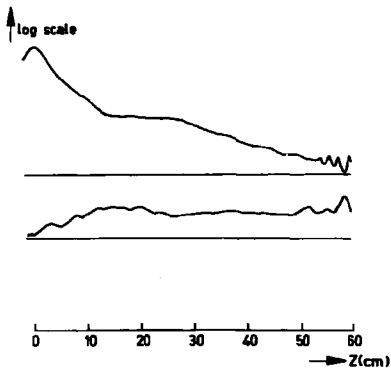


Fig. 1 - Spatial decay of the large amplitude wave (upper curve) and growth of the lower sideband (lower curve);  $f_0 = 35$  MHz;  $k = 1.05$ ;  $\omega_0/\omega_p = 0.55$ .

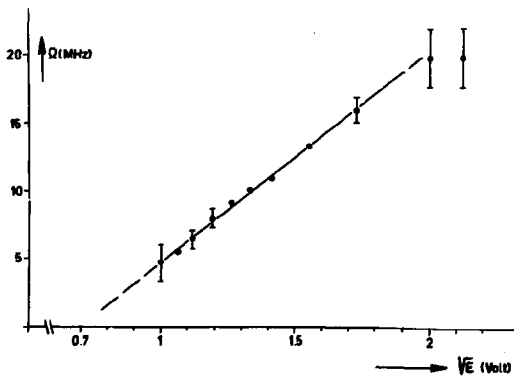


Fig. 2 - Frequency separation  $Q$  vs. the square root of the applied signal amplitude  $f_0 = 35$  MHz;  $k = 1.05$ ;  $\omega/\omega_p = 0.55$ .

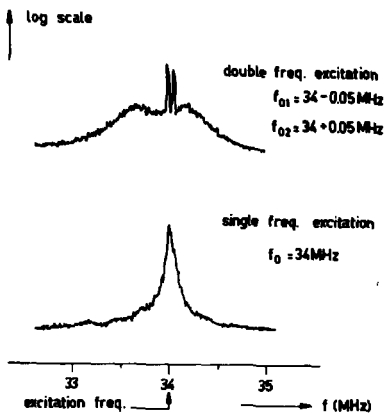


Fig. 3 - Compare double and single frequency excitation observed at  $z = 40 \text{ cm}$ .

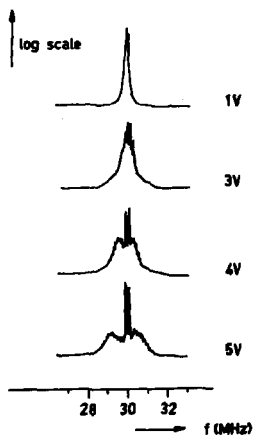


Fig. 4 - Double frequency excitation, 100 kHz separation at  $f_0 = 30 \text{ MHz}$ .  
Variation of the signal amplitude.

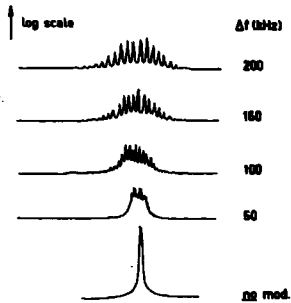


Fig. 5 - Variation of the frequency separation observed at  $z = 35$  cm,  $E = 5$  Volt.

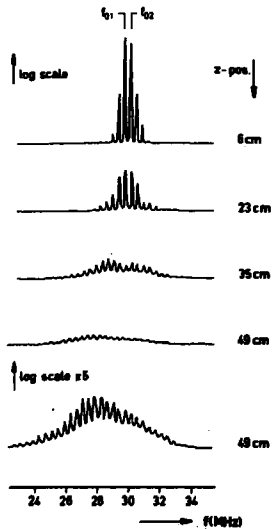


Fig. 6 - Spatial development of the spectrum with  $f_{o1} = 29.8$  MHz;  $f_{o2} = 30.2$  MHz;  $E = 5$  Volt.



Test Wave Amplification and Instability  
Caused by Electron Trapping

R.N. Franklin\*, S.M. Hamberger, H. Ikezi<sup>f</sup>, G. Lampis, G.J. Smith\*

UKAEA Culham Laboratory, Abingdon, Berkshire, England

Abstract

When the electric field of an electron plasma wave is sufficiently large, electrons are trapped by, and oscillate in, the potential wells of the wave. The paper shows that sidebands to the main wave are produced by a resonance between the trapped electrons and small amplitude electron waves propagating in the plasma (e.g. as noise or as a test wave).

The frequency differences between the large amplitude wave and the side-bands are shown to be consistent with the theory. The growth rates of the sideband and of a test wave are shown to be the same.

This paper describes some experiments on the high frequency propagation properties, of a one-dimensional, collisionless plasma perturbed by a single, coherent, finite amplitude electron plasma wave. It is known that the dispersion relation for electrostatic waves is modified by the existence of a class of resonant electrons which, because they move with mean velocities close to the phase velocity of the wave,  $v_{\phi} = \omega_0/k_0$ , become trapped in the potential well which moves with the wave.

For example<sup>1</sup>, it can be shown that, provided the fraction of trapped electrons is not too high, a small amplitude test wave  $(\omega, k)$  which satisfies the dispersion relation,  $\epsilon(\omega, k) = 0$ , will grow when the following resonance condition is satisfied:

$$\omega - kv_{\phi} \approx \pm \sqrt{2N+1} \omega_B \quad \dots (1)$$

where  $\omega_B = k_0 \left( \frac{e\phi_0}{m} \right)^{1/2}$  is the characteristic oscillation frequency of the electrons trapped in the potential well of the wave,  $\phi_0$  is the amplitude, and  $e, m$  the electronic charge and mass.  $N$  is a non-negative integer. The condition  $N=0$  corresponds to a simple resonance between the test wave and the Doppler-shifted frequency of oscillation of the trapped particles, and has also been derived by others<sup>2,3</sup>.

In an actual experiment the frequencies  $\omega$  may, provided their growth rate is sufficiently large, appear in the frequency



spectrum in the neighbourhood of the original (carrier) wave  $\omega_0$ . Such 'side-bands' were first reported by Wharton et al<sup>7</sup>, who found their frequency displacement  $\Delta\omega = |\omega - \omega_0|$  to be given by

$$\Delta\omega = \omega_B. \quad \dots (2)$$

Qualitatively similar effects have also been seen by others both in laboratory<sup>7</sup> and computer simulation<sup>8,9</sup> experiments, although the relation (2) did not necessarily hold. Recently Ikezi et al<sup>10</sup> have demonstrated that equation (1) provides a good description of the side-band frequencies generated by ions trapped in finite amplitude ion waves.

We show here that equation (1) in fact holds also in the case of electron waves; that the 'side-bands' are propagating electron waves which grow along the column from the initial noise level with the same amplification experienced by a test wave at the same frequency; that the phenomenon is due to the existence of trapped electrons and can be eliminated by preventing trapping from occurring; and that the relation (2) is valid only for rather special dispersion conditions which were satisfied in reference (6).

Our experiments were conducted in a single ended, thermally ionized Na plasma column, diameter 2.5 cm, length 80 cm, density  $\sim 3 \times 10^7 \text{ cm}^{-3}$  ( $\omega_{pe}/2\pi \sim 30 - 60 \text{ MHz}$ ) and uniform to within 1% over its length, confined in a uniform magnetic field  $\geq 2 \text{ kG}$ . The waves were launched and detected in the usual way, using either thin wire probes or the cold end-plate as antennae, and the linear plasma dispersion properties measured as described in the accompanying paper<sup>11</sup> using very small amplitude waves. The absolute amplitude of the waves  $\phi_0$  was measured using a probe with very high input impedance ( $\sim 1 \text{ M}\Omega$ ) matched to the  $50 \Omega$  line by a PET amplifier close to the probe tip<sup>12</sup>.

In general we find that for high phase velocities of the carrier two lower and one upper side-band appear, but for frequencies  $\geq \omega_{pe}$  only one lower side-band, with appreciable frequency spread, is seen. For example the upper portion of Fig.1(a) shows the spectrum detected by a receiving probe 20 cm from the exciter, exhibiting clearly two lower and one upper side-band. The appropriate dispersion curve is shown in the lower part of Fig.1(b) with the same frequency scale. From this diagram we can find the appropriate value of  $\omega - kv_0$  for the two lower side-band maxima; their ratio is  $1:1.7 \pm 0.1$ , in good agreement with the ratio  $1:\sqrt{3}$  according to Eq. (1) if they correspond to  $N = 0, 1$  respectively.

A more quantitative comparison for  $N=0$  (when only one lower side-band appears) is shown in Fig.2, where the frequency shift  $\Delta\omega = \omega_0 - \omega$  is plotted against  $\omega_B$ ; in Fig.2(a)  $\omega_B$  is varied by changing the amplitude  $\phi_0$  at constant carrier frequency  $\omega_0$ , and in Fig.2(b) the amplitude was fixed and the frequency  $\omega_0$  changed, thus varying  $v_0$  over a wide range. The solid lines are calculated according to (1) and the known linear dispersion curve. The line  $\Delta\omega = \omega_B$  is shown dashed for comparison. The solid line clearly provides a much closer agreement with both sets of data than the line  $\Delta\omega = \omega_B$ . In fact, from (1) and the

dispersion relation, it is easy to show that for  $N = 0$ ,  $\Delta\omega \ll \omega_0$ ,

$$\Delta\omega \approx \frac{\frac{\partial\omega}{\partial k}}{v_{\phi} - \frac{\partial\omega}{\partial k}} \omega_B \approx \omega_B$$

if, as in the conditions of ref. (6),  $\partial\omega/\partial k \approx 0.5 v_{\phi}$ . Thus the earlier results, though somewhat misleading, are not in conflict with these.

The amplification produced by the carrier could be measured by introducing a second, small amplitude test wave from a separate transmitter probe, and measuring its amplitude variation along the column. When the test wave frequency was in the vicinity of the observed side-band, exponential growth occurred only in the direction of the carrier. Fig.3 shows the spatial variation of amplitude of:

- (a) the carrier wave at amplitude sufficiently increased to produce the growing side-band, showing enhanced damping due to the non-linear generation of the side-band;
- (b) the same wave at very small amplitude, showing normal weak Landau damping;
- (c) the side-band signal itself, showing exponential growth along the column;
- (d) the test wave at the same frequency as the centre of the side-band.

Notice that the growth rates of (c) and (d) are the same. Thus it seems clear that the side-bands appear by amplification of some waves originally present (e.g. as noise) in the column, and are not generated directly by the non-linear currents in the wave.

The measured growth rate of the test wave as a function of frequency is compared with the side-band amplitude spectrum in Fig.4.

Fig.5 shows the variation of amplification with amplitude. The proportionality of  $k_i/k_r$  with  $\omega_B$  is similar to that found in computer simulation for the temporal growth rate<sup>a</sup>. Further, since it  $\propto \omega_0^{1/2}$ , it can clearly be distinguished from other decay instabilities, e.g. non-linear Landau damping, for which the growth rate  $\propto \omega_0^{3/2}$ .

Increasing the carrier wave amplitude also increases the range of growing frequencies: this is demonstrated in Fig.6, which shows both the increased frequency shift  $\Delta\omega$  and frequency spread  $\delta\omega$  of the side-band with increasing  $\omega_0$ . This effect can be deduced from the dispersion relation given by Kruger et al<sup>2</sup>.

To demonstrate that the origin of the above effects is indeed associated with the trapped electrons, we have measured the amplitude of the side-band in the presence of a second

perturbing wave whose frequency is far from those in the unstable region. The result, shown in Fig.7, is that as the amplitude of the second wave is increased the growth of the side-band rapidly decreases. When both waves have comparable amplitude, thus effectively destroying the potential well necessary to sustain ordered motion of the trapped electrons, the side-band completely disappears.

The phase velocity of the individual frequency components in a side-band has been measured from the space-time correlation between two receiving probes. The results show that they lie on the same dispersion curve,  $\epsilon(\omega, k) = 0$ , as for small amplitude electron plasma waves.

Finally, we should comment that the effects described here can and do occur concurrently with other non-linear effects which lead to enhanced decay, e.g. the induced decay into ion-waves<sup>14</sup>, and the resonant decay into other electron wave modes<sup>15</sup>, both of which are described elsewhere.

We are happy to acknowledge the excellent technical assistance of Mr W.J. McKay.

The research was supported jointly by the UKAEA and the Science Research Council.

References

- \* Also at Department of Engineering Science, Oxford University.  
/ On leave from Plasma Physics Institute, Nagoya, Japan.
- <sup>1</sup> K. Mima and K. Nishikawa, J. Phys. Soc. Japan, 30, 1722 (1971)
- <sup>2</sup> W.L. Kruer, J.M. Dawson and R.N. Sudan, Phys. Rev. Lett., 23, 838 (1969)
- <sup>3</sup> M.V. Goldman, Phys. Fluids, 13, 1281 (1970).
- <sup>4</sup> M.V. Goldman and H.L. Berk, Phys. Fluids, 14, 801 (1971).
- <sup>5</sup> W.M. Manheimer, Phys. Rev. A., 3, 1402 (1971).
- <sup>6</sup> C.B. Wharton, J.H. Malmberg and T.M. O'Neil, Phys. Fluids, 11, 1761 (1968)
- <sup>7</sup> R.N. Franklin, G.J. Smith, S.M. Hamberger and G. Lampis, Proc. 4th Int. Conf. on Fusion and Plasma Physics, Rome, 1970, p.158.
- <sup>8</sup> W.L. Kruer and J.M. Dawson, Phys. Fluids, 13, 2747 (1970).
- <sup>9</sup> J. Denavit and W.L. Kruer, Phys. Fluids, 14, 1782 (1971).
- <sup>10</sup> H. Ikezi, Y. Kiwamoto, K. Mima and K. Nishikawa, in Risø Report No. 250 (1971) 334-340.
- <sup>11</sup> R.N. Franklin, S.M. Hamberger, G. Lampis and G.J. Smith, in Risø Report No. 250 (1971) 144-150.
- <sup>12</sup> H. Ikezi, P.J. Barrett, R. White and A.Y. Wong (to be published in Phys. Fluids).
- <sup>13</sup> K. Gentle and A. Malein, Phys. Rev. Lett., 26, 625 (1971).
- <sup>14</sup> R.N. Franklin, S.M. Hamberger, G. Lampis, G.J. Smith, Proc. Xth Int. Conf. on Phenomena in Ionized Gases, Oxford, (1971), p.324. (to be published in Phys. Rev. Lett.)
- <sup>15</sup> R.N. Franklin, S.M. Hamberger, G. Lampis, G.J. Smith. (to be published in Phys. Letts. A.)

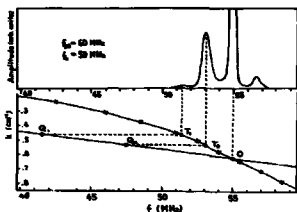


Fig.1

Upper: Carrier wave with  $N=0,1$  lower sidebands and  $N=0$  upper sideband  
 Lower: Experimental dispersion(x); straight line  $\omega_k 0 = \omega_0 k$ .  $T_0 Q_0$  represents  $\omega_B$  and  $T_1 Q_1$  represents  $\sqrt{3} \omega_B$  [see equation (1)]

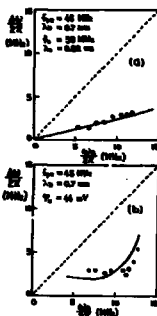


Fig.2

Observed frequency difference  $\Delta^0$  between carrier and  $N=0$  lower sideband versus  $\omega_B$ . (a) constant  $\omega_0$ , amplitude varying; (b) constant amplitude, varying  $\omega_0$ . Solid curves from Eq. (1)

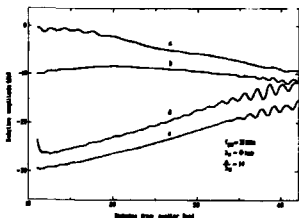


Fig.3

Spatial variation of: large amplitude wave  $\omega_0$  (a); linear wave (b); amplitude of  $N=0$  lower sideband frequency  $\sim \omega$  (c); test wave  $\omega$ , excited by probe 10 cm from that exciting large wave(d).  $\omega_0/2\pi = 34 \text{ MHz}$ ;  $\omega/2\pi = 30 \text{ MHz}$

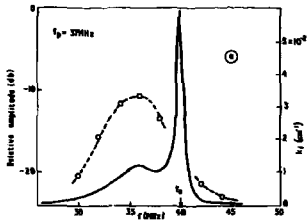


Fig. 4  
Carrier wave and  $N=0$  sideband.  
Open circles represent spatial  
growth rate of test wave for  
different frequencies  $\omega$

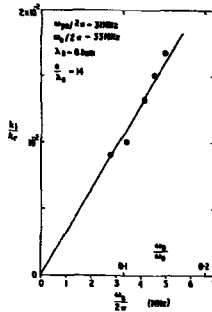


Fig. 5  
Variation of normalized  
spatial growth rate of  
 $N=0$  sideband with  $W_B$

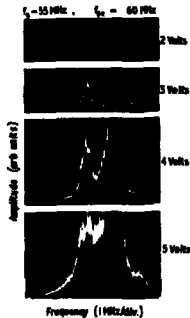


Fig. 6  
Variation in  $\delta\omega$  with  $\phi_0$   
R.M.S. voltages are those  
applied to end plates

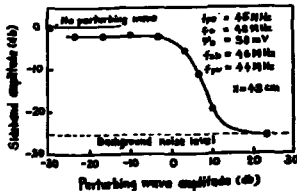


Fig. 7  
Variation of amplitude of  $N=0$   
lower sideband with amplitude  
of second perturbing wave

Trapped-Ion Instability  
in Ion-Acoustic Waves

H. Ikezi and Y. Kawanoto

Institute of Plasma Physics, Nagoya University, Nagoya, Japan

K. Mima and K. Nishikawa

Department of Physics, Kyoto University, Kyoto, Japan

Abstract

The growth of the sideband waves has been observed when a relatively large-amplitude ion-acoustic wave ( $\bar{N}/n_0 = 0.02 \sim 0.05$ ) propagates in a collisionless plasma. The structure of the frequency spectrum, growth rate and the conditions for the instability are consistent with the theory for trapped-ion instability.

Since Wharton, Malmberg and O'Neil<sup>1</sup> observed growth of sidebands of a large-amplitude electron plasma wave, the stability of a non-linear stationary wave<sup>2</sup> received considerable attention<sup>3-7</sup>. Krner, Dawson and Sudan<sup>3</sup> pointed out that the particles trapped in the potential troughs of a large-amplitude wave cause unstable sidebands.

Physically, the trapped-particle instability can be viewed as a parametric instability of upper and lower sideband waves where the coupling is being strengthened by the bouncing motion of the trapped particles. In the weak-coupling limit (i.e. when the trapped particle density is sufficiently low), the theory predicts the growth of a couple of modes specified by  $(\omega, k)$  and  $(\omega - 2\omega_0, k - 2k_0)$  when one

of the following conditions is satisfied<sup>5</sup>.

$$(i) \frac{\omega_0}{k_0} = \frac{\omega - \sqrt{2N+1} \omega_B}{k} \quad \text{and} \quad \epsilon(k, \omega) \approx 0, \quad (1a)$$

$$(ii) \frac{\omega_0}{k_0} = \frac{\omega + \sqrt{2N+1} \omega_B}{k} \quad \text{and} \quad \epsilon(k, \omega) = 0, \quad (1b)$$

$$(iii) \quad \epsilon(k, \omega) = 0 \quad \text{and} \quad \epsilon(k - 2k_0, \omega - 2\omega_0) = 0. \quad (2)$$

Here  $\omega_0$  and  $k_0$  are the frequency and wavenumber of the large-amplitude wave (hereafter to be called the carrier wave),  $\omega$  and  $k$  are those of an unstable sideband wave,  $\omega_B$  is the bounce frequency of the ions trapped in the carrier wave,  $N$  is a non-negative integer, and  $\epsilon(k, \omega)$  is the dielectric function<sup>8</sup>. The two mutually conjugate modes,  $(\omega, k)$  and  $(\omega - 2\omega_0, k - 2k_0)$  grow with the same growth rate and their amplitude ratio is given by  $|\frac{\omega_k/\omega_{k-2k_0}}{\epsilon(k, \omega)/\epsilon(k-2k_0, \omega-2\omega_0)}| =$   
 $|\frac{\epsilon(k-2k_0, \omega-2\omega_0)}{\epsilon(k, \omega)}|$ . We remark that if the mode  $(\omega, k)$  is a lower sideband which satisfies (1a), its conjugate mode  $(\omega - 2\omega_0, k - 2k_0)$  becomes a small-amplitude upper sideband, which is well different from the mode which satisfies (1b).

The apparatus and the wave excitation method are the same in principle as those employed for the collisionless shock and the soliton experiments<sup>9,10</sup>. Two plasmas, which are produced by independent discharges, are kept separated by a negatively biased mesh grid, such that the electrons are prevented from short circuiting the plasma. The application of a potential difference between the plasmas introduces a fraction of one plasma into the other without forming any ion beams, if the potential difference is smaller than  $\sim \pi T_e/e$ . Within this range of potential differences, a sinusoidal voltage, applied between the two plasmas, drives the ion-acoustic waves which propagate in the direction away from the position of the grid. The plasma parameters are as follows: plasma density,  $n \sim 10^9 \text{ cm}^{-3}$ ; electron temperature,  $T_e = 2 - 3 \text{ eV}$ ; ion temperature,  $T_i = 0.2 \text{ eV}$ ; argon gas pressure,  $(2-5) \times 10^{-4} \text{ Torr}$ . For these values of parameters, ion-ion and ion-neutral collisions can be ignored. The plasma diameter



(40 cm) is much greater than the characteristic length of the wave. In order to increase the spatial resolution of the detector, the wave-receiver probe is biased slightly above the plasma potential, so that the probe sheath is thin. The probe detects the electron saturation current which is proportional to the electron density.

The typical experimental dispersion curve for a small amplitude wave (perturbed respect to unperturbed density ratio,  $n/n_0 \sim 10^{-3}$ ) is shown in Fig.1. At higher frequencies the phase velocity is small. If the wave amplitude is increased, and  $\tilde{n}/n_0$  reaches several percent, the following nonlinear effects appear. Near the frequency where the dispersion curve starts to deviate from a linear proportionality between  $\omega$  and  $k$ , the wave continues to propagate over a distance longer than that through which a small amplitude wave can propagate; in the meanwhile amplitude oscillations appear<sup>1</sup>. The space and time resolved ion energy distribution is measured by an electrostatic energy analyzer<sup>11</sup> through the use of sampling techniques. A group of ions near the wave phase velocity is observed to form a vortex-like motion in the phase space<sup>12</sup>. The trapped ion density is below  $5 \times 10^{-3} n_0$ . In the high frequency range, where the phase velocity is significantly smaller than the ion acoustic velocity, a significant noise is observed to grow. The frequency spectra of the received signals for six different carrier wave frequencies are displayed in Fig.2. In order to emphasize the sidebands, only lower amplitude parts of the spectra are shown. Two types of sidebands are seen: the first is the group of distinct peaks separated from the carrier wave (type A), and the second is the small-amplitude structure around the base of the carrier wave line (type B). If the carrier wave amplitude is increased from a very small value, the type B sideband appears first, then the type A sidebands start to grow when  $\tilde{n}/n_0$  exceeds 0.02 ~ 0.03. As the carrier wave amplitude is increased further, the frequency of the type A sidebands shifts away from that of the carrier wave; then finally the sidebands disappear.

The type A sidebands can be interpreted as those which satisfy the conditions (1). As seen from Fig.2, the upper sideband has much smaller amplitude than the lower sideband. The equations (1) explain the separations between the sideband peaks. Note that the separations are not equal to each other as appears in Fig.2. In this figure, the upper sideband is not the conjugate mode of the lower sideband, but is the one which satisfies (1b).

The matching condition and the dispersion relation (1a) cannot be satisfied, if  $\sqrt{2N+1}\omega_B$  is so large that  $\sqrt{2N+1}\omega_B/k > (C_s - \omega_0/k_0)$ , where  $C_s$  is the ion-acoustic velocity. This fact explains why only few sidebands ( $N = 0$  and 1 in general) can be excited. It also explains why the sidebands disappears when the carrier wave amplitude (and hence  $\omega_B$ ) is too large, as well as when  $\omega_0$  (and hence  $C_s - \omega_0/k_0$ ) is too small.

The values of  $\omega_B$  obtained from the period of the amplitude oscillations are 10 ~ 30% greater than those obtained from the frequency separations between the sidebands by using Eq. (1a) and the dispersion curve. This fact is consistent with the theory which predicts that the maximum growth is obtained in the region  $|\omega/k - \omega_0/k_0| < \sqrt{2N+1}\omega_B/k$  if the lower sideband has greater amplitude than the upper.

The spatial growth of the first lower sideband is shown in Fig.3 (curve c). The bandwidth of the receiver is narrower than the spectral line width of the sideband, therefore the total power in the sideband is larger than the amplitude shown in the figure. The sideband grows initially and saturates at a level comparable to that of the carrier wave in the most unstable case. The initial spatial growth rate is observed to be  $(0.1 \sim 0.2) \omega_B k_0 / \omega_0$ . This is in reasonable agreement with the value estimated theoretically<sup>5</sup>. It should be noted that the damping rate of the carrier wave is observed to be much greater when the sideband exists (curve a) than when it is absent, i.e. when the carrier wave amplitude is small (curve b) or when is too small for exciting sidebands.

The type B sideband is observed in a wider range in  $\omega_0$  and in the carrier wave amplitude. The growth rate is approximately proportional to  $\omega_B$  and almost the same as that of the type A sidebands. Low frequency noise, which corresponds to the difference frequency between the sideband and the carrier, is observed. However, the amplitude is so small that the sidebands cannot be attributed to nonlinear mixing of the low frequency noise with the carrier. These sidebands may reasonably be interpreted as those which satisfy the condition (2).

References

1. C.B. Wharton, J.H. Malmberg and T.M. O'Neil, *Phys. Fluids* 11, 1761 (1968)
2. I.B. Bernstein, J.M. Greene and M.D. Kruskal, *Phys. Rev.* 108, 546 (1957)
3. W.L. Krueer, J.M. Dawson and R.N. Sudan, *Phys. Rev. Lett.* 23, 838 (1969)
4. M.V. Goldman, *Phys. Fluids* 13, 1281 (1970)
5. K. Mima and K. Nishikawa, *J. Phys. Soc. Japan* 30, 1722 (1971)
6. M.V. Goldman and H.L. Berk, *Phys. Fluids* 14, 801 (1971)
7. W.M. Manheimer, *Phys. Rev. A* 3, 1402 (1971)
8. B.D. Fried and R.W. Gould, *Phys. Fluids* 4, 139 (1961)
9. R.J. Taylor, D.R. Baker and H. Ikezi, *Phys. Rev. Lett.* 24, 206 (1970)
10. H. Ikezi, R.J. Taylor and D.R. Baker, *Phys. Rev. Lett.* 25, 11 (1970)
11. H. Ikezi and R.J. Taylor, *J. Appl. Phys.* 41, 378 (1970); *Phys. Fluids* 13, 2348 (1970)
12. W.L. Krueer and J.M. Dawson, *Phys. Fluids* 13, 2747 (1970)

Figure Captions

Fig. 1 Dispersion relation for ion-acoustic waves. The dots are the experimental points; the curve shows the theoretical value for  $T_e/T_i = 20$ . The scales of  $\omega/\omega_{pi}$  and  $k/k_D$  are adjusted to fit to experimental points.

Fig. 2 Frequency spectra of received wave signals. The excitation voltage is 1 volt from peak to peak. The distance is  $x = 5$  cm.  $\omega_{pi}/2\pi = 1.1$  MHz. Only lower amplitude parts of the spectra are shown in order to emphasize the sidebands.

Fig. 3 Amplitude of the carrier waves (curve a and b) and of the first lower sideband (curve c) as a function of distance. The excitation voltage is 1 volt p-p for curves a and c and 0.3 volts p-p for curve b. No sidebands grow in the case of curve b. The gain of the receiver is increased by a factor 5 for curve c.  $\omega_c/2\pi = 0.8$  MHz.  $\omega_{pi}/2\pi = 1.1$  MHz.

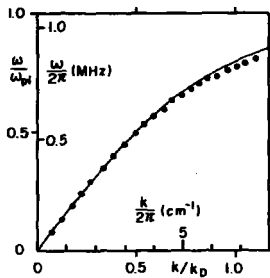


FIG. 1

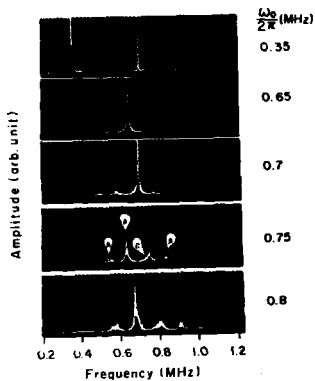


FIG. 2

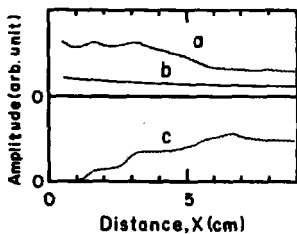


FIG. 3

Measurements on an Ion Sound Decay Instability Induced  
by a Large Amplitude Bernstein Mode in a Plasma

by

B.E. Keen and W.H.W. Fletcher

U.K.A.E.A., Research Group, Culham Laboratory, Abingdon, Berkshire, England.

Abstract

Experimental results are presented which show that a large amplitude wave of one of the Bernstein modes, above a certain threshold power, can decay into another Bernstein mode plus a low frequency ion-sound wave. At larger incident amplitudes, a whole spectrum of low frequency ion waves was observed, with frequencies extending up to the ion plasma frequency ( $\omega_i$ ). These results are compared with a previous theory and reasonable agreement is achieved.

Introduction

Recently, the parametric excitation of various plasma waves has been of considerable interest both theoretically<sup>1-5</sup> and experimentally<sup>6-10</sup>. In particular, the non-linear coupling of high frequency electric fields to low frequency density oscillations in a plasma has been demonstrated in a number of cases<sup>6-8, 10</sup>. This experiment reports the situation in which the high frequency electric field induces a Bernstein mode<sup>11</sup> at frequency ( $\omega_0$ ) close to the electron-cyclotron resonance (ecr) frequency ( $\omega_c$ ), and the non-linear coupling transfers energy to another Bernstein mode at a lower frequency ( $\omega_1$ ), plus a low frequency mode ( $\omega_2$ ), which in this case is the ion-sound decay instability ( $\omega_s$ ). This decay process requires the following relationships

between the frequencies  $\omega(k)$ , and wavenumber  $\vec{k}$ , to be satisfied:-

$$\omega_0(k_0) = \omega_1(k_1) + \omega_2(k_2) \quad \dots (1)$$

$$\vec{k}_0 = \vec{k}_1 + \vec{k}_2 \quad \dots (2)$$

where  $\omega_0$  is the incident Bernstein mode,  $\omega_1 = (\omega_0 - \omega_B)$  is another Bernstein mode,  $\omega_2 = \omega_B$  is the resultant decay instability at the ion-sound frequency, and  $\vec{k}_1 = \vec{k}_0 - \vec{k}_B$ . Equations (1) and (2) are given simply by the conservation of energy and momentum relationships, respectively.

#### Experiment and Results

The experiments were performed in an E-type (capacitively coupled) r.f. discharge ( $f \sim 27$  Mc/s), which gave peak densities in the range  $10^9 - 10^{10} \text{ cm}^{-3}$ . This discharge was run in a homogeneous ( $\sim 1\%$ ) axial magnetic field (0.1 - 1.0 kG,  $\omega_c \sim 0.28 - 2.8$  GHz) and was contained in a glass tube. The electron temperature  $T_e$  ( $\gg T_1$ ) varied between 3.5 eV and 12.5 eV depending upon the r.f. power input, or the neutral gas used ( $\text{H}_2$ , He, Ne, or Ar). This electron temperature was measured using a double probe. The electron density,  $n$ , was obtained from the double probe measurements, or alternatively, from the frequency shift in the resonant frequency of a  $\text{T M}_{010}$  mode coaxial microwave cavity<sup>12</sup>. A further check of density was afforded by a measurement of the upper hybrid frequency  $\omega_{UH} = (\omega_c^2 + \omega_p^2)^{1/2}$ , where  $\omega_p$  is the electron plasma frequency. All three methods were in good agreement.

Externally applied signals were coupled to the plasma using a Lisitano<sup>15</sup> slot line cavity device outside the glass discharge tube or by a probe inserted into the plasma. The high frequency signals were detected either by a radially movable probe inserted into the plasma or by a loop aerial outside the discharge tube. The low frequency "instabilities" were detected on a radially movable floating probe or ion-biased probe.

In these experiments, a uhf signal of frequency  $\omega_0$ , was fed to the Lisitano 'coil', and if the magnetic field was varied such that  $\omega_0/\omega_c$  was

in the range 1.05 - 1.25, Bernstein modes propagated in the plasma. At low inputs a spectral analysis near  $\omega_0$  (Fig.1a) showed a single frequency at  $\omega_0$  in the radiation emitted by the plasma. Fig.1d shows the corresponding low frequency spectrum between 0 - 1 MHz taken at the same power input. When the incident power at  $\omega_0$  was increased above a certain threshold value, the plasma was found to emit radiation at two additional frequencies  $\omega_0 - \omega_B$  and  $\omega_0 + \omega_B$ , as can be seen in Fig.1b. In this experiment the signal at  $\omega_0 - \omega_B$  was always at least one order of magnitude higher in amplitude than the signal at  $\omega_0 + \omega_B$ . The corresponding low frequency spectrum is shown in Fig.1e, and this shows also, a spectral component appearing at  $\omega_B$ . These particular experiments were carried out in a helium plasma, with  $\omega_0 = 500$  MHz, the low frequency component appeared at  $\omega_B \approx 200$  kHz,  $\omega_0/\omega_C = 1.14$ , and  $\omega_p/\omega_C = 1$  for that plasma density at the centre of the tube.

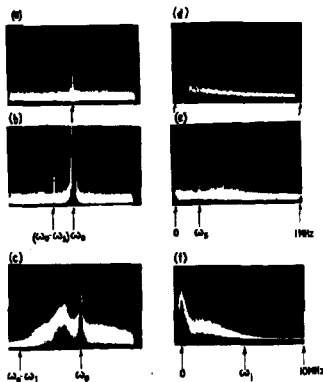


Fig.1

The possible low frequency waves are given by the following dispersion relationship for an infinite plasma<sup>13</sup>:-

$$\omega^2 = \omega_1^2 / \left[ 1 + \left( \omega_1^2 M_1 / k^2 T_e \right) \right] \quad \dots (3)$$

where  $\omega_1 = (4\pi n e^2 / M_1)^{1/2}$  is the ion plasma frequency, and  $M_1$  is the ion



mass. For radial waves, it has been shown<sup>13</sup>, that in a bounded plasma, there is a low frequency cut-off given by:-

$$\omega_g = (2.405/\pi d)(T_e/M_1)^{1/2} \dots (4)$$

where 'd' is the diameter of the containing tube. There is, also, an upper frequency cut-off, in the short wavelength ( $= 2\pi/k$ ) limit given by:-

$$\omega = \omega_1 \dots (5)$$

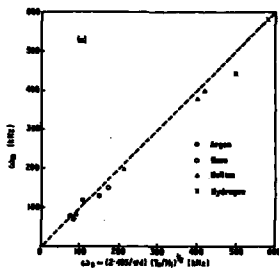


Fig. 2

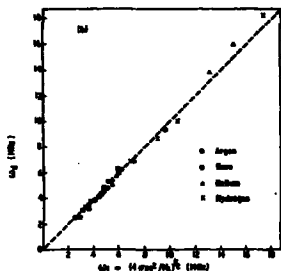


Fig.3

In order to see if the measured low frequency corresponded to the value given by equation (4), the experiment was repeated in four different plasmas, ( $H_2$ , He, Ne and Ar), thus varying both  $T_e$  and  $M_1$ . A further check was afforded by repeating the experiment in three different diameter tubes, namely  $d = 6.2, 5.0$  and  $2.5$  cms respectively. Fig.2 shows the result of these experiments plotted as the measured low frequency  $\omega_g$  versus the calculated value  $\omega_g = (2.405/\pi d)(T_e/M_1)^{1/2}$ . Good agreement is obtained, and thus it is inferred that it is the radial ion sound wave instability which is excited.

These experiments were performed at various input frequencies between 0.28 and 2.8 GHz, and the magnetic field was varied such that the Bernstein mode was propagated. In each case a threshold incident power value was required before excitation at  $\omega_g$  appeared. Corresponding to the spectra in Fig.1, a plot of the ion sound wave amplitude versus the incident power at  $\omega_0 = (500 \text{ Mc/s})$  is shown in Fig.3a. It is clearly seen that a threshold value of about 5 watts ( $E \sim 30 \text{ V/cm}$ ) is required for excitation of

$\omega_B$  (~ 200 kHz). As the power level is further increased the instability amplitude increases but begins to saturate at higher power levels (~ 10 watts). At these levels it was noticed that other modes were excited and a more 'turbulent' like spectrum was apparent. Fig.1c shows a spectral analysis near  $\omega_0$  (with a logarithmic vertical scale ~ 10 d.b./div.) and in this case there appears to be a lower sideband with a range of frequencies from  $(\omega_0 - \omega_B)$  down to a cut-off frequency at  $(\omega_0 - \omega_1)$ . The corresponding low frequency spectrum (0 - 10 MHz) is shown, with a logarithmic vertical scale, in Fig.1f. Experiments were carried out in various plasmas, varying the central plasma density in each case, to measure this cut-off frequency  $(\omega_0 - \omega_1)$ . This is shown plotted in Fig.3 as the measured cut-off  $(\omega_1)$  versus the theoretical value  $\omega_1 = (4\pi n e^2/M_1)^{1/2}$ . Again, good agreement is apparent and in these conditions ion-sound waves in the range from the lower cut-off  $(\omega_1)$  to the upper cut-off frequency  $(\omega_B)$  are obtained.

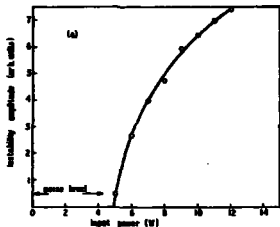
#### Theory

Tzoor<sup>4</sup>, has considered the problem of parametric excitation of ion-sound waves from the decay of Bernstein modes, in which the electronic and ionic motions are coupled by the induced electric fields in the plasma. He has shown that this decay process is possible when equations (1) and (2) are satisfied and that in this case the growth rate,  $\gamma$ , for the low frequency mode is given by:-

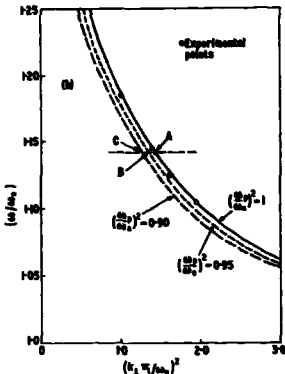
$$\gamma \approx \frac{1}{2} (1 - \epsilon_\infty/\epsilon_0) (ek_0 E_0/m\omega_p^2) (\omega_B \omega_p^2/\omega_0)^{1/2} - (\gamma_B \gamma_S)^{1/2} \quad \dots (6)$$

where  $E_0$  is the transverse electric field of the Bernstein mode,  $\gamma_B$  and  $\gamma_S$  are the effective dissipation rates of the Bernstein and the ion-sound modes, respectively, and  $\epsilon_\infty$  and  $\epsilon_0$  are the dielectric constants of the Bernstein mode at infinite and zero frequencies respectively<sup>11</sup>.

It is apparent from photographs such as those in Fig.1, that the conservation of energy (Eq.(1)) is satisfied in the process. A check of conservation of momentum (Eq.(2)) proved to be a more difficult experiment. The Bernstein



Figs. 4a and 4b



mode dispersion diagram was checked near to the conditions under which the photographs in Fig. 1 were obtained, by using an interferometric technique. The resulting experimental points are shown plotted in Fig. 4b on the  $(\omega/\omega_c)$  versus  $(k_{\perp} v_t/\omega_c)^2$  curve (here  $k_{\perp}$  was the radial wavenumber and  $v_t = (T_e/m)^{1/2}$  was the electron thermal velocity). The solid curve shows the theoretical curve<sup>11</sup> for the case  $(\omega_p/\omega_c)^2 = 1$ , which corresponds to the central plasma density, in this case. The point A on the curve corresponds to the value  $\omega_0 = 500$  Mc/s (i.e. Fig. 1). The resulting instability at  $\omega_0$ , was checked using the radial moving probe and its wavenumber  $k_2 = k_g$  was found. For the wave at  $\omega_1 = \omega_0 - \omega_g$ , the proximity of the large amplitude wave at  $\omega_0$ , swamped this wave at  $(\omega_0 - \omega_g)$ , and consequently, a direct measure of its wavenumber,  $k_1$ , was not possible. It is assumed that this wave is also a Bernstein mode, it is not possible to satisfy Eq. (2), for both the high frequency waves on the same branch of the solid curve (Fig. 4b), since the slope of this curve  $\Delta\omega/\Delta k$  is much less than  $(\omega_0 - \omega_1)/(k_0 - k_1) = \omega_g/k_g$ . However, a plausible explanation, which will satisfy Eq. (2) is the following: since the density,  $n$ , is a function of the plasma radius,  $r$ , [ $n = n(r)$ ], it follows that the Bernstein mode dispersion curve is also a function of radius. Fig. 4b shows the theoretical dashed curves calculated for  $(\omega_p/\omega_c)^2 = 0.95$  and 0.90. Therefore, if the large amplitude Bernstein wave at  $\omega_0, k_0$  (point A),

decays to another one at  $\omega_1 = (\omega_0 - \omega_B)$ ,  $k_1 = (k_0 - k_B)$ , (point B) (corresponding to the dispersion relationship at a slightly larger radius) both equations (1) and (2) can be satisfied simultaneously, in an inhomogeneous plasma. Further decay from B to C, etc. also will satisfy these equations. A decay mode from C to B or B to A etc., creates a Bernstein mode at  $\omega_0 + \omega_B$ ,  $k_0 + k_B$ , but with a smaller probability than the lower sideband<sup>14</sup>. In the same way, Eqs. (1) and (2) may be satisfied simultaneously, at any  $(\omega, k)$  related by the dispersion relationship Eq.(3), within the range  $\omega_B$  to  $\omega_1$ , by using a similar argument.

The possibility was considered that the input power creating the large amplitude Bernstein wave created a non-Maxwellian distribution in the plasma, which in turn caused the low frequency (l.f.) instability. This possibility was reduced by exciting a l.f. wave ( $\omega' \approx 50$  kHz) in the plasma and observing the 'mixing effects' produced with the Bernstein mode, below threshold. In this case, the upper and lower sidebands at  $\omega_0 + \omega'$  and  $\omega_0 - \omega'$  were observed of equal amplitude, and an order of magnitude lower in amplitude than in previous experiments. This is contrary to that expected from decay instability theory<sup>14</sup> and the experimental observations. Also, from Eq.(6), the threshold value of  $E_0$  may be obtained by equating  $\gamma$  to zero, and substituting for  $\gamma_B = \nu_i$ , ( $\nu_i$  = the ion-neutral collision frequency) and for  $\gamma_B$  as the measured decay value in the plasma. In this way, a value of  $E_0 \approx 50$  V/cm results as compared with a measured threshold value of  $E \approx 30$  V/cm (for Fig.3a), which is in reasonable agreement.

#### Conclusion

From the foregoing results, it is inferred that above a certain threshold value, a decay instability at the ion-sound frequency induced by a large amplitude Bernstein wave in the plasma, is seen in these experiments. Further, for input powers much above threshold a whole spectrum of instabilities in the range  $\omega_B$  up to the ion plasma frequency,  $\omega_1$ , is observed. Comparison of these results with a previous theory shows good agreement.

References

1. D.F. Dubois and M.V. Goldman. Phys. Rev. Letters 14, 544, (1965).
2. V.P. Silin. Zh. Eksperim. i. Teor. Fiz., 48, 1679, (1965)  
[Engl. Transl. Soviet Phys. J.E.T.P. 21, 1127, (1965)].
3. E.A. Jackson. Phys. Rev. 153, 230, (1967).
4. N. Tzoar. Phys. Rev. 178, 356, (1969).
5. Y. Pomeau. Physics Fluids 10, 2695, (1967).
6. S.A. Stern and N. Tzoar. Phys. Rev. Letters 17, 903, (1966).
7. S. Hiroe and H. Ikegami. Phys. Rev. Letters 19, 1414, (1967).
8. R.A. Stern. Phys. Rev. Letters 22, 767, (1969).
9. P.M. Porkolab and R.P.H. Chang. Phys. Rev. Letters 22, 826, (1969).
10. A.Y. Wong, D.R. Baker and N. Booth. Phys. Rev. Letters 24, 804, (1970).
11. I.B. Bernstein. Phys. Rev. 108, 10, (1965).
12. S.J. Buchsbaum and S.C. Brown. Phys. Rev. 106, 196, (1957).
13. F.W. Crawford. Phys. Rev. Letters 6, 663, (1961).
14. V.N. Tsytovich, "Non-linear effects in a Plasma" (Plenum Press, 1970).
15. G. Lisitano, "Proceedings of the 7th International Conference on Phenomena in Ionized Gases", (Belgrade, 1965), vol.1, p.464.

Observations of Nonlinear Scattering  
from a Plasma Column

by

R. L. Bruce, F. W. Crawford and K. J. Harker

Institute for Plasma Research, Stanford University  
Stanford, California 94305, USA

Abstract

An analysis of nonlinear mixing for signals propagating as  $\exp j(\omega_{\alpha,\beta} t - k_{\alpha,\beta} x)$ , incident on an unmagnetized cold plasma column oriented along the  $x$ -axis, shows that if only quasistatic dipolar fields are considered in the vicinity of the column, the nonlinearly generated component at  $\omega_{\gamma} (\approx \omega_{\alpha} + \omega_{\beta})$  has a quadrupolar radiation pattern with maxima at  $\pm \pi/4$  and  $\pm 3\pi/4$  to the  $x$ -axis. This paper considers the interaction when the quasistatic approximation is not made, and concludes that the nonlinearly generated quadrupole component should be accompanied by an appreciable dipole component oriented with its maxima at  $\pm \pi/2$ . Experiments of previous workers, and our own preliminary observations show strong nonlinear forward-scattering, however. In our experiments, this spurious result has been traced to the effect of the Earth's magnetic field. When this is cancelled, predominantly quadrupolar radiation is observed, in agreement with theory.

Introduction

One of the classic problems of plasma physics is the scattering of a microwave signal normally incident on a cylindrical plasma column. An extensive bibliography has built up on the phenomenon, and has been well summarized by Vandenplas [1]. It is now well known that there is a dipolar resonance, given by cold plasma theory, and an additional series of (Tonks-Dattner) resonances which can only be predicted satisfactorily by taking into account electron thermal velocities and radial inhomogeneity of the column. So far, work has been directed primarily to small signal theory, but some attempts

have been made to predict and to observe nonlinear interaction effects when one or more strong signals are incident on the column. In particular, Stern [2] and Tzoer [3] have observed second harmonic generation and frequency mixing, and Messiaen and Vandenplas [4] have observed second harmonic generation. The latter authors have given a comprehensive theory of the interaction for a cold homogeneous column in a dielectric tube.

A curious feature of the experiments is that forward-scattered power is observed for the nonlinearly generated signal, whereas the theory suggests a null for forward- and back-scattered power, in contrast to the predominantly dipolar radiation of the linearly scattered signals which is maximum for 0 and  $\pi$ , i.e. in the direction parallel to the wave propagation [5]. The studies to be reported here were carried out to determine whether the defects lay with the theory or the experiments. We considered first frequency mixing in the quasistatic limit, assuming dipolar excitation at frequencies  $\omega_{\alpha}, \omega_{\beta}$  to produce  $\omega_{\gamma} (\approx \omega_{\alpha} + \omega_{\beta})$  in either a homogeneous or an inhomogeneous plasma column [6]. The radiation at  $\omega_{\gamma}$  was found to be quadrupolar, with its maxima at  $\pm \pi/4$  and  $\pm 3\pi/4$  to the direction of propagation of the incident signal.

In this paper, the theory for a uniform plasma is examined, without making the quasistatic assumption. If it is found that the nonlinearly generated quadrupole component is only modified slightly, for practical conditions, but that there is an additional dipole component oriented with its maximum at  $\pm \pi/2$  to the direction of propagation of the incident signal. It is shown that no multipolar component can give a forward- or back-scattered signal. This implies that there is some spurious element in the previously reported experiments. Our own preliminary measurements indicated that this was so, since a strong dipolar radiation pattern was observed for a nonlinearly generated second harmonic signal, with its maxima at 0 and  $\pi$ . This could be removed, however, by cancelling the effect of the Earth's magnetic field. Predominantly quadrupolar radiation was then observed, as predicted.

### Theory

The time Fourier transforms of the momentum transfer equation and Maxwell's equations are given by

$$j\omega_{\gamma} \underline{v}_{\gamma} - \eta \underline{E}_{\gamma} = - \sum_{\alpha, \beta} [(\underline{v}_{\alpha} \cdot \nabla) \underline{v}_{\beta} - \eta \underline{v}_{\alpha} \times \underline{B}_{\beta}], \quad (1)$$

$$\nabla \times \underline{H}_{\gamma} - \rho_{\alpha} \underline{v}_{\gamma} - j\omega_{\gamma} \epsilon_{\alpha} \underline{E}_{\gamma} = \sum_{\alpha, \beta} \rho_{\alpha} \underline{v}_{\beta}, \quad \nabla \cdot \underline{B}_{\gamma} = 0,$$

$$\nabla \times \underline{E}_{\gamma} + j\omega_{\gamma} \underline{B}_{\gamma} = 0, \quad \nabla \cdot \underline{E}_{\gamma} - \frac{\rho_{\gamma}}{\epsilon_0} = 0,$$

where the subscripts  $\alpha, \beta, \gamma$  denote variation as  $\exp j\omega_{\alpha} t$ , etc.;  $\eta$  is the electronic charge-to-mass ratio, and the synchronism condition,

$$\omega_{\gamma} = \omega_{\alpha} + \omega_{\beta}, \quad (2)$$

is satisfied. For generality, we assume  $\omega_{\alpha} \neq \omega_{\beta}$ . The modifications necessary to specialize the results to the second harmonic case ( $\omega_{\alpha} = \omega_{\beta}$ ) will be stated later.

Linear terms have been collected on the left-hand sides of the expressions in Eq. (1) and nonlinear coupling terms on the right-hand sides. The nonlinear coupling terms may be simplified by substituting in them the small signal solutions obtained by initially ignoring the nonlinear terms. For the Maxwell equation which has a nonlinear driving term we obtain

$$\nabla \times \underline{H}_{\gamma} - j\omega_{\gamma} \epsilon_0 \epsilon_{\gamma} \underline{E}_{\gamma} = - \frac{j\rho_0 \eta^2}{\omega_{\alpha} \omega_{\beta} \omega_{\gamma}} \nabla(\underline{E}_{\alpha} \cdot \underline{E}_{\beta}) + \sum_{\alpha, \beta} \rho_{\alpha} \underline{v}_{\beta}, \quad (3)$$

where  $\epsilon_{\gamma} (= 1 - \omega_p^2/\omega_{\gamma}^2)$  is the equivalent plasma permittivity. The two nonlinear driving terms are due to the electromagnetic pressure gradient, and to volume currents. The latter are zero for a uniform column since  $\rho_{\alpha} = 0$  [6].

To proceed further, Eq. (3) and the second Maxwell curl equation must be solved for the small signal fields. These are then used to simplify the right-hand side of Eq. (3). The two curl equations are finally solved, including the nonlinear driving terms.

### Linear Scattering

It is convenient to work in terms of the magnetic field,  $H_{z\alpha}$ . Solution of the wave equation inside and outside the plasma then gives



$$\begin{aligned}
 H_{n\Omega} &= H_{0n\Omega} \sum_{-\infty}^{\infty} A_{n\Omega} J_n(k_{p\Omega} r) \exp jn\theta \quad (r \leq a), \\
 H_{n\Omega} &= H_{0n\Omega} \sum_{-\infty}^{\infty} B_{n\Omega} H_n^{(2)}(k_{\alpha} r) \exp jn\theta + H_{0n\Omega} \exp(-jk_{\alpha} x) \\
 &= H_{0n\Omega} \sum_{-\infty}^{\infty} [B_{n\Omega} H_n^{(2)}(k_{\alpha} r) + J_n(k_{\alpha} r)/J_n^{\prime}(k_{\alpha} a)] \exp jn\theta \quad (r \geq a).
 \end{aligned} \tag{4}$$

Constants  $A_{n\Omega}$ ,  $B_{n\Omega}$  are evaluated by matching  $H_{n\Omega}$ ,  $E_{\theta\Omega}$  at  $r = a$ :

$$\begin{aligned}
 A_{n\Omega} &= \frac{2\epsilon_{\alpha}^{1/2}}{j^{n-1} \pi k_{\alpha} a} \left( \frac{1}{H_n^{(2)}(k_{\alpha} a) J_n^{\prime}(k_{p\Omega} a) - \epsilon_{\alpha}^{1/2} H_n^{(2)\prime}(k_{\alpha} a) J_n(k_{p\Omega} a)} \right), \\
 B_{n\Omega} &= -\frac{1}{j^n} \left[ \frac{J_n(k_{\alpha} a) J_n^{\prime}(k_{p\Omega} a) - \epsilon_{\alpha}^{1/2} J_n^{\prime}(k_{\alpha} a) J_n(k_{p\Omega} a)}{H_n^{(2)}(k_{\alpha} a) J_n^{\prime}(k_{p\Omega} a) - \epsilon_{\alpha}^{1/2} H_n^{(2)\prime}(k_{\alpha} a) J_n(k_{p\Omega} a)} \right].
 \end{aligned} \tag{5}$$

Although the rf space-charge density is zero in the column, there is a discontinuity in  $E_{r\Omega}$  at  $r = a$ , indicating a surface charge density given by

$$\rho_{s\Omega} = -\frac{(1 - \epsilon_{\alpha})}{\omega_{pe} \epsilon_{\alpha}} H_{0n\Omega} \sum_{-\infty}^{\infty} n A_{n\Omega} J_n(k_{p\Omega} a) \exp jn\theta. \tag{6}$$

### Nonlinear Scattering

When we combine the Maxwell curl equations, we obtain a wave equation which does not depend on the (curl-free) nonlinear driving term. Solutions are consequently

$$\begin{aligned}
 H_{z\gamma} &= \sum_{-\infty}^{\infty} a_{\ell} J_{\ell}(k_{p\gamma} r) \exp j\ell\theta \quad (r < a), \\
 H_{z\gamma} &= \sum_{-\infty}^{\infty} b_{\ell} H_{\ell}^{(2)}(k_{\gamma} r) \exp j\ell\theta \quad (r > a).
 \end{aligned} \tag{7}$$

For the nonlinear surface current, we have

$$J_{s\theta\gamma} = \sum_{\alpha, \beta} \rho_{s\alpha} v_{\theta\beta} \Big|_{s-} = \frac{\eta}{\epsilon_0} \sum_{\alpha, \beta} \frac{\rho_{s\alpha}}{\omega^2 \beta} \frac{\partial H_{z\beta}}{\partial r} \Big|_{s-} = \sum_{-\infty}^{\infty} J_{s\gamma l} \exp j l \theta ,$$

$$J_{s\gamma l} = - \frac{\eta^2 p_{\alpha} H_{0\alpha} H_{0\beta}}{\epsilon_0 s^2 \omega^2 \alpha^2 \beta^2 \epsilon_{\alpha} \epsilon_{\beta}} \sum_{\alpha, \beta} \frac{k_{\beta\beta} s}{\omega \alpha} \sum_{l=-n+m}^n n A_{n\alpha} A_{m\beta} J_n(k_{\rho\alpha} s) J_m'(k_{\rho\beta} s) . \quad (8)$$

Continuity of  $H_{s\gamma}$  at  $r = s$  yields the relation

$$b_l H_l^{(2)}(k_{\gamma} s) - a_l J_l(k_{\rho\gamma} s) = - J_{s\gamma l} . \quad (9)$$

We now have to apply continuity of  $E_{\theta\gamma}$ . Using Eq. (3), we obtain

$$\epsilon_{\gamma} \frac{\partial H_{s\gamma}}{\partial r} \Big|_{s+} - \frac{\partial H_{s\gamma}}{\partial r} \Big|_{s-} = - \frac{j \rho_0 \eta^2}{s m \omega \alpha \beta \gamma} \frac{\partial}{\partial \theta} (E_{\alpha} \cdot E_{\beta}) \Big|_{s-} = \frac{1}{s} \sum_{-\infty}^{\infty} d_l \exp j l \theta ,$$

$$d_l = \sum_{l=D+n} \frac{\eta^2 p_{\alpha} H_{0\alpha} H_{0\beta} A_{n\alpha} A_{m\beta}}{\epsilon_0 s^2 \omega^2 \alpha^2 \beta^2 \epsilon_{\alpha} \epsilon_{\beta}} \left[ n m J_n(k_{\rho\alpha} s) J_m(k_{\rho\beta} s) - k_{\rho\alpha} k_{\rho\beta} s^2 J_n'(k_{\rho\alpha} s) J_m'(k_{\rho\beta} s) \right] .$$

Substituting from Eq. (7) gives

$$\epsilon_{\gamma} b_l k_{\gamma} a H_l^{(2)'}(k_{\gamma} s) - k_{\rho\gamma} a a_l J_l'(k_{\rho\gamma} s) = d_l , \quad (11)$$

and solution of Eqs. (9) and (11) yields, finally,

$$a_l = \frac{j^{l+1} k_{\gamma}}{2 \epsilon_{\gamma}} A_{l\gamma} \left[ J_{s\gamma l} \epsilon_{\gamma} k_{\gamma} a H_l^{(2)'}(k_{\gamma} s) + d_l H_l^{(2)}(k_{\gamma} s) \right] ,$$

$$b_l = \frac{j^{l+1} k_{\gamma}}{2 \epsilon_{\gamma}} A_{l\gamma} \left[ J_{s\gamma l} k_{\rho\gamma} a J_l'(k_{\rho\gamma} s) + d_l J_l(k_{\rho\gamma} s) \right] . \quad (12)$$

### Long Wavelength Limit

In our experiments,  $k_{\gamma} s \ll 1$ . For this situation, the expressions in Eq. (12) may be greatly simplified. In particular, we then find that only  $b_1$  and  $b_2$  are significant, i.e. that only dipole and quadrupole radiation components are to be expected. The amplitude  $b_2$  corresponds to the value obtained elsewhere for a uniform column located in the quasistatic approximation [6], and can be shown to be related to  $b_1$  through

$$b_1 = j b_2 \left( \frac{3\omega^2 - 4\omega \omega}{\omega^2 \alpha \beta} - 1 \right) , \quad (13)$$

Both  $b_1$  and  $b_2$  show resonance for  $1 + \epsilon_{\alpha, \beta, \gamma} = 0$ , so that for our experimental condition of second harmonic resonance ( $\alpha = m, \beta = m, \gamma = 2, 1 + \epsilon_{\alpha} = 0$ )

$$b_1 = j b_2 / 2. \quad (14)$$

Turning now to the fields, Eq. (7) indicates that the power received by a probing antenna will be

$$\begin{aligned} P_{\gamma} &\propto \left| \frac{1}{2} H_1^{(2)}(k_{\gamma} r) \sin \theta + H_2^{(2)}(k_{\gamma} r) \sin 2\theta \right|^2 \\ &\propto \left| \frac{1}{2} \sin \theta + \sin 2\theta \right|^2 \quad (k_{\gamma} r \gg 1). \quad (15) \end{aligned}$$

We note that no forward- or back-scattered power is to be expected at  $\theta = 0$ . Figure 1 shows a polar plot corresponding to Eq. (15).

### Experiments

Figure 2 shows the arrangement of the plasma and antennas used in our experiments. The plasma is a mercury-vapor positive column in a small pyrex tube (outside diameter 5 mm, inside diameter 3 mm). The transmitting antenna is an S-band horn with a dielectric lens. The receiving antenna is a 24 mm dipole supported on small diameter 50  $\Omega$  rigid coax line. At a current of 130 mA, the plasma column is dipole resonant at the applied frequency (2.20 GHz). At this point there is maximum harmonic generation.

In the course of our preliminary experiments, it was noted that weak magnetic fields, the Earth's magnetic field in particular, had a strong effect on the second harmonic radiation pattern. This effect does not seem to have been mentioned before in the literature. The presence of a magnetic field produced a strong component of dipolar radiation. This suggests that agreement with the theory outlined above can only be expected after the Earth's field has been cancelled. In our recent experiments, we have been taking scattering data with the Earth's magnetic field cancelled by applying an equal but opposite field with a large diameter ( $\approx 1$  m) 25-turn coil. Without such a coil, the radiation pattern is essentially dipolar, as shown in Fig. 3(a). With the coil, radiation lobes closer to those suggested by theory are obtained. This is illustrated by the polar pattern of Fig. 3(b), taken with the receiving antenna 7.5 cm from the plasma column axis.

This work was supported by the National Aeronautics and Space Administration and the National Science Foundation. Some of the results shown in Fig. 3 were obtained by our colleague J.M. Larsen.

References

- [1] P. E. Vandenplas, Electron Waves and Resonances in Bounded Plasmas (Interscience Publishers, New York, N. Y. 1968).
- [2] R. A. Stern, Phys. Rev. Letters 14, 517 (1965).
- [3] R. A. Stern and N. Tzoar, Phys. Rev. Letters 15, 550 (1965); 16, 785 (1966).
- [4] A. M. Messiah and P. E. Vandenplas, Plasma Phys. 10, 851 (1968).
- [5] W. D. Hershberger, Phys. Fluids 4, 740 (1961).
- [6] R. L. Bruce, F. W. Crawford and K. J. Harker, Proc. Tenth International Conference on Phenomena in Ionized Gases, Oxford, England, September 1971 (Donald Parsons, Oxford 1971), p. 326.

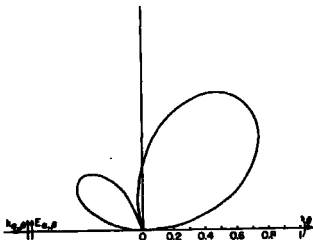
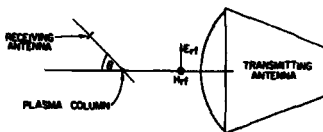
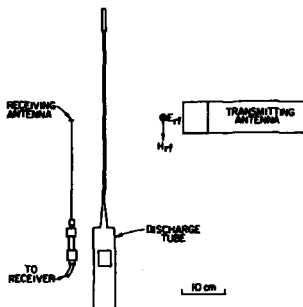


FIG. 1. Polar Plot of  $|P_y|^2$  as a  
Function of  $\theta$ .



(a) PLAN VIEW



(b) SIDE VIEW

FIG. 2. Set-Up for Studying Scattering from a Plasma Column.

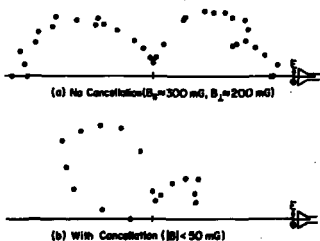


FIG. 3. Second Harmonic Radiation Pattern showing Effect of Cancelling the Earth's Magnetic Field.

Acquisition and Processing of Plasma Fluctuation Data  
Using FFT Spectral Analysis Techniques

by

D. E. Smith, E. J. Powers, and R. E. Rowberg  
Department of Electrical Engineering and Electronics Research Center  
The University of Texas at Austin, Austin, Texas 78712 USA

Abstract

An analog-digital spectral analysis system suitable for studying plasma fluctuation data is described. The data is initially recorded on a 7-channel, 1.5 MHz, analog, instrumentation-type tape recorder and later digitized for subsequent analysis on a general-purpose computer. The computer output consists of plots of auto- and cross-power spectra, and coherence spectra. An application of spectral analysis to studies of plasma-wave behavior in a noisy or turbulent-like plasma is described.

Introduction

The problem of analyzing plasma fluctuation data associated with instabilities and waves in a turbulent-like plasma may be viewed as a basic problem in analyzing random-type data. In addition to the usual space-time correlation studies, power spectral-density analysis techniques often yield considerable insight into the physics of the situation. The spectral analysis approach has been successfully utilized in a number of different areas of science and engineering (geophysics, propagation through turbulent media, communications, etc.). The approach developed to reach this goal is analog-digital in nature in that the implementation encompasses not only the digital computation of the power spectral density function but also the acquisition and digitization of the analog data need for the spectral analysis. Such an approach is based primarily on the utilization of the fast Fourier transform (FFT) algorithm<sup>1</sup> which allows one to transform the data into the frequency domain in a computationally efficient fashion. Previously, we have described this system in detail with respect to instrumentation and implementation.<sup>2</sup> In this paper we wish to emphasize three topics not previously presented. First is the enhancement of the overall system bandwidth to 1.5 MHz. Secondly, we will compare an on-line mini-computer approach to spectral analysis with our general-purpose computer, off-line, approach. Finally, we will demonstrate the use of the phase and coherence spectra in analyzing plasma wave data.

Computing Power Spectra Digitally

We will begin with a review of the theoretical background and practical considerations of a digitally implemented spectral analysis technique.

Let  $f_1(t)$  and  $f_2(t)$  denote two fluctuating signals which might, for example, represent fluctuations in plasma density or potential at two different points in the plasma. In the "classical" computation of power spectra, one would first correlate  $f_1(t)$  and  $f_2(t)$  and then Fourier transform the cross-correlation function to get the cross-power spectrum  $P_{12}(\omega)$ . In the digital

approach,  $f_1(t)$  and  $f_2(t)$  are first digitized and then Fourier transformed (using the FFT algorithm) by the computer to yield  $F_1(\omega)$  and  $F_2(\omega)$ , respectively. The resultant cross-power spectrum  $P_{12}(\omega)$  is computed from  $P_{12}(\omega) = F_1(\omega)F_2^*(\omega)$ , where the asterisk denotes complex conjugate. In general,  $P_{12}(\omega)$  is complex and may be expressed as an amplitude spectrum  $|F_1(\omega)||F_2(\omega)|$  and a phase spectrum  $\theta_{12}(\omega) = \theta_1(\omega) - \theta_2(\omega)$  where  $\theta_1(\omega)$  and  $\theta_2(\omega)$  denote the phase of  $F_1(\omega)$  and  $F_2(\omega)$ , respectively. It is important to note that the phase spectrum is a measure of the phase difference between corresponding spectral components contained in  $f_1(t)$  and  $f_2(t)$ .

In the case where  $f_1(t) = f_2(t)$ , we obtain the auto-power spectrum  $P_{11}(\omega) = |F_1(\omega)|^2$  which is real and positive. Another function which is of particular use in studying wave phenomena in a noisy background is the coherence function which is defined as  $\text{COH}(\omega) = |P_{12}(\omega)| / [P_{11}(\omega)P_{22}(\omega)]^{1/2}$ .

### Other Considerations in Digital Spectral Analysis

Finite Data Length: Since one must work with a finite length of data recorded in the time domain, the computed power spectrum will only be an "estimate" of the true power spectrum. A number of techniques which incorporate various types of "windows" can be used to improve the spectral estimate (see, e.g., ref. 3). The spectra shown in this paper were computed using a Hanning window on each data length. This window has the advantage of being easily applied in the frequency domain as a three-point convolver.

Aliasing: In digitizing data one is generally working with a fixed digitizing or sampling rate  $f_s$ . In order to avoid violating the sampling theorem there should be no frequency components present in the data above  $f_s/2$  (the Nyquist frequency). If frequency components higher than  $f_s/2$  are present, they will be "folded back" into the lower frequency spectrum giving rise to erroneous spectral estimates. This phenomenon is known as "aliasing" and is avoided by passing the analog data through a low-pass filter (known as the aliasing filter) with the upper cut-off frequency set at  $f_s/2$ .

Smoothing of Data: In computing power spectra digitally the various discrete components of the power spectra will be separated by the elementary frequency bandwidth  $\Delta f = 1/T$  Hz, where T is the duration in seconds of the sampled data. In this case the statistical error, or confidence limit, is usually very large. In order to reduce the statistical error to acceptable levels the spectra are smoothed, or averaged, over several adjacent elementary frequency bands. The spectra displayed in this paper have been averaged over 50 elementary bands. A detailed discussion of the quantitative relationship between smoothing and confidence limits may be found in ref. 4.

### System Description

A 7-channel, 1.5 MHz, analog instrumentation-type tape recorder (Ampex 1800-H) is used to initially record up to seven channels of plasma data. The data are later digitized by an XDS 930 computer and stored on digital magnetic tape for later processing on a CDC 6600 computer. The output of the CDC 6600 computer consists of auto- and cross-power spectra, and coherence functions. This system, as described in earlier papers, had an effective analysis bandwidth of 384 kHz which was set by the XDS 930 computer's digitizing capabilities.

The XDS 930 facility, currently used in digitizing the data, possesses an approximate 12 kHz maximum sampling rate for a single-channel analog-to-digital conversion. This 12 kHz sampling rate capability in conjunction with the time expansion (or frequency reduction) capability of the multispeed analog recorder (i.e., we record at 120 ips and digitize at 1-7/8 ips, a factor of 64 in frequency reduction) yields an effective sampling capability of 768 kHz at 120 ips. This corresponds, according to the sampling theorem, to an analysis bandwidth of 384 kHz which is well below our 1.5 MHz data recording capability. Efforts to improve the overall data processing bandwidth of the existing system are, consequently, directed toward increasing the effective sampling rate of the digitizer. This goal is achieved using multi-time-delay sampling.<sup>6</sup> In this approach a 12 kHz pulse train, known as the initial timing chain, is recorded on one channel of the analog tape recorder. On playback of the analog data into the digitizer the timing chain is used to trigger a pulse generator which, in turn, controls the computer's digitizing rate. In this manner data from the analog recorder is accepted by the computer, digitized, and stored on digital magnetic tape. At this point the system still has an effective analysis bandwidth of 384 kHz. To increase the effective sampling rate the analog tape unit is rewound and positioned at the initial starting pulse of the recorded timing chain. The data is now played back a second time with the timing chain triggering the pulse generator. In this case, however, the output of the pulse generator is delayed a time  $\tau$  before being applied to the XDS 930 computer. Consequently, the data is again digitized at a 12 kHz rate but at different points in time. This data is stored on digital tape in a second file. The process can be repeated with a number of different time delays and is limited only by the number of times that one can subdivide the initial pulse interval. For a 12 kHz initial timing chain division of the basic 83  $\mu$  sec time interval by a factor of 4 is feasible. In this case four separate files of data are stored on digital magnetic tape. Computer programs are used to read each file of data, multiplex the data and then write the multiplexed data in a new file, which is four times the original file length. The end result, now stored on digital tape, is a digital version of the original analog data signal which has been effectively sampled at a rate four times higher than the maximum sampling rate capability of the digitizer. This increase in sampling rate results in an effective analysis bandwidth of 1.536 MHz at 120 ips which is compatible with the analog recorder's 1.5 MHz capability.

In using this technique phase differences between data channels which might be caused by inter-channel recorder timing delays or non-identical amplifier and filter phase responses must be compensated for to successfully interpret the phase spectra. Calibration and correction using known signals should be incorporated with each data run. Without such compensation very serious errors in the phase spectra may result.

In addition to the approach utilizing general purpose computers described above, one might also utilize a mini-computer technique to perform spectral analysis. The latter approach may be used on-line whereas the former approach involves off-line analysis of the data. With respect to cost, one is trading off the capital cost of the mini-computer vs. the cost of computer time on a general purpose computer. To fully exploit the capabilities of the mini-computer, it is often desirable to program in machine language. For the non-computer expert the general purpose computer may be more attractive



since all programs are written in a language such as FORTRAN and are, therefore, easily modified or changed. Compared to the large core storage of a general-purpose computer, the storage associated with the mini-computer is usually quite small. This means working with a relatively small number of data points which in turn implies high statistical error. This error may be reduced by averaging over an ensemble of many (often a few thousand) spectra. This requires a time period which may be several minutes long and over which the experiment must remain statistically stationary. In contrast, the power spectra displayed in this paper were computed from a data length of 2.13 sec. In addition the larger core storage capability permits the general purpose computer user finer frequency resolution than that afforded by a mini-computer, while the tape recorder's multi-speed, time-expansion capability permits greater overall system bandwidth to be achieved for a fixed digitizing rate.

#### Applications of Power Spectral Analysis to Wave Phenomena

To apply spectral analysis to studies of plasma-wave phenomena we assume that within a given frequency range of interest that the plasma fluctuations at point  $\bar{r}$  may be represented by a harmonic wave expansion of the form

$$f(\bar{r}, t) = \int_{-\infty}^{\infty} N_0(\omega) e^{i(\bar{k}(\omega) \cdot \bar{r} - \omega t)} d\omega,$$

where  $\bar{k}(\omega)$  is an unknown function of frequency. A detailed analysis<sup>7</sup> of this situation shows that within this frequency range the coherence function  $\text{COH}(\omega)$  is unity. The phase spectrum, which is equal to the phase difference between the fluctuations measured at the two points, will be for the wave case under consideration equal to  $\bar{k}(\omega) \cdot \Delta\bar{r}$ . Here  $\Delta\bar{r}$  is the known vector distance of separation of the two points at which the fluctuations are monitored, and  $\bar{k}(\omega)$  is the wave number. Once the wave number  $\bar{k}(\omega)$  and the frequency  $\omega$  are known, the phase velocity  $\omega/\bar{k}(\omega)$  associated with that spectral component can be determined.

As a preliminary application of the system we have performed some measurements on a class of low frequency drift-type waves occurring in a weakly-ionized RF magneto-plasma. These waves occur at pressures ranging from few tens to hundreds of microns and weak magnetic fields of a few hundred gauss. The analysis we will present involves investigation of the waves using the power, phase, and coherence spectra. The measurements were taken by two fixed double probes, azimuthally displaced in the plasma  $\theta_{\text{probe}}$  radians, but at the same axial and radial position. Therefore, the phase spectrum will give us azimuthal information only. The azimuthal mode number  $m(\omega)$  is given by  $m(\omega) = \theta_{\text{probe}}(\omega) / \theta_{\text{probe}}$ . We have made no attempt, as yet, to compare the results to a theoretical analysis.

Figure 1 gives a computer-generated cross-power amplitude and phase spectra for  $B=430\text{G}$ . The amplitude spectrum shows a large peak at 94 kHz and two smaller peaks, or "sidebands", equally spaced on either side. The corresponding phase spectrum shows the central peak to have a phase shift of 0.90 radians which is an  $m=1$  mode. This  $m=1$  mode line has been adjusted to compensate for interchannel timing errors in the recorder system. In addition the two smaller peaks have the same phase shift as the large peak. This demonstrates a major advantage of our analysis system in that the phase shifts for all modes present are displayed with good frequency resolution. Thus one is able to determine the phase shift, and hence the mode number

for two rather closely spaced sidebands.

In Fig. 2, B has been raised to 455G and a second mode appears at 47 kHz. No sidebands appear with this mode, but the peak at 94 kHz still retains the sideband characteristic. The phase spectrum for this case shows the low frequency peak to be an  $m=2$  mode. The upper frequency peak still exhibits  $m=1$  behavior as does its sidebands. Figure 3 shows a coherence plot for this magnetic field and the amplitude spectrum for comparison purposes. Note the peaks at 47 kHz and 94 kHz have a coherence of 1.00 while the sidebands have a coherence  $>0.87$ . This indicates that all of these modes are strongly coherent and are, therefore, waves, not random signals producing statistically large amplitude peaks in the power spectra. This is significant as far as the sidebands are concerned because their observation is very difficult from the time signals alone. Therefore, the coherence spectra adds to the evidence that the two peaks on either side of the  $m=1$  mode are probably sidebands generated by some non-linear phenomena. The fact that we have easily obtained this information again points up the benefits of our system.

Raising B still further to 480G produces a sharp change in the spectra as indicated in Fig. 4. The amplitude spectra for 455G has been repeated in this figure for reference purposes. Here the sidebands are greatly enhanced apparently at the expense of the  $m=1$  carrier wave. This observation is corroborated by the coherence spectrum (not shown) which shows a sharp drop in coherence of the 94 kHz wave to about 0.78 while the sidebands increase to 0.98. Other modes are also evident whose origin is as yet not known. However, the frequencies of the various peaks occur at such values that wave mixing could be possible in forming some of these waves. For example, the mode at 145 kHz and the peak at 78 kHz could mix to produce the wave at 67 kHz. The corresponding phase spectra tend to confirm this possibility, but further data must be gathered before the question of wave origin is answered.

We conclude that our spectra yields at least two phenomena of interest. First the plasma exhibits unstable modes whose frequency varies inversely with mode number. Secondly, we note the appearance of sidebands for the  $m=1$  mode suggesting the presence of a non-linear modulation of the plasma. Additionally, there is an apparent shift of plasma energy from the  $m=1$  mode into the sidebands as we reach a critical magnetic field as seen in Fig. 4.

The above discussion indicates some of the benefits of the digital spectral analysis system in performing plasma wave analysis. The detailed display of the spectra gives us a complete picture of the power and phase information for a given plasma condition. In this way we can ascertain much information about the wave process without having to perform lengthy observations on the analog signal. Further, in the form the data is displayed, direct theoretical analysis is possible because the wave number and phase velocity can be readily calculated. In connection with this we have performed a calculation relating the power spectrum for a linear wave excitation process to the linear dispersion relation.<sup>8</sup> Finally, the use of the power and coherence spectra provides one with a method of determining energy transfer between waves by displaying relative changes of the various modes in the spectra. This is quite useful in investigating non-linear wave coupling processes.

---

This work was supported by the Texas Atomic Energy Research Foundation and the Joint Services Electronics Program.

### References

1. G. D. Bergland, "A Guided Tour of the Fast Fourier Transform", IEEE Spectrum, vol. 6, pp. 46, July 1969.
2. D. E. Smith, E. J. Powers, and R. E. Rowberg, "Computer Processing of Plasma Data Utilizing a Fast-Fourier-Transform-Generated Spectral Analysis Approach", to be published in the IEEE Trans. on Nuclear Science, August, 1971.
3. R. B. Blackman and J. W. Tukey, The Measurement of Power Spectra, New York:Dover, 1959.
4. G. M. Jenkins and D. G. Watts, Spectral Analysis and Its Applications, San Francisco:Holden-Day, 1969.
5. E. J. Powers and D. E. Smith, "Diagnostics of Plasma Fluctuations Using Digital Spectral Analysis", Proceedings of the Tenth International Conference on Phenomena in Ionized Gases (Contributed Papers), Oxford, England, September 13-18, 1971, p. 437.
6. D. E. Smith, C. W. Thomas, and E. J. Powers, "A 1.5 MHz, Digital, Plasma-Data Acquisition and Processing System Using Multi-Time Delay Sampling", to be presented at the IEEE Nuclear Science Symposium, San Francisco, California, November 3-5, 1971.
7. E. J. Powers and D. E. Smith, "Applications of Spectral Analysis Techniques to the Diagnostics of Plasma Fluctuations", Biannual of Electronics Research No. 11, Electronics Research Center, The University of Texas at Austin, May 15, 1970, pp. 232-246.
8. R. E. Rowberg, "A Transfer Function Model of Plasma Drift Waves", Biannual of Electronics Research No. 12, The University of Texas at Austin, November 15, 1970, pp. 249-256.

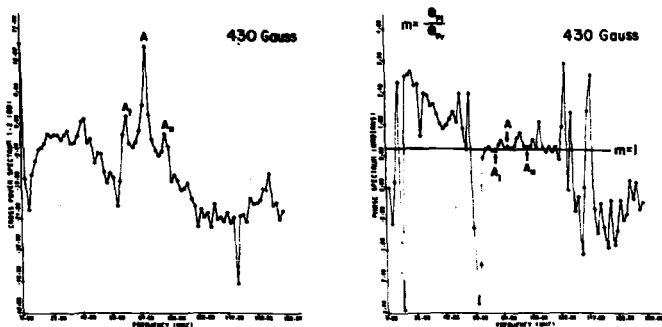


Figure 1. Cross-power amplitude and phase spectra for the case of a single, unstable mode (A) and "sidebands" ( $A_1$  and  $A_2$ ). The probes (1 and 2) are displaced in the azimuthal direction by the angle  $\theta_p$ . The wave phase difference is  $\theta_{p1}$ . The latter is clearly determined for all modes displayed in the amplitude spectrum.

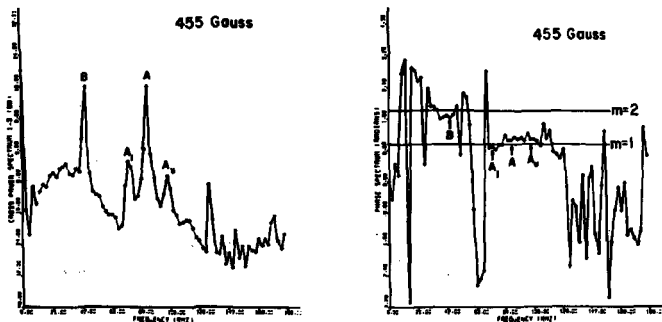


Figure 2. Amplitude and phase spectra for the case of two unstable modes (A and B). Note the mode number increases as the frequency decreases.

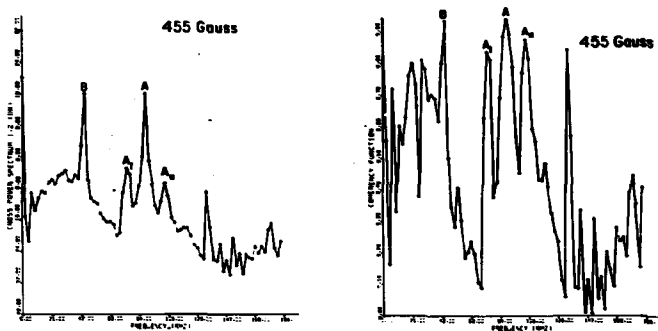


Figure 3. Amplitude and coherence spectra for the same conditions of Fig. 2. The value of the coherence for A and B is  $\approx 1.0$ , and for the "sidebands",  $A_2$  and  $A_1$ , it is  $\approx 0.87$ , indicative of wave phenomena. This demonstrates the value of the coherence function in identifying true wave motion.

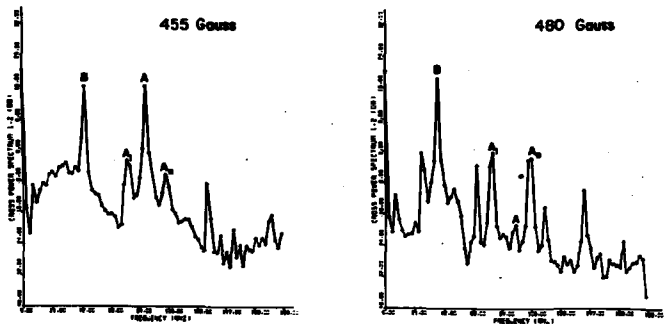


Figure 4. The change in amplitude spectra as we raise the magnetic field above a critical value ( $B_c \approx 480$  Gauss). The "sidebands" ( $A_2$  and  $A_1$ ) are enhanced while peak A is considerably reduced. These curves show the value of displaying power spectra in this manner in clearly determining changes in the mode structure as plasma conditions are changed.

Potential Surrounding a Moving Test-Particle in a  
Quiescent Plasma

by

K.C. Hines

University of Melbourne, Australia

Abstract

The self-consistent Vlasov and Maxwell equations can be solved for the effective potential surrounding a test-particle in a plasma. The solution is in the form of a 3-dimensional k-space integration.

Several authors have recently attempted to evaluate the integral analytically, but succeed only for limited ranges of the test-particle velocity,  $V$ , and range  $r$ .

We present first, preliminary results of a numerical evaluation of the potential valid for all values of  $V$  and  $a$ . The accuracy of these results was in some doubt because of numerical problems, and a new method of numerical analysis was therefore developed which is identical to that of Nishimura. However, the results obtained by the old method agree very well with Nishimura's work.

The long range part of the interaction is found to differ both from the standard Coulomb and from the static Debye forms. Contrary to expectations it appears to be impossible to represent the potential in the form  $1/r^p$  with any  $p$  valid over a worthwhile range of  $V$  and  $r$ .

Attention is drawn to the effect of the new form for the potential on the plasma transport processes, particularly the test particle energy loss problem.

The comparison with the gravitational case is also instructive, and an additional term occurs in the self consistent expression for the potential.

### 1. Potential Surrounding a Moving Test Particle

In 1967 Joyce, Montgomery and Sugihara [1],[2] obtained evidence for a radial fall off in the potential surrounding a test charge of the form  $1/r^3$ . This result was obtained for the situation of a plasma with two counter-moving electron streams in a uniform positive background, that is to say a marked anisotropy in the plasma velocity distribution function. It is natural to ask whether this sort of departure from the usual static Debye type screening exists for all situations with velocity anisotropies, and in particular for the physically more obvious case of a test particle moving with velocity  $\underline{V}$  through a Maxwellian plasma.

Analytic studies of this latter problem have appeared since, the first by Cooper [3] and the second by James and Vermeulen [4]. These authors obtained a series expansion for the dielectric coefficient of the plasma which, for calculation of the potential, was truncated after the term with

$$n = 2: \quad \epsilon(\underline{k}, -i\underline{k} \cdot \underline{V}) = 1 + \sum_{n=0}^{\infty} a_n (\hat{\underline{k}} \cdot \underline{V} / v_{\text{therm}})^n \quad \dots (1)$$

Use of this form for the dielectric function in the expression for the potential surrounding the moving test particle enabled this to be integrated in closed form for the two limiting cases of test particle - field point distance very much greater than and very much less than the Debye radius,  $\lambda_D$ . If  $\phi$  is the potential, the results of this work were:

$$\text{For } r \ll \lambda_D \text{ (inside the Debye sphere), } \phi \sim (q/r) \exp(-r/\lambda_D)$$

$$\text{For } r \gg \lambda_D \text{ (outside the Debye sphere), } \phi \sim \text{const}/r^3.$$

In between these two limiting regions is a transition region where neither of the above approximate expressions for the potential is adequate. In this transition region the expression for the potential cannot be integrated in closed form and numerical methods must be invoked. James and Vermeulen have demonstrated that the transition region moves outwards away from the test particle as  $\underline{V} \rightarrow 0$ , thus recovering the correct zero velocity limit.

### 2. The Potential and its Evaluation

The expression for the potential,  $\phi$ , which forms the basis for all this work is obtained from the usual self-consistent Vlasov and Maxwell equations. In the electrostatic approximation the only relevant Maxwell equation is

$$\nabla \cdot \underline{E} = -\nabla^2 \phi(\underline{r}, t) = 4\pi [\rho_{\text{ext}} - ne \int f^{(1)} d\underline{v}].$$

Fourier-Laplace transformation of this equation, together with the Vlasov equation, and the subsequent elimination of the perturbed distribution

function  $f^{(1)}$ , leads to the following expression for the potential in wave number and frequency space:

$$\phi(\underline{k}, \omega) = \frac{4\pi \rho_{\text{ext}}(\underline{k}, \omega)}{k^2 \left[ 1 - \frac{4\pi q_e e^2}{m R} \frac{(\underline{k} \cdot \underline{v}_0 / \omega - \underline{k} \cdot \underline{v})}{\omega + \underline{k} \cdot \underline{v}} \right]} = 4\pi \rho_{\text{ext}}(\underline{k}, \omega) / k^2 \epsilon(\underline{k}, \omega) \quad \dots (2)$$

The external charge density due to the test particle may be written

$$\rho_{\text{ext}}(\underline{r}, t) = q \delta(\underline{r} - \underline{r}_0 - \underline{v}t)$$

and this may be Fourier-Laplace transformed to yield

$$\rho_{\text{ext}}(\underline{k}, \omega) = 2\pi q \delta(\omega + \underline{k} \cdot \underline{v}).$$

This delta function in the numerator of the potential expression (2) enables us to perform the  $\omega$ -integral in the inversion of  $\phi(\underline{k}, \omega)$ , so yielding

$$\phi(\underline{r}, t) = (q/2\pi^2) \int d\underline{k} \exp(i\underline{k} \cdot \underline{R}) / [k^2 \epsilon(\underline{k}, -\underline{k} \cdot \underline{v})] \quad \dots (3)$$

with  $\underline{R} = \underline{r} - \underline{v}t$ ,  $\underline{r}_0 = 0$  and

$$\epsilon(\underline{k}, -\underline{k} \cdot \underline{v}) = 1 - \frac{\omega_p^2}{k^2} \int \frac{\underline{k} \cdot \partial f_0 / \partial \underline{v}}{\underline{k} \cdot \underline{v} - \underline{k} \cdot \underline{v}} d\underline{v} \quad \dots (4)$$

The idea behind the numerical work is to evaluate equation (3) at a number of points and so find the coefficients and parameters of an algebraic expression describing the potential,  $\phi$ , in various velocity and radius domains.

A reduction of equation (4) suitable for numerical work is

$$\epsilon = 1 + (k_D^2/k^2) [1 + i \sqrt{\pi} (\underline{k} \cdot \underline{U}) W(\underline{k} \cdot \underline{U})], \quad \dots (5)$$

where  $k_D = 1/\lambda_D$  and  $\underline{U} = \underline{v}/v_{\text{therm}}^{1/2}$ . This enables equation (3) for  $\phi$  to be written

$$\phi(\underline{R}) = (q/2\pi^2) \int d\underline{k} \exp(i\underline{k} \cdot \underline{R}) / [k^2 + k_D^2 F(\underline{k} \cdot \underline{U})], \quad \dots (6)$$

In the above equations  $W$  is the plasma dispersion function. From the asymptotic behaviour of this function [5] one readily finds that for  $|\underline{U}| \ll 1$ ,  $F \sim 1 + i0$ , so giving the usual Debye shielding at zero test particle velocity. On the other hand, for  $|\underline{U}| \gg 1$ ,  $F \sim 0 + i0$  over most of the range of integration, giving the unshielded Coulomb  $1/r$  potential in this limit. This corresponds physically to the fact that for a fast test particle the plasma has no time to respond, and no polarization cloud forms behind the external charge. The most interesting region from the point of view of plasma transport properties corresponds to  $|\underline{U}| \sim 1$ , and this is the region which is hardest to evaluate. Of course the restriction must always apply that the particle velocity is not so large that distortion in the potential leading eventually to a Cerenkov shock-wave becomes important, since the



derivation of  $\phi$  does not include the possibility of such an effect.

A numerical evaluation of the potential in this region was begun last year by R. Bruhns of the Melbourne plasma group.

The  $\phi$ -integrand contains the W function, which can be represented in simple form only by an infinite series and an asymptotic expansion, and a numerator reminiscent of Bessel functions. This suggests that, if complete accuracy is required,  $\phi$  can be represented by nothing less complex than, say, an infinite series in  $r$ , with coefficients functions of velocity and angle. In the light of the required  $1/r$  dependence very near the source, it will not be adequate to take simply a linear combination of  $1/r^3$  and  $e^{-r}/r$  in the hope of describing  $\phi$  for all  $r$ , even when there is a restriction to low velocities.

In Bruhn's numerical calculation the integral is first split into two parts

$$\Phi = \Phi_1 + \Phi_2 = \frac{q}{2\pi^2} \int_0^{k_{\max}} dk \int_0^{\pi} d\varphi' \int_0^{\pi} d\theta' \frac{k^2 \sin\theta' e^{ik \cdot \underline{R}}}{k^2 + k_D^2 F} + \frac{q}{2\pi^2} \int_{k_{\max}}^{\infty} dk \int_0^{\pi} d\varphi' \int_0^{\pi} d\theta' \frac{k^2 \sin\theta' e^{ik \cdot \underline{R}}}{k^2 + k_D^2 F} \quad (7)$$

With  $k_{\max}^2 \gg k_D^2$  the integral  $\Phi_2$  may be treated by rotating the  $0$ - $z$  axis to lie along  $\underline{R}$  if  $F \sim 1$ , since then the integrand no longer contains any reference to  $U$ .  $\Phi_2$  may then be reduced to

$$\Phi_2 = \frac{2q}{\pi R} [\pi/2 - \text{Si}(k_{\max} R)]$$

An approximate expression for the Sine integral in  $x \gg 1$  is

$$\text{Si}(x) = \pi/2 - f \cos(x) - g \sin(x),$$

where  $f$  and  $g$  are tabulated in Noble's book [6].

After considerable reduction of  $\Phi_1$ , the final expression used in the computation by Bruhns becomes

$$\frac{\Phi}{k_D q} = \frac{q}{2\pi^2} \int_0^{k_{\max}} dk \int_0^{\pi} d\varphi' \int_0^{\pi} d\theta' \frac{k^2 \cos(kR \sin\theta \sin\theta' \cos\varphi') \sin\theta'}{[(k^2 + f_R(U \cos\theta))^2 + f_I^2(U \cos\theta)]^{1/2}} \times \\ \times \{ [k^2 + f_R(U \cos\theta)] \cos(kR \cos\theta \cos\theta') + f_I(U \cos\theta) \sin(kR \cos\theta \cos\theta') \} + \frac{1}{R} [f \cos(k_{\max} R) + g \sin(k_{\max} R)] \quad \dots (8)$$

Here  $k$ ,  $k_{\max}$  have been normalized to  $k_D$ ,  $R$  is now expressed in units of  $\lambda_D$  and  $f_R$  is an approximation for the real part of  $\epsilon$ .  $f_I$  is the imaginary part of  $\epsilon$ .

In determining the potential for a given  $(U, r, \theta)$ ,  $(k, \phi', \theta')$  - space is divided into orthorhombic cells with a uniform spacing in the  $k$  and  $\phi'$  directions. Note that  $\theta$  is the angle between  $\underline{R}$  and  $\underline{U}$ , whilst  $\theta'$  is the angle between  $\underline{U}$  and  $\underline{k}$ . The integrand is then evaluated at the centre of each  $(k, \phi')$  rectangle for every  $\theta'$  step.

Preliminary integration results for  $\theta = 0$  (potential in the forward direction) are given in the following table. The values listed are of  $\phi/k_D q$ .

|               |        | TABLE  |        |        |        |      |
|---------------|--------|--------|--------|--------|--------|------|
| $R/\lambda_D$ | 0.     | .100   | .200   | .400   | .707   | ∞.   |
| 0.5           | 1.21   | 1.21   |        |        | 1.29   | 2.00 |
| 1.0           | .368   | .384   |        |        | .461   | 1.00 |
| 2.0           | .0677  | .0743  |        |        | .122   | .500 |
| 3.0           | .0166  | .0197  |        |        | .0477  | .333 |
| 6.0           | .00041 | .00151 | .00245 | .00453 | .00800 | .167 |
| 8.0           | .00004 |        |        |        | .00272 | .125 |

Some tentative conclusions can be drawn from these results. Firstly, a uniform reduction in shielding is observed as the velocity is raised from zero to  $v_{\text{therm}}$ . Within a Debye length, however, the change in potential is not great (<20%), verifying Cooper's reference to Nishimura's finding that  $\exp(-r)/r$  is reasonable out to the vicinity of  $r = \lambda_D$ . Secondly, no sign of the suggested  $1/r^p$  potential for  $p$  a constant (at least for a specific test particle velocity) has been found within 8 Debye lengths. Thirdly, results for directions not parallel to the motion (not shown in the table) suggest that shielding persists to a greater extent in the perpendicular direction. This is intuitively plausible since the relative motion between a stationary point and the test charge is least for this case. On present indications, however, the anisotropy is likely to become important only at distances far outside the Debye length and so this velocity effect may not lead to appreciable distortion of the Debye sphere itself.

Detailed study of the numerical procedures outlined above has revealed some unsatisfactory features. The most important concerns the behaviour of the integral referred to as  $\phi_1$  in equation (7) as a function of the upper limit,  $k_{\text{max}}$ . Instead of approaching a constant value for sufficiently large  $k_{\text{max}}$ , the integral  $\phi_1$  displayed oscillations which were significant enough to throw some doubt on the accuracy of the results obtained.

In view of this difficulty a new method of numerical integration of equation (6) was developed and programmed by E. Toime, also of the Melbourne group. In this approach equation (6) is integrated numerically by introducing a polar coordinate system with  $R$  directed along the  $z$ -axis and  $U$  lying in the  $xz$ -plane. In this new coordinate system the reduction of the potential, equation (6), to a form suitable for evaluation (that is to

say the equivalent in this new approach of equation (7)) is

$$\phi/k_D q = (1/\pi^2) \int_0^\infty dk k^2 \int_0^\pi d\theta \sin\theta \int_0^\pi d\phi \{A \cos(kR \cos\theta) - B \sin(kR \cos\theta)\} / (A^2 + B^2) \quad \dots (9)$$

where  $A = 1 + k^2 - \sqrt{\pi} \times \text{Im } W(x)$

$B = \sqrt{\pi} \times \exp(-x^2)$

and  $x = |U|(\cos\theta \cos\beta + \sin\theta \sin\beta \sin\phi)$

Here  $\beta$  is the angle between  $\underline{R}$  and  $\underline{U}$ , and  $R$  is again in units of  $\lambda_D$ .

At this stage in the work it came to the attention of our group that an identical reduction of equation (6) leading to equation (9) had been performed by Nishimura [7]. His numerical evaluation completed the calculations which Toime had started independently, and there was no point in pressing on to duplicate what appears to be a thorough and accurate determination of  $\phi$ . The values listed in the table (determined by the earlier numerical procedure), although of limited scope, agree with Nishimura's results to within 5%. Furthermore, the conclusions stated earlier as a result of this work are also borne out by much more complete results of Nishimura.

Similar conclusions have also been obtained from a study by Laing, Lamont and Fielding [8] of a two-dimensional system. One of the distinctive qualitative features of the situation is that the electrons will be sucked out of the background plasma by the field of the test particle, but will be directed to its retarded position. By the time they get there the test particle will have moved on, leaving a negative excess charge behind. As a consequence of this the potential ahead of the test particle will be more positive than for the spherically symmetric Debye potential. This negative charge build up behind the test particle is in effect a heavily damped plasma oscillation. As  $U$  increases the numerical studies of Laing et al on the two-dimensional system show that the damping decreases. Finally a fully developed plasma oscillation is established behind the test particle.

### 3. Effects of the Potential on Plasma Transport Properties

Since all test particle problems in a plasma involve the interaction of the test particle with the plasma via the  $\phi$  of equation (3), one sees that all plasma transport properties must be considered again in the light of the Nishimura potential. We may follow tradition in plasma theory by discussing the implications of the new form for the potential under the two headings of a binary collision effects and b collective effects.

a. Binary Collision Effects: N.E. Frankel of the Melbourne group has pointed out that in this case the transport properties are obtained by evaluating integrals of the type

$$Q_n = \int (1 - \cos^n \theta) \frac{d\sigma}{d\Omega} d\Omega$$

where  $n = 1$  corresponds to energy transport, and it is to be noted that the interesting physics comes from the small scattering angles,  $\theta \ll 1$ . For these small angles one may use the impulse approximation and find

$$\theta \approx \Delta p/p = - \int (\partial\phi/\partial r)(b/r) dt/p, \quad \dots (10)$$

where  $p$  is the momentum of the test particle and  $b$  is the classical impact parameter. The evaluation of this integral for the Coulomb  $1/r$  potential, giving the logarithmic divergence and consequent cut-off at small angles is well known. The more difficult evaluation for the Debye static potential has been carried through by Liboff [9]. It is important now to calculate the impulse approximation integral of equation (10) with the correct numerically evaluated form for the potential  $\phi$ . This will answer the question of what happens in between the Coulomb and static Debye situations and we will then know whether cut-offs are required or not for the partially screened potential. This calculation is made more difficult by our inability to represent the numerical results for the potential in the  $1/r^p$  form for which the transport integrals can be readily carried through. Nevertheless, we are hoping to represent Nishimura's results in a form which will enable these integrals to be done approximately. If cut-offs are required the asymmetry of the Debye shielding surface will be important.

b. Collective Effects: An example would be the calculation of the energy loss of a test particle moving through a plasma. This problem has been considered, for example, by Hines and Sigmar [10] and the result may be written

$$\text{energy loss} \sim \text{const} \int \frac{d\underline{k}}{k^2} \int_c \frac{\underline{k} \cdot \underline{v}}{c} \text{Im}(1/\epsilon(\underline{k}, \omega)) \frac{e^{i(\omega + \underline{k} \cdot \underline{v})t}}{\omega + \underline{k} \cdot \underline{v}} d\omega.$$

This expression diverges for large  $k$  and either a cut-off must be introduced or a unified theory used which combines the effects of binary collisions and collective effects to some degree of approximation (see for example May [11]). Although it is true that the correct dynamic screening is automatically taken into account by the existence of a pole in the  $\omega$ -integration for  $\omega = -\underline{k} \cdot \underline{v}$ , thus ensuring that the proper  $\epsilon(\underline{k}, -\underline{k} \cdot \underline{v})$  is employed for the calculation, there is another problem. The cut-off normally employed for this work assumes a symmetric screening cloud, and therefore the same value of

$k_{\max}$  independent of direction. If we can model the Nishimura potential mathematically, it will be possible to take account of asymmetric screening for these calculations by making  $k_{\max}$  depend on angle. This of course couples the angle and wave number integrations together in a much more complicated way. The implications of this complication for the unified theories will also have to be investigated.

#### 4. The Gravitational Analogue of the Potential

The Landau-Vlasov theory may be applied to systems of interacting stars. The new features are just the different sign of the force and the absence of a charge neutrality condition, since all the 'particles' are of the same 'sign' in the gravitational case. As a consequence of these differences one can show, from an analysis of the first two equations of the BBGKY hierarchy, that the decay of correlations (described by the pair correlation function) goes as

$$p(r_{12}) \sim \cos(k_G r_{12})/r_{12},$$

$r_{12}$  being the distance between the two interacting particles and  $k_G$  the gravitational analogue of the plasma  $k_D$ .

This means that for the gravitational system the test-star potential at zero velocity will be of the form  $\cos(kr)/r$  instead of the static Debye result. We expect that this form for the potential, combined with the formulae for stellar transport, will lead to conditionally convergent results for, say, the energy transport in a gravitating system.

An analogous development to that leading to equation (3) results in the following expression for the self-consistent potential surrounding a moving test-star in a uniform, homogeneous stellar system:

$$\Phi_0(\mathbf{z}, t) = - \frac{4\pi G M}{(2\pi)^3} \int d\mathbf{k} e^{i\mathbf{k}\cdot\mathbf{R}} / k^2 \epsilon_0 - \frac{4\pi G n_0 m}{(2\pi)^3} \int d\omega \int d\mathbf{k} e^{i(\omega t + \mathbf{k}\cdot\mathbf{z})} \delta(k) / \omega k^2 \epsilon_0$$

where

$$\epsilon_0 = 1 + \frac{4\pi G n_0}{k^2} \int \frac{\mathbf{k} \cdot \partial f_0 / \partial \mathbf{V}}{\omega + \mathbf{k} \cdot \mathbf{V}} d\mathbf{V}$$

is the equivalent of the plasma dielectric function. Here  $G$  is the gravitational constant,  $M$  the mass of the test-star,  $m$  the mass of the other stars in the system and  $n_0$  the number density.

The first term is well-behaved and is the analogue of the plasma potential evaluated in the earlier sections whereas the second term arises because of the absence of a neutralizing background. It is an infinite potential term arising from the infinite homogeneous charge distribution assumed in this model.

5. References

- [ 1 ] G.R. JOYCE and D. MONTGOMERY, *Physics Fluids*, 10, 2017 (1967).
- [ 2 ] D. MONTGOMERY, G. JOYCE and R. SUGIHARA, *Plasma Physics*, 10, 681 (1968).
- [ 3 ] G. COOPER, *Physics Fluids*, 12, 2707 (1969).
- [ 4 ] C.R. JAMES and F. VERMEULEN, *Canadian Journal of Physics*, 48, 349 (1970).
- [ 5 ] B.D. FRIED and S.D. CONTE, *The Plasma Dispersion Function*, Academic Press (1961).
- [ 6 ] B. NOBLE, *Numerical Methods 1*, Oliver and Boyd (1966).
- [ 7 ] K. NISHIMURA, UCRL-71754 (1969).
- [ 8 ] E.W. LAING, A. LAMONT and P.J. FIELDING, *Journal of Plasma Physics*, 5, 441 (1971).
- [ 9 ] R.L. LIBOFF, *Physics Fluids*, 2, 40 (1959).
- [ 10 ] K.C. HINES and D.J. SIGMAR, *Conference on Phenomena in Ionized Gases*, Vienna (1967).
- [ 11 ] R.M. MAY, *Australian Journal of Physics*, 22, 687 (1969).

A Measurement of  $T_{\perp}$  of Ba Plasma in a Q-Machine

by

I. Katsumata<sup>†</sup>

Max-Planck Institut für Plasma physik, EURATOM-Association,  
Garching near Munich, Federal Republic of Germany

Abstract

Ion temperatures perpendicular to the magnetic field, electron temperatures, plasma densities, and plasma potentials of Ba plasmas in a single-ended Q-machine are measured in a low density regime by means of an ion sensitive probe. Data obtained are compared with the predictions of a collisionless theory of Q-machine plasma. Satisfactory agreement is found. In particular, within experimental accuracy of 10%, the measured ion temperatures agree with the corresponding temperatures of the plasma generating plate.

Introduction

In a Q-machine, ions are produced by thermal contact ionization of alkali or alkali earth atoms on the surface of a hot refractory metal. On the plate, the ion energy distribution function is expected to be Maxwellian of a temperature identical with the generating plate. They are supplied into the plasma across a sheath either of electron (electron rich regime) or ion (ion rich regime). In the absence of any dissipation mechanism of directed energy, the energy distribution function perpendicular to the magnetic field should keep its initial temperature in the plasma in both the regimes, though the parallel energy distribution function in the electron rich regime becomes a truncated Maxwellian due to the acceleration in the electron sheath<sup>1)</sup>.

A measurement of  $T_{\perp}$  was already made in Cs plasmas in a single-ended Q-machine by means of an ion sensitive probe and good agreement was observed between measured  $T_{\perp}$  and corresponding plate temperature as long as plasmas were in ion rich regime.<sup>2)</sup> In that experiment, however, the hot plate was a 45° type and the elevation of  $T_{\perp}$  depends on experimental conditions in very complicated manner in electron rich

regime.

The purpose of the present experiment is to measure  $T_{i2}$  under more refined conditions, where the hot plate has been a perpendicular type and plasma densities have been varied down to a collisionless region. A combination of a Re plate and Ba has been used in the present experiment to enable to make both the regimes in the low density region of  $\approx 10^9/\text{cm}^3$ . Temperatures of ion and electron have been measured by means of an ion sensitive probe<sup>3,4)</sup> and are compared with that of the hot plate. By the way, plasma densities and plasma potentials have been measured with the same probe and are compared with the prediction of a collisionless theory proposed by Hashmi et. al.<sup>5)</sup>. In the calculation of theoretical curves, following values have been used; ionization potential of Ba=5.21 V, electron and ion emission work functions of Re =4.93 V and 5.43 V respectively, and the coefficient of the Richardson equation =  $200 \text{ A/cm}^2 \text{K}^{2/6}$ .

#### Experiment

Q-Machine The Q-machine Barbara has been used<sup>7)</sup>. The machine is a vertical type and has two end plates of 32 mm in diameter. A distance between two plates is 50 cm, so that the critical density, at which the collision mean free path is the same as the length of the plasma column, is about  $10^9/\text{cm}^3$ . The upper plate has been heated and illuminated by a Ba atomic beam. After some measurements, an aperture limiter 30 mm in diameter has been attached to the upper plate to avoid the ion emission from the Ba illuminated side of the plate assembly and to control the potential distribution around the plate. The lower plate has been kept at floating or biased at -9 V during the measurement, which is very important to suppress the plasma heating by the current induced instabilities in this type of experiment. The magnetic field has been kept at 5 kG throughout the experiment. The probe has been inserted into the plasma in the middle between both the end plates.

Probe The ion sensitive probe used is illustrated in Fig. 1. The probe consists of an inner, plane ion collector and an outer cylindrical guard electrode which is to prevent the electron current to the inner electrode.



The plane of the ion collector, which is a flat end of a Mo or Cu rod, should be oriented parallel to the magnetic field. Under adequate conditions, the inner electrode collects only ions even when the probe is biased positive to the plasma, so that one can measure the ion temperature from a current-voltage characteristics with a familiar method in retarding potential energy analyzer. The depth of the ion collector, denoted as  $h$  in Fig. 1, should be selected larger than a critical value which depends on the electron gyro radius, the Debye distance and the diameter of the probe.<sup>8)</sup> The same voltage must be applied to both the electrodes, which is to avoid the electron current to the ion collector due to  $E \times B$  drift in the case of positive voltage excess of the ion collector and also to avoid the deformation of characteristics in the case of negative voltage excess of the ion collector.

To make possible the selection of the smallest value of  $h$ , the ion collector of the probe used has been made movable. In the present experiment, values of  $h$  have been from 0.1 to 0.15 mm. Generally in metal vapor plasmas, the work function of a probe changes appreciably by coverage of the plasma constituent metal on it. A trouble, which has been expected and, indeed, been observed in Ba plasma, is the change of work function under the bombardment by plasma electrons during voltage sweep. This difficulty has been overcome by covering the whole surface of electrodes of the probe exposed to the plasma by thin layer of Ba metal. This has been made daily before the measurement by exposing the probe in a high density plasma produced in double end operation.

A typical example of  $\log I-V$  curve is illustrated in Fig. 2, where the curve of electron has been taken by the outer-electrode. In the course of experiment, the ion collector extruded beyond the outer electrode has also been used as a Langmuir probe.

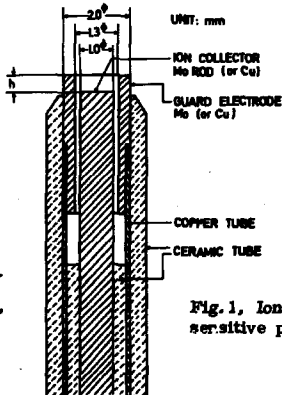


Fig. 1, Ion sensitive probe

In order to measure the plasma density  $n$ , the ion saturation current  $I_i$  and the ion temperature measured have been used. To eliminate the shadow effect of the guard electrode for ions of small gyro radii,  $I_i$  has been obtained graphically from the cross point of two straight lines extrapolated from the saturation and the exponential fall regions of  $\log I_i - V$  curve. A well-known relation

$$I_i = (1/4)ne\bar{v}_i s$$

has been used in the calculation of the plasma density, where  $e$  is the charge of proton,  $\bar{v}_i$  the mean thermal velocity of ion given by  $(8kT_i/\pi M_i)^{1/2}$  and  $s$  is an effective

area of the ion collector corrected by a geometrical factor as given below. The correction has been made introducing a simple approximation that ions, enter through the opening of the outer electrode, are collected by each electrode depending on their relative area. Then,

$$s = \pi r_g^2 \cdot \pi \left\{ (r_g + r_p)/2 \right\}^2 / (2\pi r_g h + \pi r_g^2),$$

where  $r_g$  and  $r_p$  are inner radius of the guard electrode and the radius of the ion collector, respectively. This relation has been experimentally checked, where the ion saturation current has been measured as a function of  $h$  and compared with the relation above. Satisfactory agreement has been found. The deviation between them increases with  $h$ , however, it is smaller than 20% at a rather large value of  $h = 0.5$  mm.

### Results

Figure 3 illustrates typical results obtained at a atomic beam intensity  $J_0 = 3 \times 10^{14} / \text{cm}^2 \text{sec}$ , where  $T_i$ ,  $T_e$  and plasma potentials are presented as functions of hot plate heating power together with corresponding plate temperature  $T_p$ . For reference to the plasma potential, the theoretical curve is also presented. Plasma densities range from  $8 \times 10^8$  to  $3 \times 10^9$

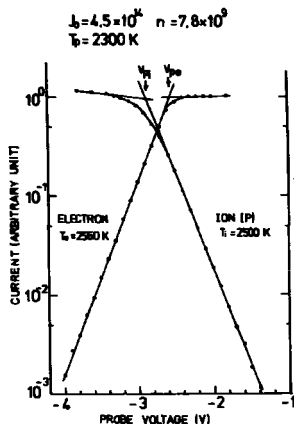


Fig. 2. Typical characteristics of the probe

per  $\text{cm}^3$  in present data. The actual sheath transition can be found out in the figure at a plate heating power near 1.0 kW corresponding to a plate temperature 2400 K. This transition is also clear in the case of the plate temperature dependence of the plasma density as seen later in the next figure. An interpretation on the discrepancy between measured plasma potentials and the theoretical prediction will be given later. As seen in the figure, measured ion and electron temperatures agree well with corresponding plate temperatures in respective regime.

Because the deflection mean free path of electron in ions is comparable or shorter than the plasma column, the increase of electron temperatures in ion rich regime may be attributed to the dissipation of parallel energy through the collision with ions. The heating of ions observed in electron rich regime can, evidently, not explained by the collision with electrons. At a lower atomic beam intensity of  $6 \times 10^{13} / \text{cm}^2 \text{ sec}$ , any distinguishable heating of ion has not been observed. On the contrary, at a higher atomic beam intensity, the heating of ion has become much more clear, namely, a sudden elevation of the temperature has been observed immediately after the sheath transition into the electron rich regime. This heating effect may be interpreted in terms of viscous heating as discussed below.

The temperature distribution of the hot plate has a ring-shaped maximum corresponding to the position of a ring cathode for electron bombardment heating of the plate. The probe has been placed at the corresponding position to this temperature maximum during the measurement presented here. The sheath transition does not take place at the same time over the plate. For example, when the sheath transition takes

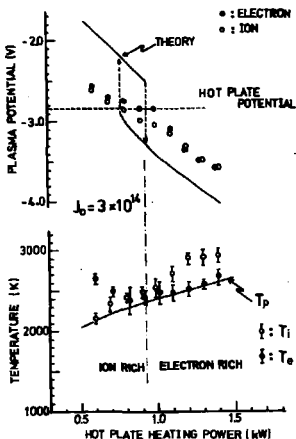


Fig. 3 Results of temperature and plasma potential measurements

place at the position of the temperature maximum, the remaining part of the plasma is still in ion rich regime. Then, the radial electric field changes its polarity within the radius of the plasma. In such a composite regime, a shear of the drift velocity will be enhanced than in a pure regime. Thus the viscous heating will become evident when the ion-ion collision mean free path becomes shorter than the plasma column. A rough estimation based on the analysis of Braginsky<sup>9)</sup> on the viscous heating agrees with the experimentally observed heating rate within the order of magnitude. A more detailed analysis along this line is now under the way.

In the theoretical curve of plasma potential, two dashed lines represent the sheath transitions, which take place at different plate temperatures depending on the direction of transition. This phenomenon was, at first, pointed out by A. L. Eichenbaum and K. G. Hernqvist<sup>10)</sup> in terms of the space charge instability in their analysis on collisionless synthesized plasma, where, as a criterion for stable sheath, a monotonic potential distribution along the plasma column was assumed. In experimental data presented here, the collisionless theory does not hold in electron rich regime but in ion rich regime, since the ion deflection mean free path in electrons is much longer than the plasma column as mentioned before. As origins of the discrepancy between the measurement and the theory, there may be two possibilities. One is a error in the plate temperature measurement and the other is the adoption of the inadequate values for the constants in the Richardson equation in the theoretical calculation. The plate temperature has been measured by means of a optical pyrometer calibrated by a standard tungsten lamp and the correction due to

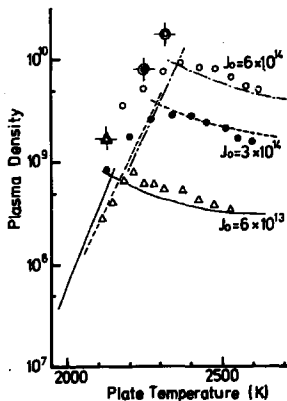


Fig. 4 Results of density measurements

emissivity of Re has also been made.<sup>11)</sup>

If the discrepancy would be due to the error in the plate temperature measurement, it should be about 150 degrees. This value can not be explained, because the error of the optical pyrometer used has been within 20 degrees and a 10% increase of the emissivity causes 1% lowering of the measured temperature. On the other hand, the lowering of 150 degrees correspond to, for example, a increase 0.3 V in the electronic work function of the plate, provided that the used coefficient in the Richardson equation ( $200A/cm^2K^2$ ) is valid. It can be, therefore, concluded that the discrepancy is mainly caused by the use of inadequate values of constants in Richardson equation.

Results of density measurements made at three atomic intensities are presented in Fig. 4 together with corresponding theoretical curves. Three points with cross in the figure represent conditions for sheath free state, however, they are singular solutions of the theory and unstable<sup>10)</sup>. As expected, the agreement between experimental values and theoretical curves becomes the better for the lower atomic beam intensity. In the case of the lowest atomic beam intensity, the agreement is satisfactory except a slight shift to the right on which the interpretation has already made concerning the plasma potential. The other two curves show also good agreement in electron rich regime, as expected, where the collisionless theory still holds for.

Finally, Fig. 5 illustrates typical examples of radial temperature distributions in the plasma and on the plasma generating plate at a plate heating power 0.6 kW. The ion temperature has been measured at  $J_0 = 4 \times 10^{14}$  (ion rich regime) and the electron temperature has been measured at  $J_0 = 1.2 \times 10^{13}$  (electron rich

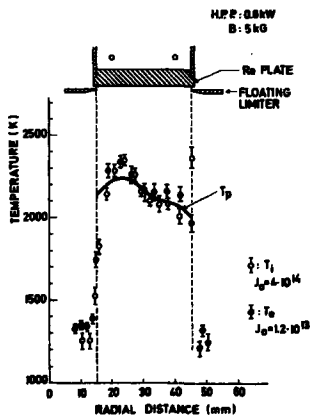


Fig. 5 Radial temperature distribution of ion, electron and the generating plate

regime). As seen in the figure, temperatures of ion, electron and the plate agree very well with each other except an ion temperature at the right hand side edge of the limiter where intense noise of the plasma has been observed.

#### Conclusion

It can be concluded that, in collision less Ba plasma in single-ended Q-machine, the ion temperature perpendicular to the magnetic field and the electron temperature agree the temperature of the plasma generating plate within experimental accuracy better than 10%, and further, agreement between the experiment and the collisionless theory is satisfactory. The latter conclusion support also the reliability of the ion sensitive probe in density measurement in the presence of drift velocity.

On the heating of ion in higher density region, more detailed study should be necessary.

#### Reference

† On leave of absence from Reseach Institute for Atomic Energy, Osaka City University, Osaka, Japan, supported by the fellowship of the Alexander-von-Humboldt-Foundation.

- 1) S.A. Anderson, V.O. Jensen and P. Michelsen, Proceeding of the IV European Conference on Cont. Fusion and Plasma Physics, Rome, 1970; 123
- 2) I. Katsumata, Annual Review of IPP Japan (Apr.1967 - March 1968) 59
- 3) I. Katsumata, M. Okazaki, Japan J. Appl. Phys., **6** 123 (1967)
- 4) I. Katsumata et.al., IV Europ. Conf. on Controlled fusion and Plasma Physics, Rome 1970, 122
- 5) M. Hashmi et. al., Nucl. Fusion **10** 163 (1970)
- 6) A. Ya. Tanteqode, E. Ya. Zandberg, Sovj. Phys. Techn. Phys. **11** 713 (1966)
- 7) M. Hashmi et. al., Nucl. Fusion **10** 173 (1970)
- 8) I. Katsumata, Collec. Pap. of Riken Symp. (Nov. 20, 1968), - in Japanese -(Publ. March 5, 1969 by Institute of Physical and Chemical Research, Tokyo, Japan), 28
- 9) S. J. Braginskii, Reviews of Plasma Physics, M. A. Leontovich, Ed. (Consultant Bureau Enterprises, Inc., New York, 1965), Vol. I, 219
- 10) A. L. Eichenbaun and K. G. Hernqvist, J. Appl. Phys., **32** 16 (1961)
- 11) Kohlrausch, Praktische Physik, (B. G. Teubner Verlag. Stuttgart, 1968) Vol. III, 70

A Small Electrostatic Energy Analyser

by

Poul Michelsen

Danish Atomic Energy Commission  
Research Establishment Risø  
Roskilde, Denmark

Abstract

A small energy analyser was constructed for measurements of the local ion velocity distribution function in a Q-machine. The outer diameter of the analyser was 2 mm and the collecting area  $2 \times 5$  mm. To avoid Cs-condensation the analyser can be heated to about  $300^{\circ}\text{C}$ . The analyser can be used in a double-ended Q-machine without disturbing the plasma too much. Measurements of the ion velocity distribution are discussed.

Introduction

The ion velocity distribution in a double-ended Q-machine plasma was measured with a small electrostatic energy analyser. Recently many wave experiments have been performed in D. E. Q-machines<sup>(1)</sup>. To compare the results of this kind of experiment with theory it is of importance to know the ion velocity distribution function both in the steady state and in the disturbed plasma. A few papers concerning energy analysers for single-ended Q-machines have been published<sup>(2-3)</sup>. These analysers had a size comparable with the diameter of the plasma column and could therefore not be used in double-ended machines. The analyser described in this paper is cylindrical, 2 mm in diameter, i. e. comparable with the ion gyro radius. The disturbance of the plasma due to the analyser is therefore relatively small.





The energy resolution of the analyser is not so good as that obtained in refs. 2 and 3, probably because of geometrical effects. However, it is possible to measure the main features of the ion distribution function.

The results were as expected. At low densities and high plate temperature the ion velocity distribution function in a D. E. Q-machine has two humps. A group of ions streams from each hot plate. At higher densities the potential drop at the hot plates decreases so the difference in velocity of the two ion groups becomes smaller. Furthermore, collisions become important, and the two groups are mixed together.

At high densities it is not possible to determine the plasma potential with sufficient accuracy, but the results indicate a single-humped distribution function with low mean velocity.

### The Analyser

The analyser is shown in fig. 1. It consists of an aluminium tube, 2 mm in diameter. This tube is oxidized to insulate it from the inner collector, which is a 1-mm tube. A hole of  $5 \times 0.5 \text{ mm}^2$  in the outer tube is covered with a copper mesh with 25 p. c. transmission and  $25 \mu\text{m} \times 25 \mu\text{m}$  holes. The inner tube contains two thermocouple wires primarily used for heating of the analyser to avoid caesium condensation.

In operation the outer tube and thus the mesh are biased by a few volts negative with respect to the plasma potential in order to reflect electrons. The distribution of ion energies is determined by measurement of the characteristic current voltage at the collector plate. By differentiation of this signal with respect to the collector voltage,  $\varphi_a$ , we get

$$\frac{dI}{d\varphi_a} \propto I \left[ v = \left( \frac{2e(\varphi_a - \varphi_{pl})}{m} \right)^{1/2} \right] \quad \text{for } \varphi_a \geq \varphi_{pl}, \quad (1)$$

where  $I$  is the collector current, and  $\varphi_{pl}$  is the plasma potential.

The Q-machine and the electric circuit connected to the analyser are shown schematically in fig. 2. A 3 kc/s signal is applied to the transformer and thereby added to  $\varphi_a$ . The corresponding ac current is measured with a PAR lock-in amplifier and displayed on the scope as a function of  $\varphi_a$ .

Capacitive currents are independent of  $\varphi_a$ , and they will therefore only give a constant output from the lock-in amplifier, which may furthermore be compensated away.

The energy resolution of the analyser was measured to be 0.1 - 0.2 V which is not as good as for the analyser described in ref. 3. The resolution

for this large analyser was less than 0.03 V. The resolution of the small analyser was measured in two ways:

First simultaneous measurements of the ion distribution function were taken in a S. E. Q-machine with the small analyser and the large one (ref. 3). The difference between the widths of the distribution functions then gives the resolution of the small analyser. The other method was based on charge exchange processes<sup>(3)</sup>. In the tube surrounding the plasma column (fig. 2) a beam of neutral Cs is induced. Because of the temperature (500°K) of the tube the Cs-atoms will not condense on the walls, and the pressure of neutral Cs is therefore considerably higher inside the tube than outside. Some of the ions in the plasma will undergo charge exchange in this region. This means that we get a group of cold ions with a very small mean velocity.

By measuring the distribution function for these ions, whose width is narrow compared with the energy resolution, it is possible to measure the latter. The group of charge-exchange-produced ions may also be used for determination of the plasma potential if there are only few slow ions in the main distribution<sup>(3)</sup>. To find  $f(v)$  from (1)  $\phi_{pl}$  must be known.

### Measurements

By means of the technique described, the ion velocity distribution function was measured in a double-ended Q-machine. The purpose of this examination was only to find the main features of the distribution function. As shown in ref. 3,  $f(v)$  in a single-ended Q-machine varies rather great with the important parameters such as plasma density, plate temperature, background pressure, etc. This means that if we want to know  $f(v)$  for comparison purposes, it has to be measured in the actual case.

In figs. 3a-b  $f(v)$  is shown measured with the analyser facing the hot plates, A and B. The density is low ( $n \approx 10^8 \text{ cm}^{-3}$ ), and the hot plates have the same temperature. The noise level is rather large because of the small signals. On the left-hand side of fig. 3a is seen the signal due to the charge-exchange-produced ions. This has disappeared in fig. 3b, but the average energy of the main group of ions is the same. This energy can be found as the distance in volts,  $\phi_0$ , between the two ion groups which is about 2.3 V. This corresponds to a velocity of

$$v = \sqrt{\frac{2e\phi_0}{m}} \approx 1.8 \cdot 10^3 \text{ m/s.}$$

The plasma potential is the same in the two pictures, and therefore the mean velocity of the ion groups coming from the two hot plates is about the same. The total velocity difference between these two groups is therefore  $3.6 \cdot 10^3$  m/s.

In figs. 4a-b the density has been increased to  $\sim 8 \cdot 10^9$  cm<sup>3</sup>. In this case the distribution is very broad because of collisions between the two ion beams. It is not possible to determine  $\varphi_{pl}$  with the charge exchange ions in this case because they disappear in the main distribution. The ion flux coming from hot plate No. 2 is smaller than that coming from hot plate No. 1 because the neutral Cs is supplied at the latter.

The effect of the temperature of hot plate No. 2 is shown in figs. 5a-c. The analyser faces this plate whose temperature is 2300, 2200 and 2100°K in the three pictures. The temperature of hot plate No. 1 is kept constant at 2300°K. The density is  $\sim 4 \cdot 10^8$  cm<sup>-3</sup>.

#### Acknowledgement

The author wants to thank M. Nielsen for constructing the analyser.

#### References

- 1) A. Y. Wong, N. D'Angelo, and R. W. Motley, Phys. Rev. 133, A436 (1964).  
H. K. Andersen, N. D'Angelo, V. O. Jensen, P. Michelsen, and P. Nielsen, Phys. Fluids 11, 1177 (1968).
- 2) J. M. Buzzi, H. J. Doucet, and D. Gresillon, Phys. Fluids 13, 3041 (1970).
- 3) S. A. Andersen, V. O. Jensen, P. Michelsen, and P. Nielsen, Phys. Fluids 14, 728 (1971).

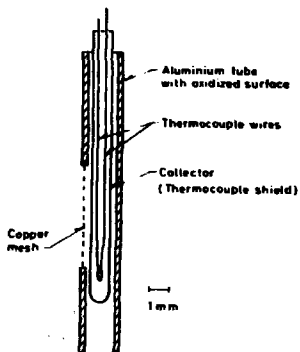


Fig. 1. The electrostatic analyzer.

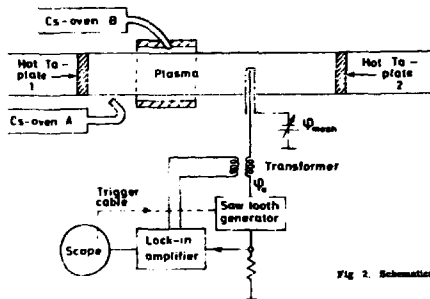


Fig. 2. Schematic of the experimental set-up.

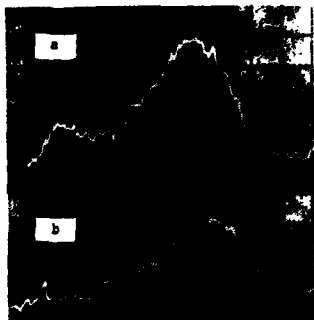


Fig. 3. Distribution functions at low density,  $n \approx 10^8 \text{ cm}^{-3}$  a) analyzer facing hot plate No. 1. The small peak is due to charge exchange ions. b) analyzer facing hot plate No. 2. Sweep 0.5 V/large div.



Fig. 4. Distribution functions in the collision-dominated range,  $n \approx 8 \cdot 10^9$   $\text{cm}^{-3}$ . a) analyser facing hot plate No. 1, b) analyser facing hot plate No. 2. Sweep 0.5 V/large div.

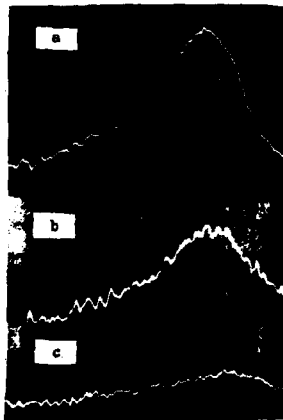


Fig. 5. Distribution functions measured with analyser facing hot plate No. 2. Temperature of hot plate No. 1:  $\approx 2200^\circ\text{K}$ . Temperature of hot plate No. 2: a)  $2500^\circ\text{K}$ ; b)  $2200^\circ\text{K}$ ; c)  $2100^\circ\text{K}$ . Sweep 0.5 V/large div.

RESONANCE CHARGE EXCHANGE CROSS SECTION  
FOR CESIUM MEASURED AROUND 2 eV

\*S.A. Andersen, V.O. Jensen and P. Michelsen

Danish Atomic Energy Commission

Research Establishment Risø, Roskilde, Denmark

ABSTRACT

The resonance charge exchange cross section for Cesium was measured in a Q-machine at energies around 2 eV. It was found that  $\sigma_{c.e.} = 0.6 \cdot 10^{-13} \text{ cm}^2 \pm 20\%$ .

TEXT

Measurements at energies under 10 eV of the cross sections for resonance charge exchange processes of the type



are interesting from a theoretical as well as from an experimental point of view. Theoretically, the cross section is expected to increase rapidly with decreasing energy, and experimentally, knowledge of the cross section is important in the construction of ion sources, in plasma physics, etc. Many

measurements in the energy range above 10 eV have been reported. Those by Marino et al.<sup>1)</sup> are supposedly the most accurate. Measurements at 10 eV or less are very difficult to perform because of the difficulties in obtaining ion beams with sufficiently well-known energy and narrow-enough energy spread. Recently Palyukh and Savchin<sup>2)</sup> reported on measurements of the cross sections for process (1) in the energy range from 100 eV to 1 eV. In this work ions are formed on a hot tungsten ribbon and accelerated through an electrode system into a charge exchange chamber with a known pressure of neutral Cesium. At the opposite end of the chamber the ions are collected on a negatively biased plate. From the current-voltage characteristics of this plate the charge exchange cross sections are deduced. There are two limitations to the energy resolution in this experiment. Firstly, the potential in the charge exchange chamber varies along the ion path, and therefore the ion energy at which charge exchange occurs is not well defined. Secondly, the exact energy of the ions entering the charge exchange chamber is not known because of lack of knowledge of the work functions of the tungsten ribbon and of the accelerating electrodes. This last point is of importance only at low energies (under a few eV).

In this paper we report on measurements of the cross section for process (1) performed in the Risø Q-machine<sup>3)</sup> at energies around 2 eV. Our technique is in principle similar to that of Palyukh and Savchin<sup>2)</sup> mentioned above. The energy resolution, however, is improved because all charge exchange processes take place at the same potential, i. e. the plasma potential, and because the energy of the ions is measured directly by an electrostatic energy analyser<sup>3)</sup>.

Using a very different technique, Dreicher et al.<sup>4)</sup> have performed measurements of resonance charge exchange cross sections for K in a Q-machine.

The experimental set-up is shown in Fig. 1. The plasma is produced by surface ionization of a beam of Cs-atoms from oven A on the hot ( 2500°K)

tantalum plate (diameter 3 cm) and is confined radially by a magnetic field of the intensity of 0.4 T. Ions formed at the hot plate are accelerated through a narrow sheath close to the plate from the plate potential down to the plasma potential,  $\varphi_{pl}$ . This potential drop is variable between 0.5 and 2.5 V<sup>3)</sup>. Once in the plasma the ions flow freely along the magnetic lines of force towards the analyser. Their perpendicular energy, which corresponds to the temperature of the hot plate ( $\sim 2$  eV), is unchanged by passing through the sheath. The ion density in the plasma is approximately  $10^9$  cm<sup>-3</sup> in this experiment, hence ion-ion collisions may be neglected.

The charge exchange processes take place in a limited region of length of the plasma column, which is crossed by a beam of Cs-atoms from oven B. A neutral detector is used to measure the flux of Cs-atoms in this region. All atoms hitting the heated tungsten wire in the detector are ionized and collected on two negatively biased collector plates. The collector current,  $I_c$ , is related to the neutral density,  $n_n$ , as follows

$$I_c = n_n \bar{c} A q \quad (2)$$

where A is the apparent area of the tungsten wire and

$$\bar{c} = (8\pi T_0/\pi m)^{1/2} \quad (3)$$

$T_0$  is the temperature of the tip of oven B, and is measured with a thermocouple ( $\sim 900^\circ\text{K}$  in the experiment). In calculating the neutral density in the plasma column from the measurement of  $I_c$ , a geometrical factor must be introduced to take into account the set-up in Fig. 1. The validity range of eq. (3) has been discussed by Lou<sup>5)</sup>; according to his work, (3) is certainly valid within the range of this experiment.

The beam of neutral Cs from oven B can be turned on/off by a shutter. To avoid reflection of atoms from this beam towards the hot Ta-plate, whence they would become ionized the beam is absorbed on a plate cooled by liquid N<sub>2</sub>. The walls of the vacuum system (not shown in Fig. 1) are



also cold. ( $\sim 25^{\circ}\text{C}$ ). A square opening in a cooled diaphragm determines the dimensions of the beam. By moving the neutral detector longitudinally it is found that the density of neutral Cesium is essentially zero outside the beam and constant within it.

The velocity distribution function of ions which have passed through the neutral beam region is examined by means of an electrostatic analyser<sup>3)</sup>. The analyser consists of a fine-meshed grid negatively biased (-6V) for reflection of electrons. The current-voltage characteristic ( $I_a - \varphi_a$ ) of a collector behind the grid is used to determine the distribution function,  $f(v)$ , since

$$I(\varphi_a) = \text{const} \int_{v_{\min}}^{\infty} v f(v) dv \quad (4)$$

where  $\frac{1}{2}mv_{\min}^2 = q(\varphi_a - \varphi_{pl})$ . The characteristic therefore shows the flux of ions with energies higher than  $q(\varphi_a - \varphi_{pl})$ . Curve (a) in Fig. 2 is an example of such a characteristic. The curve was obtained with the shutter closed, and the density in the neutral beam was therefore zero. It is seen that the majority of the ions have energies around 2 eV. Curve (b) is obtained with a neutral beam passing through the plasma column. Some fast ions undergo charge exchange with atoms to give slow ions. In the high energy range curve (b) therefore runs below curve (a). Only at very low energies ( $\varphi_a \approx \varphi_{pl}$ ) are the slow ions accepted by the analyser plate and here the two curves coincide. The difference  $\Delta I$  between curves (a) and (b) at their plateaux (where they are parallel) (see Fig. 2) is a measure of the number of ions having undergone charge exchange in the neutral cloud. The charge exchange cross section is therefore given by

$$\sigma_{c.e.} = \frac{1}{n_n l} \ln \left( \frac{I_0}{I_0 - \Delta I} \right) \approx \frac{1}{n_n l} \frac{\Delta I}{I_0} \quad (5)$$

In the experiments the neutral density was first determined from a measurement of  $I_c$  (eq. (2)). The neutral detector was then removed from the neutral beam to avoid scattering of Cs-atoms from the beam through the chamber. The characteristic (b) was taken. The shutter was then closed and characteristic (a) taken. During the experiment, fluctuation in the neutral density was about 20%. All other sources of uncertainty were small by comparison.

The result of the experiment is

$$\sigma_{c.e.} = 0.6 \cdot 10^{-13} \text{ cm}^2 \pm 20\%$$

at ion energies within a spread of 0.4 eV centred at 2.0 eV. It should be noted that these results are in agreement with the predictions of Marino et al.<sup>1)</sup>

The predominant sources of uncertainty is the neutral beam fluctuation, which occurs at the high density needed in this experiment. It should be possible to improve this technique by constructing an oven giving a more constant beam at high densities. From all other sources of error, the contribution was estimated at ~5%, which may be ignored in comparison with the uncertainty caused by fluctuations in the neutral beam density. The energy spread of the ion beam is determined by the temperature at the hot plate and fluctuations in the work function of the plate<sup>3)</sup>. We cannot see how we can improve this. The possibility of measuring the cross section at lower energies is also small - at lower energies we do not see the flat plateaux on the curves (b).

In principle, it is possible to deduce  $\sigma_{c.e.}$  versus energy in the range  $0.5 \text{ V} \leq \varphi_a - \varphi_{pl} \leq 3 \text{ V}$  from curves like those shown in Fig. 2. The energy resolution is then limited to 0.2 eV, which is the thermal spread in perpendicular energy. Within the accuracy of our experiment no variation in  $\sigma_{c.e.}$  has been observed in this energy range.

Finally it should be noted that the method described here may in principle be used for measurements at energies around 2 eV of charge exchange cross sections between ions of all alkali metals, and neutral atoms of all elements which can be brought into the vapour phase at sufficiently high densities. The use of this method does require that the charge exchange cross sections are large compared to those of inelastic collisions.

\* Present address: Technical College, Dar es Salaam, Tanzania

#### References

1. Marino, L. L., Smith, A. C. H. and Caplinger, E.  
Phys. Rev. 128, 2243 (1962).
2. Palyukh, B. M. and Savchin, L. S. Soviet Phys. Tech.  
Phys. 13, 878 (1969).
3. Andersen, S. A., Jensen, V. O., Michelsen, P. and Nielsen, P.  
Phys. Fluids 14, 728 (1971).
4. Dreicer, H., Henderson, D. B. and Mosher, D. in International  
Conference on Physics of Quiescent Plasmas, Paris, France,  
Sept. 8-13, 1969. (Laboratoire de Physique des Milieux Ionises,  
Ecole Polytechnique, Paris, 1969). Part III p. 11.
5. Lou, Y. S., Journ. App. Phys. 42, 536 (1971).

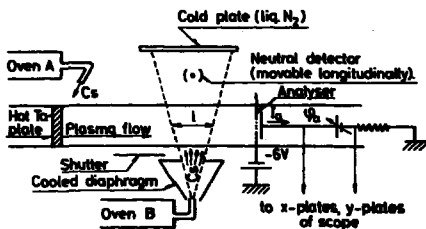


Fig. 1. Experimental set-up.

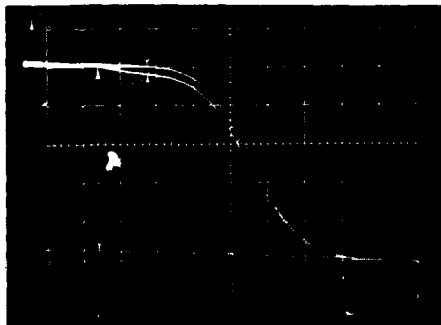


Fig. 2. Examples of measured characteristics.

Sweep: 0.5 V/large div. Curve (a) obtained without neutral beam; (b) with neutral beam  $n_n = 2 \cdot 10^{11} \text{ cm}^{-3}$   
 Plasma density  $\approx 10^9 \text{ cm}^{-3}$ . The baseline is oblique because of the final input impedance (100 MΩ) to the x-plates.

AUTHOR LIST

|                      | Page          |                                | Page              |
|----------------------|---------------|--------------------------------|-------------------|
| Abrams, R.H.         | 79            | Hamberger, S.M.                | 144, 327          |
| Alcock, M.W.         | 238           | Harker, K.J.                   | 349               |
| Alexeff, I.          | 71            | Hashmi, M.                     | 27                |
| Andersen, S.A.       | 388           | Hellberg, M.A.                 | 9                 |
| Ault, Earl R.        | 17            | Hendel, H.W.                   | 201               |
| Baker, D.R.          | 111           | Hines, K.C.                    | 365               |
| Baker, C.R.          | 9             | Honsowa, T.                    | 119               |
| Barbian, E.P.        | 317           | Houven van Oordt, A.J. van der | 27                |
| Barrett, P.J.        | 285, 290, 297 | Ikeni, H.                      | 327, 334          |
| Bartoli, C.          | 111           | Jensen, V.O.                   | 63, 87, 388       |
| Bitter, M.           | 111           | Jones, W.D.                    | 128               |
| Boissier, R.         | 246           | Jurgens, B.                    | 317               |
| Brossier, P.         | 209, 246, 261 | Katsumata, I.                  | 374               |
| Bruce, R.L.          | 349           | Kawai, I.                      | 119               |
| Burt, J.             | 254           | Kean, B.E.                     | 238, 334          |
| Buszi, J.M.          | 40, 48, 128   | Kennel, C.F.                   | 297               |
| Christoffersen, G.B. | 55, 63        | Kiwamoto, Y.                   | 334               |
| Chu, T.K.            | 224           | Krumm, P.H.                    | 9                 |
| Crawford, F.W.       | 349           | Lampis, G.                     | 144, 327          |
| Demulière, P.        | 151           | Lashinsky, H.                  | 79                |
| Deschamps, P.        | 209, 246, 261 | Lee, Y.C.                      | 224               |
| Doucet, H.J.         | 128           | Limpaecher, Rudolf             | 22                |
| Killis, R.F.         | 194           | MacKenzie, K.R.                | 17, 22            |
| Etatabrook, K.       | 71            | Marshall, T.C.                 | 136               |
| Fletcher, W.H.W.     | 334           | Matthiuseent, G.               | 275               |
| Franklin, R.N.       | 144, 327      | Messiaen, A.N.                 | 161               |
| Fried, B.D.          | 297           | Nichelsen, P.                  | 63, 103, 382, 388 |
| Fris, W.             | 217           | Kills, P.                      | 33                |
| Gravier, R.          | 209, 246, 261 | Nina, K.                       | 334               |
| Grénilon, D.         | 285, 290      | Nutley, R.V.                   | 194               |
| Guillemot, M.        | 151, 275, 304 | Miller, G.L.J.                 | 217, 230          |

|                     | Page          |                  | Page     |
|---------------------|---------------|------------------|----------|
| Nishikawa, K.       | 334           | Schlitt, L.G.    | 201      |
| Ohe, T.             | 79            | Schmitt, J.P.M.  | 177, 185 |
| Olivain, J.         | 151, 275, 304 | Self, S.A.       | 169, 267 |
| Palmer, R.S.        | 217, 230      | Sellen, J.M.     | 297      |
| Pellat, R.          | 209, 246      | Smith, D.E.      | 357      |
| Perceval, F.        | 151, 275, 304 | Smith, G.J.      | 144, 327 |
| Powers, E.J.        | 357           | Stott, P.E.      | 254      |
| Praha, L.P.         | 103           | Taylor, R.J.     | 297      |
| Quemeneur, A.       | 151, 275, 304 | Twomey, Dennis   | 95       |
| Renaud, C.          | 209, 246, 261 | Vandenplas, F.E. | 161      |
| Robertson, Harry S. | 1             | Vanak, V.        | 136      |
| Rognlien, T.D.      | 169, 267      | Weynants, R.R.   | 161      |
| Rowberg, R.E.       | 357           | Wong, A.Y.       | 285, 290 |